DEVELOPMENT AND CHARACTERIZATION OF FUNCTIONALLY GRADED Al-Si ALLOY SYSTEM AND Al-Si/SiC_P COMPOSITES USING CENTRIFUGE CASTING

Thesis

Submitted in partial fulfillment of the requirements for the degree of

DOCTOR OF PHILOSOPHY

by

KIRAN AITHAL S

(Reg. No. 070531ME07P01)

DEPARTMENT OF MECHANICAL ENGINEERING

NATIONAL INSTITUTE OF TECHNOLOGY KARNATAKA

SURATHKAL, MANGALORE-575025

JANUARY-2013

D E C L A R A T ION

By the Ph.D Research Scholar

I hereby *declare* that the Research Thesis entitled "***DEVELOPMENT AND CHARACTERIZATION OF FUNCTIONALLY GRADED Al-Si ALLOY SYSTEM AND Al-Si/SiC$_P$ COMPOSITES USING CENTRIFUGE CASTING"*** which is being submitted to the **National Institute of Technology Karnataka, Surathkal** in partial fulfillment of the requirements for the award of the degree of **Doctor of Philosophy** in **Department of Mechanical Engineering** *is a bonafide report of the research work carried out by me.* The material contained in this Research Thesis has not been submitted to any University or Institution for the award of any degree.

Register Number: **070531ME07P01**

Name of the Research Scholar: **Kiran Aithal S**

Signature of the Research Scholar:

Department of Mechanical Engineering

Place : NITK-Surathkal

Date :

CERTIFICATE

This is to *certify* that the Research Thesis entitled ***"DEVELOPMENT AND CHARACTERIZATION OF FUNCTIONALLY GRADED Al-Si ALLOY SYSTEM AND Al-Si/SiC_P COMPOSITES USING CENTRIFUGE CASTING"*** submitted by **Mr. Kiran Aithal S (Register Number: 070531ME07P01)** as the record of the research work carried out by him, is accepted as the *Research Thesis submission* in partial fulfillment of the requirements for the award of the degree of **Doctor of Philosophy.**

Dr. Vijay Desai
Guide
Date:

Dr. S Narendranath
Co-Guide
Date:

Chairman-DRPC
Date:

ACKNOWLEDGEMENT

..... It is impossible to start.....

One of the joys of completion of this thesis work is to look over the past journey and remember all the Gurus, friends, students and family, who have helped and supported me along this long but fulfilling road. It cannot be argued that the most influential persons in my career have been my Gurus. I express my gratitude with the Sanskrit stanzas on guru:

!!! Guru Brahmaa Gurur Vishnu, Guru Devo Maheshwaraha
Guru Saakshat Para Brahma, Tasmai Shri Guruve Namaha !!!

The Guru is manifested God who is the Light, the inspiration and the great exemplar. The life of the average seeker, as it is lived on the material and physical level, is barren and unproductive until it finds its focus in the Master. It requires the grace, protection and the powerful push of the Guru to release this imprisoned splendor that lies captive in each and every one of us. Expressing the gratitude to my gurus Dr Vijay Desai and Dr S Narendranath becomes my first and foremost duty, for their encouraging and constructive feedback, to shape and guide the direction of the work with careful and instructive comments. It is no easy task, reviewing a thesis, and I am grateful for their thoughtful and detailed comments.

I would like to express my heartfelt gratitude to my mentor, Dr. P G Mukunda. I could not have asked for better role model and I really thank him for his inspiration, support and care during the entire course of Ph.D work. Being proud of my academic roots, I hope to in turn pass on the research values and the dreams that he has given to me for the betterment of the research community in the technical field.

I thank Dr G C Mohan Kumar, Head Mechanical Department and also Former Head Dr T P Ashok Babu for their kind support throughout my Ph D course.

I also acknowledge and appreciate the advice of the RPAC members Dr G Umesh and Dr M B Saidutta for their critical comments which enabled me to make the necessary improvements according to their suggestions.

A good support system is important to survive and work for better results. I was lucky to be a part of one. We the group of five, Dr Shailesh Rao, Dr Sudheer Reddy, Mr Madhusudan, Mr Desai Gowda and myself formed the core of research in the institute and were always there for one another and have taught ourselves and each other many tools and issues. I like to thank all the core team members for their sincere advice and support. At this outset I also like to thank my supporting staff members Mr Naresh and Mr Bhaskar for their help in developing the Centrifuge machine and producing castings. I also wish to convey my thanks to Dr N R Shetty our director, Dr H C Nagaraj our principal, Dean Academic Prof Ranganatha Setty, Dr P B Shetty HOD, Mechanical department, Mrs Rashmi of NMIT for their support and encouragement throughout my Ph.D. I sincerely thank to my students Hemanth, Adarsh, Sachin, Anoop, Sharat, Shashi kiran, Sandeep, Pankaj, Maqsud, Saurabh and Cyril.

Finally, I take this opportunity to thank my mother Vanajakshi, wife Kavitha, my daughter Kshithi, brother Praveen, each of whom extended whole hearted support and cooperation and made contributions in their own way during the entire period of my research. Most importantly, the moral and emotional support was, of course, something that kept me going all through the arduous period of my research and made it possible to finally complete this thesis, which I dedicate in the memory of my father.

The list goes on and there are many others I should mention. There are people who have helped me all the way and provided me support when I didn't even realize I needed it, or needed it now, or needed it constantly. Listing all of them would fill a book itself, so I merely will have to limit myself to a few words: I THANK YOU ALL!

ABSTRACT

FGM is a material that shows change in magnitude of property values from one end of a specimen or component to the other end. FGM has an intermediate layer whose structure, composition and morphology vary smoothly from one end of the specimen to the other end. Fabrication of FGM and their components with gradient microstructures and properties are challenging. Most of the investigations which focus on material behavior of FGMs are limited to analytical or numerical studies. One of the major bottlenecks with experimental studies is the preparation of FGMs having large property gradation. This necessitates the development of a suitable technique to produce such FGMs with reproducibility of structure and properties. The present work aims at developing a manufacturing technique for the FGMs in order to meet the wide range of and also suitable mechanical and tribological properties for specific thermal and mechanical engineering applications.

Among the processing techniques available the most commonly used is horizontal centrifugal method, but, this method is used to produce mainly hallow cylinders. In this work a centrifuge setup is fabricated and FGMs have been successfully developed to produce solid castings. The major advantage of this machine when compared to the conventional machine is that the pouring is done while the mold is stationary and machine operates about a vertical axis. The principal advantage of this is good mold filling combined with microstructural control, which usually results in improved mechanical properties. In this process, when the melt is subjected to high G forces the lighter particles segregate towards the axis of rotation, while the denser particles move away from the axis of rotation depending on the density difference between melt and the reinforcement. This segregation depends on several process parameters such as mold rotational speed (G Factor), pouring temperature, mold temperature etc.

The use of aluminum, its alloys and aluminum based composites in the present day has shown many advantages through its unique combination of physical and mechanical properties. The light weight, strength, formability, corrosion resistance, of

aluminum, its alloys give it the potential to meet a wide range of design challenges. Taking into consideration the advantages such as high wear resistance, controlled thermal-expansion coefficient, good corrosion resistance, and improved mechanical properties over a range of temperatures that Al alloys and its composites can provide, in this work manufacturing and characterization Al-Si FG alloys and Al-Si-SiC_P FG composites have been taken up. Two Al-Si alloys eutectic (12%Si) and hypereutectic (17%Si) were used for producing FG alloys. Further effect of 3 mold rotational speed 200, 300, 400rpm, 2 pouring temperatures 800^oC , 900^oC and 2 mold temperatures ambient and preheating the mold at 180^oC temperature were studied. Similarly FG composites were also produced using Al-17%Si and Al-12% Si as matrix with SiC_P as reinforcement. Three different volume fractions of SiC_P were used to produce FG composites. The FG composites were produced using 900^oC pouring temperature with preheating the mold at 180^oC under 200, 300, 400rpm mold rotational speed.

The structure and properties of the FG alloys and Composites are studied to understand the effect of different process parameters. The Al-Si FGM specimens are studied for distribution of Si along the length of the specimen (from bottom to top) using optical microscope. The hardness's is measured along the length of the specimen using Brinell hardness tester. Sliding wear tests at room temperature are conducted at normal loads of 40, 60, and 80N and at 1.466m/s sliding speed for a constant sliding distance 879.6m in order to measure the wear resistance and friction characteristics. Similar tests were carried out for FG composites. Diametral compressive strength were conducted to know the strength of the specimen along the length at bottom, middle and top regions. It is found that the FG alloy and Composites are produced successfully using centrifuge technique. In both alloy and composite the gradation occurs at higher rpm, teeming temperature and mold temperature. The experimental findings of hardness and the wear tests provide adequate proof on the gradation characterization (% volume fraction of primary Si, % volume fraction of SiC_P and rim thickness) done using microstructural studies.

Key words: *Functionally Graded Material, Centrifuge, Segregation, Hardness, Wear*

CONTENTS

LIST OF TABLES

LIST OF FIGURES

NOMENCLATURE

m = Mass of the melt (kg)

R = Radius of rotation (m)

ω = Angular velocity (rad/sec)

g = Gravitational force (m/s^2)

W = Load for hardness indentation (kg)

d = Diameters of the indentation (mm)

D= Diameter of the indenter (mm)

T_m = Mold Temperature (^oC)

T_p = Teeming Temperature (^oC)

SWR = Specific wear rate ($mm^3/N\text{-}mm$)

COF = Coefficient of Friction

σ_t = Tensile strength (N/mm^2)

P = Load applied for diametral compression test (N)

D_c = Diameter of the specimen for diametral compression test (mm)

t = Thickness of the specimen for diametral compression test (mm)

ρ = Density

PFZ = Particle Free Zone

T400 = Casting at 400rpm (89.42g), tested for top end of the casting

B400 = Casting at 400rpm (89.42g), tested for bottom end of the casting

T300 = Casting at 300rpm (50.3g), tested for top end of the casting

B300 = Casting at 300rpm (50.3g), tested for bottom end of the casting

T400 = Casting at 200rpm (22.35g), tested for top end of the casting

B400 = Casting at 200rpm (22.35g), tested for bottom end of the casting

1. INTRODUCTION

Functionally Graded Material (FGM) is a novel concept for the realization of innovative properties and functions that cannot be achieved by conventional homogeneous materials. FGM is a material that shows change in magnitude of property values from one end of a specimen or component to the other end. FGM has an intermediate layer whose structure, composition and morphology vary smoothly from one end of the specimen to the other end. These transition profiles are predesigned and intentional in order to achieve the desired properties (Kawasaki et al 1997). FGMs multifunctional behavior and performance, enable wide scope for applications in aerospace, automotive, electronics, and biomedical sectors. The specific properties obtained by the use of Functionally Graded Metal Matrix Composites (FGMMC) include high temperature surface wear resistance, desired friction and thermal properties, reduced internal stress, increased fracture toughness and crack retardation.

In conventional composites, the reinforced or constituent phases are evenly distributed thereby the properties on an average will be uniform. However in FGMs, the composition and microstructure vary smoothly in space and the properties and performance, therefore, vary from one end of the specimen to the other. The Functional gradient can be tailored to the specified service conditions, thus ensuring the best response of the system. One of the advantages of continuously varying volume fraction of the constituent phases is the elimination of stress discontinuity that is often encountered in laminated composites. Accordingly delamination problems are avoided and further the gradual transition also allows the creation of superior and multiple properties without any mechanically weak interface. Moreover, the gradual change of properties can be tailored to suit different applications and service environments.

The concept of FGM includes two important features. The first feature is the ability to tailor the microstructure and chemical composition as per the desired

function, while the second feature is the availability of the fabricating process which has good and controlled reproducibility of the desired properties.

The use of FG alloys and FG composites as structural materials is determined by their physical properties and their mechanical properties. The mechanical properties of a specific alloy or composite can be attributed to the individual properties of its main phase components and to the volume fraction and morphology of these components. In Al-Si alloys and Al-Si- SiC_P composites the tensile properties and fracture behavior depend on secondary dendrite arm spacing, Si shape and size, volume percentage of SiC_P. Thus, mechanical properties of Al-Si alloys and their composites depend not only on chemical composition but, more importantly, on micro-structural features such as morphology of α-Al dendrites, eutectic Si particles, SiC_P shape and size and other intermetalics that are present in the microstructure. The components such as part of turbine, rocket nozzle, medical implant, tool inserts and optical devices need to meet functional performance requirements that vary with location within the component. FGM provides best solutions under such situations (Birman et al 2007). In the last two decades, more attention is given to the research on production techniques of FGMs that include, powder metallurgy, deposition techniques, centrifugal casting, electromagnetic separation etc. (Kiebact et al 2003). But each technology has particular aspects that interfere with the generation of a desired microstructure and consequently affect the mechanical properties adversely.

To produce a wear resistant material with considerable strength, a material of heterogeneous microstructure can be designed in which a high volume fraction of hard particles is dispersed at the surface, where better wear properties are needed, and a gradually decreasing lower volume fraction of hard particles below the surface where better strength and ductility are desired. Centrifugal casting technique allows producing a material of desired tribological surface at one end and with good strength on the other end (Qudong et al 2005).

As compared to conventional casting, in centrifugal casting the mold itself will be spinning during the melt solidification. The centrifugal casting process utilizes the

inertial forces caused by rotation to distribute the molten metal into the cavities in the mold. This method was suggested in the early part of 19th century (Royer et al 1988). The parts made from centrifugal casting exhibit a denser, close grained structure with vastly improved physical and mechanical properties. This process yields castings of good quality, dimensional accuracy and external surface details. The disadvantages include its applicability to limited sizes and shapes.

In centrifugal casting process for producing FGM the alloy melt or alloy melt with reinforcement particle melt is subjected to centrifugal force. Two distinct zones, one with enriched and the other with depleted primary alloy phase and particles, with an intermediate graded zone are formed. The extent of particle segregation and relative locations of enriched and depleted particle zones within the casting are mainly dictated by the densities of the particles, melt temperature, melt viscosity, cooling rate, particle size and magnitude of centrifugal acceleration. Depending on the density of particles, the lighter particles segregate towards the axis of rotation, while the denser particles segregate away from the axis of rotation (Rajan et al 2008).

Traditionally the centrifugal casting process has been mainly used for obtaining cylindrical parts. There are two types of centrifugal casting machines: the horizontal, where the mold rotates about a horizontal axis, and the vertical, where the mold rotates about a vertical axis. Horizontal centrifugal casting process is usually adopted to manufacture pipe, tube, bushings and vertical casting process is used to produce gear blanks, pulleys, etc.

Centrifugal casting is also a very common method for obtaining FGMs. Most of the work based on centrifugal casting is mainly on composite materials, such as SiC_p reinforced Al based FGMs wherein the two materials have reasonably high density difference and low mutual solubility. However, there are almost no studies emphasizing the fact that the centrifugal process can be successfully used for obtaining solid cylindrical FGMs. One of the objectives of the present work is to produce solid cylindrical FGMs of Al-Si alloy system and Al-Si-SiC_P composites using the principle of centrifugal casting.

Aluminum matrix composites are tailored to possess the toughness of the alloy matrix and the hardness, stiffness and strength of hard ceramic reinforcements. As a result composite materials exhibit a good combination of strength and toughness. In the earlier work on Al-Si FGMs and Al-Si-SiC_P FGMMCs produced by different methods, it has been shown that the performances of these depend heavily on their microstructures. The morphology, volume fraction, size and distribution of the primary phase and the eutectic constituent in the microstructures will depend both on the composition and the solidification/ casting process involved (Srivatsan et al 1991).

Along with research in processing of FGMs, in early stages of evolution, the basic experimental and theoretical studies on the mechanics of these materials must be taken up. There are several important areas being addressed in FGM research: design (Ogawa et al 2006), processing (Song et al 2006), (Zhang et al 2009), (Peng et al 2007) and modeling (Panda et al 2006). However, considering the mechanics of FGMs, most of the research work has been without much experimental testing on wear and mechanical properties, particularly along the radial direction. This clearly conveys the message for the need for development of a suitable manufacturing technique for the FGMs to meet the demand for lightweight materials, with suitable mechanical and tribological properties for a range of engineering applications. Major part of the available literature on FGMs is based on the centrifugal technique to produce hallow cylinders. Very little literature is available on producing solid blocks which is of prime importance in the automobile sector.

From the above discussion, it is clear that many mechanisms can play significant role in the sliding behavior and mechanical properties of FGMs. In order to meet the growing demand for high performance Al-Si based FGMs, it is thus essential that investigations be carried out to search for the role of Si, SiC_P and process parameters on dry sliding behavior.

2. LITERATURE REVIEW

2.1 Introduction

Over the last two decades reasonably significant work has been carried out on FGM. A large volume of information is available on FGM exploring the mechanical properties and processing techniques but still many problems exist that needs to be addressed. The structured literature survey done so far on FGM will help in planning the research work. The literature is collected based on the objectives of the present research work and is presented under the following headings.

- **History of FGM**
- **FGM Processing Techniques**
- **FGM through Centrifugal Technique**
- **Al-Si and Al-Si-SiC_P system**
- **Characterization of FGMs**

2.2 History of FGM

FGMs are characterized by continuous, smooth variations in composition and/or microstructure within the material so as to meet functional performance requirements that vary with locations within the part. This shows that their transition profiles have been designed and introduced intentionally in such a way that the desired properties are achieved. This separates the FGMs from the conventionally homogenous composite materials.

From the historical point of view, the production of FGMs dates back to 1972 (Bever et al 1972). Research work carried out by Nath et al indicate that mica particles are gradiently dispersed in Al-Cu-Mg alloy in centrifugally cast hollow cylinders (Nath et al 1981). The cast hollow cylinders showed two distinct zones: an outer free of mica zone and an inner zone with majority of mica particles distributed from top to bottom. The authors have illustrated that the mica particles near the inner

periphery can serve as good as a solid lubricant, whereas the mica free zone having nearly the same strength as the matrix alloy would serve as a good backing material.

However the concept of Functionally Gradient Materials was proposed in 1984 by a materials scientist in Sendai, Japan as a means of preparing thermal barrier materials (Koizumi 1997). In the fiscal year 1987, a national project entitled 'Research on the Basic Technology for the Development of Functionally Gradient Materials for Relaxation of Thermal Stress' was initiated in Japan, The aim of the project was to develop advanced heat shielding structural material for space vehicle application wherein the material at the surface is expected to withstand temperatures as high as 2100K and a temperature difference of 1600K. As a result, the concept of FGM was shown virtually and the term 'Functionally Gradient Material' was introduced for the first time. The report of this project has cited CVD/PVD, powder metallurgy, plasma spray for processing FGM.

Apart from thermal barrier coatings, FGMs are nowadays used for many applications such as gradient structural alloy materials to obtain wear resistance. MMCs with considerable strength and with a high volume fraction of hard particles at the surface for better wear properties, and a gradually lowered volume fraction of hard particles below the surface where better strength and ductility can be achieved. Also they have considerable potential to be extended from structural, to electrical, chemical, optical, nuclear and biomedical areas (Kato et al 2006), (Muller et al 2003), (Zhou et al 2010), (Pompe et al 2003), (Mishina et al 2008).

2.3 FGM Processing Techniques

In order to use FGMs in structural and functional applications, a suitable fabrication technique is needed that makes it possible to produce the required microstructure and compositional gradient and also assures high reproducibility of the gradient. Thus FGMs can meet functional performance requirement that vary with the location within a work piece such as in a turbine blade, rocket nozzle, medical implant, tool inserts and optical devices (Birman et al 2007). Nowadays with the

usefulness of FGMs being established, more attention is paid to research on production techniques of FGMs.

The manufacturing process of a FGM is classified according to methodology of obtaining spatially inhomogeneous structure known as 'Gradation' and transformation of this structure into a bulk material known as 'Consolidation'. Gradation processes can be classified into constitutive, homogenizing and segregating processes. Constitutive processes are based on a stepwise buildup of the graded structure from precursor materials or powders. In homogenizing processes a sharp interface between two materials is converted into a gradient by material transport. Segregating processes start with macroscopically homogeneous material which is converted by an external field (viz. gravity or electric field). Homogenizing and segregating processes produce continuous gradients, but have limitations concerning the types of gradients which can be produced (Kiebact et al 2003).

The prevailing techniques used in practice to fabricate FGM include powder metallurgy technique, deposition techniques, power ultrasonic technique, electromagnetic separation, power ultrasonic, gradient slurry disintegration technique, directional metal remelting and quenching technique, centrifugal casting etc.

An overview of the processing techniques (Kiebact et al 2003) is tabulated in Table 2.1 and in the following sections these techniques are explained in detail.

Table 2.1 Overview of processing techniques for FGMs

Process	Variability of Transition Function	Layer thickness	Versatility in phase content	Type of FGM	Versatility in component Geometry
Powder stacking	Very good	M, L	Very good	Bulk	Moderate
Sheet lamination	Very good	T, M[b]	Very good	Bulk	Moderate
Wet powder spraying	Very good	UT, T[b]	Very good	Bulk[C]	Moderate
Slurry dipping	Very good	UT, T[b]	Very good	Coating	Good
Jet solidification	Very good	M, L	Very good	Bulk	Very Good
Sedimentation / Centrifuging	Good	C	Very good	Bulk	Poor
Filtration / Slip casting	Very good	C	Very good	Bulk[C]	Good
Laser cladding	Very good	M	Very good	Bulk, Coating	Very Good
Thermal spraying	Very good	T	Very good	Coating, Bulk	Good
Diffusion	Moderate	C	Very good	Joint, Coating	Good
Directed solidification	Moderate	C	Moderate	Bulk	Poor
Electrochemical gradation	Moderate	C	Good	Bulk	Good
Foaming of polymers	Moderate	C	Good	Bulk[C]	Good
PVD, CVD	Very Good	C	Very good	Coatimg	Moderate
GMFC process	Very good	M, L, C	Moderate	Bulk	Good

L:Large (>1mm); M: Medium (100-1000μm); T: Thin (10-100μm); UT: Very Thin (<10μm); C: Continuous
[b]Depending on available powder size
[c]Maximum thickness is limited

2.3.1 Powder Metallurgy

Kawasaki et al have extensively worked on FGM from the late 1990s. Powder metallurgy (Kawasaki et al 1990) technique involves the selection of a material combination of metals and ceramics, optimum compositional distribution, stepwise or continuous stacking followed by die compaction, isostatic pressing and sintering. Among all the steps sintering is the most important process. Any imbalance in sintering process will cause various faults such as warping, frustum formation, splitting and cracking. Later the authors have shown that this imbalance can be avoided by pressure sintering i.e., by hot pressing and hot isostatic pressing (Kawasaki et al 1997). However there are also drawbacks in this production route. Practical considerations towards an efficient process design suggest the use of powder mixtures with changing average particles size or composition during deposition of the material prior to the forming operation. The method applied for powder deposition determines whether smooth change or a stepwise variation is obtained in the green compact. Since the consolidation of the green parts during sintering or pressing

requires high temperature, there may be adverse microstructural features associated with the sintering, in particular porosity and interfacial reaction products.

Lin et al developed a mechanical working process which eliminates the need for sintering (Lin et al 1999). An additional mechanical vibration step was introduced in the mechanical working route, in order to improve the continuity of the composition gradient. This working process was successfully employed for the production of SiC/Al 2124 FGMs. It was found that the vibration stage modified the SiC distribution from a layered structure to a smoothly changing SiC content with position in the sample. The vibration process also improved local homogeneity by breaking up the coarse SiC agglomerates which tend to form in high SiC content regions of the FGMs.

Jingchuan Zhu and others produced ZrO_2-Ni FGM by hot pressing and pressure less sintering (Zhu et al 2001). This Powder metallurgy technique was developed to optimize the FGM fabrication process and further improve its performance. The FGM produced had continuity of both components and eliminated the macroscopic interface.

Xie et al have extensively worked on W-Cu FGMs. They have shown that it is difficult to fabricate W-Cu graded materials with nearly full density even by liquid phase sintering after mechanical alloying. By increasing the holding time and sintering temperature sintering quality of W-Cu composites improves. It develops structural homogeneity and changes the initial composition design (Xie et al 2005). To overcome this they used particle size adjustment method wherein two kinds of powders with different particle sizes are added to powder mixtures to promote sintering density. This caused production of W-Cu graded heat sink materials with nearly full density at a sintering temperature of 1060^0C, pressure of 85 MPa and holding time of 3hrs (Liu et al 2008).

2.3.2. Deposition Techniques

The concept of coating techniques to produce FGM is to achieve reliability and longevity. The graded coatings are mainly used to protect metallic or ceramic substrates used in space shuttles, jet engines, nuclear fusion equipment and gas turbines against oxidation, heat protection, wear and corrosion (Cetinel et al 2003). Depending on the application and the specific loading conditions, various approaches are used to generate the gradients (Schulz et al 2003). The various thermal spray techniques used include High-Velocity Oxy-Fuel (HVOF) spraying, Low-velocity Oxy-Fuel (LVOF) spraying, Plasma Spraying (PS), Arc Spraying (AS), and Layered Manufacturing Technique (LMT). The coating is used as an alternative approach to the conventional thermal barrier coatings in order to reduce the mismatch effect, thermal expansion and interfacial stresses (Wayne et al 1990).

Under coating techniques Vapor Plasma Spraying (VPS) is more often employed. In this process the powder particles of the material to be deposited on a given substrate are blown into a plasma plume produced by a certain gas mixture in an ambient argon atmosphere at 120Mbar. The particles are melted, accelerated towards the substrate and finally each particle is deposited on the substrate in a splat like structure using mechanical bonding. Using this technique Pintsuk fabricated W/Cu composites for applications involving extreme thermal conditions (Pintsuk et al 2007).

An alternative technique for FGM is Layered Manufacture Technique (LMT). This technology can produce virtually free form geometries using different materials. Selective laser sintering, direct laser remelting and laser cladding which are based on powder and laser interaction are the processes used under LMT.

Selective laser sintering works with fine layers of powder deposited over a platform. Each layer is selectively sintered through the energy delivered by the laser beam. The laser beam sinters a new layer adding it to the previous one and the process is repeated until the part is built. Direct metal laser sintering is based on the same process of selective method but it uses the power of the laser to fully process the

powder, without necessity for special post processing in an oven to increase the density of the part. Laser cladding works by spraying powder with a shield gas over a high power density laser spot. Selective laser fusion works with fine powder layers spread over a platform and they are fully melted layer by layer by scanning the laser (Beal et al 2006).

2.3.3. Electromagnetic Separation Technique

Song et al, developed a new process called electromagnetic separation method for in situ multilayer FGMs. The principle behind this method is that when the melt is exposed to the electromagnetic field an electromagnetic force will be induced in the liquid metal. Smaller force will be induced in the primary particles of the alloy such as Si in Al-Si alloy, due to their lower electrical conductivity. So when the melt containing primary particles is exposed to the electromagnetic field, the electromagnetic Archimedes force will act on the primary particles because of the difference in the electrical conductivity between the primary particles and the parent melt. During solidification, when the melt temperature is below the liquidus temperature, primary particles will precipitate from the parent melt and then move with a particular speed in the direction of the resultant force to the one side of the sample. With the temperature decreasing further, primary particles precipitate on one side of the sample. So by adjusting the electromagnetic force and solidification rate of the melt, the desirable distribution of the primary particles can be obtained and the in situ FGMs are produced. Based on this in-situ multi-layer FGMs using alloy Al-22%Si-3.9%Ti-0.78%B are produced (Song et al 2005). Results show that there are three layers, namely the layer of the primary ternary intermetallic compound Al-Si-Ti particles with rich Si, the layer of the primary Si particles and the layer of Al-Si eutectic structure. The ternary Si rich intermetallic compound Al-Si-Ti particles are formed above 700^{o}C, the Si particles are precipitated in the range of eutectic temperature 720^{o}C to about 577^{o}C and the eutectic reaction occurs at the eutectic temperature 577^{o}C. The interfaces between the layers show gradient transition in the microstructure from one layer to another in the situ multilayer FGM.

By using the method cited above Song et al produced Al/Mg_2Si alloy FGMs (Song et al 2006), (Song et al 2007). In this work the authors have analyzed the process parameters such as electromagnetic force, preheating temperature of the mold and melt temperatures. It was shown that as the electromagnetic force increases, the maximal volume fraction of primary Mg_2Si particles in the lower part of the sample increases, and the length of the particle free region increases. As a result the volume fraction gradient increases with the increase of the electromagnetic force. Moreover the particle size decreases with the increase of the electromagnetic force. When the mold temperature increases, the maximal volume fraction of the particle packed regions increases, and the length of the particle packed regions becomes shorter. As a result, the volume fraction gradients become greater. The change in the pouring temperature for 750^{o}C to 850^{o}C showed no effect on the volume fraction distribution of primary Mg_2Si particles.

Al-Si alloy FGM with microstructure showing a gradient from hypereutectic structure to hypoeutectic structure through intermediate eutectic region from one side of the sample to the other has been successfully produced (Song et al 2007). The sample yielded gradient of volume fraction of Si particles and the hardness. The continuation of work on electromagnetic separation method to produce Al/Al_3Ni alloy FGM (Song et al 2007) investigated the primary particle distribution and the effects of alloy composition on microstructural and hardness gradient. Three compositions were investigated; Al-12wt%Ni, Al-17wt%Ni, and Al-23wt%Ni. The result shows that the volume fraction and size of primary Al_3Ni particles are of gradient distributions from one side to the other in Al-Ni samples. The particle volume fraction gradient of Al-17wt%Ni sample is highest among all compositions. It is reported that major axis of primary Al_3Ni particles tends to be perpendicular to the direction of the electromagnetic Archimedes force at the lower part. However orientation arrangement of primary particles is random due to the small effect of the electromagnetic force in the upper part.

2.3.4. Power Ultrasonic Technique

The method of preparing Al-Si alloy containing 18%Si FGM using power ultrasonic field and water cooling system was reported by Zhang et al (Zhang et al 2009). The alloy was heated to 750^{o}C and held for 30 min to achieve uniform Si distribution. Further the melt was poured into a preheated cylindrical graphite crucible. During solidification ultrasonic vibration was started at 710^{o}C. When the temperature decreased to 620^{o}C, water cooling system was used to spray water on the crucible wall. After the sample was cooled to room temperature, the Al-Si alloy FGM produced under ultrasonic field was obtained. Ultrasonic vibrations leads to the vigorous migration of primary Si, and water cooling increases the solicitation velocity. The viscosity, concentration gradient of the outer melt increase rapidly. Due to this, most of the primary Si particles are rapidly trapped in the outer region by the engulfment of solidification interphase, which causes the graded distribution of primary Si in the sample. Since the hardness is mainly affected by the content of primary Si, the hardness of the FGM sample decreases from outer to inner side of the sample. It was shown that volume fraction of primary Si varies from 30% to zero from outer to the inner side of the FGM sample. In accordance to this even the micro hardness and wear resistance also showed better graded character.

Gupta et al have exclusively worked on gradient slurry disintegration and deposition process (Gupta et al 2000). The process involved ultrasonic assisted super heating of Al strips in a graphite crucible up to 950^{o}C. For the synthesis of Al–Cu/SiC_P and Al–Mg/SiC_P FGMs, the same procedure is carried out, except for the extra addition of the respective alloying elements (Cu or Mg) upon reaching 950^{o}C. SiC_P, preheated for an hour at 950^{o}C was added to the molten Al via a vibratory feeder and stirred at a particular speed. The FGM melt was poured through a centrally drilled hole in the base of the graphite crucible and the melt slurry was disintegrated using two linear argon gas jets. The disintegrated melt slurry was then deposited into a metallic substrate. Several studies have been carried out using this method to find the effect of weight % of SiC_P, stirring speed (Gupta et al 2002) for different compositions such as Al-Cu/SiC_P (Gupta et al 2002) and Al-Mg/SiC_P. Very

significant hardness values were observed at the extreme ends of the FGMs as a result of large weight % of SiC_P. For Al/ SiC_P and Al-Mg/ SiC_P composite FGMs distinct high SiC_P and low SiC_P ends were observed and also wear resistance improved gradually from low end to high end. However in case of Al-Cu/ SiC_P system the wear resistance showed a lower value (Gupta et al 2003).

2.3.5. Centrifugal Casting Process

The process of centrifugal casting differs from the conventional casting processes in that, the mold itself is rotating during the time the molten metal is solidifying. The application of centrifugal force to a metal as it solidifies can be used to distribute the molten metal into mold cavities and to achieve a dense sound casting (Janco 1998). This method was developed in the early 1800s. There are various types of casting machines used for the production of centrifugal castings such as:

- Horizontal axis and
- Vertical axis machines.

Horizontal centrifugal casting machines are generally used to make pipes, tubes, bushings, cylinder sleeves (liners) and cylindrical or tubular castings that are simple in shape. The range of application of vertical centrifugal casting machines is considerably wider. Components that are not cylindrical, or even symmetrical, can be cast using vertical centrifugal casting. The centrifugal casting process uses rotating molds to feed molten metal uniformly into the mold cavity. Directional solidification results in clean, dense castings with physical properties that are often superior to those of the static casting processes. In a vertical casting machine, the mold is placed vertically and the molten metal is poured from the top. Horizontal machines are used to produce castings having a true cylinder as their inside diameter (Janco 1998).

The centrifugal force of the rotating mold forces the molten metal against the interior cavity (or cavities) of the mold under constant pressure until the molten metal has solidified. Cylindrical castings are generally preferred for the centrifugal casting process. Tubular castings produced in permanent molds by centrifugal casting usually

have higher yields and higher mechanical properties than castings produced by the static casting process. Centrifugal casting is the most economical method of producing a superior-quality tubular or cylindrical casting with regard to casting yield, cleaning cost, and mold cost (ASM 1992).

The components made from centrifugal casting process exhibit a dense, fine grained structure with vastly improved mechanical properties. The desirable properties are improved up to 30% over those castings produced by conventional, gravity or static casting processes. The process produces castings of good quality, dimensional accuracy and external surface finish. Some of the disadvantages of the process are limited size and shape. Researchers by utilizing the outstanding advantage created by the centrifugal force of rotating molds, started producing highly engineered FG castings in the form of pipes and tubes. Nowadays by slight modification in the processing technology, castings of solid blocks, circular plates are produced. Next section elaborates the work done by the researchers to produce FGMs using the centrifugal casting process.

2.4 FGM through Centrifugal Technique.

The concept of producing FGMs using centrifugal casting process is based on the centrifugal force. The centrifugal force, applied to a homogenous melt suspension, helps the formation of the desired gradation. The gradient is achieved primarily by the difference in the centrifugal force produced by the difference in density between the molten metal and solid particles. Fukui proposed this technique to produce the FGMMCs (Fukui 1991). During mold rotation, the particle suspended in the liquid is subjected to both centrifugal and gravitational forces. The centrifugal force acting on a particle along the radial direction is given by '$mr\omega^2$' and the gravitational force is given by 'mg'. The ratio of centrifugal force to the gravitational force is called the gravitational coefficient (G) or G number given by equation 2.1

$$G = \frac{m R \omega^2}{m g} = \frac{R \omega^2}{g} \qquad 2.1$$

where

m = mass of the melt in kg

R= radius of rotation in m

ω= angular velocity in rad/sec

From the above equation it can be noted that, as the angular velocity increases, the G value also increases. Since the centrifugal force acting on the particle is G times higher than the gravitational force 'g', the latter is negligible when compared to the former. Thus, as the rotational speed increases, the force acting on the particle to segregate it also increases.

Even though the concept of production of FGM came into light by 1986, Nath and Rohatgi (Nath et al 1981) had worked on use of segregation of particles in 1981 without terming it as FGM. They studied the effects of pouring temperature and particle size on the distribution of mica particles in the hollow cylindrical castings produced by centrifugal and static casting processes. The mica-free zone width increased with an increase in the particle size of the mica and the pouring temperature of the melt. By carrying out experiments on the static casting they reported that mica segregation is mainly due to density difference and not due to rejection by the solidifying front. Centrifugal casting of mica (120/μm) dispersed aluminum alloy when poured at 760^{o}C can result in mica concentration up to 9% at the inner periphery of the casting whereas it is difficult to make static castings containing more than 3% mica. The mica particles near the inner periphery can serve as good solid lubricant when the cylindrical castings are used as bearings even after considerable machining, whereas the mica free outer zone having nearly the same strength as the matrix alloy would serve as a good backing material (Nath et al 1981).

The fabrication of the FGMs made through the centrifugal action can be classified into two categories based on the melting point of the reinforcement particles. If the melting point is significantly higher than the processing temperature,

the reinforcement particle remains solid in a liquid matrix. This is known as centrifugal solid-particle method. If the melting point of the reinforcement particle is lower than the processing temperature, centrifugal force can be applied during the solidification both to the matrix and to the reinforcement particle. This solidification is similar to the production of in-situ composites using the crystallization phenomena and is known as centrifugal in-situ method.

Y Watanabe et al have worked exclusively on centrifugal casting of FGMs. They showed that the particle size distribution as well as the volume fraction of particles in composites play an important role in controlling mechanical properties. They studied in detail the particle size distribution to predict the mechanical properties of FGMs. In Al/Al_3Ni FGMs the Al_3Ni primary average particle size is gradually distributed and found that as the G number becomes larger, the particle size of the ring's outer region becomes smaller. It was concluded that the difference in the particle size distributions is caused by the cooling rate (Y Watanabe et al 2001).

The mechanical properties of the platelet and particle reinforced composites are strongly affected by the platelet orientation, particle size and the volume fraction of reinforced material as well. The detailed knowledge of distributions of platelet orientation and particle size will help in predicting the mechanical properties of the FGMs. To evaluate this a detailed observation was done on Al-(Al_3Ti+Al_3Ni) FGMs (Y Watanabe et al 2001). It was found that a large number of Al_3Ti platelets are arranged with their platelet planes nearly perpendicular to the direction of centrifugal force but no preferential direction at the ring's inner region (Y Watanabe et al 2001). The position dependence on the orientation parameter along the centrifugal force direction was found. The orientation parameter increases with the normalized thickness and the graded profile in the orientation parameter increases with increasing G number.

The velocity of particles in a viscous liquid is proportional to the square of the particle diameter under a centrifugal force. Therefore the migration distance is greater in the case of large particles. So to determine the particle size distribution in FGMs

fabricated by the centrifugal solid particle method, the authors used FGM tubes fabricated from plaster matrix composite materials containing corundum particles of five different particle sizes. It was found that average particle size is gradually distributed and the average particle size at outer region is greater than that in the inner region. Particle size gradient becomes steeper by increasing the G number or by decreasing the mean volume fraction. It was clearly shown that FGM can be fabricated by using multi-sized particles (Y Watanabe et al 1998).

From the above findings it was concluded that the larger particles migrate faster than smaller particles and the gradient of particle sizes arises. The gradients depending on the character of particles can be controlled by the difference of migration rate among particles contained in the melt. Consequently, the density of the ring will increase toward the outer periphery of the ring when the density of particles is greater than the melt matrix. If the FGM is fabricated using a melt containing two kinds of particles i.e., large particles with a low density and small particles with a high density, the large particles can have high velocity. To study this a simulation was done considering the relative motion of large particles with low density and small particles with high density in a molten metal (Y Watanabe et al 2002). The large particles with low density showed higher migration rate compared with small particles with high density, if the difference in diameter is significantly large. Thus large particles migrate and prevent the movement of small high density particles. This phenomenon provides the unique density gradation and can obtain the FGM with designed density gradients (Y Watanabe et al 2005a) (Y Watanabe et al 2006).

Centrifugal solid-particle method is influenced by various processing parameters. The authors used Al-Al_3Ti FGMs to find wear behavior (Y Watanabe et al 1999) and the effect of platelet size and volume fraction of platelets on graded distribution (Y Watanabe et al 2007). It has been reported that steeper compositional gradients are obtained in the case of larger platelet size and larger mean volume fraction. The graded distribution of orientation becomes steeper as the platelet size and mean volume fraction increases.

Zinc Aluminum alloy has many advantages namely, excellent tribological prosperities, superior mechanical properties, relatively lower density and it can be processed easily. Sui Xiandong reported on the mechanical properties for Zinc Aluminum alloy ZA27 reinforced with SiC_P (Xiandong et al 1997). It is reported by the author that the SiC particles on the outer portion of the cast sleeve are fairly uniformly distributed within the matrix. For a 30% volume reinforcement of SiC_P a remarkable 43% increase in the volume fraction at the outer periphery is observed. SiC_P content shows gradation from outer periphery to the inner periphery. Thus the closer their location to the outer layer, the higher is the volume fraction of the particles

Gang Chen has reported on the various process parameters for centrifugal casting which influenced the macrosegregation in ZA27 alloy (Chen et al 1999). The primary phase produced from the melt will float to the inner surface due to the density difference between primary phase and melt. If the pouring time is long or the pouring temperature is low, only a small amount of primary phase could float in the melt. It was concluded that the longer the pouring time or lower the pouring temperature, the less is the degree of the macrosegregation. The macrosegregation is caused due to the density difference between Zinc and Aluminum. The addition of Manganese in ZA27 alloy reduces the macrosegregation and makes the centrifugal casting of ZA27 alloy viable.

Functionally graded MMCs with a reinforcement concentration higher on the surface than in the interior offer new opportunities to the designer like providing high surface hardness as well as high resistance to crack growth towards the interior. In the case of an Al/ SiC_P FGM composite, the volume fraction of the reinforcement (SiC_P) changes gradually along the thickness to give a predetermined composition profile. Due to their novel mechanical, tribological and thermal behavior, Al/SiC_P FGMs have attracted several investigators to work extensively on them. R Rodriguez-Castro presented a centrifugal method for processing Al/SiC_P FGM composite blocks of appropriate dimensions. SiC_P of 20% by volume was reinforced in A359 aluminum alloy for investigation (Castro et al 2002). A centrifuge machine was designed for this

purpose wherein the pouring needs to be done while the mold is stationary. Since mold takes some time to reach its designed rotational speed, faster pouring and high mold temperature are used. It was found that the concentration of SiC particles increases in the direction of the centrifugal force for all the experiments, and concentrations as high as 44 vol% are obtained at the chill zone. A region completely denuded of particles was also observed for all the experiments in the mold surface in contact with the chill plate (chilled zone), and this region was larger with increased centrifugal force.

In centrifugal castings since high centrifugal forces are involved, particles are restricted to move in the direction of the centrifugal force increasing angular velocities. The solidification front moves in a direction opposite that of the force i.e. towards the inner circumference of the casting at a speed that depends on mold rpm. It was observed that cooling rate enhanced with increase in mold speed. This is because of better heat transfer at the chill plate and also due to the presence of thermally insulating SiC particles. The high cooling rate gives rise to a much finer cast microstructure. These conditions favour the Al/ SiC_P composites to be cast at high centrifugal accelerations to obtain very uniform distribution of particles. In the first place, the particles are less likely to be rejected by the solidification front due to the high relative velocity between the solid-liquid interphase and the particles. Secondly, a finer microstructure (high cooling rates) produces a more even SiC distribution due to restricted cell growth, which causes the reinforcement particles to be pushed to shorter distances (Duque et al 2005).

The concentration of particles was very homogenous in castings cast at high G forces, whereas at low G force clustering of particles was detected. The rejection and clustering of SiC particles is because of the interaction between solidification fronts and particles as well as the size of the micro-constituents of the matrix structure. At high solidification rates the cell size or dendrite spacing is smaller than the particle size and the distribution of particles in the solidified composites remains the same as in the liquid state. There is engulfment rather than rejection of particles due to the interaction of solid-liquid interface at high velocity. When the dendrite growth occurs

at lower cooling rates, and if the cells and the particles are comparable in size, then the particles are geometrically trapped in inter-dendritic region, while for further dendrite growth and increasing cell sizes, particle agglomeration is enhanced due to more particle pushing and less geometrical trapping.

The matrix structure is modified in the reinforced region as a consequence of solidification taking place rapidly in very restricted spaces. Also breaking of dendrites by the combined loading action of accelerated particles against loaded dendrites causes further reinforcement. Quench modification of the eutectic structure was observed with a fully modified structure at the chill end and an unmodified structure at the opposite side of the casting.

Tensile tests were conducted on FGMs at various levels of reinforcement content. The effect of SiC content is significant in the composite cast at 700rpm. The 1300 rpm cast composite showed no improvement in ultimate strength in the static test. The effect of SiC particulate reinforcement on strengthening of the alloy is limited up to a certain volume fraction. There is a continuous increase in tensile and yield strength at corresponding increments of SiC_P volume fraction in the range of 20-30%. On the contrary there is a reduction in tensile and yield strength for SiC_P concentration in the range of 30-40% volume fractions (Castro et al 2002).

Fracture mechanics tests were conducted on Al/ SiC_P FGMs with cracks oriented parallel to the gradation and it was observed that for this orientation the crack growth resistance improved. At higher SiC_P concentrations, plastic deformation of the matrix at the crack tip was restrained by the presence of the stiff reinforcing particles. Fracture toughness of the FGM composite was low for small crack lengths due to the limited dissipation of energy. On the contrary, for longer crack lengths SiC content decreased energy dissipation and the material surrounding the crack tip was able to plastically deform more. Therefore there was more absorption of the energy imposed on the external loads and as a result the fracture toughness of the composite was increased (Castro et al 2000).

One of the recent innovations in FGM is Aluminum matrix composites centrifugally cast for cylinder liner applications. Bollono et al, investigated the cylinder liners made from Al-Si alloy and Al-Al_2O_3 composite for different process parameters in order to optimize the reinforcement distribution at the inner surface of the liner (Bollono et al 2004). Al-7%Si (A357) and Al with Al_2O_3 reinforcement of 10%wt was considered in this work. In Al alloy it was found that in the inner and central zones, dendrites were columnar in structure, while the outer zones were equiaxed. For low mold temperatures, the presence of surface defects and porosity were clearly visible. This is due to the fact that at too low mold temperatures, melt does not have enough time for a complete and homogenous distribution of ceramic particles along the mold length before solidifying. FGMMC liners were produced for different mold temperatures, melt temperatures and cooling rate. Material prepared at low melt temperature, low mold temperature and high rate of cooling (ΔT) was having uniform ceramic distribution radially, increasing from inner to outer surface but having low metallurgical quality. At medium melt temperature, high mold temperature and low ΔT the material exhibited a partition line between the particle free inner zone and the particle rich outer zone with reduced porosity. For medium melt temperature, high mold temperature, when the ΔT was increased to medium level the material yielded the best results in terms of distribution gradient wherein the gradient increased towards the outside with excellent metallurgical quality showing no porosity. It was concluded that the optimal combination of the parameters were T_{Al} 750^{o}C. T_{mold} 350^{o}C for 15% reinforcement.

The work carried out by Wang Kai aimed at segregating 20% SiC particles in a Zl104 (Zl104: Si9.24%, Mg 0.54%) aluminum alloy using compo-casting technique to achieve uniformly distributed SiC_P/Zl104 composites (Kai et al 2009). Microstructural characteristics of these centrifugally cast composites were studied as a function of position along the radial direction of casting in order to investigate the effect of differing centrifugal force along the radial direction. The SiC particles were dispersed uniformly in the aluminum matrix except for some congregated SiC particles, and also very few voids were observed. The SiC particles were segregated totally towards the outer side of the castings. The middle zone of the casting is

particle free. This confirms that the SiC particles in composite segregate to external circumference completely. The volume fraction of SiC particles in samples decreases gradually with the increase in radial distance. The higher volume fraction for larger diameter specimens is found and the difference of volume fraction at different positions in external zone is very small. SiC particles in SiC_P /Zl104 composites have different bulk density hence they move in different directions during centrifugal casting. Uniformly scattered SiC particles segregate to the external circumference of the cylinder, while alumina oxide, pores and voids migrate to the inner circumference of the cylinder during centrifugal casting. In the case of congregated SiC particles, some of them get scattered and segregate to the external circumference and others with low bulk density migrate to the inner circumference under centrifugal force. Quick cooling of inner circumference of cylinder prevents the movement of the SiC particles so that some particles remain at the inner circumference. The volume fraction of SiC particles located in the inner particle zone, therefore, increases a little compared with that in raw 20% SiC_P /Zl104 composites. There is a corresponding increase in Brinell hardness with the increase of volume fraction of SiC particles gradually and large difference in hardness between external reinforced zone and free particle inner zone is seen. The decrease of hardness at inner reinforced zone is due to formation of voids and congregated SiC particles.

The intermetallic compound Mg_2Si exhibits a high melting temperature, low density, high strength and low coefficient of thermal expansion. This makes the metal matrix composites with Mg_2Si as reinforcement, an attractive candidate material for aerospace, automotive and other applications. At the same time the existence of hard and fragile primary Mg_2Si particles would decrease the strength and ductility of the material. Jian Zhang et al have proposed centrifugal technique to overcome this problem by gradient distribution of primary Mg_2Si (Zhang et al 1999). Tubes of different Mg_2Si content in aluminum alloy matrix were prepared by centrifugal casting process. It was found that tubes contained three layers, fine particles in an aluminum alloy matrix near the outer periphery of the tube, a particle free region in the middle area of the tube thickness and inner layer showing a gradation in high volume fraction of Mg_2Si particles. Process parameters such as speed of rotation and

cooling rate also influenced the particle distribution in the casting. It was found that lower rotation speed resulted in better gradient distribution of Mg_2Si primary particles, but at the cost of higher volume fraction of the casting defects. With increase in rotation speed an apparent change of the particle distribution profile on the outer periphery was observed. High cooling rate achieved by using Cu mold with water cooling lead to very fine microstructure in the outer periphery compared to the tubes cast in Graphite mold (Zhang et al 2000).

Zhai Yan-bo et al studied two kinds of Al based functionally gradient composite tubes, one with reinforcement of primary Si particles alone and the other with primary Si/ in-situ Mg_2Si particles prepared by hot mold centrifugal casting. The structural and mechanical properties of both the materials were compared (Yan-bo et al 2010). It was seen that in the case of composite reinforced with primary Si particles, the particles get distributed both in inner and outer layers. In contrast to this, composite in which reinforcement was primary silicon / Mg_2Si particle jointly, the FGMMC shows particle distribution only in the inner layer and shows a sudden change of particle distribution across the section of inner and outer layers. The hardness and wear characteristics were better in the inner layer for Al-19Si-5Mg tube. At the same time, because Silicon is consumed to form Mg_2Si by adding Mg into the melt, the quantity of primary Si particles in Al-19Si-5Mg tube is lower than that in the Al-19Si tube. The authors also concluded through theoretical analysis that the existence of Mg_2Si particle is the key factor to form sudden change of gradient distribution of two kinds of particles, citing the reason that in the centrifugal force field the centripetal acceleration of Mg_2Si particles with smaller density is 13.9 times that of the primary particles Si and therefore it possesses higher centripetal velocity and impels the primary Si particle into the inner layer.

Pistons made out of Al-Si alloy are frequently damaged by burning of piston top surface due to elevated combustion temperature, and by rubbing of the first ring groove against the engine cylinder liner. To prevent pistons from these damages, some technologies were invented, such as mounting high Ni cast iron ring around the first ring groove in Al alloy piston body and thermal resistant steel on piston top

surface, and fabricating Al composite pistons by squeeze casting for enhancing the whole or local piston performance. Xuhong fabricated aluminum matrix composite pistons made of Al-20Si-4Mg by centrifugal casting. Primary Si and Mg_2Si particles were locally enriched in the regions of piston top and piston ring grooves (Xuhong et al 2011), observed as blocky phases light gray in colour, with the average diameter from 80 to 120 μm, and blocky phases with dark grayness, with the average diameters from 30 to 40 μm. The microstructures of piston skirt are eutectic in nature with low contents of primary Si and primary Mg_2Si particles. The volume fraction of primary Si and primary Mg_2Si particles in piston top and piston ring grooves are greater than that in piston skirt and the total amount of primary Si and primary Mg_2Si particles is about 26% to 28%. The distribution characteristics of hardness indicates that, in both the as-cast and heat treated conditions, the hardness on the reinforced zone of the piston is higher than that on the unreinforced zone, and, the hardness after aging is highest and the hardness of the as-cast is the lowest. It is inferred that primary Si and primary Mg_2Si particles, whose hardness is much higher than that of the matrix, segregated in piston top and piston ring grooves, resulting in higher hardness in piston top and piston ring grooves. The hardness in piston skirt without primary Si and primary Mg_2Si is relatively low and the variation of hardness is also little. In the as-cast condition, the hardness at the bottom of the piston skirt is a little higher than that in the piston skirt due to the presence of a small amount of primary Si and primary Mg_2Si particles. As the solidification velocity in the bottom region of the piston skirt is higher than the moving velocity of primary Si and primary Mg_2Si particles, primary Si and primary Mg_2Si particles will be captured at the bottom of the piston skirt. Therefore, it can be deduced that the hardness of the in situ composite piston increases with the increase of the amount of primary Si and primary Mg_2Si particles.

Intermetalics are the potential materials for high temperature applications and Al_3Ni is one of the promising material among them. Al_3Ni is a hard phase formed in Al-Ni alloys containing less than 42 wt% Ni. It is observed that Al_3Ni intermetallic compound has a density of $4g/cm^3$ which is more than that of molten aluminium. A composite having graded distribution of Al_3Ni near the outer periphery of a hollow

cylinder can be formed. Fukui et al have worked extensively on Al_3Ni (Fukui et al 2001). It was observed that the Young's modulus of FGM formed by 20 wt% Ni varies from 81-100 GPa from the inner to the outer surface of 6mm thick tube where Ni varied from 15.2-43.2 vol%. The bending strength at different crack initiation planes having varying volume fraction has shown a maximum average fracture stress of 156 MPa at the location having 24 vol% (Fukui et al 1997).

Rajan et al investigated the effect of Ni (10-40 wt%) in Al-Ni alloys on gradation and property while using vertical centrifugal casting technique. The microstructure of FGM with 10 wt% Ni contains only a very small amount of primary Al_3Ni phase near the outer periphery. The outer periphery of 20 wt% Ni shows 30 vol% of primary Al_3Ni phase and its concentration gradually decreases to zero at the inside. Similarly 30 and 40 wt% Ni FGM yielded 40 and 65 vol% of primary Al_3Ni phases in the matrix respectively. The 40 wt% Ni exhibited maximum hardness among all the FGMs while 20 wt% Ni yielded the best graded structure (Rajan et al 2006). The author also investigated the formation of different types of gradient solidification microstructures in SiC and B_4C. SiC-graphite hybrid, primary Si, Mg_2Si reinforced FG aluminum composites processed by centrifugal casting. From the above works the author has concluded that the densities and size of the reinforcements play an important role in segregation of the particles. They showed that SiC and Al_3Ni segregate towards the outer periphery and low density particles such as graphite, Si and Mg_2Si segregate towards the inner periphery. But B_4C which is close to the density of Al has given more scattered distribution compared to the other reinforcements (Rajan et al 2009).

Huisman used alumina particles as reinforcement in Aluminum matrix to cast cylinders (Huisman et al 1995). The author has claimed low density, high strength, low thermal expansion, high thermal conductivity, high elastic modulus, excellent thermal shock resistance, superior chemical inertness etc. of Al_2O_3 to be the promising properties for a better gradient FGM. Aluminum Oxide referred to as α-alumina can exist in several crystalline phases, which revert to the most stable hexagonal alpha phase at elevated temperatures. In comparison to SiC it is much more inert in Al and

it is also oxidation resistant. Centrifugally cast components showed high reliability in high bend strength tests. The parts produced showed better particle packing and smaller number and smaller size flaws. Kyung-Hee Kim et al used the concept of centrifugal casting to produce castings of alumina tubes for membrane applications (Kim et al 2002). These porous alumina tubes are used as supports for inorganic membranes. The investigators fabricated alumina tubes of larger diameters with lower centrifugal acceleration (Kim et al 2000). Microstructural examinations revealed non-uniform microstructure throughout the tubes, but there was a gradient in porosity through the thickness of the tubes. This porosity gradient was used to the benefit in membrane application. They showed that by controlling the porosity and pore size distribution permeability of the tubes can be achieved by varying particle size of alumina powders and controlling sintering temperature. Piggen rao et al, prepared Al_2O_3-15wt%ZrO_2 composite using high speed centrifugal casting process. It was observed that ZrO_2 particles were not homogeneously dispersed in Al_2O_3 matrix and large agglomerates occurred in the 80 wt% slurry. When the solid content was 60 wt%, the densities of the sample slightly increased from the top to bottom region. However, phase segregation could be effectively eliminated by starting with 78 wt% slurry (Piggen rao et al 2003).

Aluminum copper alloys are high strength-ductility cast alloys. They are commonly used for components such as bearings, particularly under heavy loads and slow speed conditions. Apart from this they have high hardness and can operate at high temperatures. Yanwei et al, prepared castings of Al-Cu11wt% alloy using centrifugal technique (Yanwei et al 2010). They investigated the effect of centrifugal radius and mold rotation speed on microstructure. It was found that the grain size decreased gradually with increasing the centrifugal radius and also at the same radius for higher rpm. The grain size was finer for higher rpm compared to that of low rpm. It was concluded that the reason for the above phenomenon is the combined effect of centrifugal force, mechanical vibration and convective flow. Alam et al, investigated aluminum bronze bushes fabricated using centrifugal casting process (Alam et al 1996). The microstructural examination revealed that the distribution of alpha phase was not uniform and inhomogeneity was due to centrifugal action on the solidification

melt. The tribological behavior showed that the centrifugally cast specimens experienced boundary lubrication conditions at the start of the test. It was also found that the wear loss of the centrifugally cast specimen was less compared to that of the forged cast specimen. It was concluded that the bushes fabricated are suitable for high load and slow speed applications. Zhang et al, worked on electromagnetic centrifugal casting accomplished within a superposed magnetic field (Zhang et al 1998). When the melt rotates in a magnetic field, Lorentz force, resulting from interaction of fluid flow motion and the magnetic field, leads to electromagnetic stirring which greatly influences solidification features of materials. Thus solidification is associated with both centrifugal and electromagnetic fields. Al-Cu33.4wt% was used in this investigation. In the absence of a magnetic field, the microstructure consists of a fine chill zone and a coarse columnar zone. When magnetic field was applied, there was a remarkable change with the chill zone and the original columnar structure size was reduced and even eliminated when the intensity of the magnetic field was increased; the coarse columnar structure was transformed into equiaxed fine columnar structure formed in the outer region. An increase of magnetic field intensity results in refinement of the generated equiaxed structure. Without electromagnetic stirring, the eutectic is typically lamellar. As solidification occurs under stirring, most of the eutectic still remains lamellar, but rod-like eutectic begins to form. When the magnetic field is further increased, more proeutectic phase is seen; the rod like eutectic and proeutectic structure steadily increase in quantity. If the magnetic flux is increased, the eutectic in the inner zone is turned into a blocky structure whose morphology is no more as typical as lamellar or rod-like eutectic.

FGMMC using Al-Si and Al-Cu as matrices and TiB_2, TiC as reinforcements were produced using horizontal centrifugal casting by Kumar et al. Influence of matrix, reinforcement, process parameters such as mold temperature, mold speed were highlighted in this work (Kumar et al 2010). A356-TiB_2 FGMMC tube had three distinct regions across the thickness; the outer region consisted of segregated TiB_2 particles in the matrix, the middle region showed a clear interface between the composite and matrix and the inner region only the matrix. The segregation of TiB_2 into the outer layers during casting is attributed to the higher density of the TiB_2

particles in comparison to that of the liquid matrix. For a given mold temperature, the normalized rim thickness decreased with increasing mold speed, and this is attributed to the increase in centrifugal force. During the mold rotation, the particle suspended in the liquid is subjected to both centrifugal force and gravitational force. Since the centrifugal force acting on the particle is G times higher than the gravitational force, the latter is negligible when compared to the former. Thus as the rotational speed increases, the force acting on the particles to segregate also increases. It was noted that as the rotational speed of the mold increases, the particle free zone shifts to the left and the peak in the TiB_2 volume fraction increases. It is reported that the volume fraction of TiB_2 obtained at the surface increases with increase in the speed and temperature. The maximum volume fraction of TiB_2 achieved is 3.6 times the mean volume fraction. The variation of hardness as a function of distance from the surface across the thickness of the casting reveals that there is an increase in hardness from the interior to the peripheral region of the casting. This increase in hardness is attributed to the increase in volume fraction of the reinforcement. Solidification rate in centrifugal casting can be controlled by the heat transfer between the casting and the mold. Preheating the mold can control the heat transfer. It was found that the increase in mold temperature leads to the narrower region of reinforcement particle region and this region shifts towards the outer periphery of the casting. A356-TiB_2 and Al-4Cu-TiB_2 composites under identical processing conditions were used to study the effect of matrix on centrifugal forces. It was reported that A356 alloy has a normalized rim thickness of 0.27, whereas Al-4Cu alloy has a normalized rim thickness of 0.16. From this result it was inferred that the difference in the densities between the solid particle and the melt play an important role in particle velocity. The Al-4Cu alloy has a liquid density of 2360Kg/m^3 and TiB_2 has a density of 4520 Kg/m^3, a difference of 2160 Kg/m^3. Similarly there is a density difference of 2090 Kg/m^3 between A356 and TiB_2. Because of the higher density difference in case of Al-4Cu and TiB_2 system particles had a greater tendency to segregate. The effect of reinforcement can be assessed by viewing the thickness of the TiC and TiB_2 particles. Since TiC particles have greater density the thickness is about 0.24 and that of TiB_2 0.27. Similarly, the volume fraction of TiC and TiB_2 are 12 and 10%, and hardness 126 and 120 HV_5 respectively.

During centrifugal casting segregation of particles occurs due to centrifugal force, either at the inner or the outer periphery of the casting depending on the relative densities of the particles and the melt, resulting in functionally gradient composites. The extent of segregation depends on various process parameters including casting geometry, melt poring temperature, solidification time, density difference between matrix and reinforcement particles and rotational scheme. Numerical investigations and process modeling have helped in predicting the behavior of the casting. Goa et al, have conducted numerical investigations on the solidification during centrifugal casting of FGMs (Gao et al 2000). They focused on the interplay between the freezing front propagation and particle migration. Authors have developed a one-dimensional solidification model, with particle transport taken into account, using pure water as the matrix and glass beads as the particle phase. Unidirectional solidification experiments were performed in a rectangular test cell to validate the multiphase model. Three factors can be identified to be responsible for creation of the particle concentration gradient: the geometrical nature of particle flow in the cylindrical mold, the angular velocity, and the solidification rate. It was concluded that by optimizing processing conditions, such as the particle size, initial concentration, rotational speed of the mold, cooling rate and superheat, one can engineer a desired gradient in the solidified part.

Kang and Rohatagi (Kang et al 1996) have described the results of a heat transfer analysis of centrifugal casting of metal matrix composites by one-dimensional analysis considering the thermo-physical properties due to particles moving as a function of temperature. In their investigations, the positions of the dispersed particles at a given instant of time are analyzed as a first step. Then, the temperature distributions in the mold and the solidifying metal are analyzed at different time intervals. Using these temperature distributions, time taken for solidification of casting at different rotational speeds, initial mold temperatures, and pouring temperatures of molten metal are estimated. Raju et al, have presented a more realistic model showing variation in the volume fraction of the particles across the thickness of the casting with time (Raju et al 2000). Their formulation is based on one-dimensional heat-transfer analysis incorporating variations in the thermo physical

properties due to particle movement on the matrix. It also considers variations in the heat-transfer coefficient and latent heat release.

Particle segregation pattern in a centrifugally cast product, temperature distribution in the casting and mold, and time for complete solidification were predicted using a one-dimensional transient heat-transfer model coupled with an equation for force balance on particles (Panda et al 2006). Emila Panda et al, have reported that for a given set of operating conditions, the thickness of the particle-rich region in the composite decreases with an increase in rotational speed, particle size, relative density difference between particles and melt, initial pouring temperature and initial mold temperature. With reduced heat-transfer co-efficient at the casting/mold interface, the solidification time increases, which, in turn, results in more intense segregation of solid particulates. Again, with increased initial volume fraction of the solid particulates in the melt, both the solidification time and the final thickness of the particulates rich region increases. It has been reported that due to the high solidification rate at the beginning, the particles adjacent to the casting/mold interface do not get a chance to move toward this interface to form a cluster. Therefore, the volume fraction of the particulates in the solidified composite is the same as in the initial melt. Thus, with finer particles, the maximum clustering of particles is seen only after a certain distance from the casting/mold interface. However, for melts with coarser particles at higher rotational speeds, maximum segregation is seen at the outer surface itself, because the particle velocity is much higher than the velocity of the solidification front and several particles from the adjoining regions are able to reach there before this layer is solidified.

Among the different centrifugal castings, vertical centrifugal casting process is considered for range of applications from hollow to solid cylinder, symmetrical to unsymmetrical parts. Parts produced by this process are of high degree of metallurgical cleanliness. Directional solidification provides clean, dense castings with physical properties that are superior to static castings. The effect of the vertical centrifugal casting process on castings is mainly due to three features: centrifugal pressure, fluid dynamics and intrinsic vibrations of the process. Chirita et al have

carried out few investigations to understand the effect of each of the variables listed above on mechanical and metallurgical properties. The authors have concluded that the centrifugal pressure exerted over a casting sample depends on angular speed, the distance from the mold cavity to the rotation axis, the quantity of the melt and the geometry of the sample. It was also found that the pressure does not promote a displacement of more dense solid phase along the direction of the centrifugal force. Centrifugal pressure does not seem to have any effect on mechanical and metallurgical properties. The vibration effect was assessed by introducing a linear vibrating movement to the mold or frame. Under these conditions of solidification observations were made that showed increase in mechanical properties i.e. rupture strength and strain by 20 and 40% respectively (Chirita et al 2008). It was also reported that vibration influenced the microstructure. These effects are similar to the one achieved by high solidification rate. It has been explained that the rate of solidification due to vibration is due to internal movement of the melt that promotes a quicker heat transfer inside the melt and to the mold. This attributes to a faster distribution of solidification germens inside the melt due to internal melt movement. The fluid dynamics is very different between gravity (Chirita et al 2007) and centrifugal castings. It was observed that turbulence is more responsible in centrifugal casting for the uniform distribution of the solidification germens and consequently will create a different solidification pattern and faster solidification rate of the casting. This faster solidification rate will lead to a finer micro structure, higher eutectic volume fraction and consequently better mechanical properties (Chirita et al 2009). This is the driving force for utilizing the centrifugal casting process for producing FGMs. They also studied the mechanical properties of the specimens produced by centrifugal and gravity casting technique which is made in three different Al-Si alloys: a hypoeutectic, a eutectic, and a hypereutectic alloy (Chirita et al 2010). It was observed that the centrifugal effect may produce an increase, approximately 50%, in rupture strength and approximately 300% in rupture strain over the gravity casting. The Young's modulus also increased by 20% and these properties are also gradated within the casting. The higher the distance in relation to rotation centre the more is the increase in mechanical properties.

Al-B alloy system containing a small wt% of boron lends itself very well to be formed as a FGM. As this alloy consists of an almost pure aluminum matrix dispersed with AlB_2 particles, the particle redistribution during centrifugal casting occurs in such a way that borides having high density form at the outer zone of the casting compared to molten aluminum. The AlB_2 phase has a higher density (3190kg/m^3) than liquid Al (2400kg/m^3) at 700^{o}C. The forced segregation of hard borides towards the outer zone of the casting provides a unique approach to improve the surface hardness and wear resistance. Humberto Melgareji et al, investigated Al-2%Mg alloys reinforced with AlB_2 particles to make FGMs using centrifugal casting technique (Melgarejo et al 2005). They characterized the microstructure as a function of the position along the radial direction. Surface hardness, micro hardness as well as wear. Tests were performed and compared with homogeneous gravity cast composites. In centrifugally cast Al-2 wt% Mg alloy composites containing 1- 4 wt% B, a gradient in the volume fraction of the AlB_2 particles along the radial direction was observed with denser distribution of di-boride particles in the outer regions of the casting due to inertia forces. The hardness of the composite increased along the radial direction and proportionally to the volume fraction of the AlB_2 particles. Appreciable increments in hardness were observed even at lower radial distances as the boron content of the alloy increased. Micro hardness test performed on the composites showed an increase with increasing boron content, an effect attributed to the higher dislocation density in the matrix due to the higher volume fraction of AlB_2 particles. The volume fraction of porosity increased with the amount of boron in the alloy, presumably due to an increase in the viscosity of the melt which inhibits the escape of entrapped air during the solidification process. Evaluation of gravity casting composites of identical compositions demonstrated microstructure and properties to be intermediate with respect to two extreme zones of FGMs (Melgarejo et al 2008).

2.5 Al-Si and SiC system

The binary Al-Si alloys belong to the eutectic system, with the eutectic temperature of 577^{o}C (Gruzleski et al 1990). The composition of the eutectic point has been reported to be ranging from 11.7-14.5% Si with the most probable value at

11.7% Si (Murray et al 1992). The eutectic composition in binary Al-Si system shifts depending on the alloying elements and the casting processes.

In addition to the above attributes the Al-Si alloy system also has the advantage of high thermal conductivity and improved mechanical properties for wide temperature range. The low density 2340kg/m^3 of Si in particular provides the following advantages in a Al-Si system.

a. It helps in reducing the overall weight of the component,
b. Si has a diamond crystal structure that provides good hardness.
c. It also has very low solubility in Al which improves wear characteristics.
d. Si content imparts fluidity and low shrinkage, resulting in good casting and welding characteristics.

The alloys are classified into 3 groups based on the Si content.

a. Hypoeutectic (<11.7%Si)
b. Eutectic (= 11.7%Si)
c. Hyper Eutectic (>11.7%Si).

Good castability and corrosion resistance characterize the binary hypoeutectic and eutectic alloys while hypereutectic alloys are known for low thermal expansion and excellent wear resistance (Prasad et al 1998).

Increasing the Si content increases the strength but at the expense of ductility (Mondolfo 1976). The use of Al-Si system as structural materials is determined by their physical properties which are primarily influenced by their chemical composition. Also their mechanical properties are influenced by chemical composition and microstructure. The characteristic property of aluminum alloys is relatively high tensile strength in relation to density compared with that of other cast

alloys. The high specific tensile strength of aluminum alloys is very strongly influenced by their poly-phase microstructure.

The silicon content in standardized commercial cast Al-Si alloys is in the range of 5 to 23 wt%. The structure of the alloys can be hypoeutectic, hypereutectic, or eutectic, as shown in the equilibrium phase diagram in Fig. 2.1. Hypoeutectic alloys are used in many applications such as marine, electrical, automotive and aircraft industries specifically to produce cylinder blocks, cylinder heads and engine body castings. It is reported that Si varying from 6% to 8.5% has been used extensively in making cylinder heads. Researchers have added grain modifiers to increase the tensile strength and ductility. Some of the modifiers such as Cu (Basavakumar et al 2006), have increased the thermal stability, lowered the thermal expansion of the hypo Al-Si alloys promoting their application in Internal Combustion Engines. Eutectic Al-Si alloy has been used in engine parts and marine castings. These alloys offer high resistance during machining, which causes tool wear. Hypereutectic alloys are used extensively these days in automotive industries because of their excellent wear resistance and low thermal expansion.

The mechanical properties of Al alloys are very strongly influenced by their poly-phase microstructure. The mechanical properties of a specific alloy (hypoeutectic, eutectic or hypereutectic) can be attributed to the individual physical properties of its main phase components α-Al solid solution, silicon crystals and to the volume fraction and morphology of these components. The tensile properties and fracture behavior strongly depend on secondary dendrite arm spacing, Mg content and in particular, the size and shape of eutectic silicon particle and Fe-rich intermatallics. Thus by changing the morphology of dendritic α-Al, eutectic Si particles and other intermatallics that are present in the microstructure, the mechanical properties can be changed.

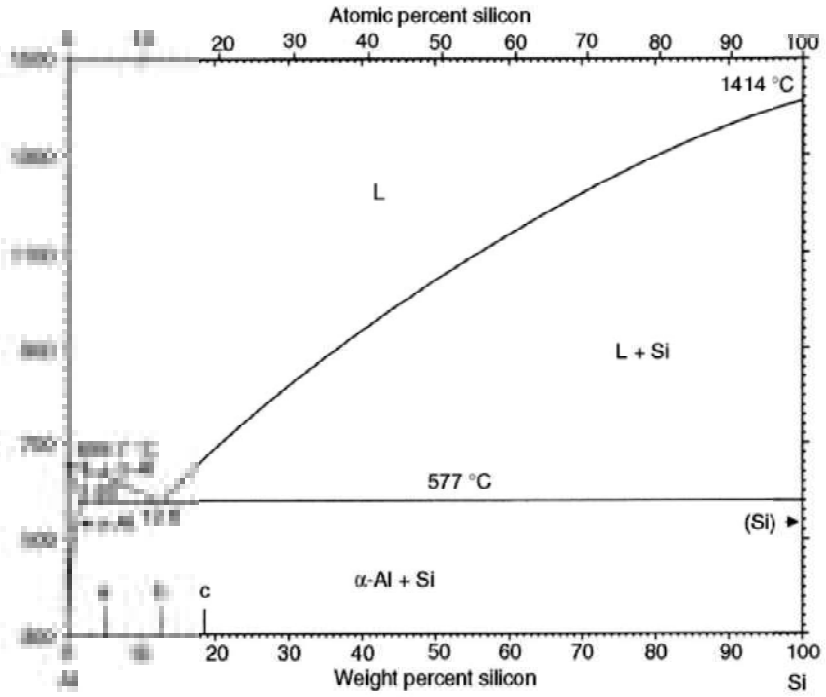

Fig. 2.1 Al-Si Equilibrium phase diagram.

Different techniques are used to control the microstructural features. These include casting technology, use of grain refiners and modifiers etc. The rapid cooling gives a fine eutectic structure, small α-Al dendrite arm spacing and reduced grain size. Slower cooling rates result in randomly oriented coarse eutectic Si needles and coarse columnar α-Al dendrites. A few researchers have reported the use of modifiers like Serenium or Sodium to obtain finely dispersed eutectic (Basavakumar et al 2008) and use of grain refiners AlB_2, etc. to reduce the size of the primary α-Al grains. The use of modifiers and refiners has led to obtaining of fine equiaxed structure during solidification which resulted in good surface finish during machining. In hypereutectic alloys primary silicon appears in different forms like star, polyhedral and dendrite. The Si morphology is highly dependent on the solidification parameters such as freezing rate, temperature gradient in the liquid and liquid composition.

The reinforcement in a Metal Matrix Composite (MMC) is expected to improve various physical, mechanical and tribological properties of the matrix. The reinforcement phase must have chemical stability and compatibility with the matrix

material not only with respect to end application of the product but also for the material fabrication. The reinforcements may be continuous in the form of fiber or discontinuous in the form of whiskers or particulates. Continuous fiber reinforced composites offer highly directional properties such as stiffness but its usage is quite restricted due to high cost and difficulty of processing. The discontinuous form of reinforcements in particular particulate reinforcements have found commercial use in many applications owing to their several advantages. The MMCs with particulate reinforcement possesses near isotropic properties and are easier to process using simple casting techniques or powder metallurgy technique (Kaczmar et al 2000). Further the particulate reinforced MMCs can be made available in large quantities for many structural applications in near net shape. The reinforcement particles suitable for MMCs include metal carbides - SiC, B_4C, WC, metal oxides -Al_2O_3, ZrO_2, SiO_2, and metal nitrides – AlN, Si_3N_4, etc.

It is evident from the literature that for automotive and aerospace applications, Silicon Carbide (SiC_P) and Aluminum oxide (Al_2O_{3P}) particulates are extensively used. Silicon Carbide (SiC_P) has a density of 3.1g/cm^3 and is constituted of tetrahedral carbon and silicon atoms with strong bonds in the crystal lattice. SiC reinforced MMCs have substantial potential in different applications as SiC retains the room temperature strength and stiffness even at higher temperatures. It also imparts low coefficient of thermal expansion and provides better wear resistance. The thermodynamic instability of SiC in aluminum forms Al_4C_3 which degrades the reinforcement and increases the corrosion. The influence of Al_4C_3 can be reduced by the following techniques: i) increasing the Silicon content in aluminum ii) providing a protective surface treatment to SiC iii) Preoxidization of SiC.

Another widely used reinforcement for MMCs is Aluminum oxide (Al_2O_3) of density 3.72g/cm^3. Al_2O_3 possesses strong inter-atomic bonding giving rise to its desirable material characteristics. It can exist in several crystalline phases and in general it is hexagonal alpha phase at elevated temperature. Its high hardness, excellent dielectric properties, refractoriness and good thermal properties make it suitable for a wide range of applications.

The performance of the MMC is also related to some parameters concerning the reinforcement particles such as volume fraction, size, shape of the particles, and distribution of particles. Higher volume fractions of reinforcement may result in melt viscosity related problems like lesser chances of particles getting embedded in the melt. This may also cause the particles to form clusters. As regards the mechanical properties, increase in volume fraction of the reinforcement in MMC increases the yield strength but decreases ductility and fracture toughness. The tendency to sink the reinforcement particles decreases with decrease in size of the reinforcement particles. In liquid state processing the vortex pushes the lesser size particles to the sides of the vortex and thus causes the particles to float on the surface (Ibrahim et al 1991).

2.6 Characterization

2.6.1 Hardness

The term Hardness, as it is used in industry, may be defined as the ability of a material to resist permanent indentation or deformation when in contact with an indenter under load. Generally a hardness test consists of pressing an indenter of known geometry and mechanical properties into the test material. The hardness of the material is quantified using one of a variety of scales that directly or indirectly indicate the contact pressure involved in deforming the test surface. Since the indenter is pressed into the material during testing, hardness is also viewed as the ability of a material to resist compressive loads.

Brinell hardness is a widely used method to study the bulk hardness of materials. In this test a hard spherical indenter is pressed under a fixed normal load onto the smooth surface of a material. When the equilibrium is reached, the load and the indenter are withdrawn, and the diameter of the indentation formed on the surface is measured using a microscope with a built-in millimeter scale. The Brinell hardness is expressed as the ratio of the indenter load W to the area of the concave (i.e., contact) surface of the spherical indentation that is assumed to support the load and is given as Brinell hardness number (BHN) denoted by HB (Revankar et al 2000).

The Al based FGMs made by using different processing techniques have reported variation in hardness from one end of the specimen to the other. A variation of hardness from 70HV to 122HV is reported for Al-28wt%. Si, produced by magnetic separation method (Song et al 2007). Al-18wt% Si processed by Power ultrasonic field technique showed a gradient of 80HV to 55HV from outer to inner region of the sample, having a primary Si volume fraction of 30% at the outer region (Zhang et al 2009). Al–Al_3Ni in situ FG composites casting using centrifugal method have shown that as the concentration of nickel increases, the hardness of the system also increases. Al–40 wt% Ni system has exhibited the maximum hardness (83±2 BHN) throughout followed by Al–30 wt% Ni (64±2 BHN). On the other hand, only Al–20 wt% Ni system has exhibited the maximum hardness gradation from 55 BHN near outer periphery to 46BHN near the inner periphery followed by Al–10 wt% Ni (45–39 BHN). This aspect is also clearly revealed in their respective microstructures (Rajan et al 2008). Aluminum-based functionally graded composites reinforced with aluminum di-boride particles were manufactured by centrifugal casting. The centrifugally cast materials showed the segregation of di-boride particles and higher superficial hardness and micro-hardness towards the outer region of the casting. The hardness increased as a function of distance from the internal zone to the external zone in the samples of Al–4wt%B–2wt%Mg composite from 60-80HR (Melgarejo et al 2005). The results revealed significantly different micro hardness values at either ends of the three FGM ingots synthesized using gradient slurry disintegration and deposition process. For Al/ SiC_P and Al–Cu/ SiC_P, micro hardness of the metallic matrix was found to increase as a function of distance from the base of the ingot. However for Al–Mg/ SiC_P, a decreasing trend of matrix hardness was observed, with an increase in the distance from the base of the ingot (Gupta et al 2002).

2.6.2 Wear

Wear is defined as damage to a solid surface that generally involves progressive loss of material and is due to relative motion between that surface and a contacting substance or substances (ASTM G40). Under normal operating parameters, the property changes during usage occur in three different stages;

- Primary or early stage or run-in period, where rate of change can be high.
- Secondary or mid-age process where a steady rate of aging process is maintained. Most of the useful or working life of the component is comprised in this stage.
- Tertiary or old-age stage, where a high rate of aging leads to rapid failure.

According to British stainless steel association the main factors affecting wear and galling (BSSA 2011) are:

- Design,
- Applied load,
- Contact area and degree of movement,
- Lubrication,
- Environment,
- Material properties like surface finish, hardness and microstructure etc.

Publications on the dry sliding wear of homogenous Al-Si system show that researchers have tried to optimize the Si content, study the transition in wear rate as a function of variations in sliding wear parameters, such as applied load and sliding distance. In the study of dry sliding wear of two Al-Si alloys (10.9 and 22.1%Si) against a steel counter face, two wear regimes were observed (Sarkar et al 1975). The first wear regime was described as a mixed mode of elastic-plastic contact where Archard's law is obeyed. The second regime, activated at a critical applied load, was characterized by gross plastic flow where the wear rate was not directly proportional to the load. It was also stated that the hyper-eutectic alloy experienced a higher wear rate than the hypo-eutectic alloy (Clarke et al 1979). Wear mechanisms in the dry sliding of Al-Si alloys have been classified as oxidative wear and metallic wear (Shivanath et al 1977);

- Oxidative wear occurred at lower applied loads. In this, aluminium oxide layer formed on both the wearing Al-Si surface and the counter face. Wear occurred firstly by oxidation of the asperities and then secondly by fracture and compaction of the oxidized wear debris into this film. The wear rate was low, due to the amount of metal removed being confined to the thickness of this oxide formation. Some localized deformation of the substrate and fracture of the Si particles was observed. Oxidative wear was considered to be generally independent of the Si content or Si particle size.

- Metallic wear mechanism was more predominant at higher applied loads. The Al-Si wear surface was characterized by plastic deformation and fracture, significant transfer of material between the sliding surfaces and wear debris formation. The amount of plastic deformation and the higher wear rate prevented the formation of an oxide layer. A higher Si content was reported to increase the load at which this wear regime was active.

Al-Si alloy samples were subjected to wear studies on a Pin on Disc machine using Steel disc. Three distinct wear regimes were identified as a function of applied load (Reddy et al 1994).

- Mild wear: At low loads, the worn surface was characterized by the formation of an iron-rich compacted debris layer.
- Severe wear: As load increased a delamination type wear mechanism was operative in which sub-surface deformation and cracking caused fragmentation of the Si particles and removal of the iron-rich protective layer.
- Seizure wear: In this wear regime, temperatures near the surface were high enough to lower the shear strength in the sub-surface layer which promoted extensive material transfer from the wearing alloy to the steel counter face.

Regarding topographical features of worn Al-Si alloys in dry sliding, the mutual transfer of material between the wearing Al-Si and the steel counter face appears to be a feature of all wear regimes and becomes more significant as load increases. The transition from mild to severe (metallic) wear is associated with the existence of a delamination wear process (Sarkar et al 1975). Although some papers reported that Si additions (4-24%Si) improved wear resistance of aluminium, no relationship between wear rates as a function of Si content was found (Reddy et al 1994). Wear rate increased linearly with applied pressure but was independent of sliding velocity. The value of the friction coefficient was found to be insensitive to applied pressure, Si content and sliding velocity (Clarke et al 1979). The frictional force and the shear resistance of Al-Si alloys, were the two main controlling factors determining the initiation of seizure. For a given alloy subjected to sliding at different temperatures, seizure was initiated at a sub-surface depth where the shear stress equaled the resistance to shear. The presence of silicon was said to provide strengthening of this sub-surface region and to help inhibit bulk shear. It was also reported that seizure was associated with features like rapid increase in wear rate, transfer of pin material to the counter face, increased noise and vibration (Reddy et al 1995).

A few efforts have been made to find the effect of Si in Al based FGM. Wear resistance of the FGM sample produced by Al-18wt.%Si, power ultrasonic method decreased gradually from outer to inner. The wear resistance distribution of the FGM sample is in good accordance with the microstructure distribution (Zhang et al 2009). For Al-Mg-B it was shown that the wear resistance increased in trend with hardness observed in the outer region. The SEM analysis revealed abrasive and oxidative wear modes, the extent of which was dependent upon the boron content (Melgarejo et al 2006). Al-(Al_3Ti+Al_3Ni) FGMs produced by centrifugal technique have shown that the size of the primary particles depends upon their location in the ring thickness and the applied G number. It was also shown that the wear resistance of these materials was superior compared to the pure Al (Y Watanabe et al 2001). A study to find the effect of lubrication using aqueous solution on Al based FGM showed that in absence of lubrication while sliding, the COF is not significantly affected by SiC content. Results showed that a lower friction and wear values are obtained as the reinforcing

particles increased. The wear rate of the FGM is not significantly affected by the presence of the aqueous solution (Gomes et al 2005). A tribological study carried out on Al/SiC_P FGM with water as lubricating medium showed that it played as a carrier agent for transfer of material. Water lubrication significantly increased wear of FGM, by facilitating catastrophic SiC particle pull out thus obviating the load carrying and anchoring role of the reinforcement (Velhinho et al 2004). To improve the wear resistance of thermal barrier coatings, hard particles were successfully introduced into the surface area by employing the HVOF technique. A graded alumina particles profile was produced in the surface area, with 25% particles in the surface area proving to be the optimum regarding good thermal shock and wear resistance (Schulz et al 2003). The FGM Al/ SiC_P and Al-Mg/ SiC_P casting using slurry integration technique has shown that both materials had better wear resistance at the high SiC_P end compared to the low SiC_P end. This increase in wear resistance has been attributed to the increased resistance to plastic shear deformation imparted by the presence of more SiC_P as a large number of cracks might have nucleated before loose debris could form and the increase in hardness of the specimen at the high SiC_P end. This might have resulted in a decrease in the rate of plastic deformation and thus led to crack propagation at shallow depth and lower crack propagation rate (Gupta et al 2003).

It is clear from the documented literature that Al-Si alloy is the most sought of alloy for many engineering applications because of their low thermal expansion coefficient, good corrosion resistance, good casting characteristics, high thermal conductivity and improved mechanical properties at wide temperature range. The performance of the alloys depends on the content of the Si and also on their microstructural characteristics. Not much of work has been done in achieving an Al based FGM with relatively high segregation of Si on one side using a very effective processing technique at low processing cost.

Wear of Al-Si alloy has been studied extensively in the past by varying the Si content. These studies only aimed at optimizing the content for maximum wear resistance. From the above discussion it was found that experimental findings are

contradictory with regards to the role of Si content on wear resistance. Some of them reported that for wear resistance the optimum Si content is near Eutectic while some contradicted saying it is in the Hypereutectic region.

We can conclude that many mechanisms can play a significant role in the sliding wear behavior of complex polyphase alloys and that it is not a simple function of composition. The wear is a complex phenomenon which depends on different parameters viz., type of the matrix material, type of the reinforcement, surface roughness, processing technique, pressure, temperature, environment, sliding speed, type of friction etc. (Bialo et al 2000).

As a matter of fact, the inconsistencies of the obtained results are not surprising. Wear resistance is not a material property. It is always uniquely correlated with strength or hardness. It depends upon the combination of all intrinsic and extrinsic factors involved in the wear process. Therefore, friction and wear must be considered the general characteristics of the friction couple as a system.

2.6.3 Diametral Compression

Tensile test is the most common test used to find the tensile strength of materials, more so, in case of ductile materials. However, for materials that are brittle in nature, this test is extremely inaccurate due to eccentricity of loading, gripping difficulties, greater sensitivity to misalignment and position of defects (Shaw et al 1975). With increased use of ceramic particles in composite materials, they tend to be brittle in nature. Due to this, researchers have used different methods to determine the tensile strength. Diametral Compression (DC) test also known as Brazilian test is more preferred than the other tests methods that include, indirect tensile test, compact crushing test and compact hardness test (Procopio et al 2003). The diametral compression test was first introduced in 1953 to measure the tensile strength of concrete (Carniero et al 1953), (Wright et al 1955) and then gained popularity because of simplified test specimen preparation, simple specimen geometry and quickness of

conducting the test (Amoros et al 2008). This test has also been used to measure tensile strength of rock, coal, polymers, cemented carbides, ceramics, MMCs, tablets etc. (Chen et al 1998), (Marion et al 1977), (Ovri et al 1987), (Bonollo et al 1994), (Fell et al 1970).

The diametral compression test is based on the fact that when a circular disc is compressed by applying load on two diametrically opposite faces, tensile stresses develop perpendicular to loading direction and are proportional to applied compressive force (Fahad et al 1996). The theoretical stress analysis in a disc subjected to two concentrated diametral forces has suggested (Thimoshenko 1982) that along the loaded diameter, the normal stress (σ_x) is tensile and constant, while σ_y parallel to the loaded diameter is a compressive stress which increases from $3\sigma_x$ at the center of disc to infinity beneath the loaded points. The shear stress is zero along the diameter plane and hence σ_x and σ_y are the principal stresses on the plane assuming a point load on the disc.

Since the failure occurs along the diametral plane of the applied load, it is commonly assumed that the nominal tensile stress causes the disc to fail. However some researchers believed that the failure is initiated under the load points rather than at the center due to high compressive stresses. Because of this, there is some disagreement about the exact mechanism of failure. In practice the load needs to be distributed over a finite area to avoid shear and/or compression failure at the loaded points (Hooper 1971), (Darvell et al 1990). An exact theoretical stress analysis was developed (Hondros et al 1959) for the case of pressure applied over two diametrically opposite arcs which results in the finite maximum compressive stress at the point of applied load.

The work of Takagi and Shaw reported that the material becomes plastic near the applied load before becoming plastic at the center of the disc causing a greater tensile stresses at the center than at any point towards the applied load (Takagi et al 1981). As a result, the tensile stresses at the center will be greater than that at any other point towards the applied load. Therefore, failure initiates at the center of the

disc. The strength values of diametral compression test are always much lower than other uniaxial test (three point bending) values. Deviation from Hooke's law by brittle materials, the influence of specimen size and the tensile strain failure criterion in brittle materials are cited as reasons for failure of tensile stress values (Wright et al 1955).

A comparative analysis of three, point bending, four point bending and diametral compression methods for the determination of the mechanical strength of green pressed compacts was presented by Amoros (Amoros et al 2008). It was found that the mechanical strength was much lower in diametral compression than in the bending tests (3B or 4B). It was found that Weibull statistics largely explained the difference in mechanical strength between 3B and 4B but it fails in explaining the reasons for lower mechanical strength in DC tests. The stress-strain curves in the bending and DC tests confirmed that plastic deformation was larger in diametral compression.

Modified form of Diametral Compression test for mechanical testing of metal matrix composites was proposed (Bonollo et al 1994). Mechanical behaviour of Different MMCs (A354- SiC_P, A354-Al_2O_3 short fibers) with respect to both test and material related parameters were investigated. Diametral compression tests were carried out on discs of 20mm diameter and 5mm thickness. The results of the diametral compression test in terms of Rupture Strength (RS) have been compared with those of conventional tensile test values of Ultimate Tensile Strength (UTS). For the same test conditions, a constant ratio of 2.5 ± 0.1 between UTS and RS has been found for short fibre (12-15%) and particle (505) reinforced Al. The work confirms the test as a quick and reliable procedure to study mechanical behavior of MMCs. The failure mechanism in all MMCs was found to be tensile.

Fahad et al reviewed the stress analysis in a diametral disc when subjected to point load, curve distributed load and flat distributed load (Fahad et al 1996). It is reported that, with a concentrated load, the failure is due to shear and compressive stresses at the loading point. In order to initiate the fracture by tensile stresses, the

load needs to be distributed over a finite area to avoid shear and/or compression failure at the loaded points. The different methods to distribute the load as mentioned by Fahad are: 1) By placing packing strips (shims) of suitable material between specimen and the loading platens, 2) distributing load over a small arc of finite width instead of a point. In this case the increase of arc decreases the compressive stress beneath the load. Though compression failure may not be initiated with arc loading, it is difficult to perform this type of loading. For an angle of $\alpha=11.45^{o}$, it was found that the compressive stress beneath the load was 8.4 times the tensile stress at the center of the disc. 3) Use of flattened disc to apply load. This method avoids local crushing. It was concluded that the width at the flattened end must be approximately 0.2 times the diameter of the disc to obtain an accurate tensile strength.

A modified diametral compression test using a disc specimen with centrally drilled hole was conducted by Holling et al (Holling et al 1996). Using this type of specimen it was observed that the build-up of compressive stresses in the loading areas is substantially reduced and failure was found solely due to tensile stress. However, the findings of the work suggest theoretical re-assessment using finite element analysis.

There are materials which are also to be characterized for brittle to ductile transition. But for this, simple compression test is not useful as it involves mixed loading. Brazilian test was used to by applying compressive forces on two opposite generatrix of a cylinder. This causes a uniform tensile stress on the plane containing the axis of the cylinder and the generatrix. The advantage of this test is to avoid expensive and random machining of brittle samples (Proveti et al 2006).

Different tests such as instrumented die, unconfined compression of a cylinder, three point bending and Brazilian disc test were used to determine the elastic modulus and tensile failure of powder compacts (Korachkin et al 2008). The failure of compacts due to Brazilian disc test show additional cracks propagating towards the end of the failure process. Diametral compression test leads to a lower failure stress, attributed to the influence of compact anisotropy. Values of Young's Modulus

obtained from uniaxial compression test were found to be higher than those from the three point bending test.

Hinoki et al, evaluated the tensile strength of 2-D CVI-SiC composites using diametral compression test for realizing the effect of specimen size and shape on the magnitude of the tensile strength. It was found that the tensile strength is independent of specimen size and shape (Hinoki et al 2008) .

2.7 Summary

FGM is a novel concept of realizing graded structure and properties within a component which is not possible to achieve in a conventional homogenous material. It is important to understand the different processes for achieving the gradation, the extent of gradation and the influence of process parameters. The literature presented in the earlier sections of this chapter clearly reveals that considerable amount of research has been carried out on different non-ferrous alloy systems and their composites. While designing FGM, one of the major requirements in terms of properties is obtaining higher hardness in the outer region compared to the inner region. This feature should also assist improvement in wear resistance of the material. From the literature studies it can be made out that not much focused work has been carried out in utilizing the centrifuge casting technique to produce Al-Si alloy and their composites having SiC particulates for producing FGMs. These FGMs show high potential for automobile and aerospace applications along with meeting the mechanical property requirements and high resistance. Throughout the literature we can find microstructural studies, variation in hardness and evaluating wear property has been considered for characterization of FGM. From the literature available we can also find that much of the work is on production of hollow cylindrical FGMs and very little work is reported on producing a solid cylindrical FGM.

2.8 Scope of Work

Based on the literature study scope for research in the area of FGM is proposed as below:

- Study the effectiveness of using centrifuge technique to produce solid cylindrical FGMs.
- Experimentally investigate the influence of centrifuge casting process parameters on quality of FGM.
- Explore the possibility of analyzing the effect of percentage Si (Eutectic to Hypereutectic).
- Study the SiC particulates reinforced Al-Si based composite FGM from the stand point of processing and volume fraction of SiC_P.
- Characterize the FGM based on microstructure, hardness, wear and diametral compression strength.

2.9 Problem statement

In view of the scope defined above the present research work is defined as '**DEVELOPMENT AND CHARACTERIZATION OF FUNCTIONALLY GRADED Al-Si ALLOY SYSTEM AND Al-Si/SiC_P COMPOSITES USING CENTRIFUGE CASTING**'.

3. EXPERIMENTAL DETAILS

3.1 Introduction

From the literature review on different processes for producing FGMs with good reproducibility, low production cost and to produce solid cylinders, it is evident that centrifuge technique is one of the promising techniques. This chapter gives an insight of the centrifuge method to produce the cast FGM. An overview of the material used to produce the casting, microstructural studies, hardness testing and wear test and the analysis of the worn specimens using Scanning Electron Microscope (SEM) are also presented. The sequence of operations to be carried out for processing and characterizing the casting are depicted in Fig. 3.1.

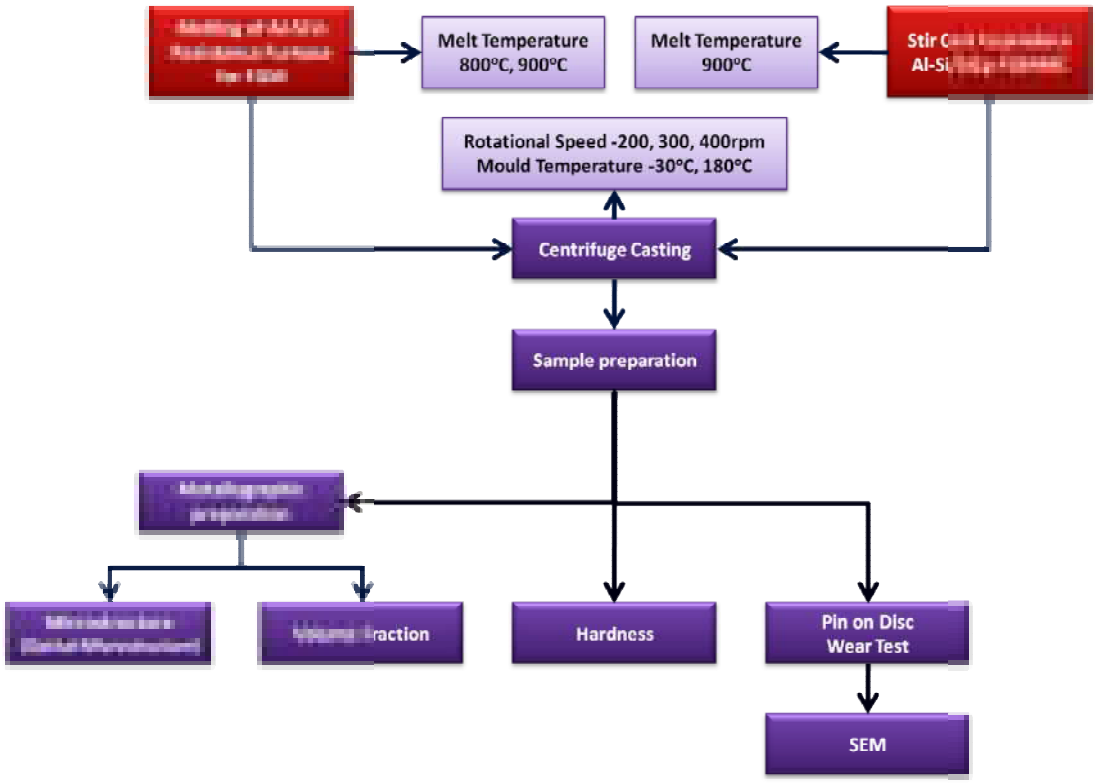

Fig. 3.1 Flow Chart showing the sequence of processes and experiments.

3.2 Material

At present industries are focusing on the development of Aluminum based alloys and their composites to achieve superior wear resistance, low coefficient of thermal expansion, high corrosion resistance, high strength to weight ratio, excellent castability, particularly in the aerospace and automotive sector (Rohatgi et al 1991). From the stand point of research as well as from industry point of view Al alloy based FGMs are able to serve better for new applications particularly in the aerospace and automotive sectors.

In Aluminum alloys Silicon is the most common and least expensive alloying element used. Silicon plays an important role in making the alloy suitable for the aerospace and automotive industry. It mainly increases castability and fluidity. In addition to lowering of aluminum alloy density to 2.34 g/cm^3 silicon increases strength to weight ratio and wear resistance of aluminum alloy.

The material used in this work is a commercially available Al alloy supplied by M/s Fenfe Metallurgicals, Bangalore, India. The composition of the material is presented in Table 3.1.

Table 3.1 Composition of Al-Si alloys used in the work

Alloy	**Composition (wt%)**					
	Si	**Fe**	**Sr**	**Ti**	**B**	**Al**
Al-12Si	12	0.1	-	-	-	Balance
Al-17Si	17	0.1	-	-	-	Balance

Aluminum-Silicon alloys are widely used for manufacturing of components like cylinder blocks, cylinder heads, pistons etc. of internal combustion engines requiring good tribological properties apart from high corrosion resistance, castability and low density. The wear resistance of Al-Si alloys is strongly dependent on the alloy composition, applied load and sliding speed (Torabian et al 1994). It has been established that the Al-Si alloys exhibit poor seizure resistance, which tends to restrict

their use in tribological applications (Reddy et al 1994). The wear resistance of these alloys can be enhanced by reinforcing ceramic particles in the soft aluminum alloy matrix.

Ceramic particles have excellent mechanical properties such as high hardness, high temperature strength and chemical stability. It has been reported (Surappa 2003) that reinforcement of hard ceramic particles in ductile metal matrices produce composites with substantial stiffness and yield strength, but they are brittle in nature when compared to the matrix alloys.

Wear and seizure resistance of Aluminum metal matrix composites (AMC) is considerably higher than the base alloys. This is due to the fact that hard reinforced particles protect the surface from the rubbing action of the abrasives by reducing the depth of penetration of the abrasives and the contact between the abrasive and the matrix (Kok 2006).

In AMCs SiC_P reinforcement is the most attractive material to produce composites for wear resistance in industrial applications as its composites can be produced by conventional processing. SiC_P of density 3.2 g/cm^3, constitutes a tetrahedral of carbon and silicon atoms with strong bonds in the crystal lattice. SiC_P reinforced MMCs have substantial potential in different applications as SiC_P retains room temperature ductility, increases the stiffness, high temperature strength, high thermal conductivity, low coefficient of thermal expansion and provides better wear resistance. It is known that chemical reactions take place at the reinforcement/alloy interface during the casting. Al_4C_3, a hard and brittle phase may be developed at the interface. It has been reported that (Hwu et al 1996) Al_4C_3 phase is unlikely to form in SiC_P reinforced AMCs. The addition of SiC_P has increased the wear resistance with increase in volume fraction and size of the dispersoids. This is attributed to the fact that the addition of SiC_P increased the hardness of the Al-Si alloy. This has given more protection to the matrix from the destructive action of the abrasive as the mean free path between the SiC particles is reduced with increase in volume fraction of SiC particle (Deius et al 1996).

A number of researchers have worked on the SiC_P reinforcement in different Aluminum alloys. In this study we have considered SiC_P supplied by M/s Fenfe Metallurgical, Bangalore and we have used volume fractions of 2%, 4%, and 6%. The average size of the SiC_P is 60 microns.

Table 3.2 gives an overview of the FGMMCs produced using different volume fractions of SiC_P.

Table 3.2 FGMMCs processed using SiC_P as reinforcement in Al-Si alloy

Base Alloy	**SiC_P reinforcement in Volume Fraction (Vol%)**		
Al-12%Si	2	4	6
Al-17%Si	2	4	6

3.3 Fabrication of Al-Si FGM and Al-Si/ SiC_P FGMMC

In order to use FGMs in structural and functional applications it has been reported that a suitable fabrication technique is needed that makes it possible to produce the microstructural and compositional gradient with a high degree of reproducibility (Birman et al 2007). Thus FGMs can meet functional performance requirements that vary with location within a work piece such as turbine component, rocket nozzle, medical implant, tool inserts and optical devices. It is surmised of late that a lot of attention is being paid to the research on FGMs production techniques through: Powder metallurgy, Deposition techniques, Centrifugal Casting, Electromagnetic separation etc (Kiebact et al 2003). These processing techniques have their own drawbacks regarding cost and limitations of production difficulties.

In the present work, using centrifuge processing technique, Al-Si alloy and Al-Si/SiC_P composite melts were solidified under a definite centrifugal force. The functionally graded alloys and composites were then characterized for microstructure and hardness along the length of the casting (along the axis). This technique used for producing FGM is very effective, low cost and it can produce solid shapes when

compared to conventional centrifugal casting process that can produce only hollow symmetric shapes.

3.3.1 Centrifuge Casting Process

In this process the centrifugal force magnitude 'G' is given by the Eq 3.1

$$G = \left(\frac{\omega^2 R}{g} \right) \qquad 3.1$$

Where 'R' is the radius of the arm in meters, 'ω' is the arm rotational speed in rad/sec and 'g' is the acceleration due to gravity. The 'G' plays an important role in positioning the reinforcement during solidification. FGMs with ex-situ and in-situ reinforcements can be processed by this technique. When particle-containing slurry is subjected to centrifugal force, two distinct zones, one with enriched and the other with depleted particles are formed, separated by an intermediate graded zone. It is reported (Y Watanabe et al 2002) that the extent of particle segregation and relative locations of enriched and depleted particle zones within the casting are mainly dictated by the relative densities of the particle and liquid, teeming temperature, melt viscosity, cooling rate, particle size and magnitude of centrifugal acceleration. The lighter particles segregate towards the axis of rotation, while the denser particles move away from the axis of rotation. The particles such as SiC, alumina and zircon in Aluminum alloy system will settle away from the axis, while the lighter Si, graphite, mica will drift towards the axis. In this work the forced segregation of hard in-situ Si particles towards the upper regions (towards the axis) of the casting by centrifugal forces provides a unique approach to production of the FGMs. This region has higher surface hardness and wear resistance in the casting, while retaining high levels of toughness in the rest of the regions.

In this study the centrifuge technique is used to process the functionally graded alloy and composites. The centrifugal force progressively increases the volume fraction of the Si and SiC_P reinforcement within the liquid Al matrix along the radial direction, owing to the density difference between the materials (ρ_{Al}=2700 kg/m^3, ρ_{Si}=2300 kg/m^3, ρ_{SiC}=3200 kg/m^3). A centrifuge machine was built for this purpose

and tested for reproducibility. The centrifuge machine is shown in Fig. 3.2. The difference between this machine and the commonly used machine is that, in this machine the pouring is done while the mold is stationary and machine operates on vertical axis. Thus, centrifugal forces are not applied immediately as in the traditional casting methods since the mold takes some time to reach its casting speed. The principal advantage of this is good mold filling combined with microstructural control, which usually results in improved mechanical properties. Apart from high production rate, time saving, and ability to cast different shapes on reproducible basis, it can produce a stable system based on the in situ nucleation and growth of the reinforcement from the parent melt.

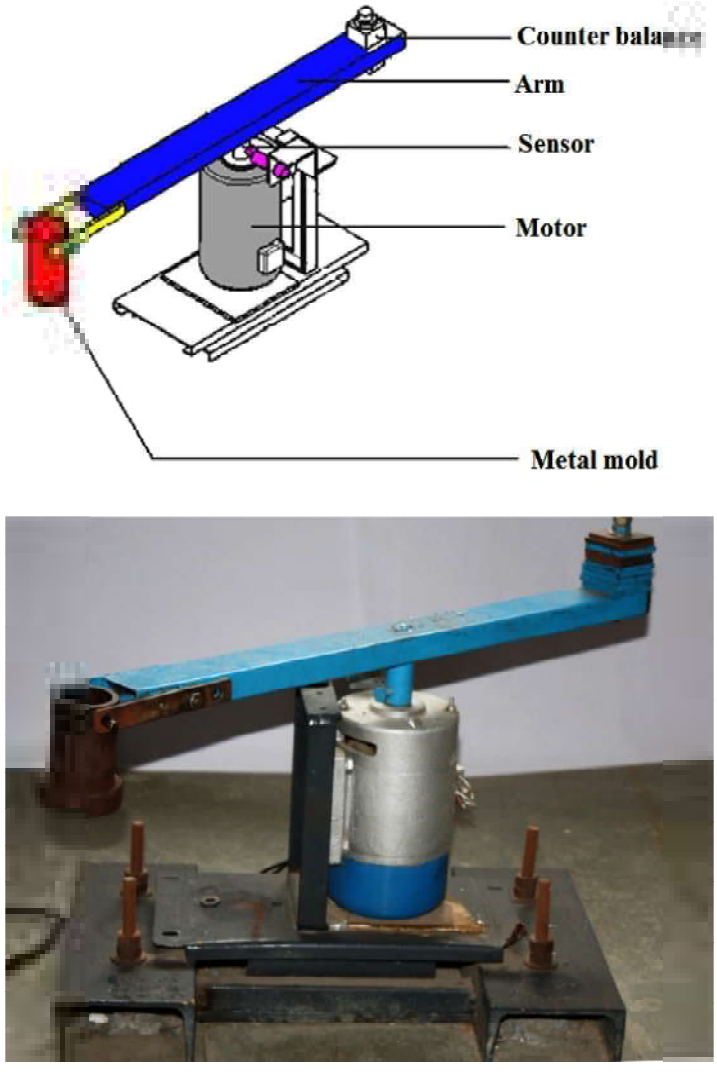

Fig. 3.2 Centrifuge Casting Machine

The experimental setup for processing of alloy/MMC FGM is fabricated in house. Fig. 3.3 shows the details of centrifuge casting machine and the solidified casting in the mold.

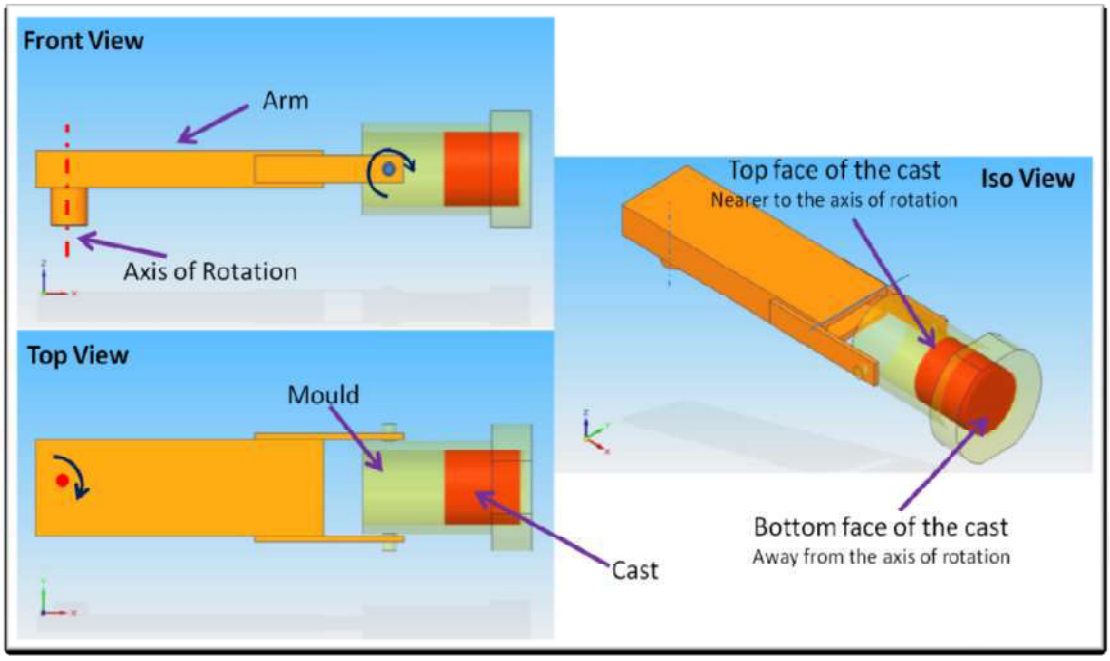

Fig. 3.3 Figure showing arm, mold and casting of the centrifuge machine

The centrifuge casting machine used in the current work mainly consists of an arm with a mold attached at one end with provision to swing and the other end is provided with a counter weight. This arm is centrally mounted on the vertical shaft of a 0.5 HP motor. The alloy was melted in a resistant furnace, heated to 800/900^{o}C temperature and held at that temperature for 20min. The melt was then poured into the metal mold hung at one end of the arm. The melting and pouring was done under controlled conditions without much exposure of the melt to the atmosphere. Hence no special degassing treatment was done. Then the arm is rotated at 400rpm. For each sample 160gms of material was cast to get the cylindrical specimen of 40mm diameter and 42mm height.

3.3.2 Stir Casting Process

The melt for Al-Si/ SiC_P FGMMCs was prepared in a stir casting machine as shown in Fig. 3.4.

Fig. 3.4 Stir Casting equipment

The unit consists of a 3 KW resistance furnace placed over a stand. The furnace constitutes a closed muffle box made with Kanthol A1 heating element. A ceramic fiber blanket of grade 128 surrounds the furnace to avoid heat loss. A clay graphite crucible of diameter 110 mm was placed in the furnace. A hole of 10 mm is drilled on the lower flat surface of the crucible. The stirrer mechanism rests on a platform/frame placed over the furnace. Stirrer set up was belt driven by a D.C. variable motor and a proximity sensor was attached to sense the speed of rotation of stirrer setup. A four blade impeller made of stainless was used.

The stirrer setup consists of a hollow tube with a large sized four blade impeller TIG welded at its lower end. A solid rod of diameter smaller than the inner diameter of hollow tube was made to pass through the hollow tube and the impeller. Bearing placed inside the tube permits hollow tube with impeller to rotate keeping the solid rod in still position. A graphite plug was screwed to the bottom of the solid rod which closes the opening provided at the bottom of crucible during the melting and stirring operations. The hollow tube passes through a pulley which in turn is driven by a belt

driven D.C. motor. A graduated stainless steel rod coated with Al_2O_3 was used to control the depth of immersion of impeller in the melt before of rotation of the impeller. This necessitates the bottom pouring of melt into the mold to retain the suspension. To achieve this, a hole was drilled at the bottom of muffle box which runs along the bottom side thickness of the furnace. During melting and stirring conditions, graphite plug screwed to the solid rod closes the opening of the crucible. After incorporation of reinforcement particles and stirring the matrix melt, lifting of entire stirrer setup i.e, impeller attached hollow tube and solid rod with graphite plug causes the MMC melt to flow down through a ceramic tube opening into the centrifuge machine mold attached to the arm of the rotor. The melt consisting of dispersed reinforcements in the alloy was then cast in the centrifuge casting machine. The cast specimen is shown in Fig. 3.5 with marker.

Fig. 3.5 Centrifugally Cast Specimen

3.4 Process parameters

Several parameters determine the microstructure and the distribution of phases/ particles in the FG casting. These parameters include the size and initial concentration of particles / alloying element, the centrifugal force, solidification rate, cooling rate, which in turn are controlled by: temperature of the mold and pouring temperature (Kumar et al 2010). The process parameters used in the present work are provided in Table 3.3. Full factorial design is used to conduct the experiments.

Table 3.3 Process parameters for centrifuge casting

	Process parameters	**Levels**
Al-Si FGM	Pouring Temperature (T_P), ^oC	800, 900
	Mold Temperature (T_m), ^oC	30 (room temperature), 180
	Rotational Speed, rpm	200, 300, 400
	'G' Number	22.35, 50.3, 89.42
	Silicon wt.%	12, 17
Al-Si/SiC_P FGMMC	Pouring Temperature (T_P), ^oC	900
	Mold Temperature (T_m), ^oC	180
	Rotational Speed, rpm	200, 300, 400
	'G' Number	22.35, 50.3, 89.42
	Base alloy, Al-Si	Al-17wt.%Si, Al-12wt.%Si
	Silicon Carbide particle, wt% (vol. %)	2(1.7), 4(3.3), 6(5)

3.5 Microstructural Characterization

In the case of FG alloys or MMCs, before carrying out any tests for mechanical and tribological properties it becomes necessary to perform microstructural characterization to provide an insight into:

- Distribution of primary Si along the length of the specimen and also to find the volume fraction.
- Distribution of SiC_P along the length of the specimen and also to find the volume fraction.
- Phase structure and solidification structure.
- Presence and distribution of porosity.
- Nature of interfacial bonding between the metallic matrix and SiC_P.

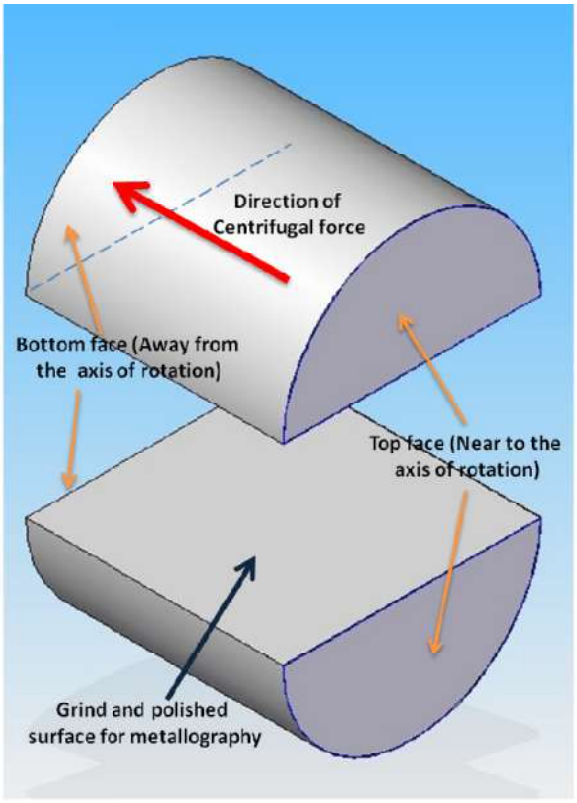

Fig. 3.6 Metallographic specimen

The metallographic specimen of the cast cylindrical FG alloy or MMC is cut along the length ie. Parallel to the centrifugal force as shown in Fig. 3.6. The sectioned surface obtained by cutting the casting on a milling machine was prepared for metallographic studies by initially grinding and then polishing with a series of abrasive papers starting from mesh size 1000, 600, 220, 4/4, ...1/4. Final polishing was performed on a series of disc polishers using fine SiC powder in water and then with 15 micron diamond paste until the surface was scratch free (ASTM-3-95E 1995). The samples so obtained were etched with keller's reagent (2.5%HNO_3 + 1.5%HCL + 1%HF + 95%H_2O) for developing the microstructure (Pace et al 2011).

The optical microscope used for microstructure characterization is shown in Fig. 3.7. An inverted microscope of Dewinter make interfaced with Metalife image analyzer software is used to capture and analyze the image. The image captured is analyzed for phase/volume fraction analysis (ASTM-E562 1995), (ASTM-E1245 1995), Si and SiC_P distribution.

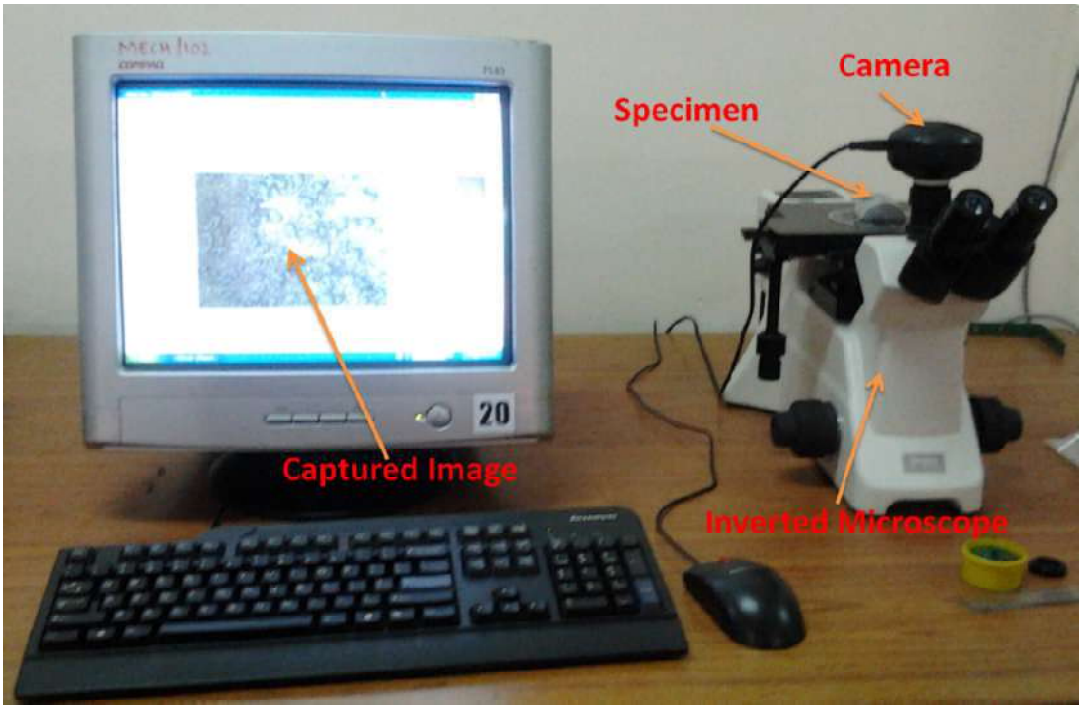

Fig. 3.7 Inverted Microscope interfaced with metalife software

3.6 Hardness

The term hardness, as used in industry, is defined as the ability of a material to resist permanent indentation or deformation when in contact with an indenter under load. Since the indenter is pressed into the material during testing, hardness is also viewed as the ability of a material to resist compressive loads (Revankar et al 2000). Hardness testing is perhaps the simplest and the least expensive method of mechanically characterizing a material since it does not require an elaborate specimen preparation, involves rather inexpensive testing equipment and is relatively quick. The theoretical and empirical investigations have resulted in fairly accurate quantitative relationships between hardness and other mechanical properties of materials such as ultimate tensile strength, yield strength and strain hardening coefficient, fatigue strength and creep. These relationships help to measure these properties with an accuracy sufficient for quality control during the intermediate and final stages of manufacturing. Many times hardness testing is the only nondestructive test alternative available to qualify and release finished components for end application.

In the Brinell hardness test, a hard spherical indenter is pressed under a fixed normal load onto the smooth surface of a material. When the equilibrium is reached, the load and the indenter are withdrawn, and the diameter of the indentation formed on the surface is measured using a microscope with a built-in millimeter scale. This method is ideally suited for inhomogeneous materials like composites, castings etc. ASTM E-10 is a standard test for determining the Brinell hardness of metallic materials The Brinell hardness is expressed as the ratio of the indenter load *W* to the area of the concave (i.e., contact) surface of the spherical indentation that is assumed to support the load and is given as Brinell Hardness Number (BHN) as shown in Eq 3.2

$$BHN = \frac{2W}{\pi D^2 \left[1 - \sqrt{\left(1 - \left(d/D\right)^2\right)}\right]} \qquad 3.2$$

where *W* is the load in kilograms, and *d* and *D* are the diameters of the indentation and the indenter respectively, in millimeters. The schematics of the hardness test is shown in Fig. 3.8.

In the present work Brinell Hardness tester (model BV-120) is used which confirms to IS-Specification 1754. Prior to the testing, the specimen is cleaned to remove dirt and oil on the surface. The type of indentor and the load to be applied are selected in accordance with ASTM E-10. In this test a ball indentor of dia 5mm and a load of 15.625 Kgs are selected. Once the load actuation button is pushed the indentor swings due to its own weight and penetrates into the specimen. The load adjusted by means of push button becomes effective and produces the impression. The produced impression is lighted and displayed on the focusing screen. The impression is magnified depending on the objective used.

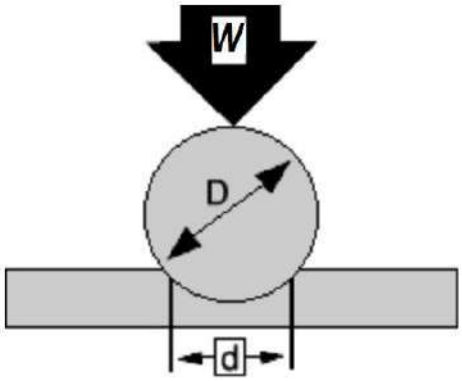

Fig. 3.8 Schematic representation of Indentation process

The hardness is measured along the length of the cast specimen for every 4mm from top to bottom of the casting. As shown in Fig. 3.9 at least five readings are taken perpendicular to the longitudinal axis. The final BHN value for each specimen is arrived at considering the statistical variation. Hardness is calculated for all the cast FG alloys (Al-12wt%Si, Al-17wt%Si) and FGMMCs (Al-12wt%Si with 2, 4, 6% SiC_P, Al-17wt%Si 2, 4, 6% SiC_P) under different process parameters.

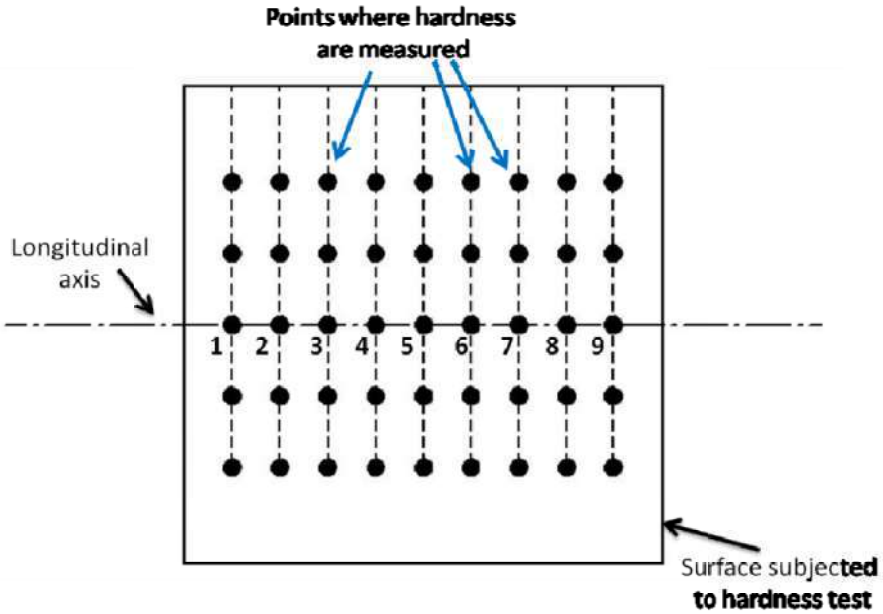

Fig. 3.9 Points of measurements in Hardness test

3.7 Wear

The concept of wear involves the presence of small particles between the contacting surfaces. It is possible that the abrading particles first penetrate the metal and then cause tearing of the surface introducing surface stress cracks, which lead to the ultimate break down of the surfaces. The complexity of wear is emphasized by a consideration of the number of factors required for its description. The main factors that influence wear and friction are as follows (Blau et al 1981):

1. Variables Connected with Metallurgy.
    - Hardness, Toughness, Constitution and Structure
2. Variables Connected with Service.
    - Contacting Materials, Normal Pressure, Sliding Speed and Temperature
3. Other Factors
    - Lubrication and Corrosion

Sliding and Adhesive wear refer to a type of wear generated by the sliding of one solid surface along another surface. Erosion, cavitation, rolling contact, abrasion, oxidative wear, fretting, and corrosion are traditionally excluded from the class of "sliding" wear problems even though some sliding (slip) may occur in some of these types of wear. Apparently, sliding wear is a category of wear that is "left over" when all other types of wear are identified under separate headings (Ludema et al 2000).

3.7.1 Wear Quantification

The material lost during dry sliding wear conditions can be measured and quantified by the following direct and indirect methods

- **Mass Loss Measures of Wear**: Measured as the difference between weight of specimen before and after wear of the material. The problem with this approach includes the need to clean the specimen carefully to

avoid having extraneous matter on the surface which will contribute to any weight difference.

- **Linear Measures of Wear:** Measures the amount of wear as dimensional change using pin-on-disc sliding wear methodology according to ASTM G99 standards.

- **Area Measures of Wear**: Measures the amount of wear over a localized area on two surfaces like wear in worn areas on gear teeth, bearing retainers and on sliding pads with contoured surfaces.

- **Volume Measures of Wear**: Measures the wear amount in volume units (mm^3), which enables a comparison of wear among materials having different densities.

Wear can be expressed in the following forms:

- Linear wear rate (K_L) = [(Thickness of the layer removed) / **(**sliding distance)]
  = (mm/mm) (Dimensionless)
- Volumetric wear rate (K_V) = (Volume of layer removed / sliding distance)
  = (mm^3 / mm-mm^2) (Dimensionless)
- Wear coefficient (K) = [(volume of the material removed x flow stress) / (Normal load x sliding distance)]
  = [(mm^3-N) / (mm^2 -N-mm)] (Dimensionless)
- Specific wear rate (SWR) = [(Volume of layer removed) / (Normal load x sliding distance)]
  = (mm^3/N-mm)

3.7.2 Pin on Disc Wear Testing Machine

In this study Wear tests were performed on a Pin-on-Disc type wear testing machine (model TR-20LE, Ducom make) shown in Fig. 3.10. The tests were conducted as per ASTM standards (ASTMG-99 1995). The normal load was applied on the pin by dead weight through a pulley string arrangement. The system had a maximum load capacity of 200N. The rpm and the sliding speed of the disc were 0-2000rpm and 0-10m/s respectively. The disc is made of En-32 steel (0.14%C, 0.18%Si, 0.52%Mn, 0.015%S, 0.019%P, 0.13%Ni, 0.05%Cr, 0.06%Mo, balance Fe), having dimensions of 160mm diameter and 8mm thickness with a hardness value of HRC65.

Fig. 3.10 Pin-on-Disc Wear testing Machine

The measurement in reduction of height of the specimen due to wear and coefficient of friction were measured continuously by electronic sensors. The LVDT used is capable of measuring a maximum displacement of $\pm$ 2 mm and the measuring range of wear is $\pm$ 2000 micron with an accuracy of $\pm$ 1µm. A load cell is used to measure frictional force. It has a maximum load capacity of 200 N and measures the frictional load at an accuracy of $\pm$ 0.1N. The data acquired was processed in the controller and transmitted to the PC using Winducom 2006 software. Wear was

measured as reduction in specimen (pin) length in microns. Frictional force and coefficient of friction data were measured as a function of time.

The tests were conducted under dry conditions and at room temperature according to ASTMG99-95a standards. The wear test was carried out at a temperature of 25^{o}C and relative humidity of 45-50%. Pins of 10 mm diameter and 42 mm length were machined as shown in Fig. 3.11 and run against a hardened and ground (Ra = 0.1 μm) EN 32 steel disc of hardness HRC 58-62 and of track dia 70mm.

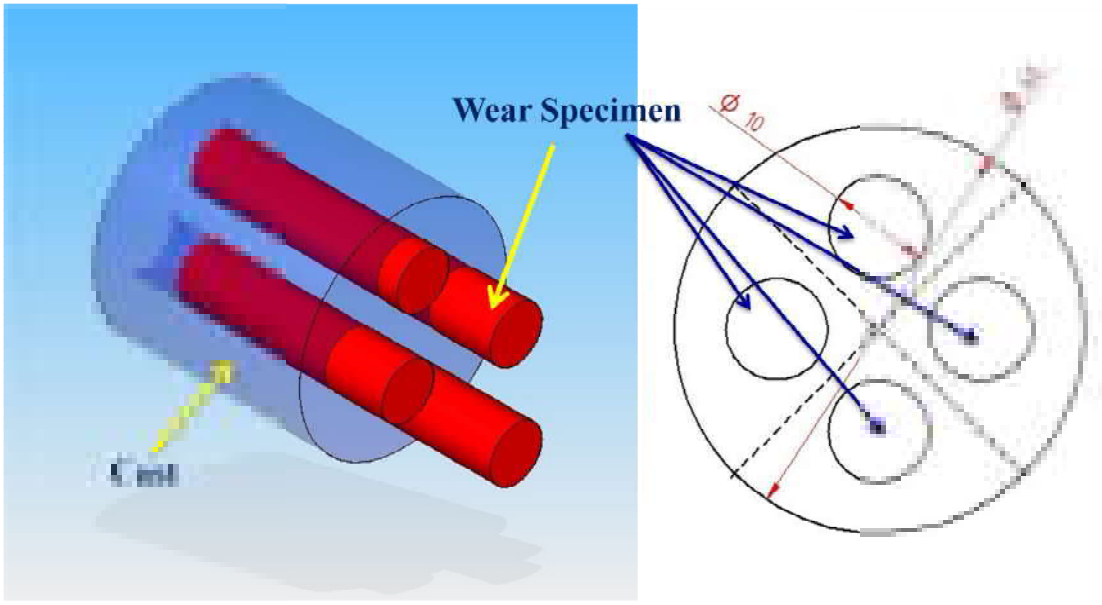

Fig. 3.11 Wear specimen

The mating surfaces of the pin and the disc were polished using 600mesh emery paper before the start of the wear test. The polished pins were cleaned and degreased using ultrasonic cleaner, first with water and soap, followed by ethanol and finally with acetone. Wear data was acquired at a rate of 10 samples per sec. Each test specimen was run under varying loads (40.0, 60.0, and 80.0N) and a constant sliding speed (1.466m/sec) for a constant sliding distance (879.6m). The wear and wear rate were calculated from the data. The frictional force generated on the specimen was monitored by using a frictional force sensor and was measured in Newton.

Specific wear rate and coefficient of friction was analyzed for FG alloys (Al-12wt%Si, Al-17wt%Si) and FGMMCs (Al-12wt%Si with 2, 4, 6% SiC_P, Al-17wt%Si 2, 4, 6% SiC_P) under different process parameters. The wear debris and worn surface of test specimens were analyzed by Scanning Electron Microscope (SEM) to understand the wear mechanism.

3.8 Diametral Compression Test

In a functionally graded alloy or composite due to gradation of a phase and / or the reinforcement properties vary from one end of the component to the other end. The extent of the variation depends on the gradation of the material. The variation in mechanical properties may be sometimes desirable. Therefore in addition to microstructural characterization it is desirable that the change in mechanical property of interest due to gradation is also evaluated. In the present study diametral compression test is considered to observe the behavior of the different regions.

A significant difference exists between bending test and diametral compression test while measuring the tensile strength. In bending test, the material is subjected only to uniaxial stress but, in the case of diametral compression test the specimen is associated with a transverse compressive stress. This is considerably larger than the tensile stress developed. Hence the results obtained from the two different methods are significantly different. Also the maximum stresses developed during loading are not limited to the surface of the material in diametral compression test as compared to bending test. Hence the failure occurring in material is not due to surface defects alone. This is important for FGM system as the properties vary based on phase/ composition and depend both on surface as well as interior of the sample.

Mathematical equations were developed to describe stress-strain for elastic discs and spheres under diametrical compression under point loading conditions as shown in Fig. 3.12 (Procopio et al 2003). The Hertz solution predicts that the maximum principal stress occurs at the centre of the disc, and is tensile in nature along the x-direction (Hertz 1895). Assuming that the maximum principal stress is

responsible for the failure of the specimen, the tensile strength obtained is given by equation 3.3

$$\sigma_t = \frac{2P}{\pi D_c t} \qquad 3.3$$

σ_t= Tensile strength in N/mm^2

P = Load applied in N

D_c = Diameter of the specimen in mm

t = thickness of the specimen in mm

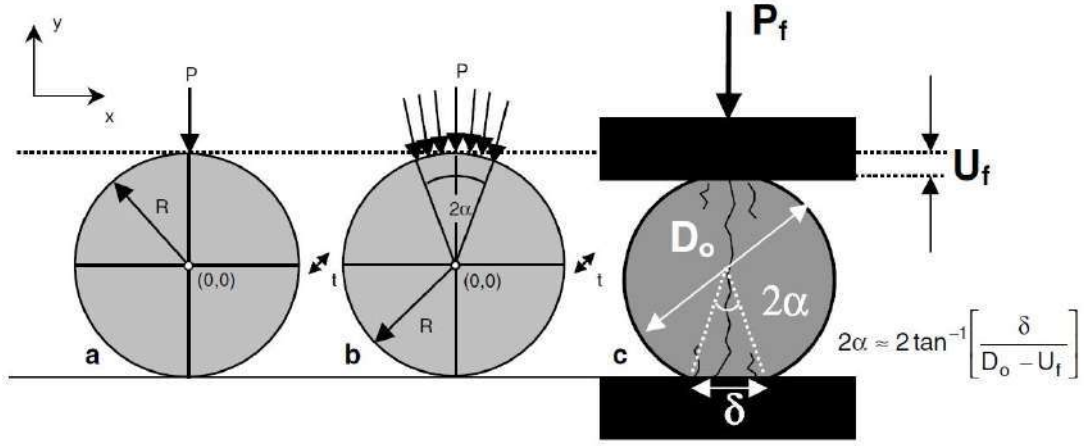

Fig. 3.12 Schematic representation of different loading conditions (a)Hertz point (b) Hondros, and (c) uni-axial diametrical compression

The work of Hertz was then modified to include distributed loading condition (Hondros et al 1959). Mathematically both solutions are exact elasticity solutions and satisfy equations of equilibrium. The analyses of both the authors converge to equation 3.3 at x=y=0. It has been discussed in the validity process of the Brazilian test (Fairhurst 1964), that failure is expected to initiate at the center of the disc, but actually the failure sometimes initiates at the loading points. The major measurable variables in the test are, P_f = failure load; D_o = initial diameter; δ = contact flattened width; 2α = contact flattened angle (Fig. 3.12).

A Universal tensile testing machine (Model TUN-600) shown in Fig. 3.13 is used to conduct the diametral compression test. The maximum capacity of the test equipment is 600 KN with flexibilitsy to select the measuring range and minimum graduation. At the point of application of load, thickness of specimens were flattened to a width equal to 0.2D (4.0 mm on either side of vertical diameter) in order to distribute the load and to obtain an accurate tensile strength (Shaw et al 1975). The deformation of the test specimen was noted down by an extensometer for every 5 KN increase of compressive load.

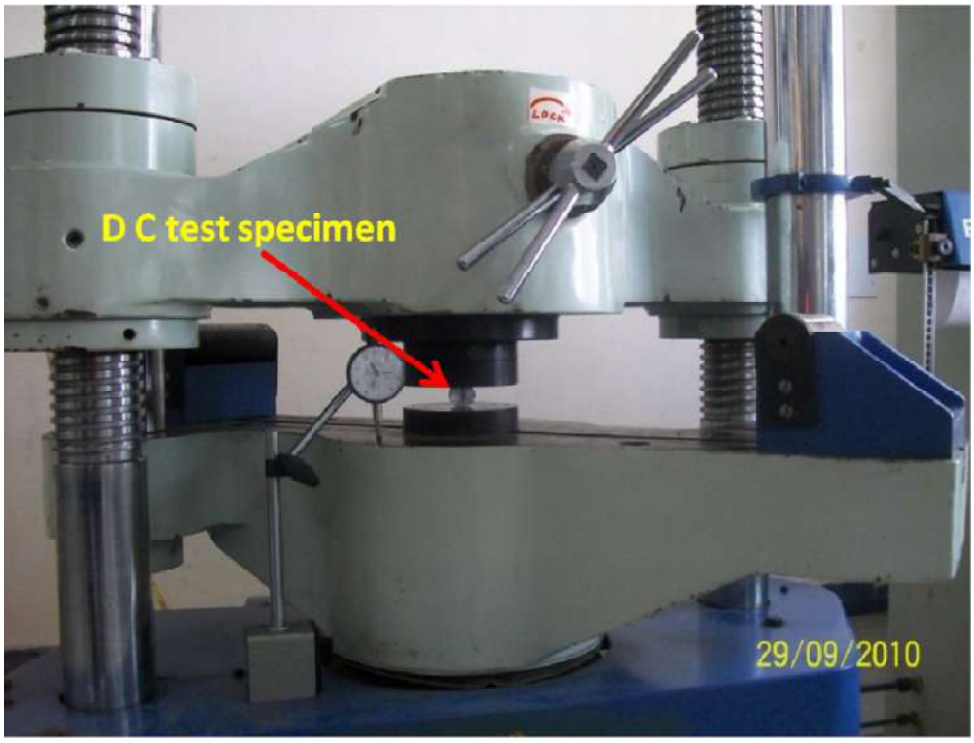

Fig. 3.13 UTM with application of Diametral compressive load

It is observed that the width of the flattened portion increased with the increase of load and thus the compressive stress in the transverse direction normal to flattened portion was assumed to act over a rectangular portion of width b and thickness t. The thickness of the flattened portion was assumed to be constant. The compressive stress in the transverse direction was considered as load at failure (maximum load) divided by the projected area of the flattened portion as $\sigma_c = P/ (b \times t)$ where b is the width of

the flat portion obtained at the end of the test. The width of flat portion (b) is determined using equation 3.4

$$b = 2 \times \sqrt{r^2 - (r - 0.5\delta r)^2} \qquad 3.4$$

where r is radius of test specimen and δr is measured radial deformation.

Assuming ductile and linear behavior of materials at low loads, the strain at low loads (5 KN) was considered in the calculation of modulus of elasticity. Modulus of Elasticity is considered as the ratio of compressive stress to compressive strain at low loads.

3.9 Designation

The designation for the test specimens for FG alloys and FGMMCs are provided in Table 3.4.

Table 3.4 Details showing designation of the test specimens of FGM alloys and FGMMCs used in the present study.

Sl. No.	Designation	Explanation
1.	T400	Casting at 400rpm (89.42g), tested for top end of the casting (end near to the axis of rotation)
2.	B400	Casting at 400rpm (89.42g), tested for bottom end of the casting (end away from the axis of rotation)
3.	T300	Casting at 300rpm (50.3g), tested for top end of the casting (end near to the axis of rotation)
4.	B300	Casting at 300rpm (50.3g), tested for bottom end of the casting (end away from the axis of rotation)
5.	T200	Casting at 200rpm (22.35g), tested for top end of the casting (end near to the axis of rotation)
6.	B200	Casting at 200rpm (22.35g), tested for bottom end of the casting (end away from the axis of rotation)

4. RESULTS AND DISCUSSION

4.1 Introduction

During the solidification of aluminum-silicon alloys, the morphology and distribution of silicon particles formed as the primary or eutectic constituents determine the mechanical properties of the castings. The alloys show increasing tensile or compressive strength, with increasing volume fraction and decreasing size of the silicon particles. As for the shape of silicon particles, spherical shapes are better compared to angular shapes from a viewpoint of stress concentration (Matsuura et al 2004). Generally, during solidification the silicon content of the melt and cooling rate are the process parameters that control the volume fraction and size of the silicon particles. Thus, mechanical properties of Al–Si cast alloys depend not only on chemical composition but, more importantly, also on micro structural features such as morphology of dendritic α-Al, eutectic Si particles and other intermetalics that are present in the microstructure.

Wear of a material is controlled by the material and microstructural characteristics as well as operating parameters such as applied pressure, sliding speed, surrounding ambience in the vicinity of the apparatus and the type of sliding interaction. Material characteristics including metallurgical and mechanical properties of the alloys significantly influence their wear resistance. Basavakumar et al have reported that morphology of the various phases present in alloys appreciably influence the mechanical and dry sliding wear behavior (Basavakumar 2007). Coarse and needle-shaped eutectic and large primary silicon particles increase adhesive wear. Fine, spherical and uniformly distributed micro-constituents (α-aluminium, eutectic, primary silicon) are known to improve the wear properties of aluminium alloys (Dwivedi et al 2004).

Centrifugal casting is a pressure casting method in which higher 'G' force is applied to molten metal by rotating or spinning the mold assembly. It has been demonstrated that a compositional gradient can be obtained to segregate phases with

different densities. In case of SiC reinforced Al / Al-Si composites, the density of SiC particles is higher than that of molten aluminium. Thus pressure castings can be used to produce Al alloy/ SiC_P FGMs. Consequently, the external zone of the part will have higher reinforcement content with good wear resistance, while the inner zone, constituted by Al alloy has high toughness. The addition of reinforcing particles to the matrix alloy greatly decreases the wear rate. As the volume fraction of particle increases effect on the wear rate is enhanced (Mondal et al 2005).

In the present work eutectic (12%Si) and hypereutectic (17%Si) Al-Si alloy FGMs are produced using centrifuge casting technique. FG Composites using same alloys with SiC particulate(SiC_P) as reinforcement are also produced using stir casting followed by centrifuge casting. Three different volume fractions of SiC_P are used. Solid cylindrical specimens have been produced under different combinations of process parameters listed below.

- 3 levels of mold speed (G force)
- 2 levels of teeming temperature
- 2 levels of mold temperature

Full factorial design is used for experiments involving FGM alloys.

The results of microstructural and mechanical characterization are presented and discussed in the following sections. Hardness, wear and diametral compression strengths are determined for mechanical characterization. The effect of L/D (length to diameter) ratio on the microstructure of the cast Al-Si FGM is evaluated and is validated further by measurement of hardness.

4.2 Al-12%Si (Eutectic) FGM

4.2.1 Microstructure

The microstructure of a material is the study of the grain structure, grain size, composition, orientation and their effect on the macroscopic behavior in terms of properties such as strength, toughness, ductility, hardness, corrosion resistance, high /

low temperature behavior, wear ability and so on which in turn governs the application of these materials in industry and manufacture. The basis of materials science is to correlate structure and property i.e., relating the desired properties and relative performance of a material in a certain application to the microstructures of that material. The major determinants of the structure of a material and its properties are its constituent chemical elements and the way in which it has been processed into its final form. These characteristics, taken together and related through the laws, govern a material's microstructure, and thus its properties.

In Centrifugal casting several parameters determine the microstructure and distribution of phases and constituents of the casting. The parameters include the mold volume and wall thickness, initial concentration of alloying element or particulate addition, centrifugal force and cooling rate which is controlled by mold temperature, pouring temperature of melt, heat transfer between the mold and the melt and G force (rpm).

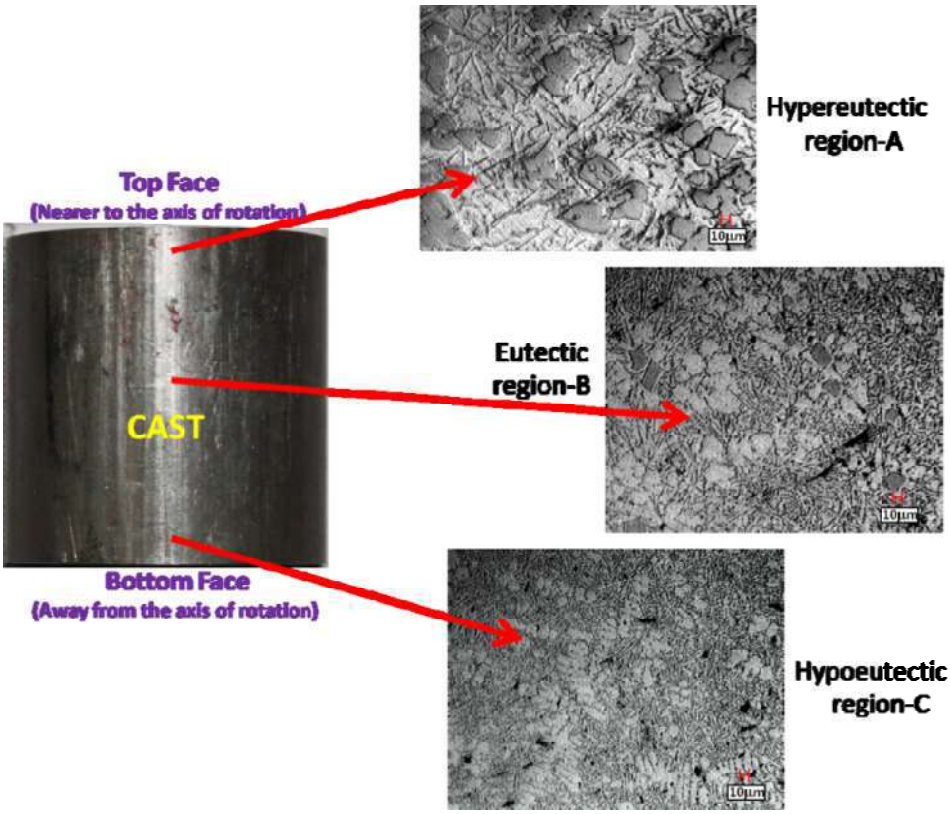

Fig. 4.1 FGM sample and the corresponding microstructures at top, middle and bottom region of a casting

Fig. 4.1 shows the centrifuge cast FGM sample of eutectic Al-Si alloy and the corresponding microstructures. The FGM consists of 3 parts: region enriched with primary silicon (A), Si particle free regions B and C. In region A, the structure is hypereutectic with a more number of primary Si particles, region B is filled with Al–Si eutectic structure and region C is hypo-eutectic containing more of Al dendrites. The three regions in the above sample show that the structure of the FGM sample changes from hypereutectic structure to eutectic structure and then to hypoeutectic structure from top to bottom of the sample. (Top: Nearer to the axis of rotation)

Referring to Fig. 4.1, it is seen that large number of primary Si are pushed to the top region of the casting. The direction of movement of the particles under centrifugal force is determined by the relative densities. If the density of the particles is more than that of the matrix, particles move away from the axis of rotation (bottom face) and if it is lower, particles move towards the axis of rotation (top face).

4.2.1.1 Effect of rotational speed (G Force)

It is observed in the cast specimens that there are three distinct regions along the length of the cylinder and these regions are; the top region consisting of Si particles in the eutectic matrix; the middle region showing a clear interface between the Si rich (top region) and Si depleted zone (bottom region): the bottom region consisting of the α-Al solid solution. Similar observations have also been reported by Y Watanabe while centrifugally casting hollow cylinders (Y Watanabe et al 2005b). The segregation of Si to the top portion of the casting is attributed to the lower density of the Si particles in comparison to that of the liquid alloy.

The microstructure and the volume fraction of primary Si for eutectic alloy under varying teeming temperature (T_P), mold temperature (T_m) and G factor (or rpm) are shown in Figs. 4.2 through 4.25. Two mold temperatures are used while pouring, one at room conditions another at 180^{o}C. For specimens cast at T_P=800^{o}C, T_m=Room temperature, the histograms shown in Figs. 4.3, 4.5 and 4.7 indicate that no primary Si

is obtained for 200rpm where as at 300 and 400rpm the primary Si is obtained at the top region of the casting showing a volume fraction of 2 and 4% respectively. It is also found that the primary Si was only up to a depth of 4mm (0.1 normalized thickness) from top.

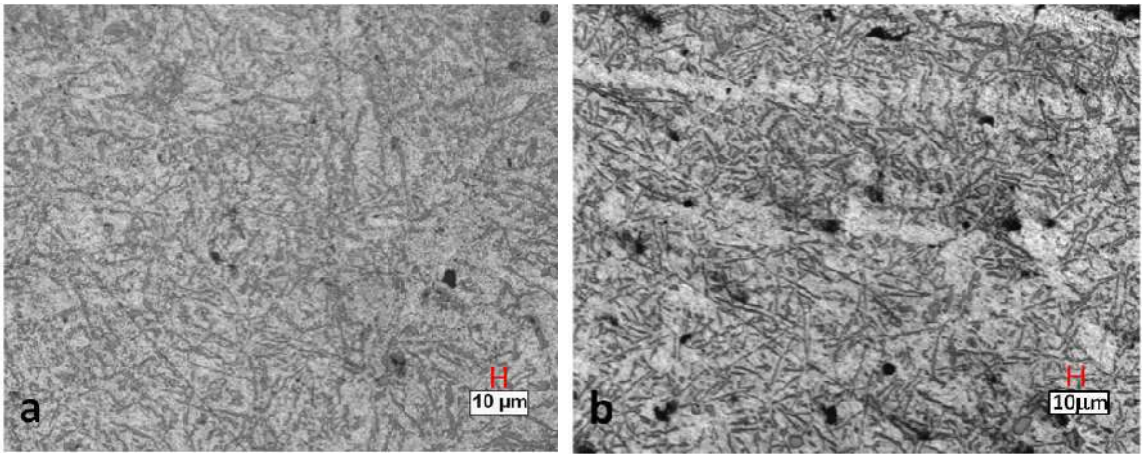

Fig. 4.2 The microstructure of the Al-12wt%Si FGM cast at, T_P =800°C, T_m =Room temp G=22.3(200rpm). a) Top end showing no primary Si, b) Bottom end showing α-Al dentritic structure

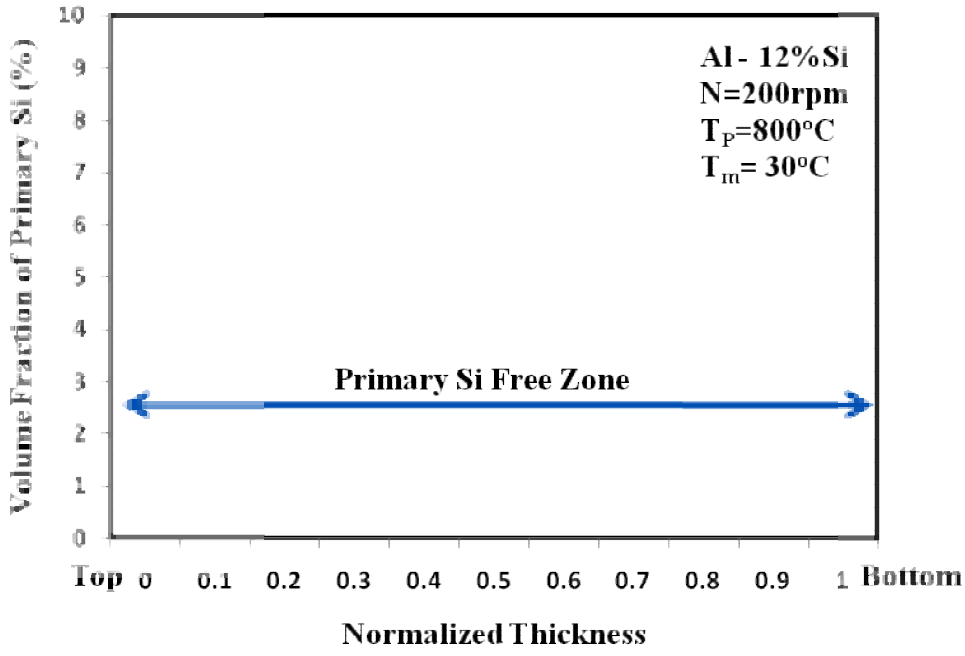

Fig. 4.3 Distribution of primary Si from top end to bottom end for Al-12wt%Si FGM cast at, T_P=800°C, T_m=Room temp, G=22.3(200rpm).

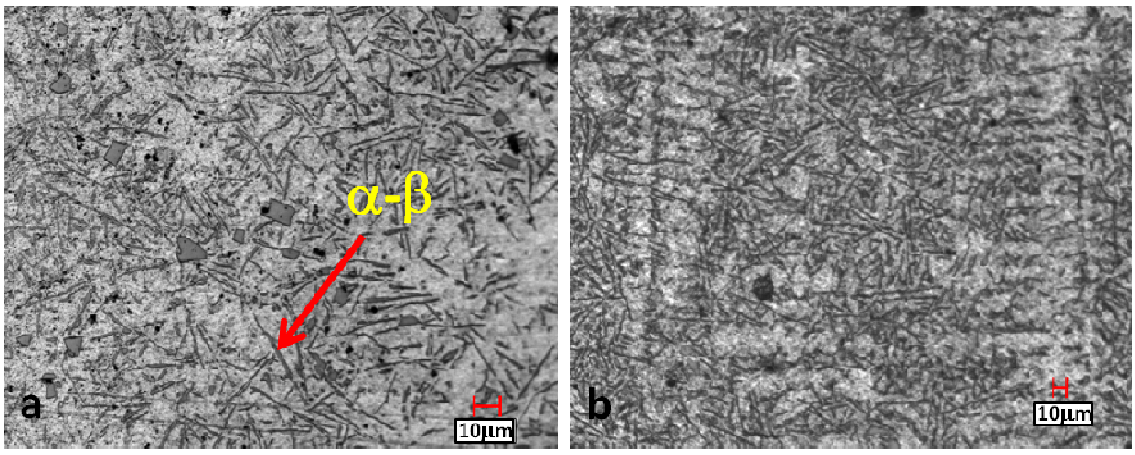

Fig. 4.4 The microstructure of the Al-12wt%Si FGM cast at, T_P=800°C, T_m=Room temp G=50.3(300rpm). a) Top end showing primary Si, b) Bottom end showing α-Al dentritic structure

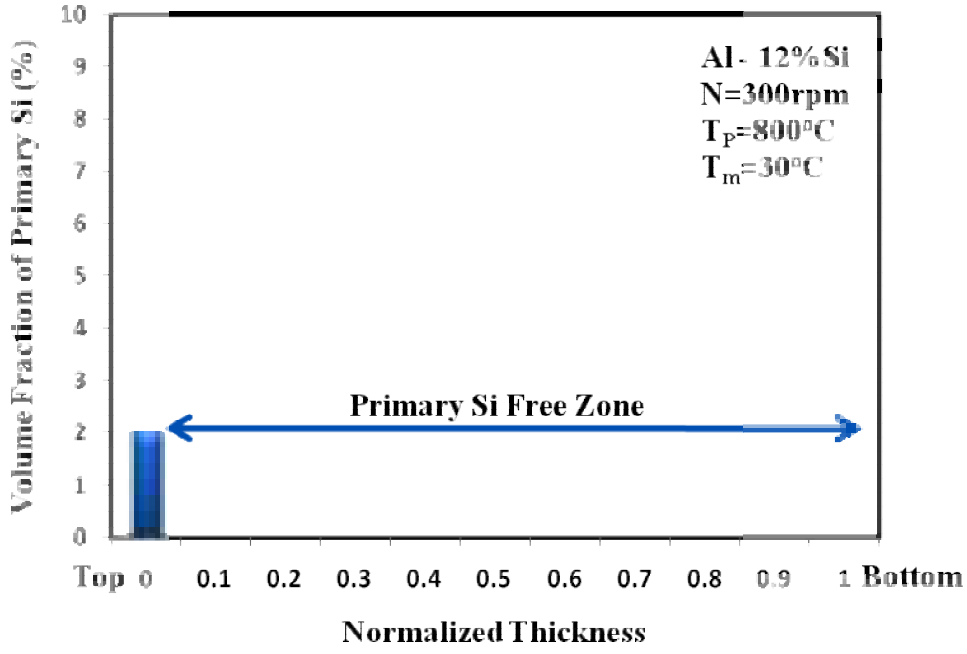

Fig. 4.5 Distribution of primary Si from top end to bottom end for Al-12wt%Si FGM cast at, T_P=800°C, T_m=Room temp, G=50.3(300rpm).

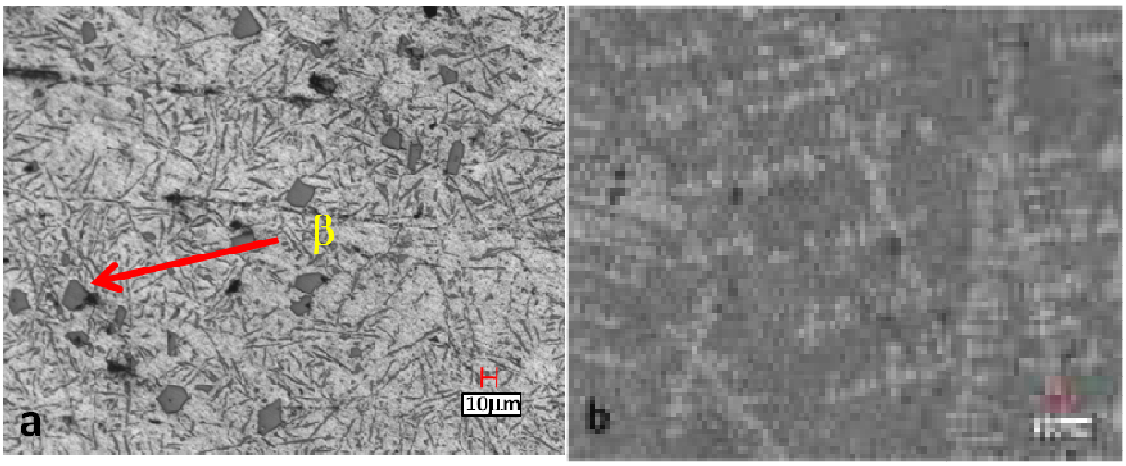

Fig. 4.6 The microstructure of the Al-12wt%Si FGM cast at, T_P=800°C, T_m=Room temp, G=89.42(400rpm). a) Top end showing primary Si, b) Bottom end showing α-Al dentritic structure

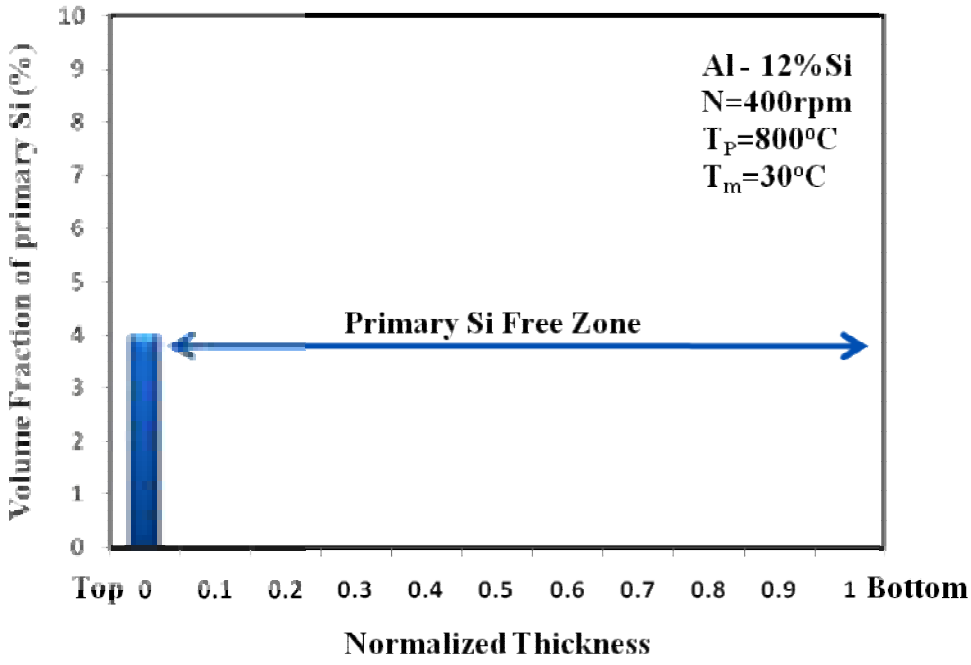

Fig. 4.7 Distribution of primary Si from top end to bottom end for Al-12wt%Si FGM cast at, T_P=800°C, T_m=Room temp, G=89.42(400rpm).

In the eutectic cast at T_P=800°C, T_m=180°C, it is found that the percentage primary Si formed has improved due to mold preheat. At 400rpm (89.42G) 7% primary Si is formed at the top of the specimen and it decreased to 3% at a distance of

4mm from the top as represented in Fig. 4.13. For the specimens cast at 300rpm (50.3G) the primary Si is found to be 4% at the top of the specimen and decreased to 2% at 4mm from the top (refer Fig. 4.11). Fig. 4.9 shows that only 2% primary Si is found at the top of the specimen cast at 200rpm (22.3G). It can thus be inferred that for a given teeming temperature the percentage of primary Si formed during solidification improves if the mold is preheated.

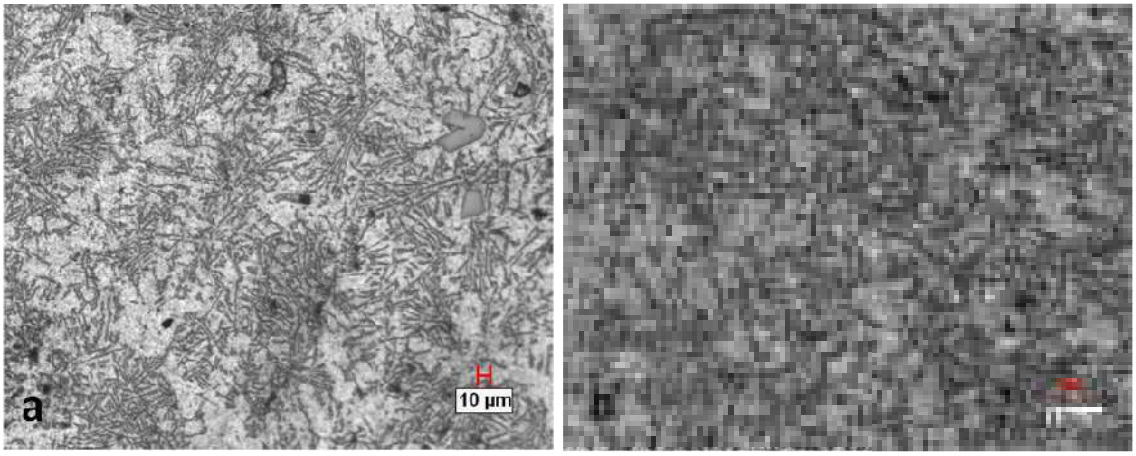

Fig. 4.8 The microstructure of the Al-12wt%Si FGM cast at, T_P=800°C, T_m=180°C G=22.3(200rpm). a) Top end showing primary Si, b) Bottom end showing α-Al dentritic structure

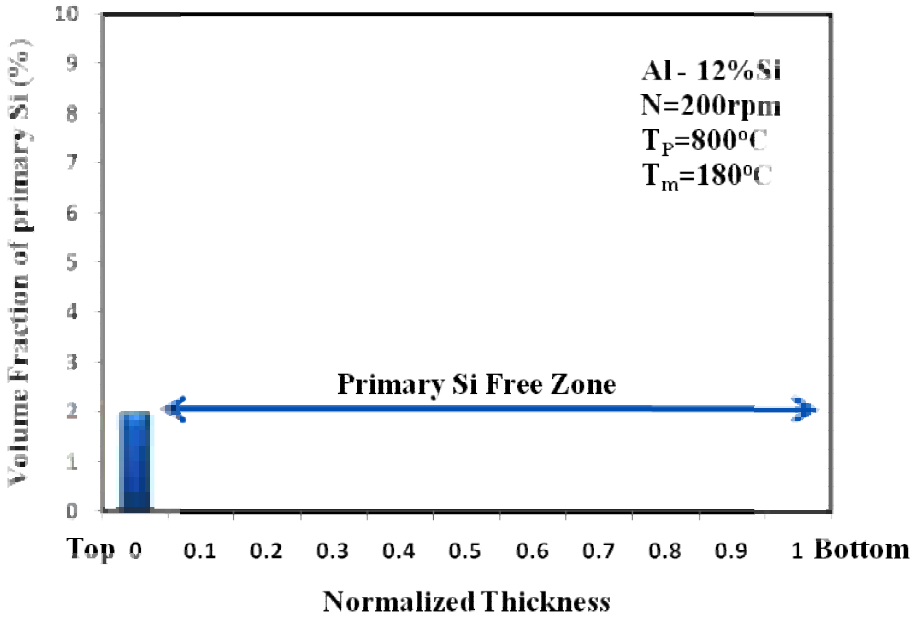

Fig. 4.9 Distribution of primary Si from top end to bottom end for Al-12wt%Si FGM cast at, T_P=800°C, T_m=180°C, G=22.3(200rpm).

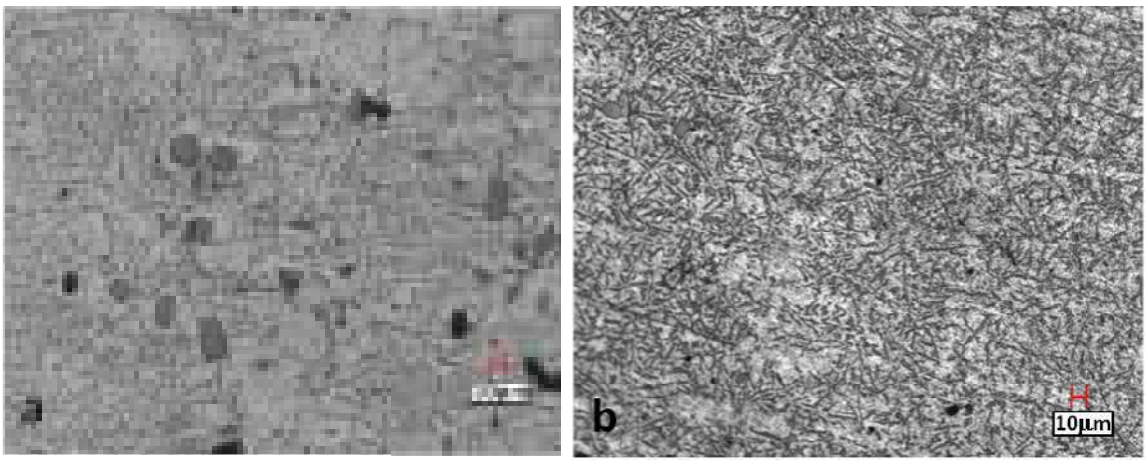

Fig. 4.10 The microstructure of the Al-12wt%Si FGM cast at, T_P=800°C, T_m=180°C G=50.3(300rpm). a) Top end showing primary Si, b) Bottom end showing α-Al dentritic structure

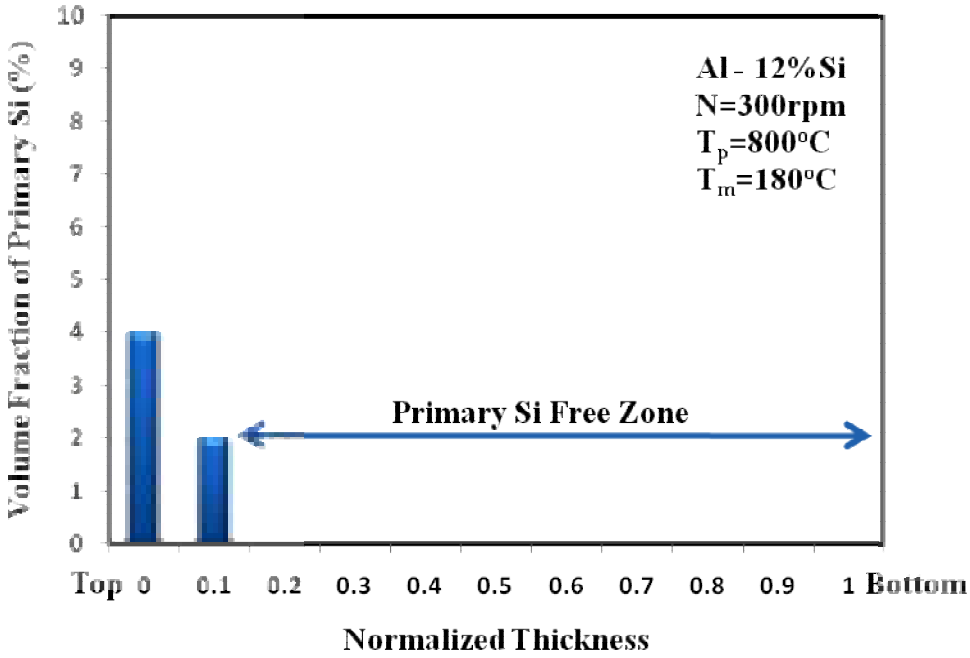

Fig. 4.11 Distribution of primary Si from top end to bottom end for Al-12wt%Si FGM cast at, T_P =800°C, T_m =180°C , G=50.3(300rpm).

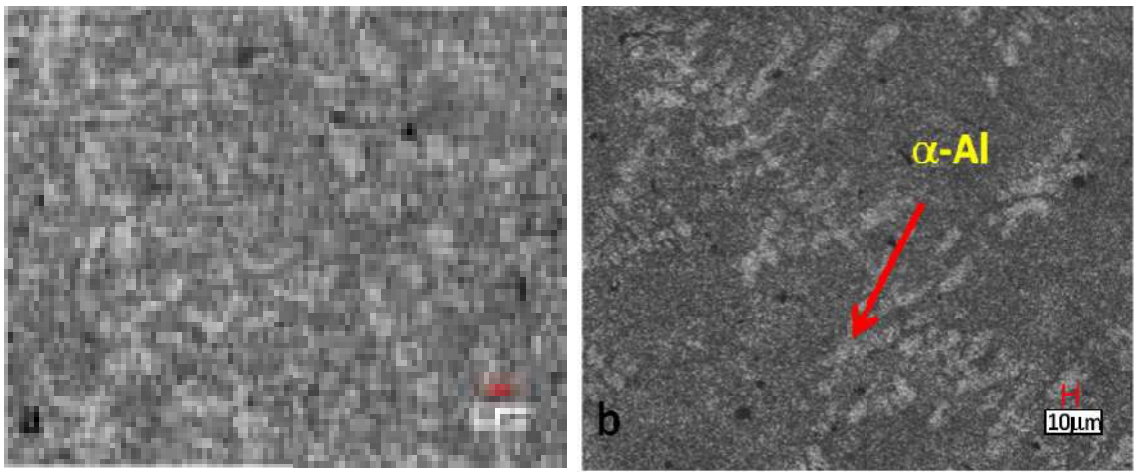

Fig. 4.12 The microstructure of the Al-12wt%Si FGM cast at, T_P=800°C T_m=180°C G=89.42(400rpm). a) Top end showing primary Si, b) Bottom end showing α-Al dentritic structure

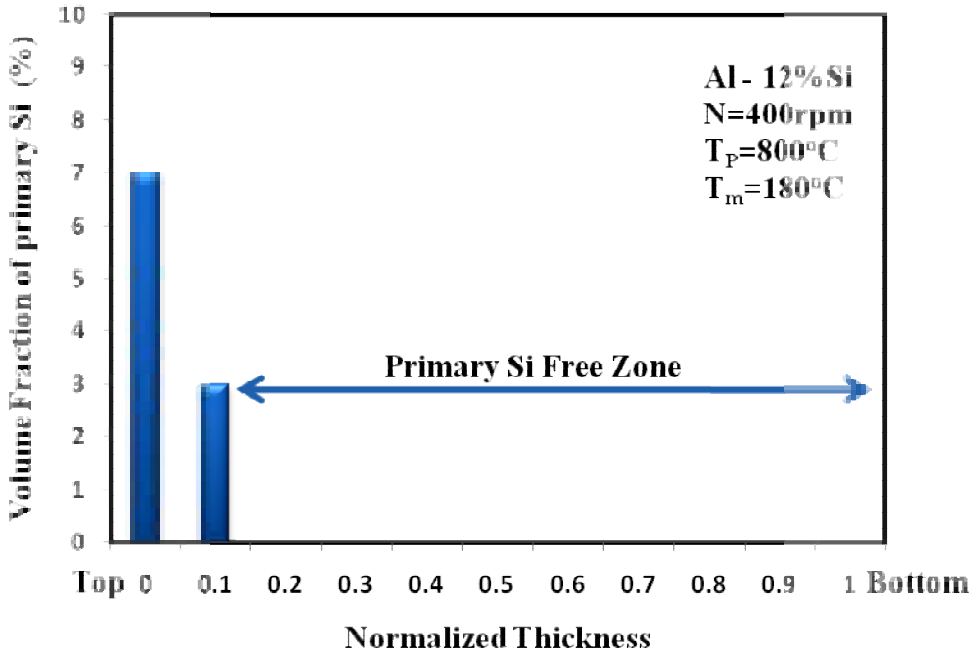

Fig. 4.13 Distribution of primary Si from top end to bottom end for Al-12wt%Si FGM cast at, T_P=800°C, T_m=180°C, G=89.42(400rpm).

For the same alloy the effect of increased teeming temperature on the volume fraction of the primary Si is studied by increasing T_P from 800^{o}C to 900^{o}C and pouring the alloy into mold held at room temperature and preheated to 180^{o}C. The microstructure and the bar chart for the segregated primary Si are shown in Figs. 4.14 to 4.25. From the microstructure and the bar chart it is evident that the volume fraction of the primary Si and also its distribution along the length of the specimen from the top face improves significantly for higher values of T_P, T_m and rpm (G factor). At T_P=900^{o}C, T_m=180^{o}C and rpm of 400 primary Si is 9% at the top and decreases uniformly to 2% at a distance of 7mm from the top.

From the micrographs we can see that the cast FG alloy specimen consists of hypoeutectic structure at the bottom and hypereutectic structure at the top. There is a gradual transition from hypereutectic to hypoeutectic structure with the middle part of the specimen showing near eutectic structure. Under high G forces the bottom part of the casting consists of primary α-dendrites and (α+β) eutectic (Fig. 4.4) and the amount of the (α+β) eutectic is more than that of the primary α-dendrites (Fig. 4.12). Further increase in speed produces a structure consisting of plate shaped particles of β-phase (Fig. 4.6) in a continuous matrix of Al-rich α solid solution. The thickness of the plates are very small compared to its length and most of the plates are isolated and are not connected with each other. The plates are randomly oriented in the matrix of the α phase. Further increase in G force makes the solidification with the formation of primary β crystals in the melt. As the solidification progresses, the amount of the β phase gradually increases at the expense of the liquid. The final microstructure consists of the primary β Si phase crystals and the eutectic (α+β) phase.

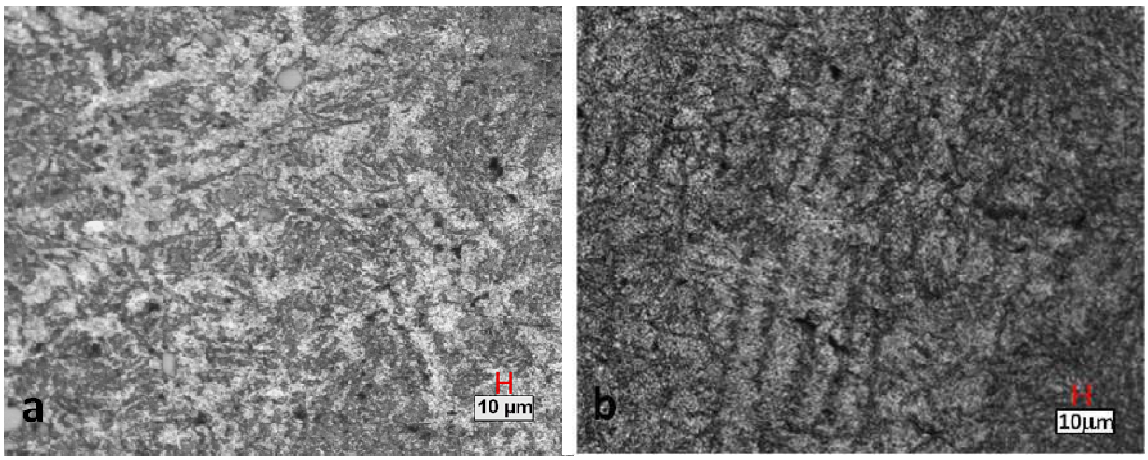

Fig. 4.14 The microstructure of the Al-12wt%Si FGM cast at, T_P=900^oC, T_m=Room temp G=22.3(200rpm). a) Top end showing primary Si, b) Bottom end showing α-Al dentritic structure

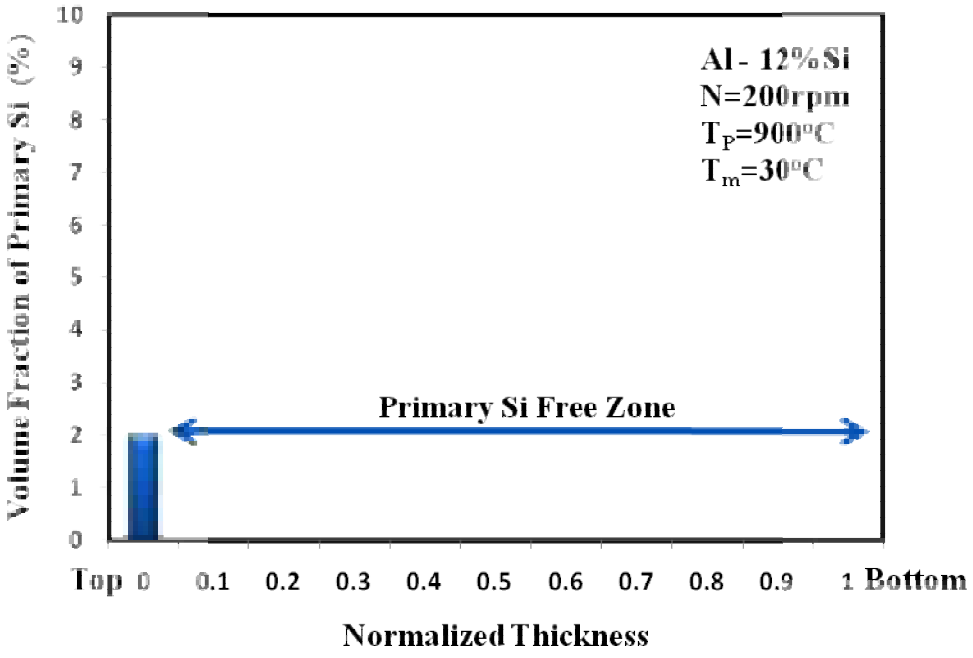

Fig. 4.15 Distribution of primary Si from top end to bottom end for Al-12wt%Si FGM cast at, T_P=900^oC, T_m=Room temp, G=22.3(200rpm).

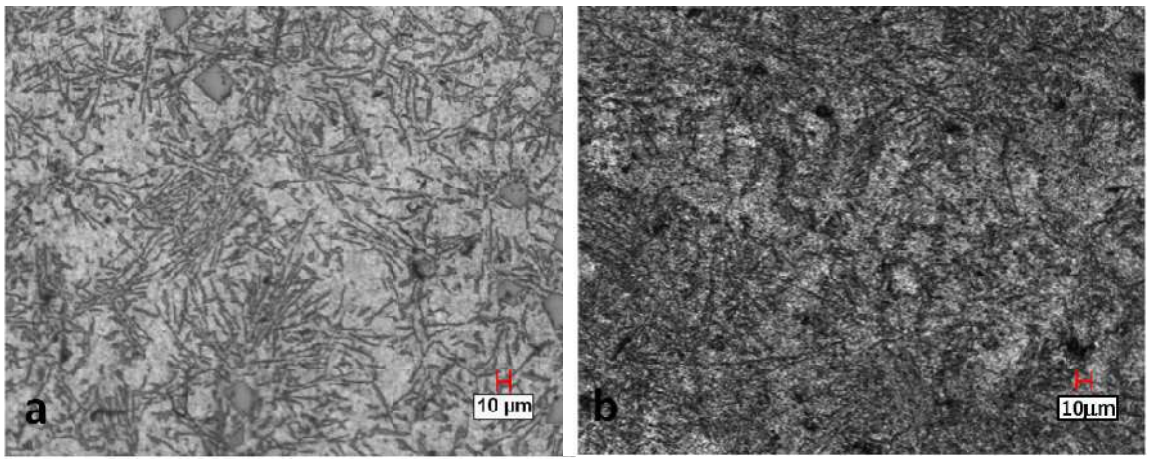

Fig. 4.16 The microstructure of the Al-12wt%Si FGM cast at, T_P=900°C, T_m=Room temp G=50.3(300rpm). a) Top end showing primary Si, b) Bottom end showing α-Al dentritic structure

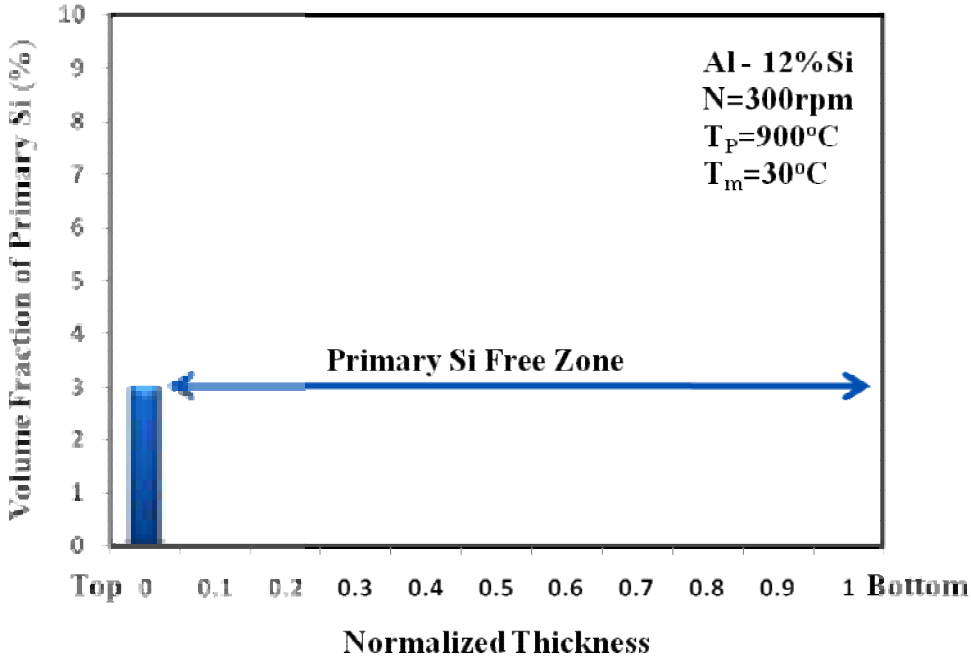

Fig. 4.17 Distribution of primary Si from top end to bottom end for Al-12wt%Si FGM cast at, T_P=900°C, T_m=Room temp, G=50.3(300rpm).

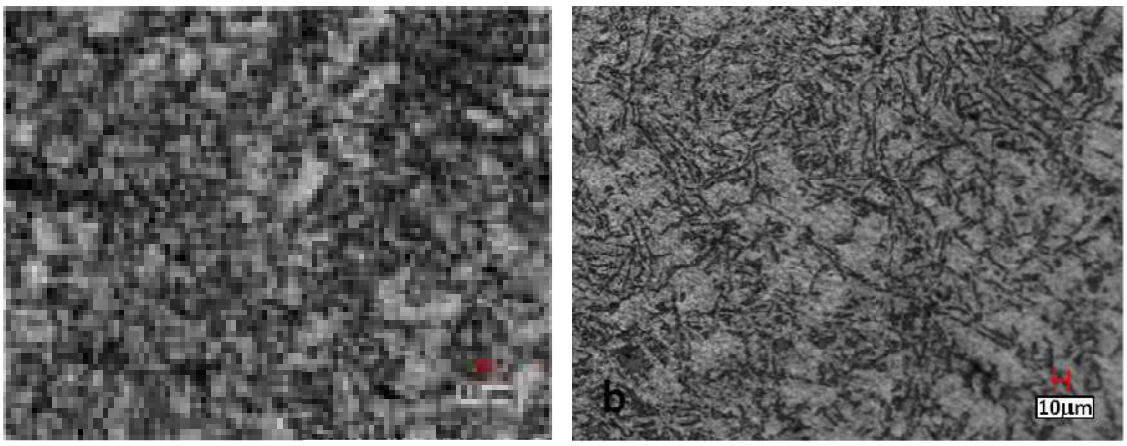

Fig. 4.18 The microstructure of the Al-12wt%Si FGM cast at, T_P=900°C, T_m=Room temp G=89.42(400rpm). a) Top end showing primary Si, b) Bottom end showing α-Al dentritic structure

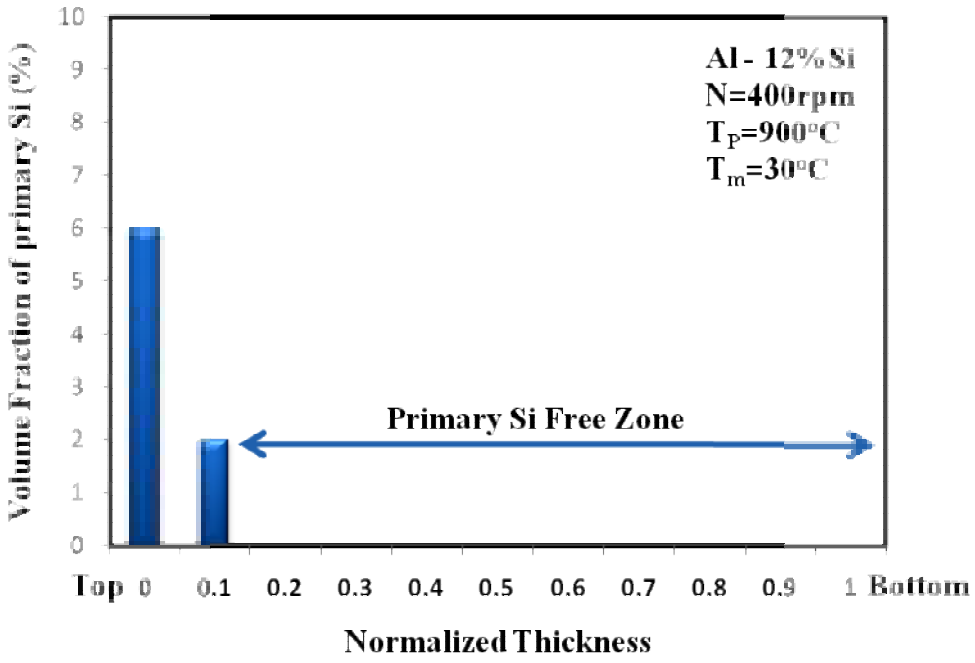

Fig. 4.19 Distribution of primary Si from top end to bottom end for Al-12wt%Si FGM cast at, T_P=900°C, T_m=Room temp, G=89.42(400rpm).

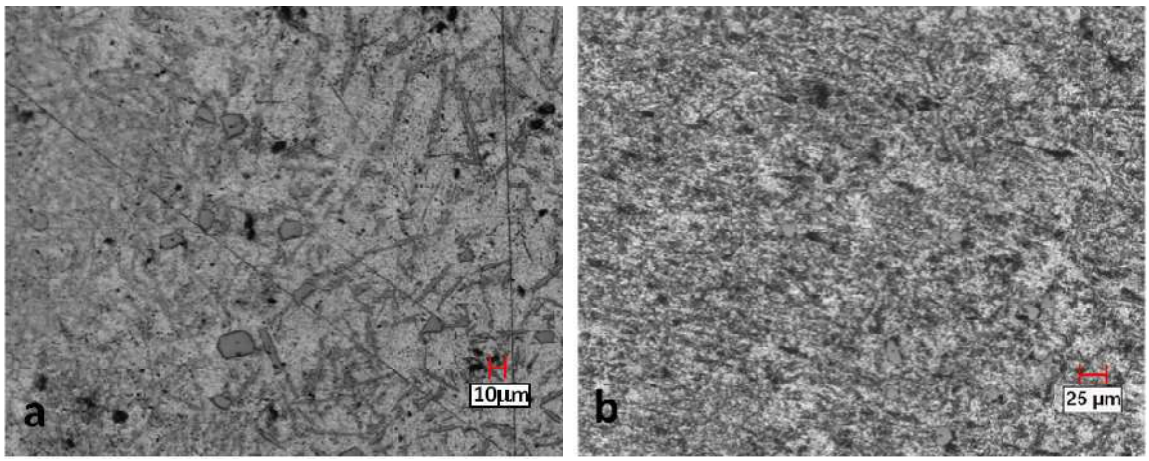

Fig. 4.20 The microstructure of the Al-12wt%Si FGM cast at, T_P=900°C, T_m=180°C G=22.3(200rpm). a) Top end showing primary Si, b) Bottom end showing α-Al dentritic structure

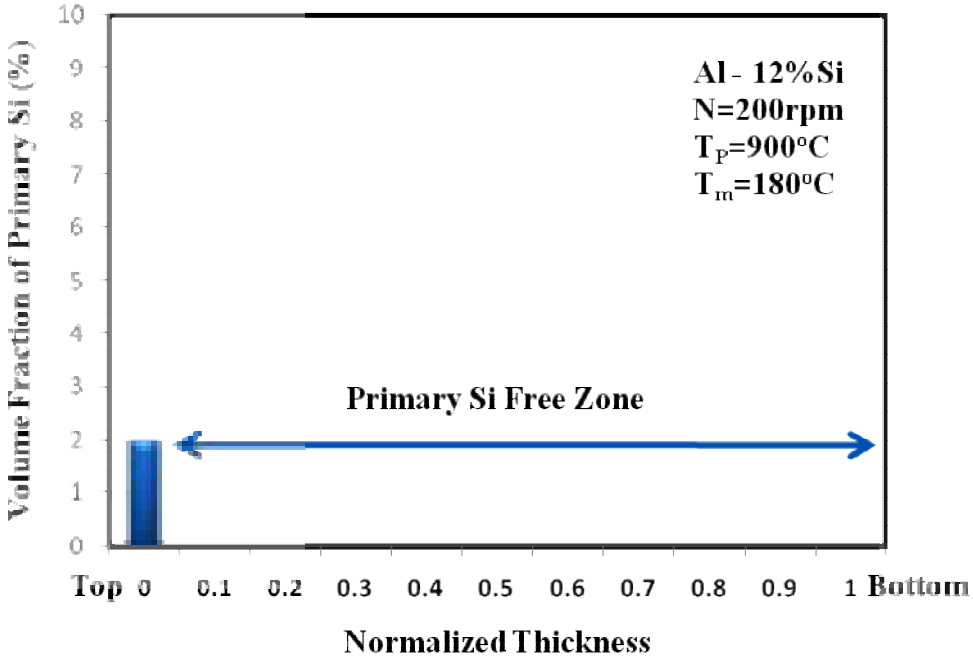

Fig. 4.21 Distribution of primary Si from top end to bottom end for Al-12wt%Si FGM cast at, T_P=900°C, T_m=180°C, G=22.3(200rpm).

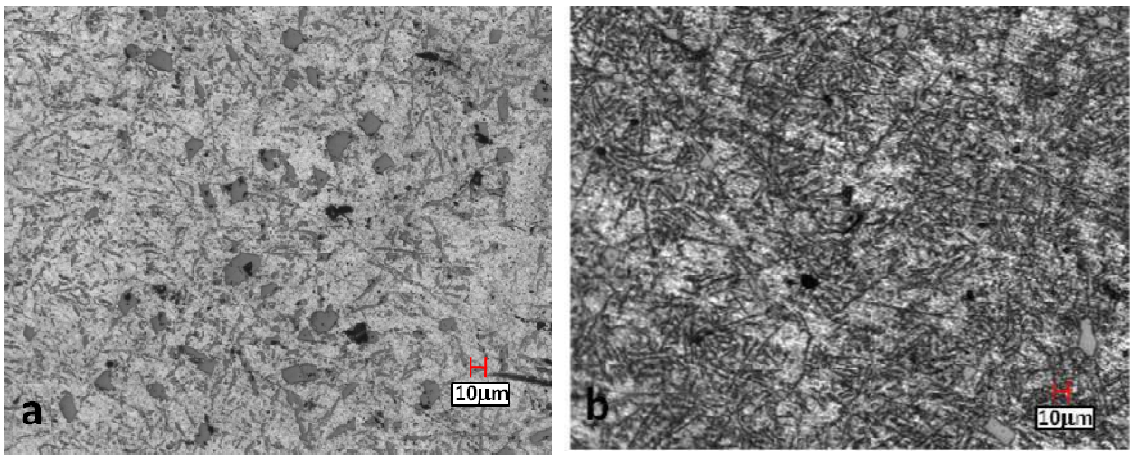

Fig. 4.22 The microstructure of the Al-12wt%Si FGM cast at, T_P=900°C, T_m=180°C G=50.3(300rpm). a) Top end showing primary Si, b) Bottom end showing α-Al dentritic structure

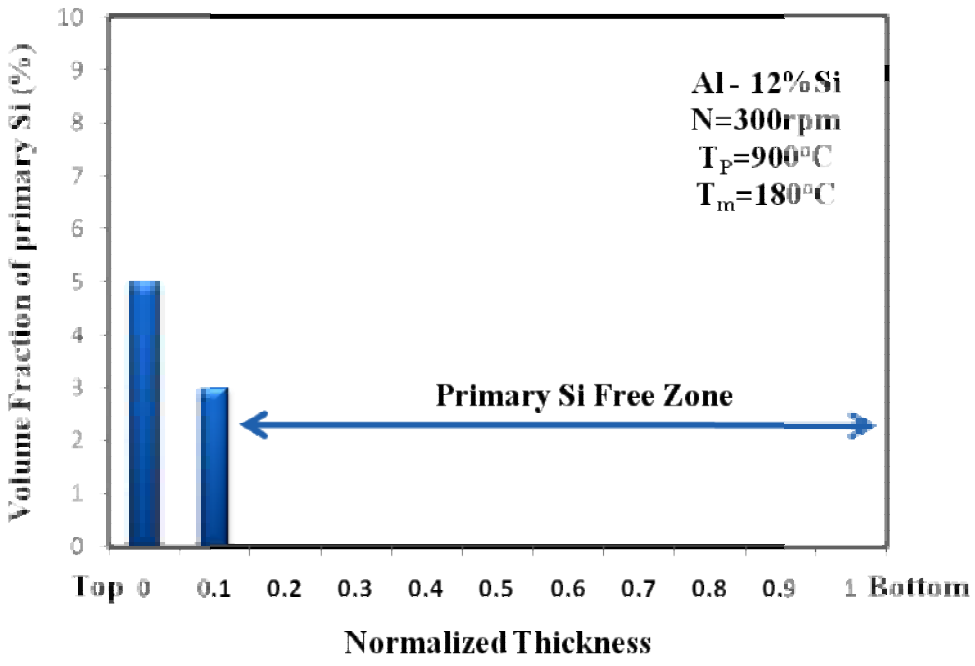

Fig. 4.23 Distribution of primary Si from top end to bottom end for Al-12wt%Si FGM cast at, T_P=900°C, T_m=180°C , G=50.3(300rpm).

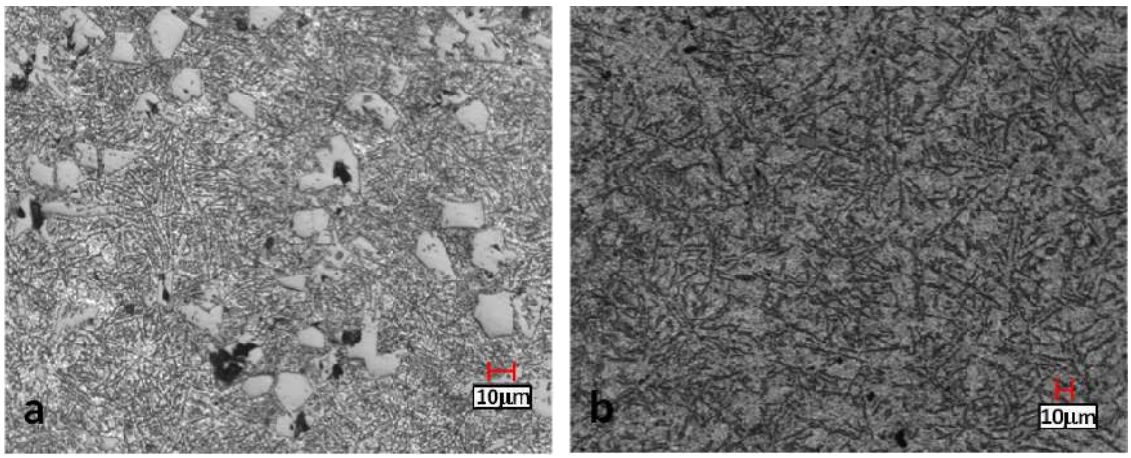

Fig. 4.24 The microstructure of the Al-12wt%Si FGM cast at, T_P=900°C T_m=180°C G=89.42(400rpm). a) Top end showing primary Si, b) Bottom end showing α-Al dentritic structure

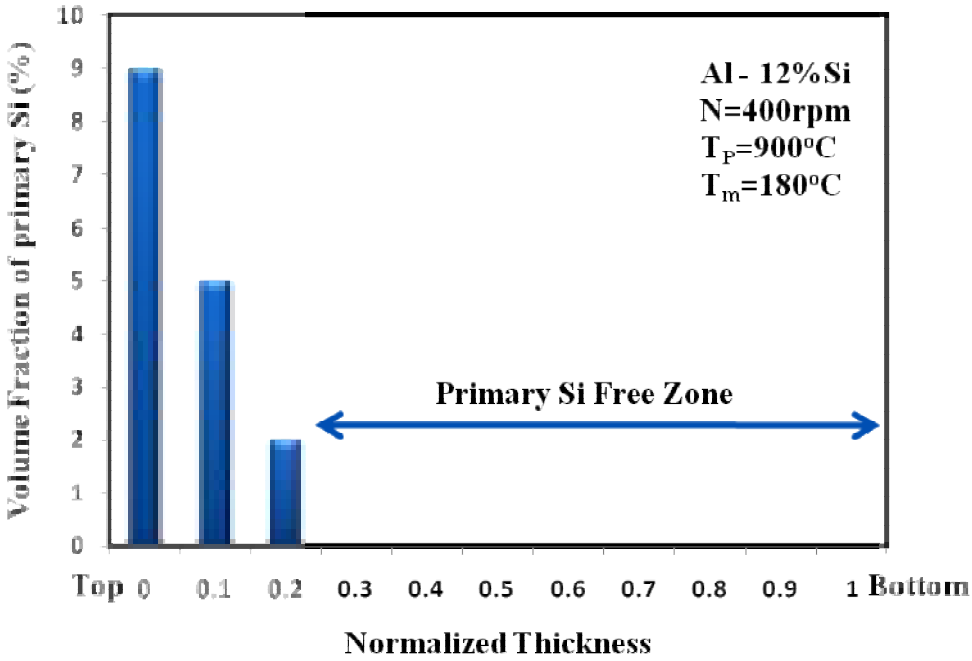

Fig. 4.25 Distribution of primary Si from top end to bottom end for Al-12wt%Si FGM cast at, T_P=900°C, T_m=180°C, G=89.42(400rpm).

It is observed that at lower G forces the eutectic microstructure changes from one end of the cylindrical specimen to the other end (i.e. along the length) with a non-uniform distribution of needle-like Si particles in the matrix of α-Al. As the G force is increased microstructure exhibits primary Si crystals along with needle-like eutectic Si phase thus signifying a hypereutectic microstructure as shown in Fig. 4.24.

The microstructures of the alloy solidified under different rpms clearly indicate that the centrifugal force generated due to centrifuging of the melt, greatly influences the solidification features of materials. For the specimen cast in the ingot, the microstructure consisted of a fine chilled zone and a coarse columnar zone (Fig. 4.26). However applying G forces on the melt resulted in reduction of the chill zone and the coarse columnar structure transformed to equiaxed structure in the top portion of the specimen. At the same time, fine columnar structure formed at the bottom portion of the casting. With the onset of solidification, elongated eutectic starts to form. When the G force was further increased, more pro-eutectic phase was frozen, the rod like eutectic and pro-eutectic structure steadily increased in quantity. With further increase in G force, the eutectic in the top portion turned into a blocky structure whose morphology no more remained as typical of needle eutectic. Refinement of the solidification structure was observed with increasing values of G force. Employing still higher G force lead to higher porosity in the top region of the casting (Zhang et al 1998).

Fig. 4.26 The macrostructure of the as-cast specimen

During the mold rotation, the particle suspended in the liquid is subjected to both centrifugal force and gravitational force. Since the centrifugal force acting on the particle is G times higher than the gravitational force, the latter can be considered as negligible when compared to the former. Thus, as the rotational speed increases, the force acting on the particles to segregate should also increase and the same has been observed in this investigation. The volume fraction of the Pro-Eutectic Si obtained at the top surface also increases with increasing speed (Fig. 4.25) (Panda et al 2006)

Micro structural examinations revealed that the structure of the specimens cast by this method was quite different from those of ingot specimens. This result has revealed that, under the equilibrium conditions, a eutectic alloy can have a hypoeutectic structure due to rapid cooling. Depending on the fastest growing phase at a given undercooling condition, a structure which consists of both primary and eutectic or only the latter develops. In the aluminium-silicon system, the primary aluminium rich phase grows dendritically, whereas the silicon grows in a facetted manner. Comparing with metallic phase α-Al, the non metallic phase Si facetted grows slower at the undercooling. The relatively low under cooling application on an eutectic alloy of a given composition causes dendritic growth in which one of the phases grows rapidly and the other phase solidifies between dendrites while higher undercooling leads to cellular growth. Based on the above statements, we conclude that the difference between microstructures of both sides is resulted from different cooling rates.

The FG eutectic alloy obtained at 200rpm hasn't revealed any primary Si at the top surface whereas castings prepared at 300 and 400rpm have shown improvement in the amounts of primary Si. This clearly signifies the importance of the G force in producing the FGM. It can be noted that as the G force is increased the segregation of the primary Si particles is increased at the top end of the casting.

4.2.1.2 Effect of Teeming Temperature (T_P) and Mold Temperature (T_m)

Several parameters determine the microstructure and distribution of particles inside the casting (Castro et al 2002). In centrifugal casting, the heat is removed only from the mold wall during solidification of the casting. Hence, the solidification rate of the centrifugal casting can be controlled by the heat transfer between the casting and the mold wall. Increasing the melt temperature and mold temperature can control heat transfer between the mold and the casting (Vassiliou et al 2008). In the present study, the melt was teemed at two different temperatures, 800^{o}C and 900^{o}C. The mold was maintained at two different temperatures, room temperature and at 180^{o}C, before the liquid metal was poured into it.

The histograms show that at 200rpm the volume fraction of primary Si at the top of the casting is zero for a teeming temperature of 800^{o}C and mold at ambient temperature. An increase in mold temperature to 180^{o}C clearly showed precipitation of 2% primary Si at the top. At 300rpm it is found that without preheating the mold, primary Si is 2% and with preheating the mold the primary Si substantially increased to 4%. It is found that further increase in speed to 400rpm increased the primary Si to 4% without preheating the mold but increase in temperature of the mold to 180^{o}C accomplished a primary Si of about 7% at the top of the casting.

Increase in teeming temperature shows drastic improvement in the formation of primary Si at the top of the casting and at 900^{o}C teeming temperature and mold at room temperature, primary Si is 2% at 200rpm. It increased to 5% at 300rpm and with preheating the mold to 180^{o}C. At 400rpm without preheating the mold the primary Si is found to be 6% but an improvement of 50% is noticed when the mold temperature is raised to 180^{o}C i.e. 9% primary Si precipitated at the top of the casting.

At the mold speed of 200rpm and without preheating the mold, no primary Si segregation was found in the microstructure. With increase in mold temperature, a segregated region was observed and further to this, increase in teeming temperature increased the precipitation of primary Si at the top of the casting. Further the

percentage of primary Si shows better improvement under higher T_P and T_m when the mold speeds are higher.

This clearly confirms that the teeming temperature, mold temperature and the rpm (G factor) together influence the precipitation of primary Si during the solidification when cast using the centrifuge action.

The influence of mold temperature on the gradient of Si inside the casting can be clearly visualized after knowing the solidification behavior of the centrifuge casting. It is assumed that the mold temperature will be constant until the liquid metal fills the mold and the centrifugal force is applied later.

It is seen that when the mold is not preheated and liquid temperature is 800^{o}C, a steep temperature gradient at the mold is expected. The higher difference in temperature (ΔT) causes lower heat transfer coefficient ($h=Q/A\Delta T$) at the mold liquid interface. This results in higher solidification rate. As the mold temperature is increased, the temperature gradient is reduced. This results in decrease of the heat transfer coefficient at the casting mold interface, leading to a slower solidification rate. At the slower solidification rate, the time for primary silicon to grow from the melt will be longer compared to that of a higher solidification rate.

The microstructures of the castings obtained by centrifuge casting show that the crystallization conditions of the melt differ in principle from top to bottom of the casting. The rotating mold in centrifuge casting makes the molten metal to rotate. In a short time the melt becomes virtually immobile in the rotating mold. At the same time, all the structural components are affected by centrifugal and centripetal forces. This situation is responsible for stratification with respect to the specific weight as well as sedimentation and floatation of solids from liquids, The light particles float to the top region and the heavier particles concentrate at the bottom of the casting (Potekhin et al 2009).

For centrifugal in-situ casting method of an alloy system of type A-B, in which A makes a matrix (Y Watanabe et al 2005b), it is reported that:

- Due to density difference and effect of centrifugal force and solidification rate, there will be a segregation of A and B metals in the liquid state.

- A chemical composition gradient is formed before the crystallization of the primary phase.

- The primary crystal to appear in the matrix will depend on local chemical composition.

- The primary crystal migrates according to density differences and a further compositional gradient is formed.

In the centrifuge casting of Al-Si eutectic alloy, during the early stage of the centrifugal in-situ method partial separation of aluminum and Si in the liquid state occurs. It results in the formation of a chemical compositional gradient prior to the crystallization of primary crystals such that, the chemical composition from the top to bottom region varies from hyper-eutectic to hypo-eutectic.

4.2.2 Hardness

In FGMs produced by centrifugal action as in centrifuging, it is expected that the properties vary with respect to the direction of centrifugal force. The segregation of hard particles or phase towards one side of the specimen will significantly improve the mechanical and tribological properties. This phenomenon is made use of to improve the mechanical properties such as hardness and tribological property such as wear. Further as seen in the literature review the improved mechanical and tribological properties are influenced by mold rotational speed, mold temperature and melt temperature.

From the results discussed in the previous section, due to the difference in density of the Si with respect to Al, primary Si is pushed to the top of the cylindrical specimen. The centrifugal force progressively increases the volume fraction of the Si within the liquid Al along the length of the specimen, owing to the density difference between the two materials (ρ_{Al} =2700 Kg/m^3 and ρ_{Si} =2300 Kg/m^3).

In this section the results of variation in hardness along the length of the specimen is explored in order to understand the effect of amount of primary Si segregated at different regions from top to bottom of the specimen. The percentage of primary Si segregated is a function of rotational speeds, melt temperatures and mold temperatures.

4.2.2.1 Effect of rotational speed (G Force)

The hardness for Al-12wt%Si FGM is plotted for three rpm's under combination of two teeming temperature and two mold temperatures. Hardness measurements are made at five locations as detailed in Fig. 3.9 and the average value of three close readings is considered. The graphs are shown in Fig. 4.27 to Fig. 4.30. Under teeming temperature of 800^{o}C and without preheating the mold, it is seen that the hardness for the casting obtained at 200rpm does not show much of the gradient and the hardness varies from 48 to 52 BHN from bottom to top of the casting. No significant change in hardness variation is observed in the specimen cast at 300rpm. The FGM cast at 400rpm has however shown some improvement in the hardness variation with top of the casting having a hardness of 54 BHN.

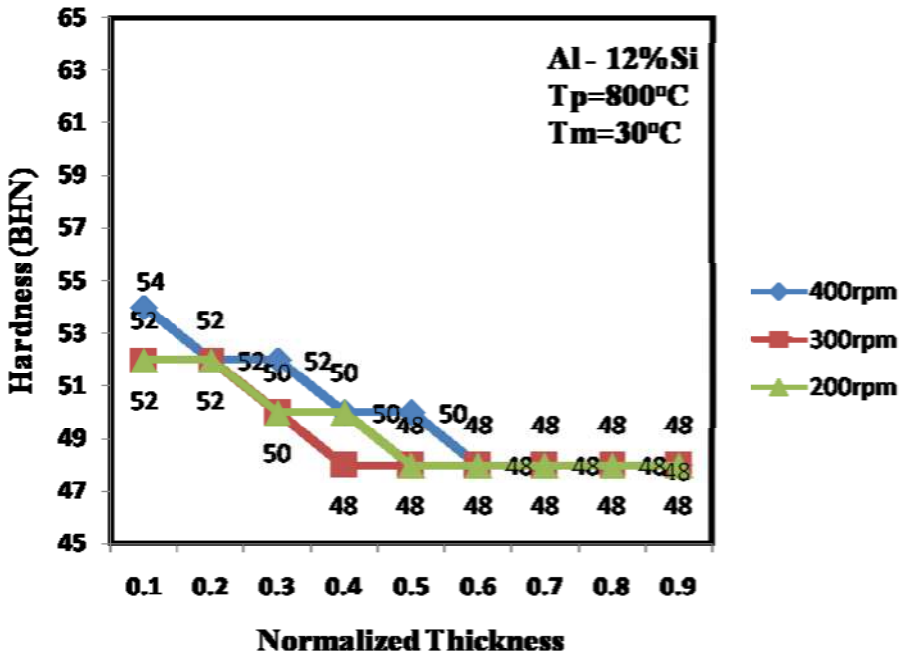

Fig. 4.27 Hardness of Al-12wt%Si FGM along the length of the casting for 800°C melt temperature without preheating the mold.

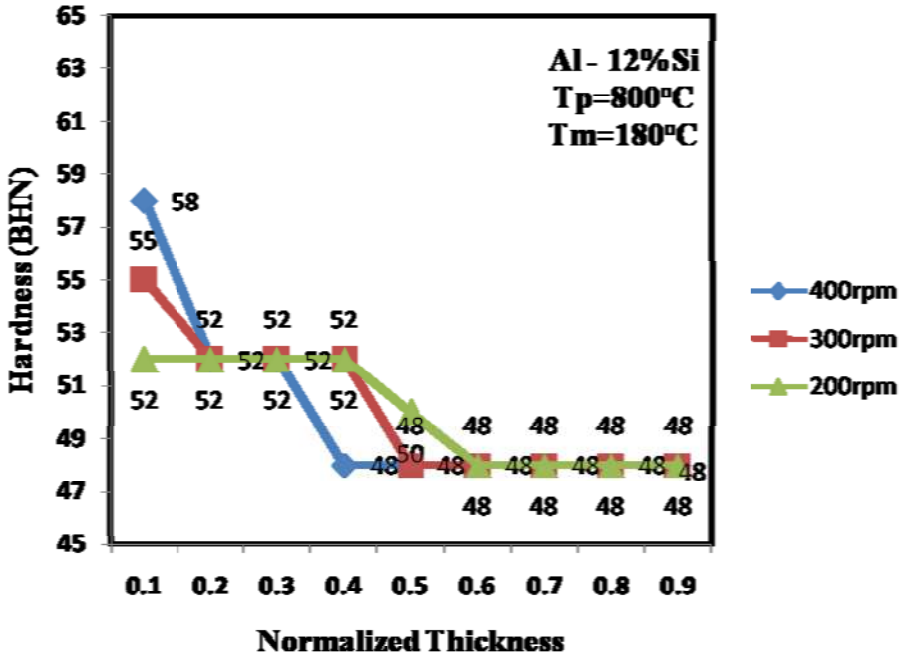

Fig. 4.28 Hardness of Al-12wt%Si FGM along the length of the casting for 800°C melt temperature with preheating the mold at 180°C.

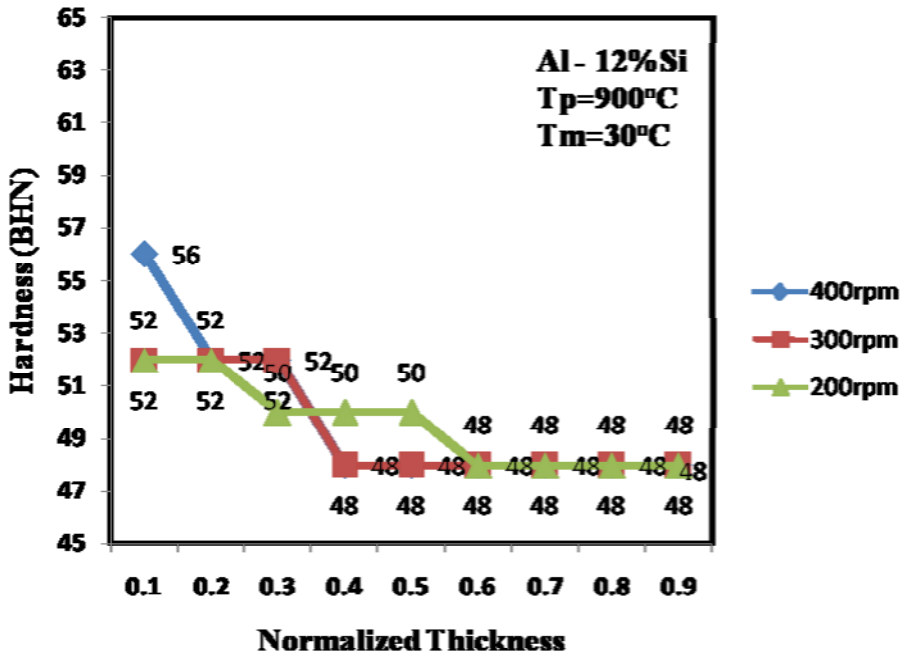

Fig. 4.29 Hardness of Al-12wt%Si FGM along the length of the casting for 900°C melt temperature without preheating the mold.

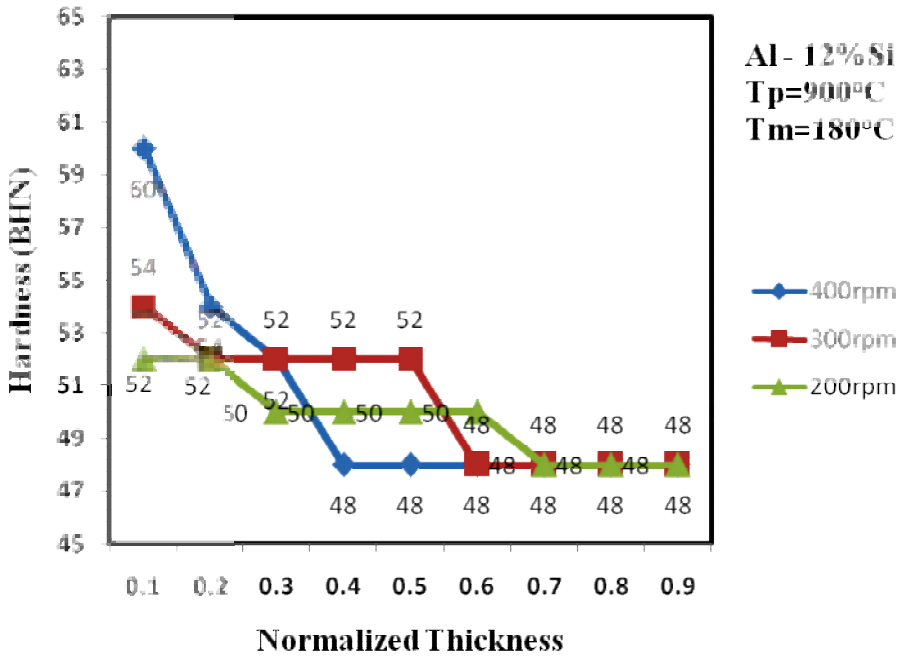

Fig. 4.30 Hardness of Al-12wt%Si FGM along the length of the casting for 900°C melt temperature with preheating the mold at 180°C.

With the preheating of mold to 180^{o}C, at 200rpm the variation in hardness is not much altered as compared to the earlier results, but at 300rpm the hardness improved from 52 BHN to 55 BHN at the top face. Further at 400rpm the hardness was measured as 58 BHN.

The values of hardness at the bottom and top face of the specimen cast under teeming temperature of 900^{o}C and without preheating the mold conditions at 200, 300 and 400 rpm were 48 to 52 BHN, 48 to 52 BHN and 48 to 56 BHN respectively.

Similarly castings produced with teeming temperature of 900^{o}C and mold temperature of 180^{o}C have shown corresponding hardness variations as 48 to 52 BHN, 48 to 54 BHN and 48 to 60 BHN.

From the above results it can be said that the hardness at the top face of the specimen has improved with higher rotational speed of the mold under both conditions of melt and mold temperatures. The factor contributing to the hardness of the specimen is the amount of primary Si (hard phase) that has segregated in varying volume fraction from top face to the bottom of the specimen. The improvement in hardness values from bottom to top face of the specimen with increasing rpm indicate that the primary Si volume fraction at the top face has increased. This is in agreement with results of microstructure discussed in the previous sections. Similar results are reported by researchers while producing hollow cylindrical specimens using centrifugal casting technique. The authors have made the inference that at the same rotation speed, firstly, Si contents drop sharply from external to internal casting walls and then rise slowly. If the mold rotation speed rises, the centrifugal force acting on heavy particles intensifies segregation of Si in casting section (Halvaee et al 2001). Severe segregation of Si at higher rotation speeds is due to rejection of the liquid metal rich in Si from dendrites.

Goa et al (2000) have identified three factors to be responsible for creation of the particle concentration gradient: the geometrical nature of particle flow in the cylindrical mold, the angular velocity and the solidification rate, which captures the

desired gradient — it is the interruption of particle migration by the solidification front that creates gradients in the particle concentration. It is also predicted that in centrifugal casting the particle segregation depends on the solidification time and solidification time is dependent on one of the process parameters - rotational speed of the mold, decreasing with an increase in speed (Kang et al 1996). The primary Si segregated at the top of the casting (increased volume fraction) leads to better hardness, mechanical properties and wear resistance (Rajan et al 2009). These observations further provide the basis for the graded distribution of primary Si and the hardness obtained in the current work.

4.2.2.2 Effect of Teeming Temperature (T_P) and Mold Temperature (T_m)

The results of the hardness presented in the previous section for Al-12wt%Si FGM indicate that at lower mold speeds the segregation of Si is lower. The segregation of the particles also depends on the solidification time. So by increasing the solidification time i.e, decreasing the solidification rate it is possible to increase the volume fraction of the particles in the direction of the centrifugal force depending on the density difference between melt and reinforcement (Panda et al 2006). By decreasing the solidification rate the time for melt to solidify will be increased. This, in turn, gives more time for the particles to precipitate and segregate within the melt (Kumar et al 2010). Based on this fact, experiments were conducted at two values of teeming and mold temperature for the three rpm's studied above.

For the same mold rotational speed, higher mold and melt temperatures resulted in significant improvement in the hardness and also variation in the hardness from the bottom to the top of the casting. Changes in hardness or hardness gradient are not significant at 200rpm even if the melt and mold temperatures are increased. At 300rpm an increase in mold temperature has increased the hardness by 5% at the top of the casting while there is no effect due to increase of the teeming temperature.

At 400rpm, it was noted that by increasing the mold temperature an increase of 7.4% in hardness was recorded. Similarly by increasing the teeming temperature, an

increase of 3.7% in hardness was noted, but combined effect of temperatures i.e an increase in mold temperature and increase in teeming temperature yielded an increase in hardness of 11.11%. This result further supports the higher degree of segregation of primary Si, at higher melt and mold temperatures.

4.2.3 Wear

Loss of material is one of the prime areas at presently engaging the attention of most of the technologists. One of the outcomes expected out of this investigation is to realize that the highly potential Al-Si alloy, if functionally graded, should be capable of replacing some of the conventional materials in the automotive, aircraft and aerospace industries where the tribological properties of the materials are a major requirement (Sarkar et al 1980), (Subramanium et al 1991), (Dwivedi et al 2001), (Bai et al 1987), (Jasim et al 1987). The industrial interest in FGMs is mainly related with the opportunity of controlling the gradation of the physical and/or chemical properties, through microstructural manipulation.

Functionally graded alloy materials contain the alloying phase with its volume fraction varying continuously from the inner to the outer sections of the part thereby providing for a controlled non-uniform microstructure with continuously changing properties. This balance of properties may not be achievable in many cases in monolithic or homogeneous alloys when cast by conventional methods. In FGM we can achieve a material wherein the external zone of the casting will present higher, harder alloying phase content, strongly affecting the wear resistance, while the inner zone will be mainly constituted by matrix presenting high toughness. The process parameters also affect the gradation pattern.

In this study the effect of centrifuge process and the parameters such as centrifugal force, melt temperature, mold temperature are studied with reference to gradation of primary Si in Al-12%Si alloy with respect to specific wear rate and coefficient of friction.

4.2.3.1 Specific Wear rate

Previous sections indicate that the cast FGM specimens have two structures at the top and bottom of the casting that are totally different in their nature i.e., hypereutectic and hypoeutectic respectively. Wear tests are conducted to determine specific wear rate under different normal loads with constant sliding distance and at a constant sliding speed. The specific wear rate is a function of volume loss, sliding distance and normal load. Generally, under the constant sliding distance the specific wear rate is inversely proportional to the normal load. The actual area of contact becomes equivalent to the nominal area with the increase in the normal load on the pin, resulting in an increase in the magnitude of the frictional force between the pin and the disc and hence an increase in the magnitude of wear. Presence of asperities between the contacting surfaces determines the magnitude and nature of wear. It has been examined by the earlier investigators that the abrading particles start penetrating the softer of the two metals, leading to the introduction of cracks due to surface stresses which in turn result in the breakdown of the surface. Wear resistance is one of the important dependent parameters which can describe the wear process quantitatively.

Figs. 4.31 through 4.34 show the specific wear rate for the top and bottom parts of the castings produced at different mold speeds, mold temperature and teeming temperature. It is clearly observed that the specific wear rate for a specific load is more at the bottom surface of the casting than at the top of the casting surface. It is also noticed that the specific wear remains constant at the bottom of the casting for a specific load for different mold speeds.

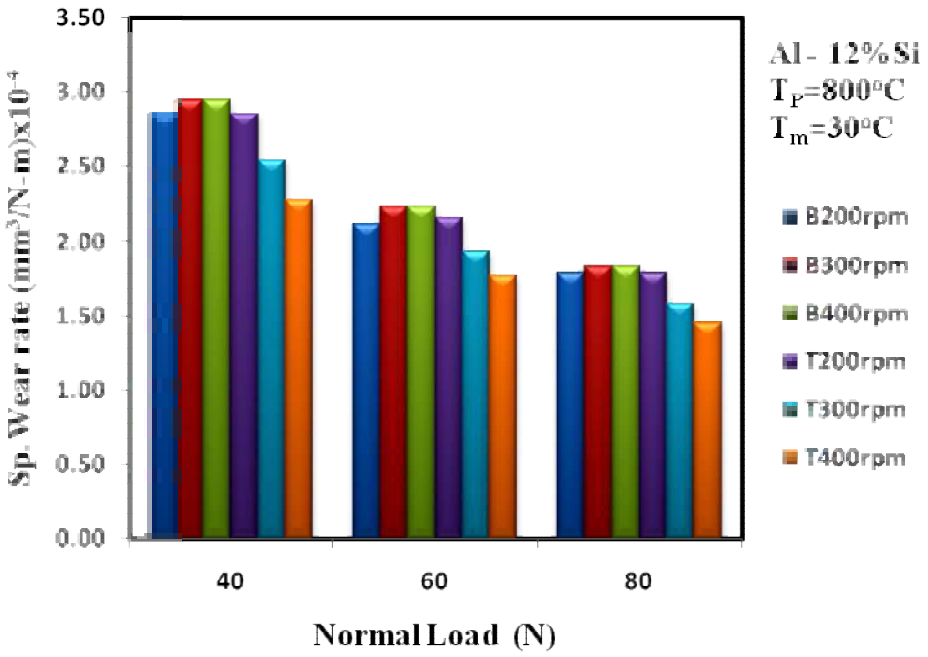

Fig. 4.31 Specific wear rate of Al-12wt%Si FGM vs Normal load of the casting for 800^{o}C melt temperature without preheating the mold.

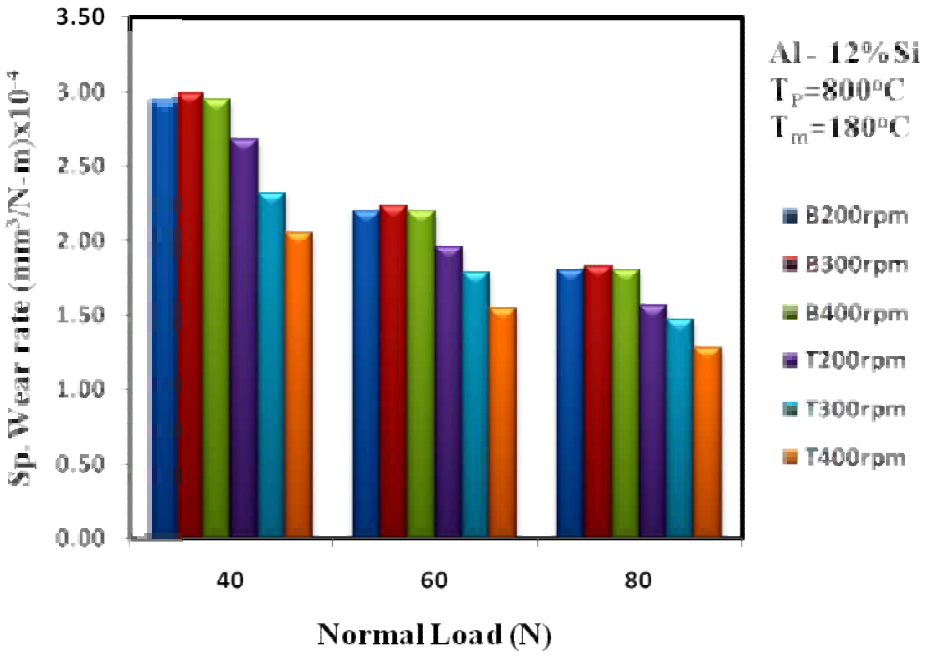

Fig. 4.32 Specific wear rate of Al-12wt%Si FGM vs Normal load of the casting for 800^{o}C melt temperature with preheating the mold.

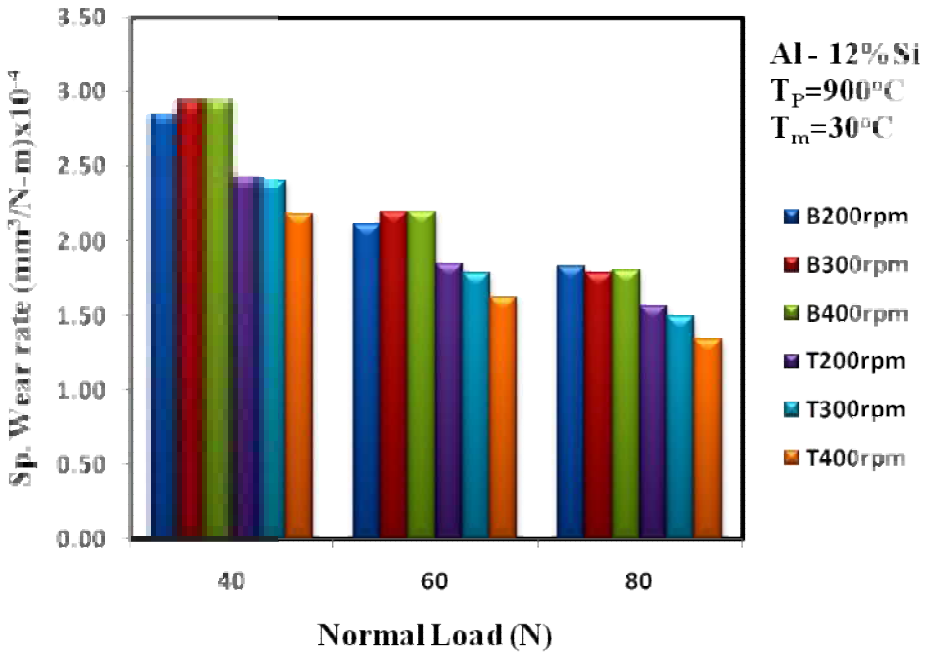

Fig. 4.33 Specific wear rate of Al-12wt%Si FGM vs Normal load of the casting for 900^{o}C melt temperature without preheating the mold.

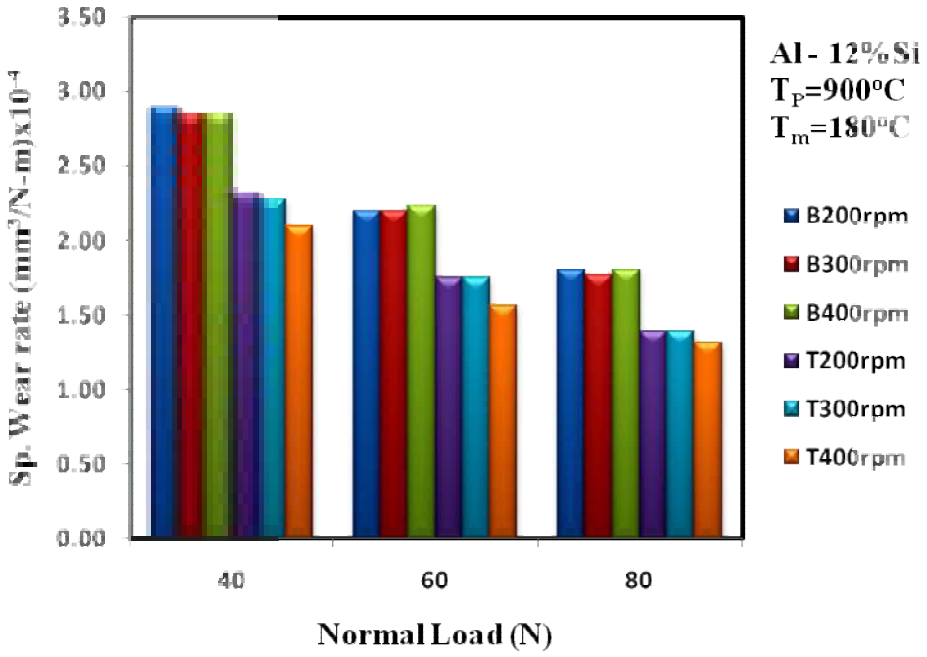

Fig. 4.34 Specific wear rate of Al-12wt%Si FGM vs Normal load of the casting for 900^{o}C melt temperature with preheating the mold.

Table 4.1 shows the percentage decrease in specific wear rate at the top surface of the casting manufactured at 900^{o}C teeming temperature, 180^{o}C mold temperature and at 400rpm as compared to those of other castings. It has also been noticed that castings produced at higher speeds show lesser specific rate compared to the lower speeds

Table 4.1 Percentage decrease in specific wear rate for the castings produced using 900^{o}C T_P, 180^{o}C T_m at 400rpm in comparison with other castings.

Rpm	**T_P (^{o}C)**	**T_m (^{o}C)**	Decrease of sp. wear rate in %		
			40N	**60N**	**80N**
400	900	30	6.53	4.81	4.35
	800	180	2.17	0.96	2.61
	800	30	10.87	14.42	13.04

From the Figs. 4.31-34 it can also be seen that there is a significant improvement in the specific wear rate for the castings produced at higher mold and teeming temperatures. By improving the mold temperature from room temperature to 180^{o}C an improvement of 4.3%, 7.2% and 12% in the SWR is achieved at 400rpm, 300rpm and 200rpm respectively for 80N normal load at 900^{o}C teeming temperature.

The mold rotational speed has a very significant effect on the specific wear rate. At a constant teeming temperature and mold temperature it is found that the specific wear rate decreased for specimen cast at higher mold speeds. It is also seen that there is no significant effect of mold rotational speed as far as the lower part of the casting. At the bottom region it is found that on an average the specific wear rate remains constant for all samples for different process parameters. The decrease in the specific rate at the top can be attributed to the more amount of Si present at the top of the casting which has been revealed through microstructure and hardness studies. Crack nucleation generally occurs at some depth below the surface, rather very near to the surface, owing to the very high hydrostatic compressive pressure acting near the asperity contact. Thus, once a crack is nucleated, its propagation is slow and seizure

does not occur, owing to the presence of well distributed particles in the matrix (Jahanmir et al 1977).

The specific wear rate is distinctly different for the top and bottom surfaces. The toughness and strength of the FG alloy increases with the presence of primary Si which leads to decreased wear rate as compared to the bottom region where primary Si is absent. This could be due to the fact that at lower silicon content dislodging of material is more when compared to the higher silicon content.

4.2.3.2 Coefficient of Friction (COF)

Figs. 4.35-38 provide evidence that the coefficient of friction increases uniformly with increasing load. The COF testing of the top of the casting was lower than that of the bottom of the casting at all the normal loads. It is attributed to the density difference between the Si and Al matrix, wherein Si is having lower density compared to Al which caused Si to push towards the top of the casting. Here more amount of harder Si will lead to reduced COF.

From Figs. 4.35 to 4.38 we can see that COF remains constant at a specific load for the bottom of the casting. Whereas at the top of the cast specimen, COF is different for different castings and it is also lower for castings produced at higher rpm. The COF castings produced at 800^{o}C teeming temperature without preheating the mold at 40N normal load was found to be 0.52 for the castings at 200rpm and 0.47 for 400rpm. The same trend continued for the 60N and 80N also. It is seen that by increasing the mold temperature for the same teeming temperature the COF decreased to 0.51 and 0.46 for the castings produced at 200 and 400rpm respectively. By increasing teeming temperature to 900^{o}C and mold temperature to 180^{o}C the COF reduced significantly to 0.47 and 0.45 for the castings produced using the speeds of 200 and 400rpm respectively.

It is also found that the COF gets reduced in sample cast at higher rotation speed at the top of the specimen for a given mold and teeming temperature. It is

clearly mentioned in the previous sections that as the speed increases the G force on the melt increases. This allows more Si to be pushed to the top of the casting in the direction opposite to the direction of the centrifugal force. Similarly keeping the mold rotation speed constant and increasing the mold and teeming temperature it is found that the COF is decreased for samples made with higher teeming temperatures. This high temperature allows more time for the solidification of the melt giving more time for the precipitation and segregation of the Si at the top of the casting.

It has been found that there is a sudden increase in the friction coefficient at very high loads indicating adhesion of the pin to the sliding surface. Such adhesion was due to the seizure of the pin on to the disc. The rise in the COF with increase in wear load may be attributed to the enhanced true area of contact resulting in rupture of Al_2O_3 further causing cross welding of surfaces. The deep furrows on the pin surface may also be accounted for by the cutting action of the hard particles of Si or Al_2O_3 formed. A simultaneous work hardening of the matrix by plastic deformation helped in reducing the extent of wear of the samples at high normal loads. During wear at normal loads, the temperature increases appreciably lowering the strength of the materials in contact resulting in increased contact area and COF. Rise in temperature within limit increases the ability of soft aluminum matrix to accommodate hard and brittle second phase silicon particles (Bai et al 1987). If temperature goes beyond a certain critical value, thermal softening of the material in sub surface region takes place which leads to large scale plastic deformation during the sliding under external normal load. Under such conditions metallic wear takes place. Increased solid solution strengthening, formation of intermetallic compound and precipitation hardening in the presence of alloying elements may be attributed to comparatively better wear resistance and hardness at the top compared to the bottom.

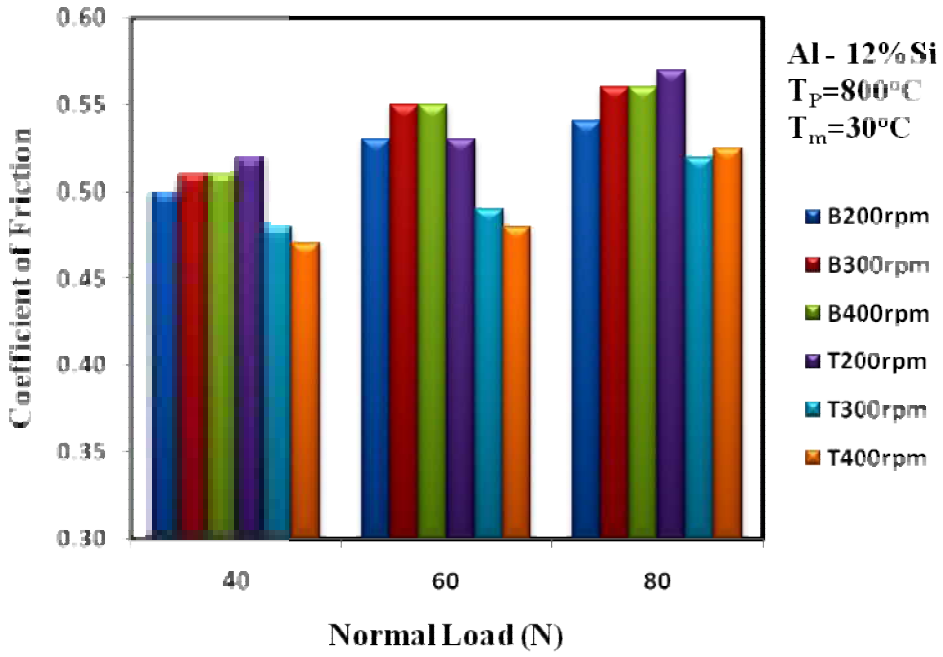

Fig. 4.35 COF of Al-12wt%Si FGM vs Normal load of the casting for 800°C melt temperature without preheating the mold.

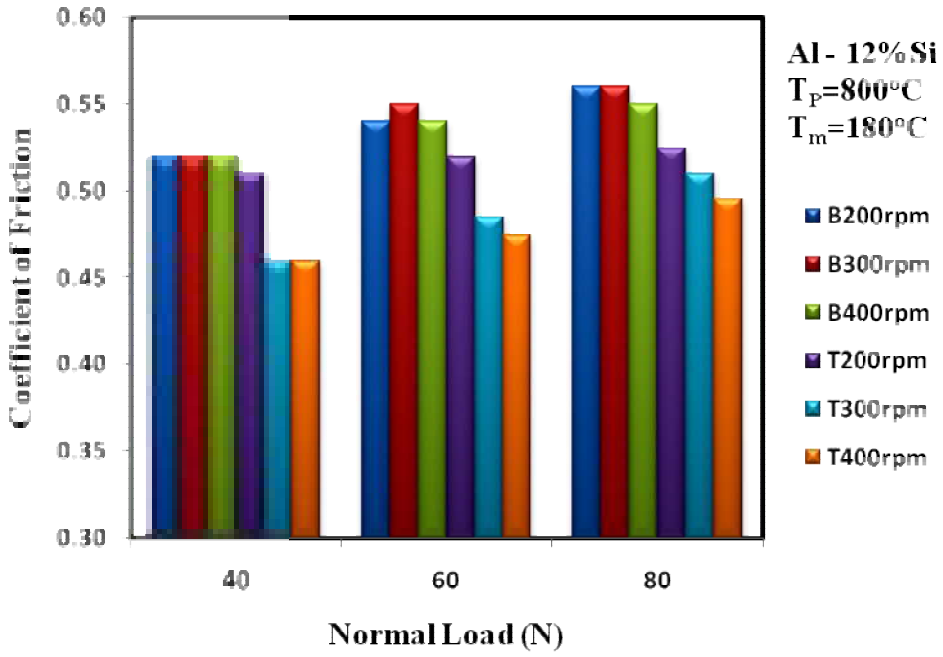

Fig. 4.36 COF of Al-12wt%Si FGM vs Normal load of the casting for 800°C melt temperature with preheating the mold.

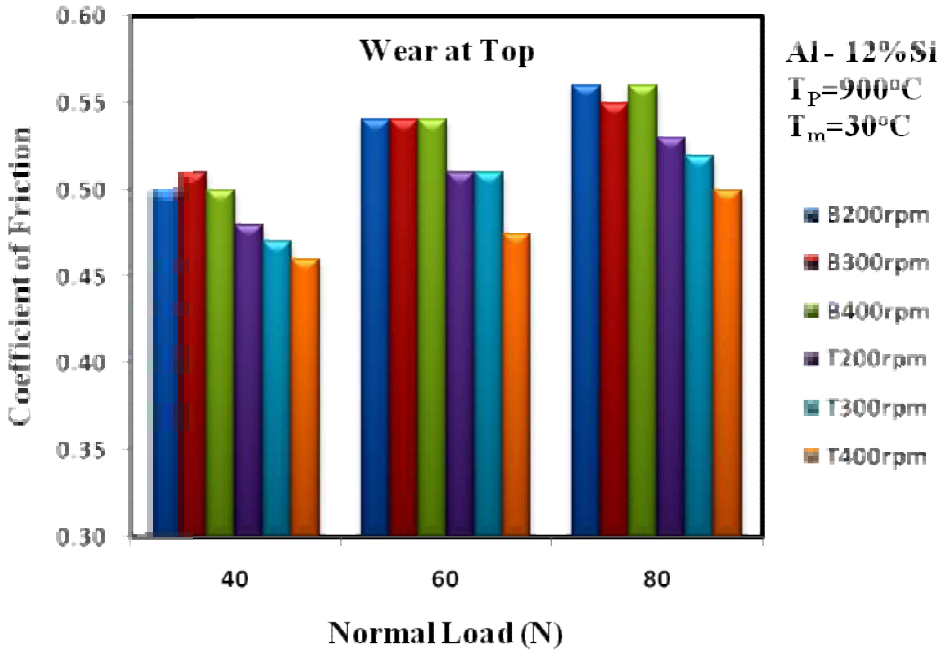

Fig. 4.37 COF of Al-12wt%Si FGM vs Normal load of the casting for 900°C melt temperature without preheating the mold.

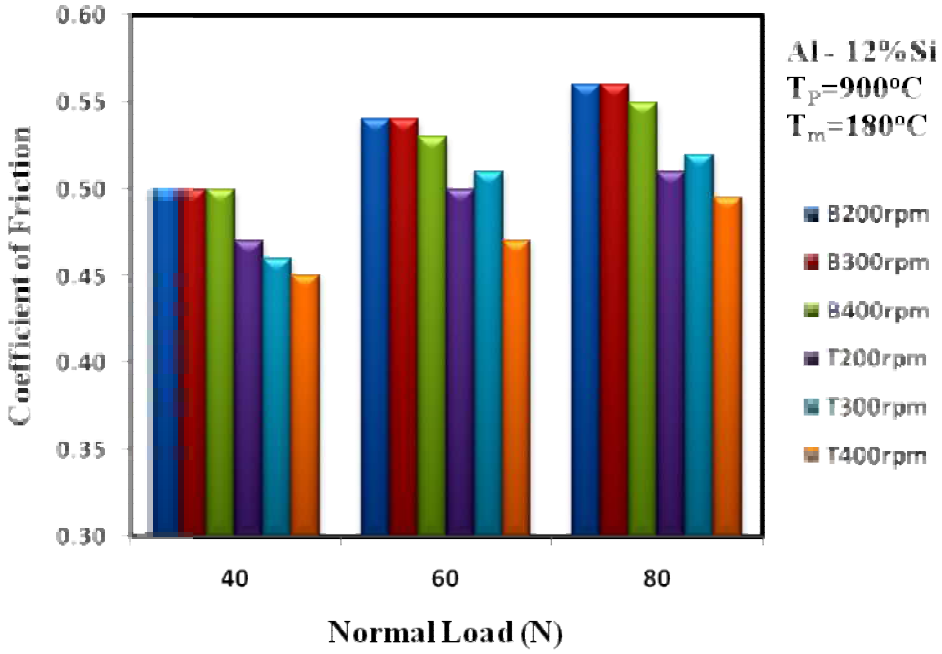

Fig. 4.38 COF of Al-12wt%Si FGM vs Normal load of the casting for 900°C melt temperature with preheating the mold.

4.3 Al-17wt%Si FGM

4.3.1 Microstructure

The microstructural features of hypereutectic (Al-17wt%Si) FG alloy shows a variation of structure from bottom to top of the casting with eutectic structure sand wiched between the hypoeutectic and hypereutectic structures. At the bottom, dendritic primary α-Al solid solution appears while at the top end of the casting it shows primary Si with eutectic. This is due to the combined effects of fast cooling and centrifugal action. Fast cooling of 17%Si alloy at the lower end suppresses primary silicon nucleation and results in near hypoeutectic structure.

The microstructure of all the hypereutectic FG alloy specimens revealed features of non-equilibrium crystallization that are characteristic features of castings in metallic molds, i.e, the microstructure contained individual primary crystals of α-solid solution of aluminum in a dendritic shape and fine crystalline eutectics in the inter-dendritic grains. The dendrites of the primary solid solution in non-equilibrium crystallization can be present in large amounts in binary eutectic in addition to primary crystals of silicon of a non-eutectic region (Silaeva et al 2000).

4.3.1.1. Effect of rotational speed (G Force)

The segregation and precipitation of Si at the top of the casting during the centrifuge casting is attributed to the density difference between the Si and the melt. The Si crystals are pushed to the top by the centrifugal force acting downward. The mold rotational speed, the mold and teeming temperatures have strongly influenced the structure development and the distribution of the primary Si. Figs. 4.39 to 4.44 show the effect of rpm or the G force on distribution of the primary Si. During mold rotation, the particle suspended in the liquid is subjected to centrifugal force acting on a particle given as $mr\omega^2$ and the gravitational force given by mg. The ratio of the centrifugal force to the gravitational force is called the gravitational coefficient (G) or G number. The rim thickness is defined as the thickness of the Si rich (primary) layer

which indicates the extent to which particles have segregated along the length of the specimen. The rim thickness decreased with increased mold speed for a given mold and teeming temperature. This is attributed to the increase in cooling rates at higher rpm. It can be noted that, as the angular velocity increases, the G factor increases. Since the centrifugal force acting on the particle is G times higher than the gravitational force, the role of gravitational force can be ignored. Thus as the rotational speed increases, the force acting on the particles to segregate is expected to increase, as is observed in the study.

For the casting produced under the lower levels of teeming and mold temperatures i.e 800^{o}C and room temperature respectively, the specimen centrifuged at 22.3G (200rpm) showed no remarkable gradation of Si (Figs. 4.39-4.40). The rim thickness of Si is observed to be 26mm. The maximum primary Si volume % obtained at this 'G' force is 8%, slightly higher than normal primary Si in this alloy. Similarly we can see from Figs. 4.41and 4.42 that, for casting produced at 300 rpm speed, the transition from hypereutectic microstructure to that of fine eutectic takes place at about 23mm (rim thickness) from the top surface. The primary Si is about 9%. At 400 rpm we can observe a rim thickness of 16mm and a volume fraction of 14% as shown in Fig. 4.44.

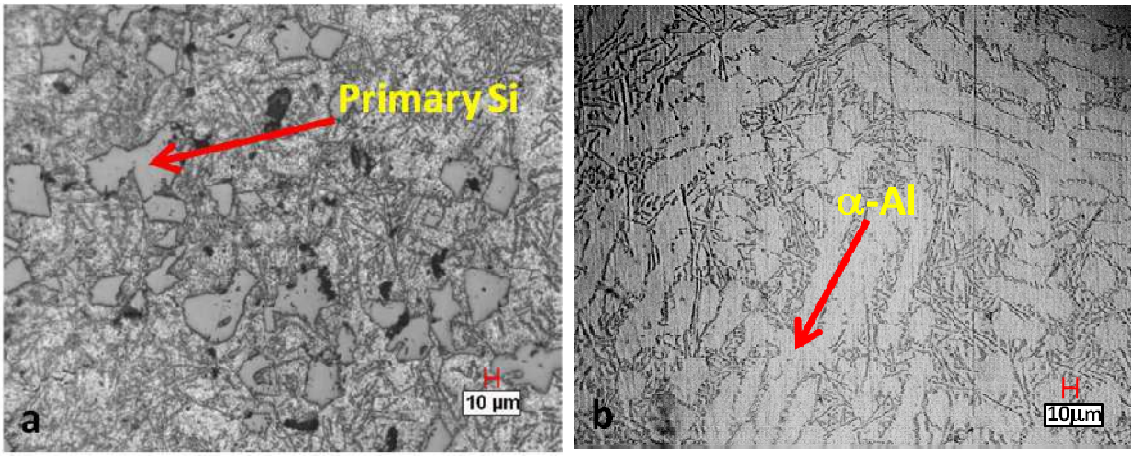

Fig. 4.39 The microstructure of the Al-17wt%Si FGM cast at, T_P=800^{o}C, T_m=Room temp., G=22.3(200rpm). a) Top end showing primary Si, b) Bottom end showing primary α-Al dentritic structure

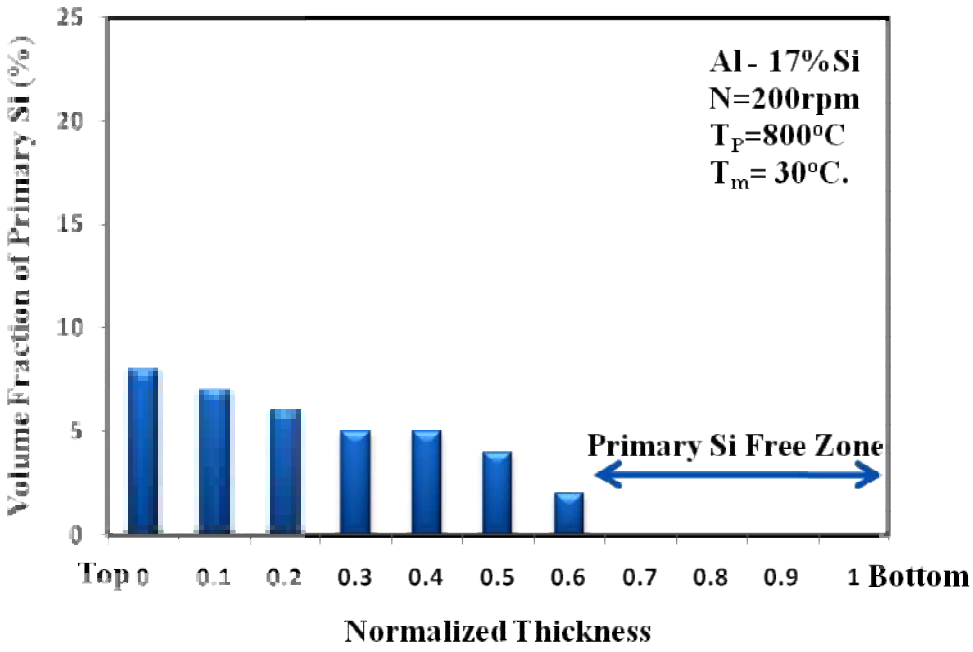

Fig. 4.40 Distribution of primary Si from top end to bottom end for Al-17wt%Si FGM cast at, T_P=800°C, T_m=Room temp, G=22.3(200rpm).

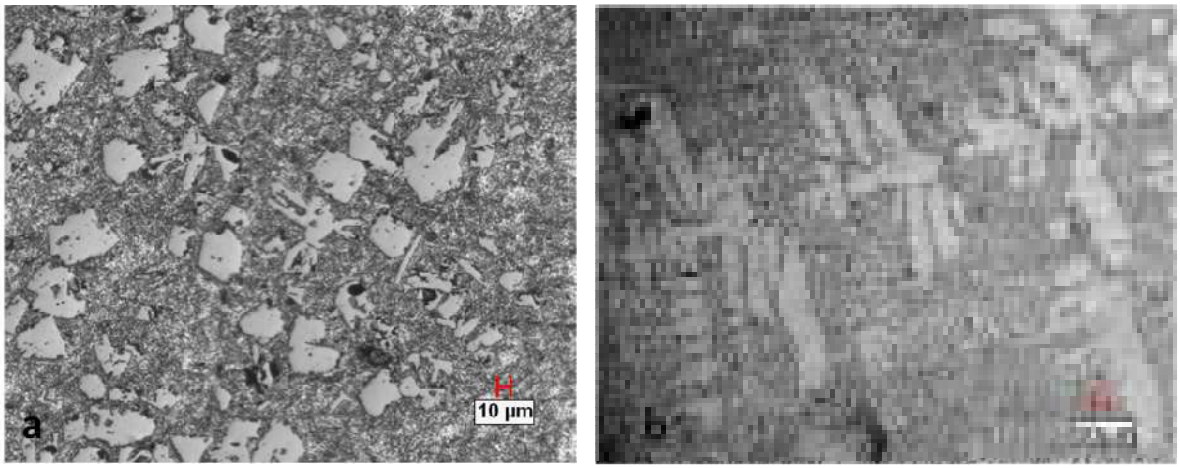

Fig. 4.41 The microstructure of the Al-17wt%Si FGM cast at, T_P=800°C, T_m=Room temp G=50.3(300rpm). a) Top end showing primary Si, b) Bottom end showing primary α-Al dentritic structure.

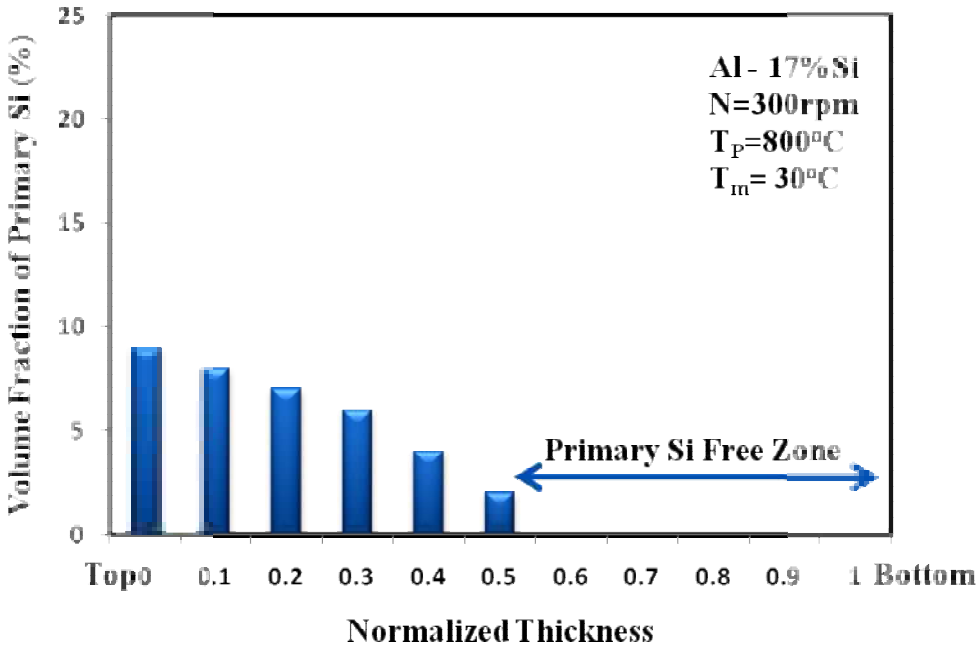

Fig. 4.42 Distribution of primary Si from top end to bottom end for Al-17wt%Si FGM cast at, T_P=800°C, T_m=Room temp, G=50.3(300rpm).

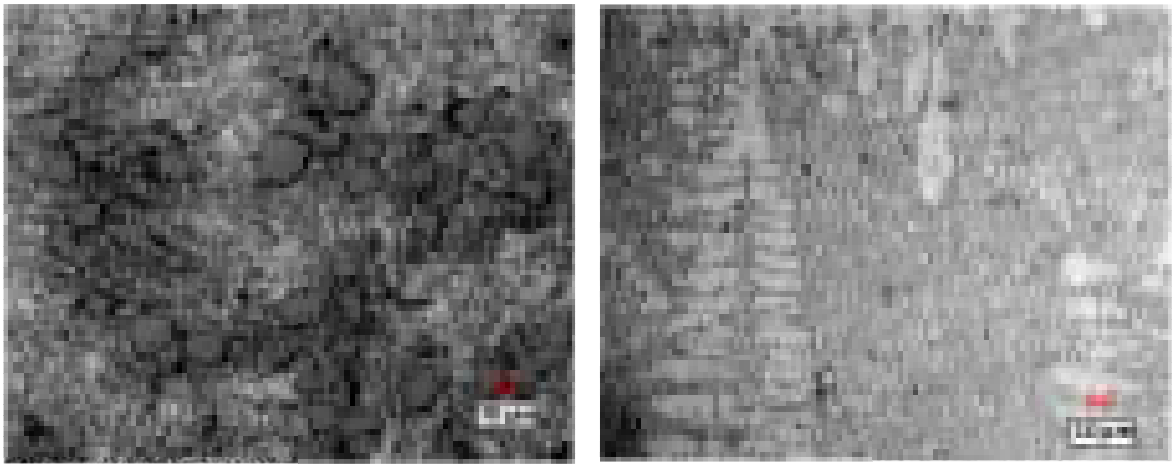

Fig. 4.43 The microstructure of the Al-17wt%Si FGM cast at, T_P=800°C, T_m=Room temp G=89.42(400rpm). a) Top end showing primary Si, b) Bottom end showing primary α-Al dentritic structure

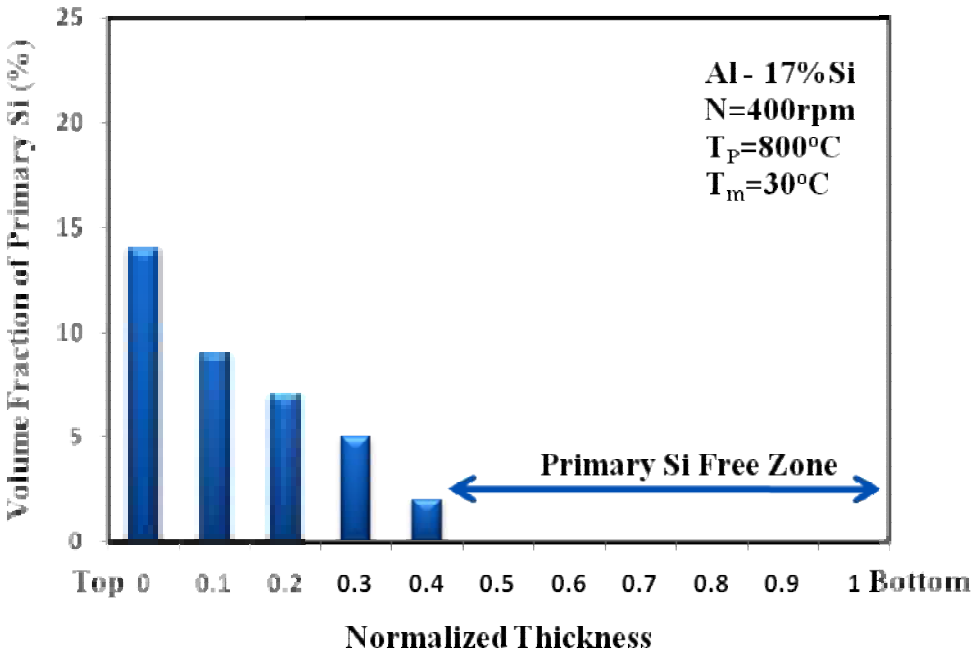

Fig. 4.44 Distribution of primary Si from top end to bottom end for Al-17wt%Si FGM cast at, T_P=800°C, T_m=Room temp, G=89.42(400rpm).

For the FG alloys cast at 800°C pouring temperature, the influence of higher mold temperature is studied at different rpm's for evaluating the percentage Si segregated and the rim thickness. In the present work mold temperature of 180°C is chosen. It was observed that at 22.3G (200rpm) the volume fraction of Si was 9% with a rim thickness of 24mm. At 50.3G(300rpm) and 89.42G(400rpm) the primary Si volume fraction was found to be 14% and 18%, whereas the rim thickness reduced to 21mm and 14mm respectively. This gives an indication that the segregation of the primary Si forming a narrow Si rich region is influenced by the mold rpm and also the solidification rate (influenced by the mold temperature).

The optical micrographs of specimens in Fig. 4.45, show microstructures with a non uniform distribution of needle-like Si particles in the matrix of α-Al (eutectic) at the bottom of the casting. As we move towards the top region, micrographs showed similar microstructure, except with increasing primary Si concentration. At the top region of the casting, the FG alloy exhibits not only needle-like eutectic Si phase but also large faceted massive primary Si crystals that signify a high silicon hypereutectic

microstructure. The bar graphs for volume fraction of primary Si against normalized thickness are shown in Fig. 4.46. The rpm influences primary Si free zone (compliment of rim thickness) and the PFZ increases as the speed (G force) is increased.

This result has revealed that, under the non-equilibrium conditions, a hypereutectic Al-17wt% Si alloy can have a hypoeutectic structure due to excessive under cooling. Depending on the fastest growing phase at a given undercooling condition, a structure which consists of both primary and eutectic phases or only the latter develops. In the aluminium-silicon system, the primary aluminium-rich phase grows dendritically, whereas the silicon-rich phase grows in a facetted manner. Compared to the dendritic phase, the facetted phase grows slower at under cooling. Relative high under cooling application on an alloy of a given composition causes dendritic growth in which one of the phases grows rapidly and the other phase solidifies between dendrites while lower under cooling leads to cellular growth. The difference between microstructures of both sides resulted from different cooling rates also under the influence of high G forces.

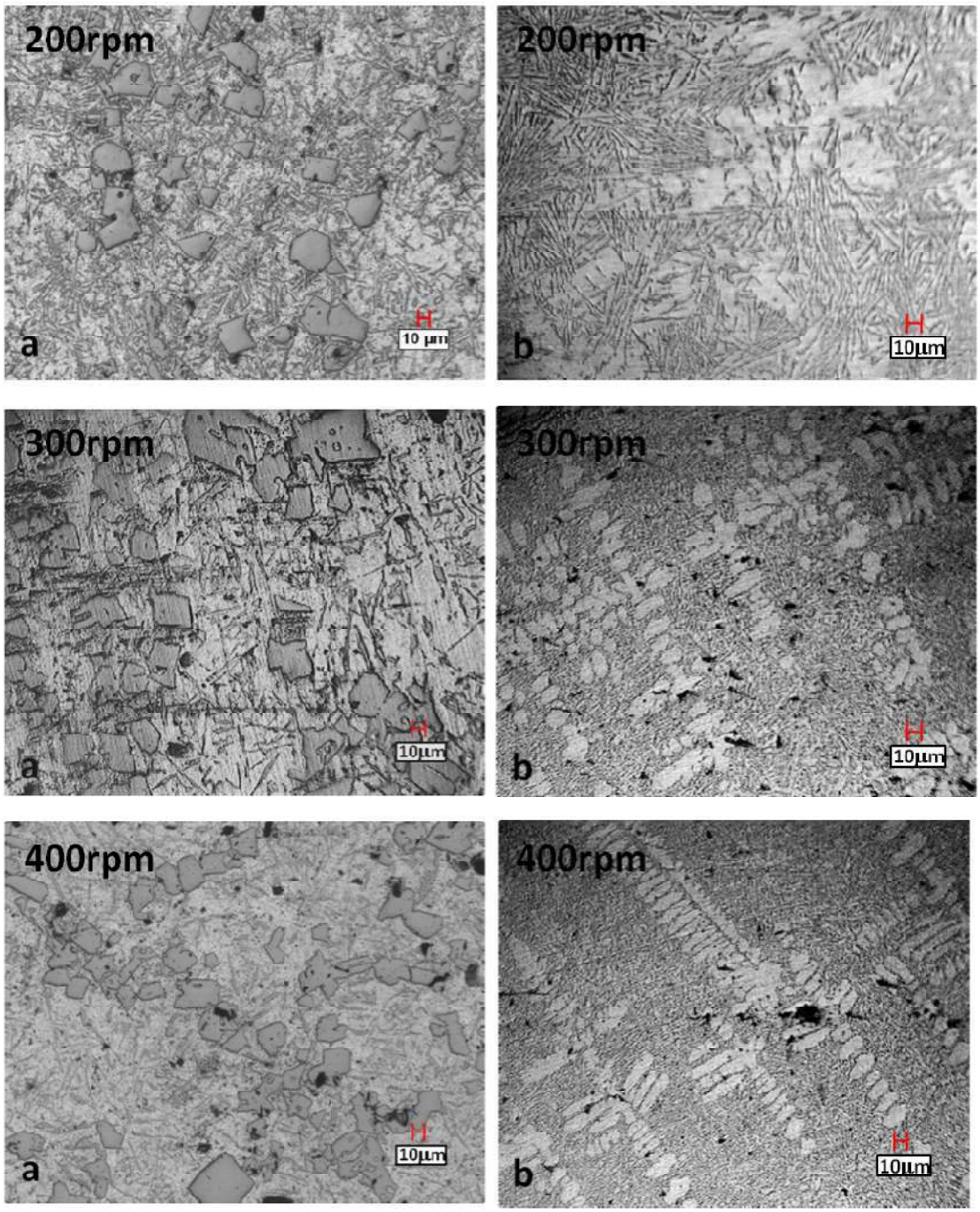

Fig. 4.45 The microstructure of the Al-17wt%Si FGM cast at, T_P=800^{o}C, T_m=180^{o}C G=22.3(200rpm), 50.3(300rpm), 89.42(400rpm). a) Top end showing primary Si, b) Bottom end showing primary α-Al dendritic structure

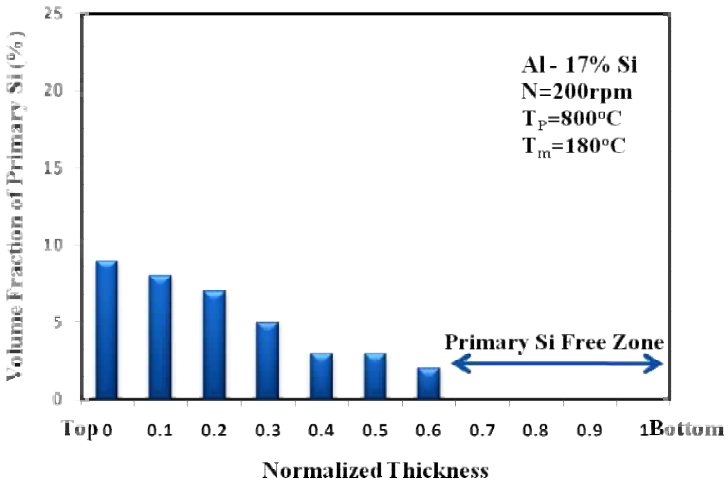

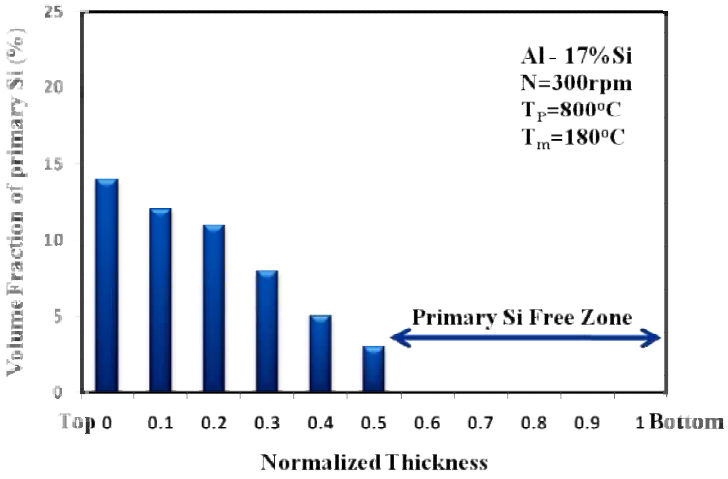

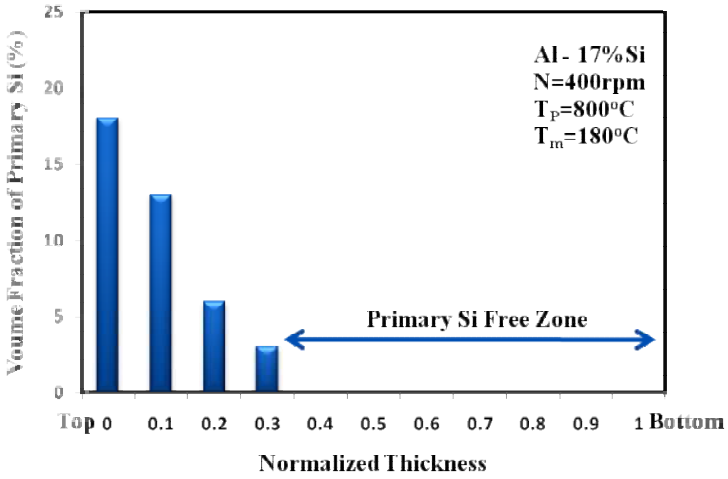

Fig.4.46 Distribution of primary Si from top end to bottom end for Al-17wt%Si FGM cast at, T_P=800°C, T_m=180°C, G=22.3(200rpm), 50.3(300rpm), 89.42(400rpm).

Similar to the controlling of solidification rate by changing the mold temperature, it can also be controlled by changing the teeming temperature. Hence the effect of teeming temperature on solidification rate and also the formation of primary Si is observed by casting the FG alloy at teeming temperature of 900^{o}C under two conditions of mold namely, with and without preheating to 180^{o}C. In either case the castings were prepared at three rpms as indicated above. The variation in % primary Si and rim thickness for two mold temperatures and three rpms and at a teeming temperature of 900^{o}C is shown in Table 4.2.

Table 4.2 Percentage of primary Si and rim thickness for a T_P of 900^{o}C

Mold Temp (^{o}C)	Rpm		
	200	300	400
Room Temp	12% & 24mm	15% & 20mm	19% & 14mm
180	14% & 24mm	18% & 16mm	23% & 12mm

The micrographs and the bar graphs for the six combinations are shown in Figs. 4.47 and 4.48. Micrographs reveal the primary silicon particulates, of varying size, distributed randomly through the FG alloy matrix. FG alloy produced showed somewhat thick primary crystals with less sharp structures, resulting in greater strength and hardness. Also, due to the effect of high G forces the primary silicon crystals and eutectic silicon needles tend to spheroidize to a certain extent, i.e., sharp corners become rounded.

The non-uniform size and distribution of the particulates resulted in particulate-rich and particulate depleted regions. The particulates were aligned in the direction of G force. Besides the presence of block like silicon particulates, isolated pockets of a eutectic silicon phase, having a flake-like morphology with large aspect ratio, was also evident. Formation and presence of the particulate-like silicon phase is the end result of a competition between nucleation and growth in front of the solid / liquid interface in the top layer. The formation of large silicon particulates from the melt provides the necessary impetus for enhanced nucleation through an epitaxial growth mechanism. Thus, a highly heterogeneous mixture of microstructures eventually collects as a highly dense preform.

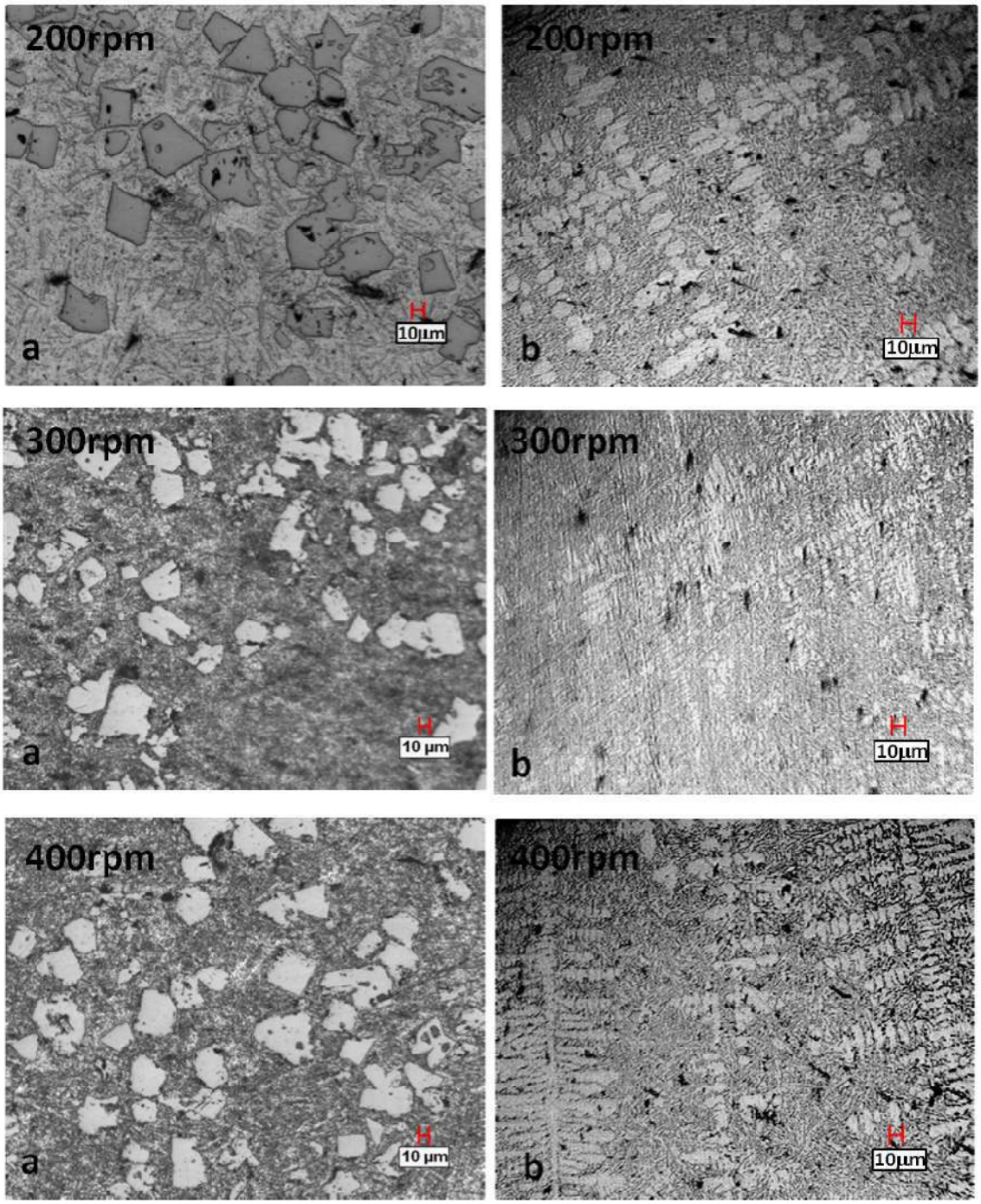

Fig. 4.47 The microstructure of the Al-17wt%Si FGM cast at, T_P=900^oC, T_m=Room temp. G=22.3(200rpm), 50.3(300rpm), 89.42(400rpm). a) Top end showing primary Si, b) Bottom end showing primary α-Al dendritic structure

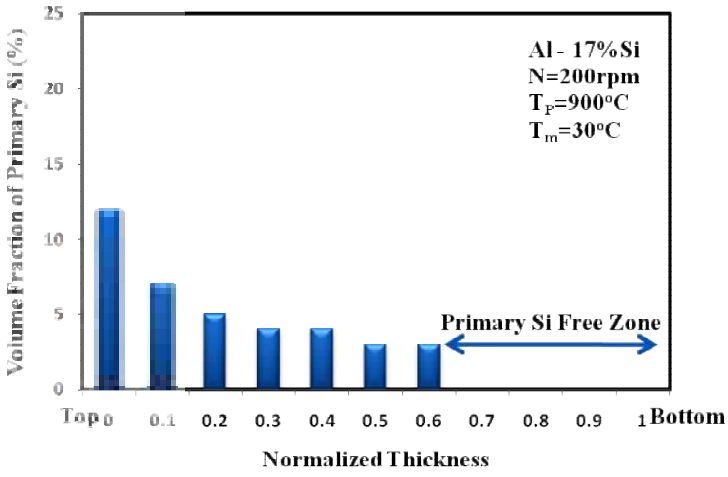

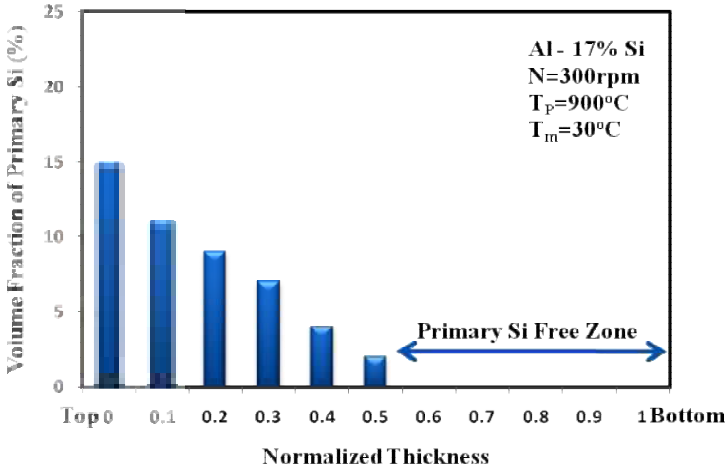

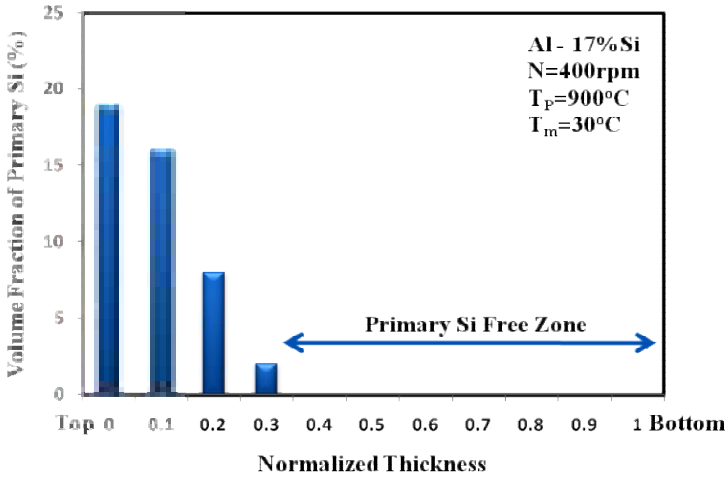

Fig. 4.48 Distribution of primary Si from top end to bottom end for Al-17wt%Si FGM cast at, T_P=900°C, T_m=Room temp. G=22.3(200rpm), 50.3(300rpm), 89.42(400rpm).

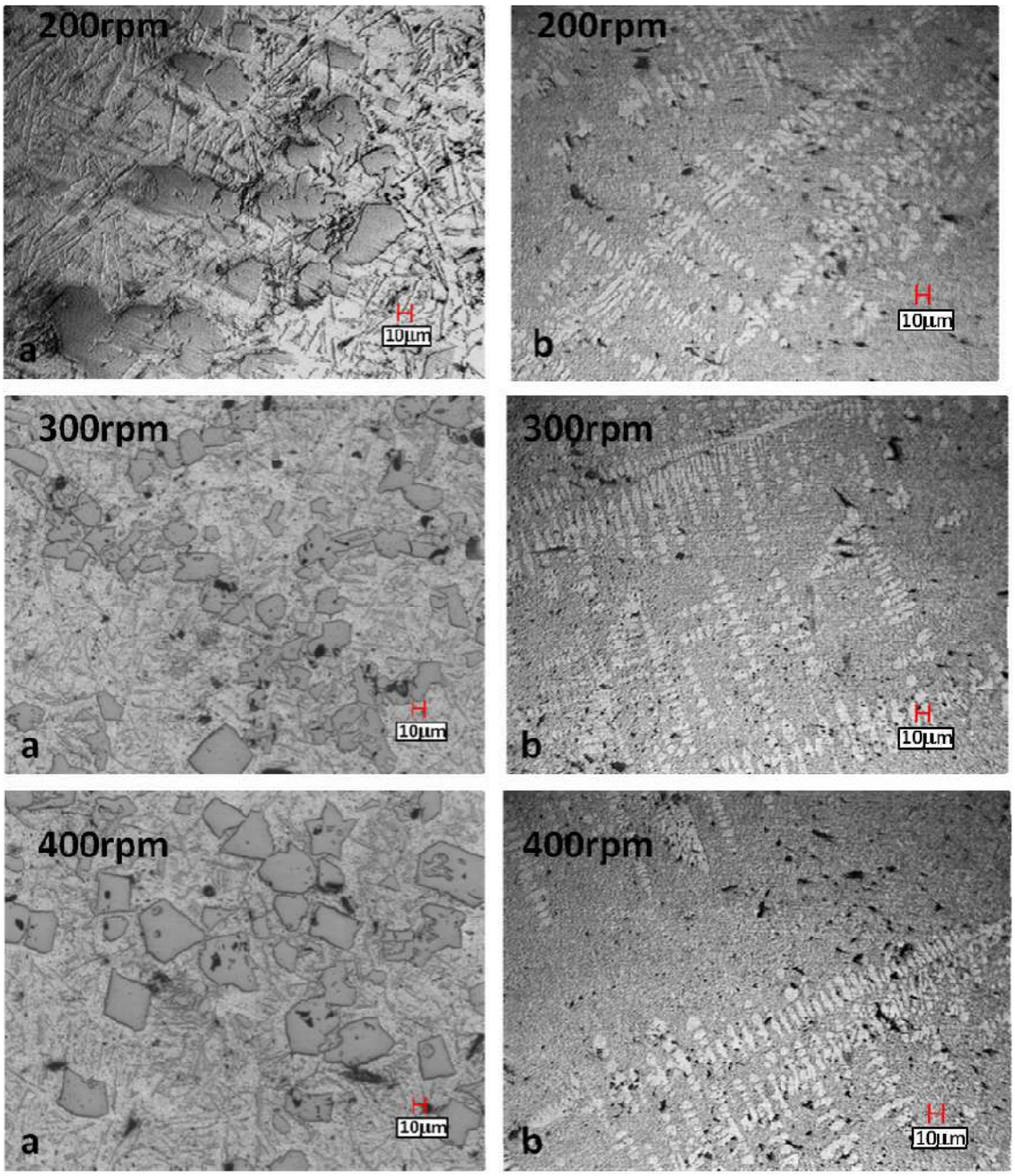

Fig. 4.49 The microstructure of the Al-17wt%Si FGM cast at, T_P=900^{o}C, T_m=180^{o}C G=22.3(200rpm), 50.3(300rpm), 89.42(400rpm). a) Top end showing primary Si, b) Bottom end showing primary α-Al dendritic structure

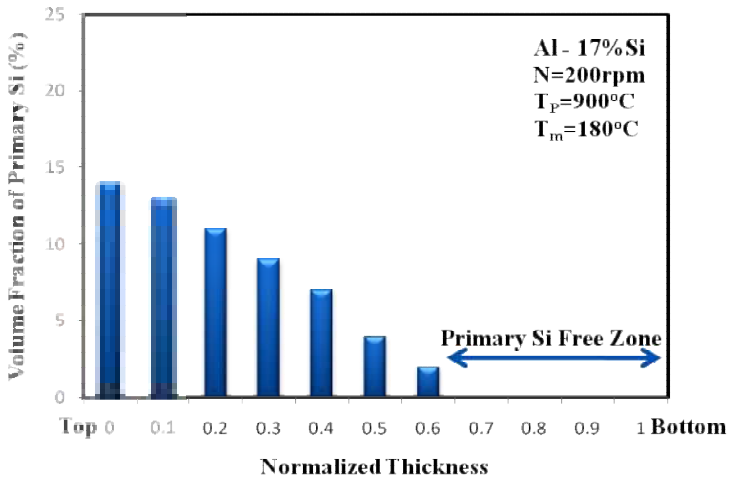

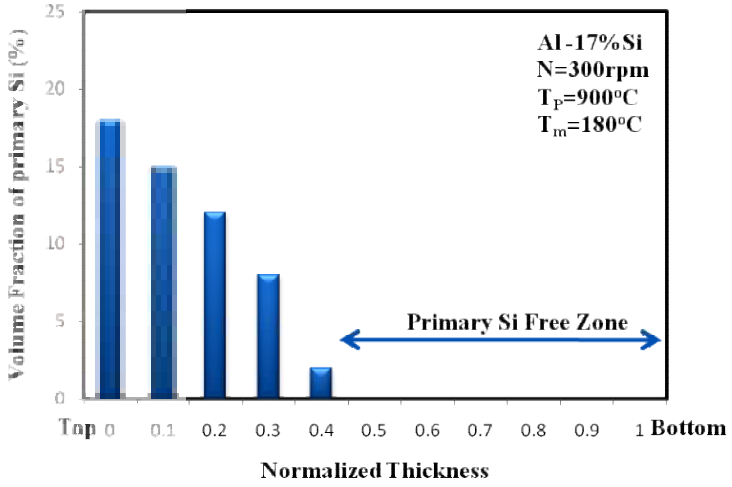

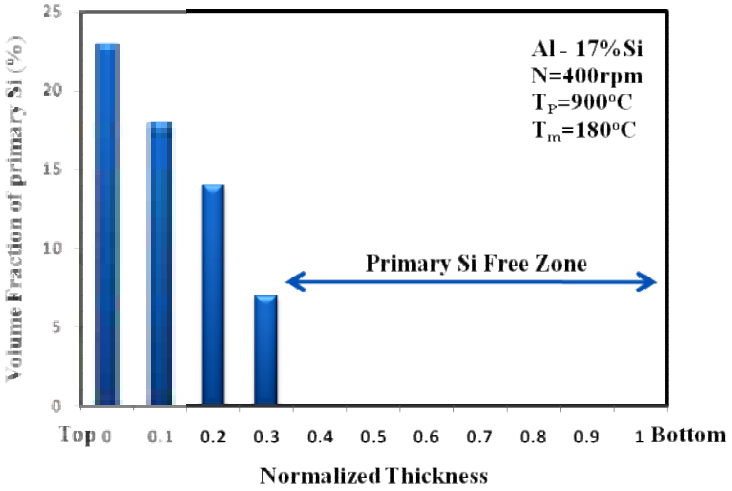

Fig.4.50 Distribution of primary Si From top end to bottom end for Al-17wt%Si FGM cast at, T_P=900°C, T_m=180°C, G=22.3(200rpm), 50.3(300rpm), 89.42(400rpm).

The microstructure of the preform is critically dependent on the concurrent and mutually competitive influences of solidification characteristics. The presence of a concentration gradient in front of the solid/liquid interface causes or promotes the dendritic or planar growth front to be replaced by an equiaxed structure. For the hypereutectic aluminium-silicon FG alloy, the silicon growth front rejects the aluminium atoms into the liquid alloy. Consequently, there exists a localized region having a low concentration of silicon present in front of the solid-liquid interface.

The distribution of primary Si from top to bottom surface of the centrifugally cast Al/Si FGM at 200, 300, 400rpm has shown a gradation. The most effective among all the castings is the casting processed at 89.42G (400 rpm). This has produced better volume % of primary Si at the top surface when compared to the other two. The comparison of distribution pattern of centrifugally cast FGM for 200rpm, 300rpm and 400rpm shows that there is a sharp transition between Si enriched and Si depleted zones in 400rpm casts. The primary Si particles formed are segregated as a graded layer in the top surface of the casting leading to a better hardness and improved wear resistance of that surface.

The origin of the graded structure is due to the density difference between melt and Si, wherein the density of the Si is much less and the centrifugal force enables stratification resulting from sedimentation a flotation of solids from liquids. Further partial separation of aluminum and Si in the melt occurred during the early stage of the centrifuging, resulting in the formation of a melt with compositional gradient prior to the crystallization of primary crystals. Such that the composition varies from hyper-eutectic to hypo-eutectic forms. Hence Si and aluminum crystals nucleate at top and bottom of the casting respectively (Y Watanabe et al 2005c).

From the bar graphs (Figs. 4.46, 4.48, 4.50) it is evident that the graded distribution of the primary Si is achieved at all the three rpms. Primary Si is a strengthening phase in Al–Si alloy, so the hardness is strongly affected by the primary Si content. The variation in distribution of volume fraction of Si along the length of the casting is studied. It is again seen from the bar graphs that, as the

rotational speed of the mold increases, the Particle Free Zone (PFZ) shifts to the left (towards the bottom of the casting) and the primary Si volume fraction increases. By subjecting a homogenous melt to a centrifugal force, a maximum volume fraction of 23% is obtained for the casting fabricated at 89.42G(400rpm) at the top end leading to a selective improvement in specific properties such as hardness and wear resistance (Fig. 4.50). The region near the top surface is rich in primary Si whose concentration decreases towards the bottom. Further it is graded to needle shaped eutectic phase The region near the bottom of the casting shows a very fine primary Al dendrites structure. This is in agreement with observations made by earlier workers on similar works on similar materials (Kumar et al 2010), (Y Watanabe et al 2001), (Rajan et al 2009).

4.3.1.2 Effect of Teeming Temperature (T_P) and Mold Temperature (T_m)

Literature reveals that the mold and pouring temperatures play an important role in segregation of the alloying particles in a melt subjected to centrifugal action during solidification. This is true due to the fact that increasing the mold and teeming temperature decreases the solidification rate which allows more time for the particle to precipitate in the matrix and segregate towards the influential side depending on the density difference between the melt and particle.

At teeming temperature of 800^{o}C and mold speed of 200rpm, the rim thickness is 26 mm for mold at room temperature and 24 mm when mold is preheated to 180^{o}C. Similar trend is observed at 300 and 400rpm. It is observed that when the mold temperature is increased the volume fraction increased by 12.5% for 200rpm, 55% and 28% for 300rpm and 400rpm respectively.

The rim thickness and volume fraction of primary Si show improved values at all the three rpms when the pouring temperature is increased to 900^{o}C. Observing the values of the two parameters: primary Si and rim thickness that are evaluated at two mold temperatures and three rpms with the pouring temperature increased from 800^{o}C to 900^{o}C, it appears that the effect of increasing the teeming temperature is more

predominant when the casting is done at higher rpm compared to the use of preheated mold.

From the above results it is clearly demonstrated that the minimum thickness of the rim (particle enriched zone) is achieved at higher mold temperature and increased teeming temperature at all mold speeds. It can be seen from the graphs (Fig. 4.46, 4.48, 4.50) that at a particular speed with the increase in mold and teeming temperatures the particle enriched zone is narrowed and PFZ is clearly visible. An increase in the PFZ could be noted at all the mold speeds. It is also observed that an increase in mold temperature and teeming temperature increased the primary volume fraction of the Si at the top of the cast specimen. The combined effect of higher T_m, T_P and rpm used in the present work have provided best values of primary Si and rim thickness.

The properties of a casting significantly depend on the solidification time or cooling rate. This is controlled by either mold temperature or melt temperature. The fluidity of the melt is also affected by the melt temperatures. This increase in temperatures will decrease the heat transfer rate between the mold and the melt. This reduces the solidification rate and in turn, more time will be available for the formation of Si in the melt and its segregation to take place. At a slower solidification rate, the time to obtain a required rim thickness of the casting will be longer compared to that of a faster solidification rate.

When the melt is retained for a long time in the two-phase region above the eutectic time, the primary silicon gets more time to float to the top. Similarly when the teeming temperature is further increased which is above the liquidus temperature of the alloy, the time the liquid spends in the mold under the centrifugal force is further increased. As a result the particles are pushed towards the top and segregate as shown in Fig. 4.50.

4.3.2 Hardness

4.3.2.1 Effect of Processing parameters

Hardness of Al-17wt%Si FGM specimens cast under 800^{o}C melt temperature without preheating the mold is examined along its length. Specimen cast at 400rpm has exhibited maximum hardness of 68 BHN at the top surface and it also showed gradation in hardness from the top to bottom from 68 to 50 BHN. The hardness values and gradation did not change much at 300 rpm (66 to 48 BHN), However at 200rpm specimen showed much smaller hardness at the top (59 BHN) even though the Si gradient remained more or less constant. At the same melt temperature with preheating the mold to 180^{o}C, specimen cast at 400rpm exhibited a maximum hardness of 79 BHN at the top surface. This is about 16% higher as compared to the mold at ambient temperature. Further the rim thickness also reduced when the mold is preheated but the hardness at the bottom of the specimen did not change. Similar results were obtained at 300 and 200 rpm also but with reduced hardness values at the top (74 and 68 respectively). The variation of hardness from top to bottom of the casting for two mold conditions and three rpms and at 800^{o}C teeming temperature is shown in Figs. 4.51 and 4.52.

The hardness values at the top end of the casting are higher at higher G values (rpm). The rim thickness also reduces at higher rpm indicating that enhanced hardness values can be obtained over a short length of the specimen at higher rpm. This effect is further enhanced when the mold is preheated.

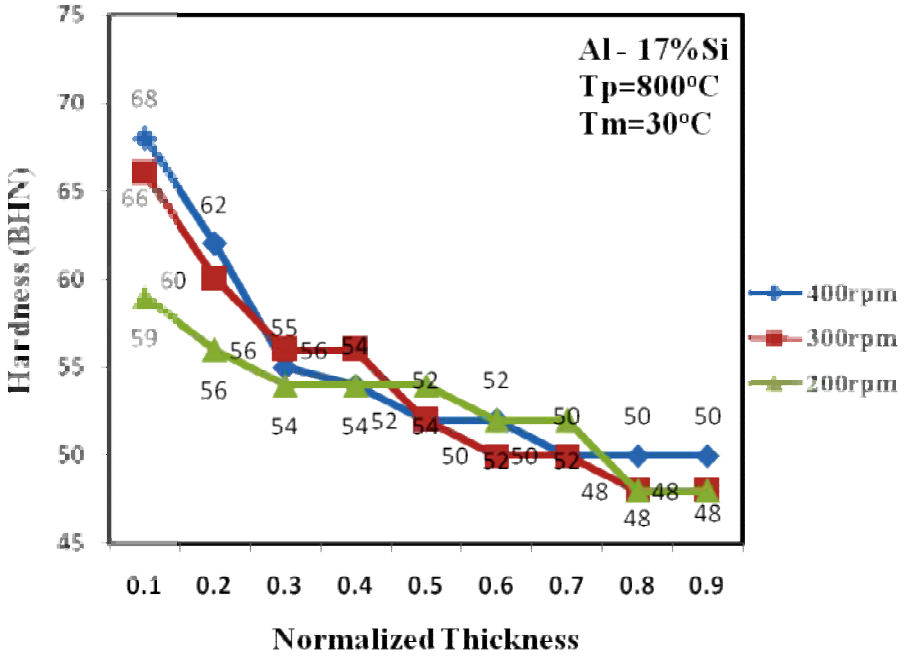

Fig. 4.51 Hardness of Al-17wt%Si FGM along the length of the casting for 800°C melt temperature without preheating the mold.

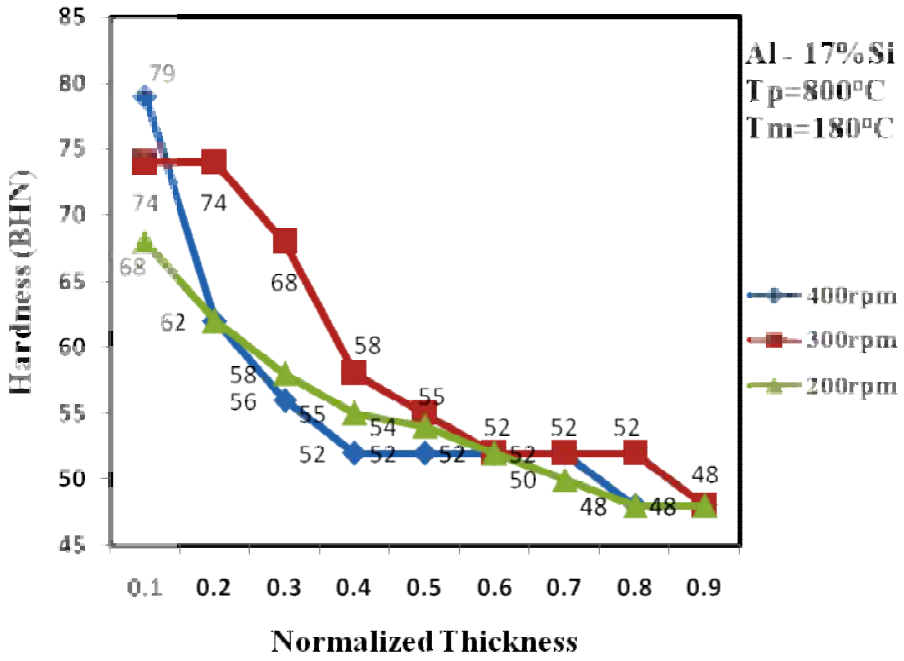

Fig. 4.52 Hardness of Al-17wt%Si FGM along the length of the casting for 800°C melt temperature with preheating the mold at 180°C.

The effect of the third variable in the process i.e the teeming temperature on the maximum hardness and rim thickness is also studied by using a teeming temperature of 900°C. Castings are produced at this temperature with two mold conditions and three rpms. It is observed that a maximum of 92 BHN is obtained at the top surface for the specimen cast with preheating the mold and at 400rpm. It also exhibited a good gradation of hardness from top to bottom face with the hardness at the bottom equal to 50 BHN. The variation of hardness from top to bottom of the casting at 900°C teeming temperature is shown in Figs. 4.53 and 4.54.

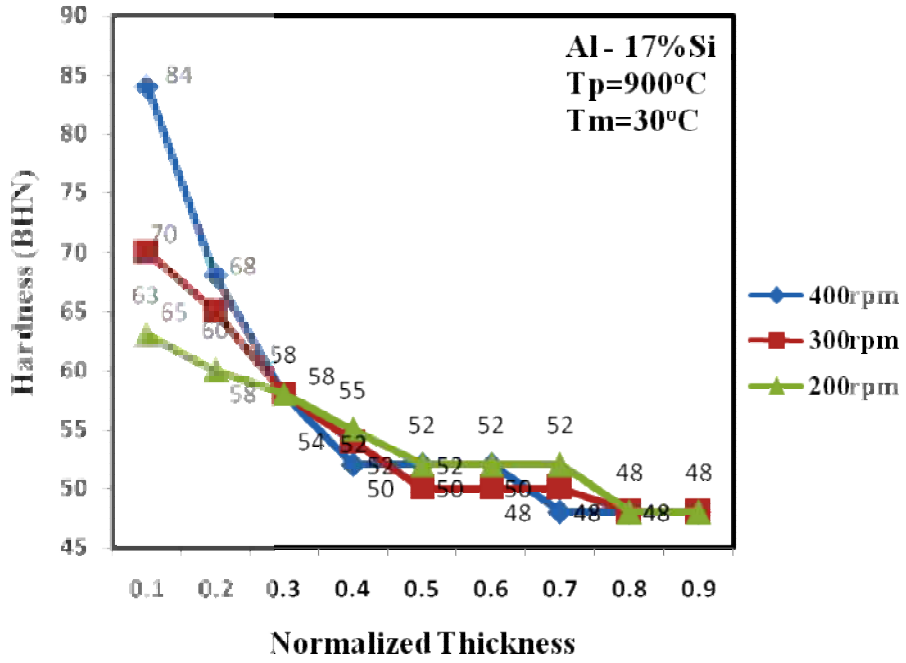

Fig. 4.53 Hardness of Al-17wt%Si FGM along the length of the casting for 900°C melt temperature without preheating the mold.

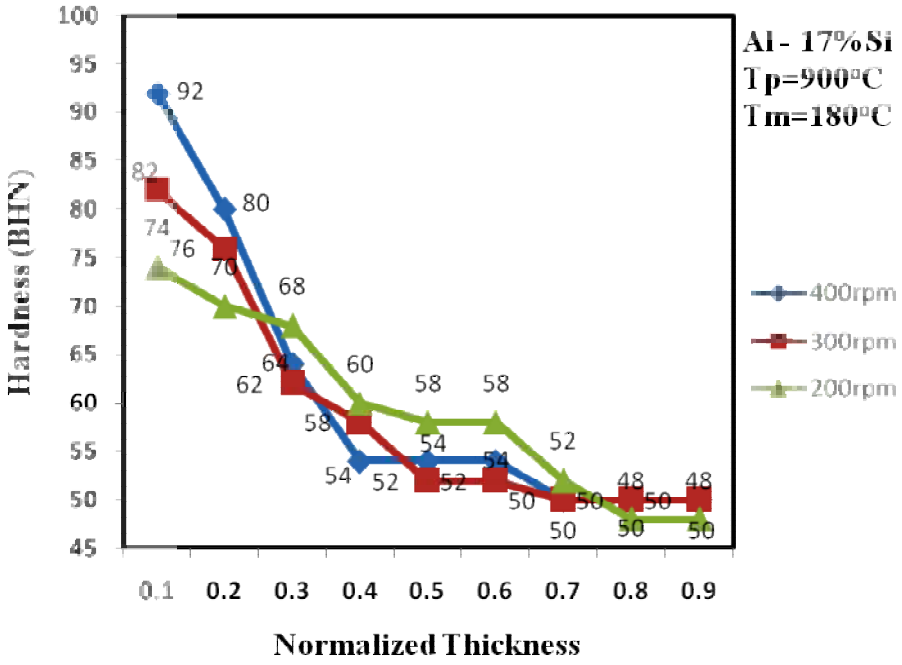

Fig. 4.54 Hardness of Al-17wt%Si FGM along the length of the casting for 900°C melt temperature with preheating the mold at 180°C.

This increase in hardness is consistent with volume fraction of the Si particles present along the length and as the volume fraction of the harder reinforcement particle increases, the bulk hardness of the casting increases. Similar observations have been reported by Y Watanabe et al. (2005b).

It can be seen that the hardness increases with the centrifugal force or the mold speed. It has also been found that in the FGM the gradation becomes steeper (smaller rim thickness) with increasing the mold rotation speed (G number). This is in relation to the volume fraction of primary Si found in the cast specimens as discussed in the previous section.

Thus, during the formation of the graded composition in the FGM produced by the centrifuge method, on pouring the molten Al-Si alloy and rotating the mold, the α-Al primary crystals nucleate before the Si crystals form. However, at this time, volume fraction of solid is high enough, and the α-Al primary crystal particles cannot

migrate any more. Therefore, α-Al primary crystal particles always migrate toward the bottom. Then, the remaining molten Al-Si alloy will solidify. At a eutectic temperature, 94% liquid phase with a eutectic composition will be retained, and the retained liquid phase may transform into the solid phase by the eutectic reaction. This means, the volume fraction of the Si increases toward the top position. The hardness of the specimen becomes larger than that of the bottom region, since the hardness of Al-Si intermetallic compound is larger than that of α-Al.

For given teeming and mold temperatures higher hardness at top end and smaller rim thickness (steeper gradation) are obtained at higher rpms. When the mold temperature is increased the hardness further increases but rim thickness decreases. Similar trend is observed when the teeming temperature is increased. Compared to T_P=800^{o}C, T_m=30^{o}C and 200rpm the hardness value improved by 15.25% when rpm is increased to 400. It further improved by 16.17% when T_m is raised to 180^{o}C and by 16.45% when T_P is raised to 900^{o}C. Thus the mold and teeming temperature and rpm affect the segregation of the primary Si towards the top of the casting. In the current work it was possible to produce FG alloy having different hardness values and gradation in that range. The highest hardness values and the smallest rim thickness were obtained under the processing conditions of: T_P=900^{o}C, T_m=180^{o}C and rpm=400.

4.3.3 Wear

4.3.3.1 Specific wear rate

Dry sliding behavior of Al-Si alloy has been found to be primarily a function of silicon content and independent of initial structure and distribution of silicon phase. Figs. 4.55 to 4.58 show the specific wear rate values obtained for Al-Si FGMs.

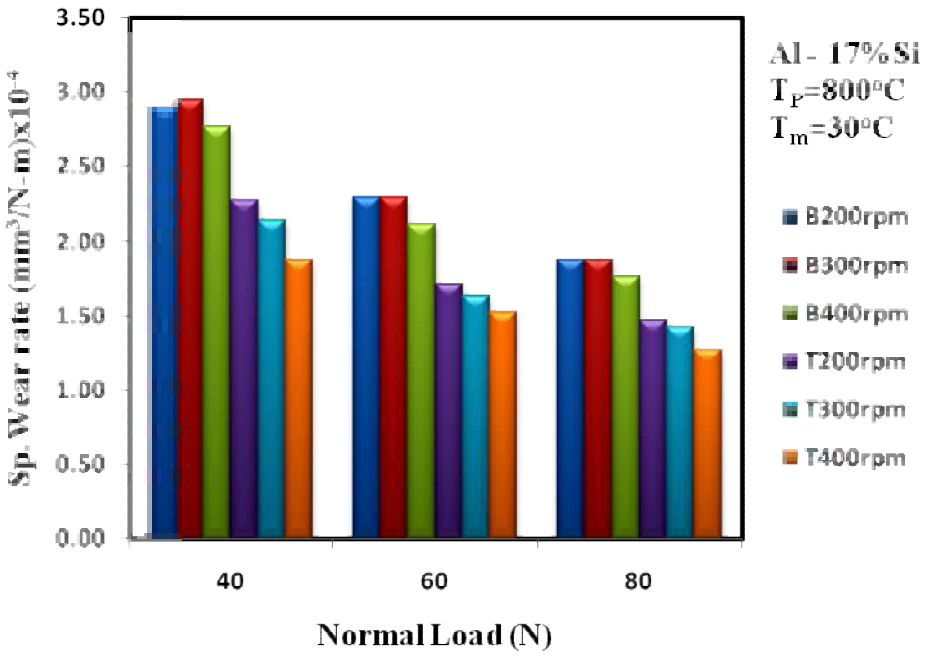

Fig. 4.55 Specific wear rate vs Normal load of Al-17wt%Si FGM for 800°C melt temperature and no preheating of the mold.

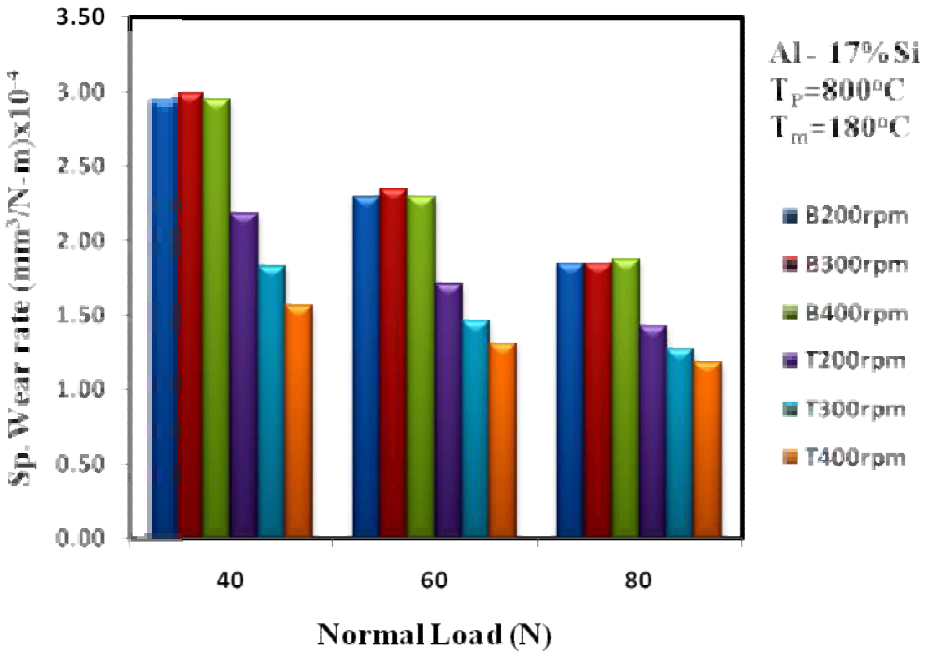

Fig. 4.56 Specific wear rate vs Normal load of Al-17wt%Si FGM for 800°C melt temperature and 180°C mold temperature.

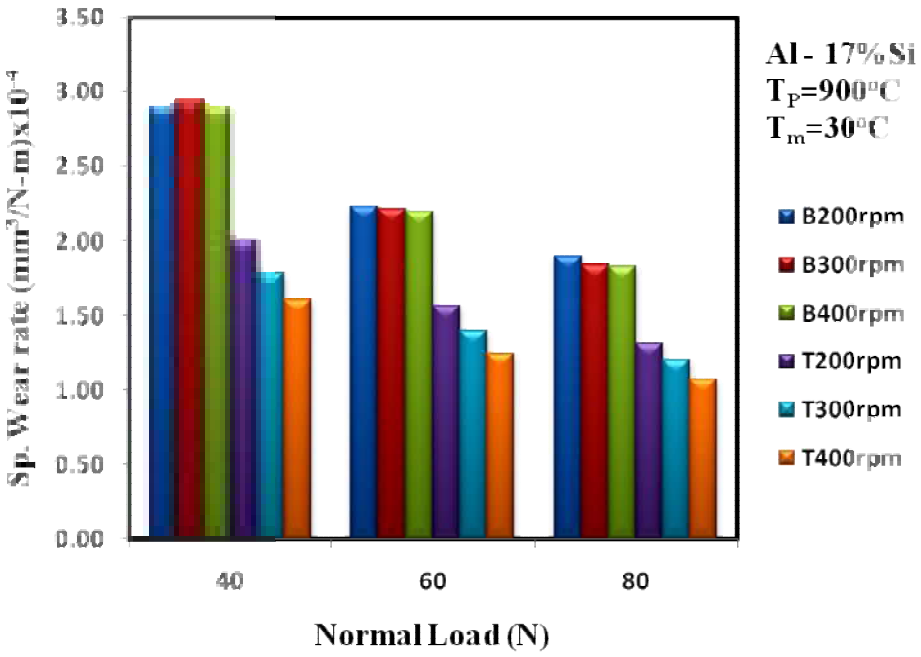

Fig. 4.57 Specific wear rate vs Normal load of Al-17wt%Si FGM for 900°C melt temperature and no preheating the mold.

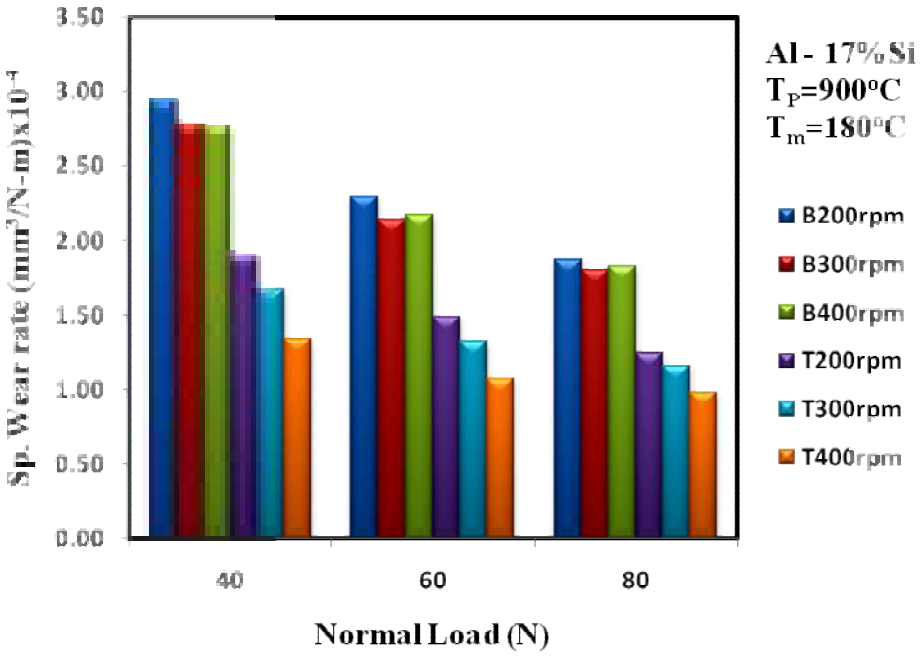

Fig. 4.58 Specific wear rate vs Normal load of Al-17wt%Si FGM for 900°C melt temperature and 180°C mold temperature

From the figures shown above it is evident that there is no significant change in specific wear rate in the bottom region of the casting for all the castings made under different process parameters. However under favorable process parameters the segregation of Si towards the top region has resulted in a decrease in specific wear rate which strongly depends on the Si volume fraction.

It can be noted that for a specific load of 40N the specific wear rate of Al-17wt%Si FGM cast with preheating mold and a teeming temperature of 900^{o}C at 400rpm decreases by 29% with respect to the casting for 200rpm. Similarly it is 28% and 21% lower for 60N and 80N tests respectively.

Table 4.3 clearly gives an idea of the amount of decrease in specific wear rate at different loads for the FG alloy produced at 900^{o}C teeming temperature, 180^{o}C mold temperature compared with other castings produced at the same speed.

Table 4.3 Specific wear rate for the specimen cast at 400rpm

Rpm	**T_P** (^{o}C)	**T_m** (^{o}C)	Decrease of Sp. Wear rate (%)		
			40N	**60N**	**80N**
400	900	30	20.00	16.67	9.09
	800	180	26.67	22.22	20.45
	800	30	40.00	41.67	29.55

From the results it can be realized that the decrease in specific wear rate is dominant at lower loads compared to the higher loads. Preheating the mold has significant effect on the specific wear rate. Casting produced in preheated mold has a greater wear resistance when compared to the other. This can be attributed to the fact that the larger segregation of the Si takes place towards the top side of the casting produced in preheated mold. This clearly shows that the result obtained during the wear test corroborates with the microstructure and hardness profile reported earlier. This can be accounted for according to the theory that the material such as anti-friction bearing alloy should have soft matrix in which hard particles are scattered in a controlled manner. The hard particles support the load, while the soft matrix can secure the hard

particle and transport the load from matrix to hard particle. The silicon particle reinforced FGM, the silicon particles support the load, so as to lessen the contact area between matrix and counter disc surface and decrease the friction, and can also prevent the scratch and cut from the hard counter face. The wear resistance of FGM is vastly improved at all lower and medium range loads. Table 4.4 provides the details of improvement in wear resistance when percentage Si in the cast alloy is higher. As observed from the results of the eutectic alloy and the hypereutectic alloy, the change in gradation due to the process parameters are same in both the cases. This feature along with the results provided in Table 4.3 justifies the use of hypereutectic graded alloy to exploit better wear resistance property at desired surfaces. Fig. 4.59 signifies the role of Si in improving the specific wear rate. The data presented is the summary of all the tests carried out. Better wear resistance properties are obtained at Si enriched regions in the casting.

Table 4.4 Increase in wear resistance of Al-17wt%Si over cast Al-12wt%Si FG alloy

T_P (°C)	T_m (°C)	Increase of wear Resistance (%)		
		40N	**60N**	**80N**
900	180	36.17	31.43	25.42
900	30	26.53	22.94	20.00
800	180	23.91	15.38	7.83
800	30	17.65	14.29	12.31

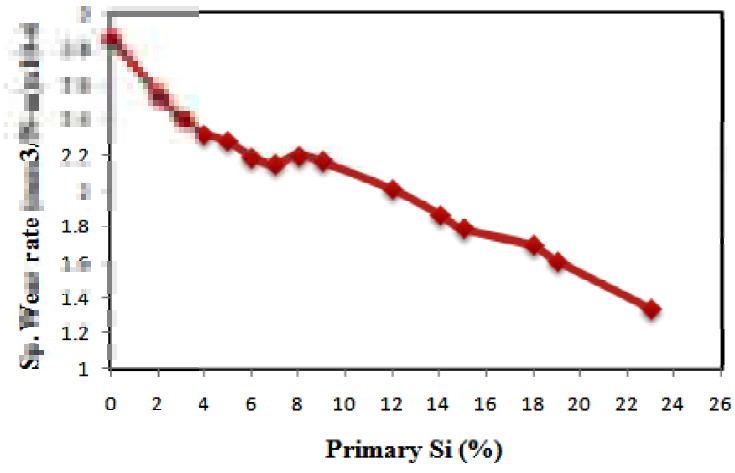

Fig. 4.59 The specific wear rate plotted as a function of the relative volume fraction of Si particles

Wear resistance is found to be better in the presence of fine and equiaxed primary α-Al grains and uniform distribution of second phase particles. The rotational speed of the mold is found to influence the quality of the microstructure of the test samples. It is found that in case of test samples cast at 400 rpm, the large primary α-Al grains are converted into fine equiaxed grains and that of eutectic silicon needle into fine particles enabling them to exhibit higher wear resistance even at higher applied loads. Crack nucleation is found to occur at some depth below the surface than near the surface of the test sample, owing to the very high hydrostatic compressive pressure acting near the asperity contact. Thus, once the crack is nucleated, its propagation is found to be slow and seizure would not occur due to the presence of well distributed particles in the matrix even at larger magnitudes of normal loads. Further increase in the load on the test samples leads to enhanced levels of plastic deformation and wear. Hardness measurements made on test samples subjected to wear at a load of 80N indicate its work hardening. The wear pattern clearly indicates the absence of steady state wear even with the increase in the applied loads on the test samples. Improvements in wear resistance of the test samples made at a rotational speed of 400 rpm are possibly due to the appreciable work hardening of the test specimen.

4.3.3.2 Coefficient of Friction

It is seen from the experiments that the COF increased to a maximum as the disc reached its set speed on starting and then smoothly decreased to a constant value. If changes in pin and disc surfaces took place, the COF rose with time on starting and reached a constant value. The variation of COF with time during the pin on disc test is shown in Fig. 4.60. Adhesion plays a main role in controlling the friction when aluminium slides on steel. Steady state of friction is due to attainment of steady state of mating surfaces from microstructure point of view. Metal transfer between interacting surfaces largely determines the friction coefficient, particularly, at early stage of sliding before steady state is achieved. At light loads a clear dependency of friction on sliding velocity and area of contact is noticed. It is noted that at light loads, oxide layer remains intact and as speed increases more lubricant is enforced into the

sliding interface so the slider may lift, giving rise to reduction in metallic contact (Zhiqiang 2005).

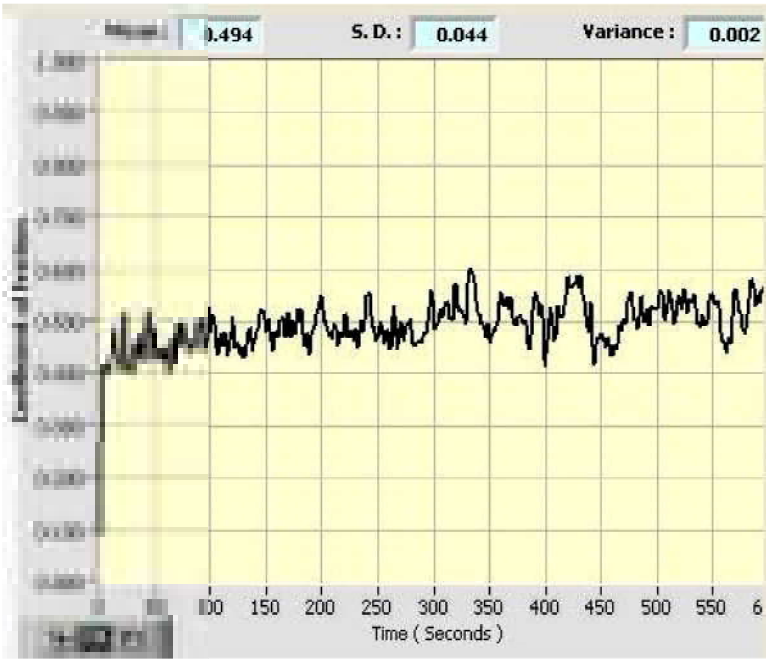

Fig. 4.60 COF vs time

The COF increases with increase in Normal load on the specimen. Reduction in COF is due to the less time available for asperity 'welding'. Increase in load, moreover increases the interface temperature. Rise in temperature with in a limit increases the ability of soft aluminum matrix to better accommodate hard and brittle second phase silicon particles which resist the thermal softening.

It is found that the Al-17wt%Si FGM produced using 900^{o}C teeming temperature with preheating the mold and cast at 400rpm which had 23% primary Si at the top showed very low COF. The COF of casting produced at 400rpm shows 8.9% and 9.4% lesser values as compared to 300 and 200rpm castings respectively; tested at 40N load, however, the FGM shows influence at increasing testing loads. At higher loads an oxide layer may form on the pin surface and reduce the friction. Two competing phenomena minimize the variation of friction coefficient with load. The plots of COF vs normal load under different processing parameters are shown in Figs. 4.61 to 4.64.

The comparison of top and bottom surface of the cast specimens clearly shows that the friction coefficient is more at the bottom. The top surface subjected to wear has significantly lower friction coefficient. This can be attributed to the increase in Si % compared to the bottom surface. At the bottom surface due to the presence of mainly dentritic Al and also with no free silicon COF is higher compared to the top surface.

From the above results it can be made out that there is a significant effect of the centrifugal force, melt temperature and teeming temperature on the friction coefficient. The comparison of top and bottom clearly acknowledges this effect. This clearly shows that the segregation of Si particle at the top surface significantly lowers the friction coefficient.

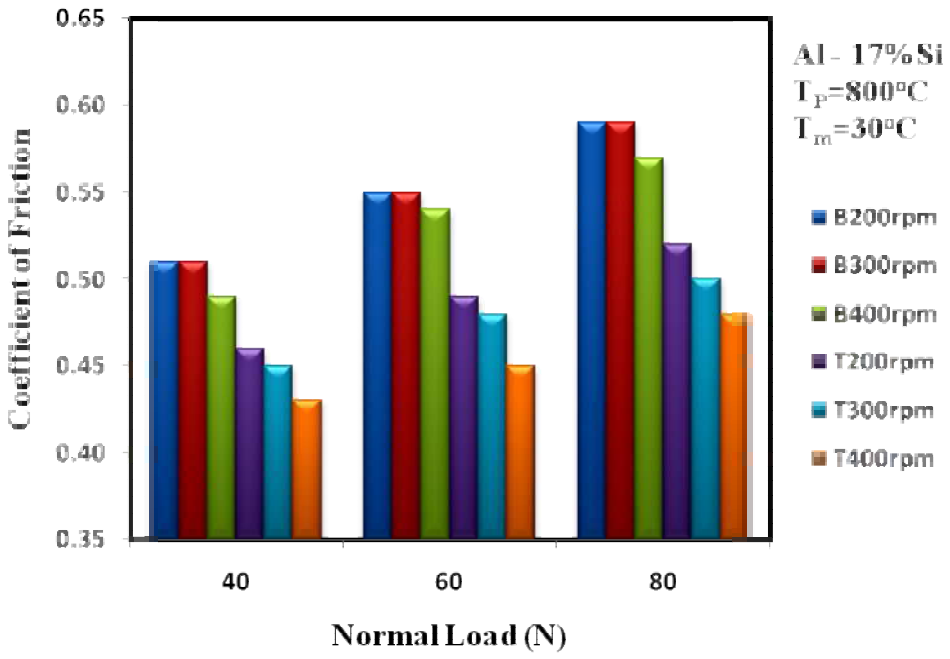

Fig. 4.61 COF of Al-17wt%Si FGM vs Normal load of the casting for 800°C melt temperature without preheating the mold.

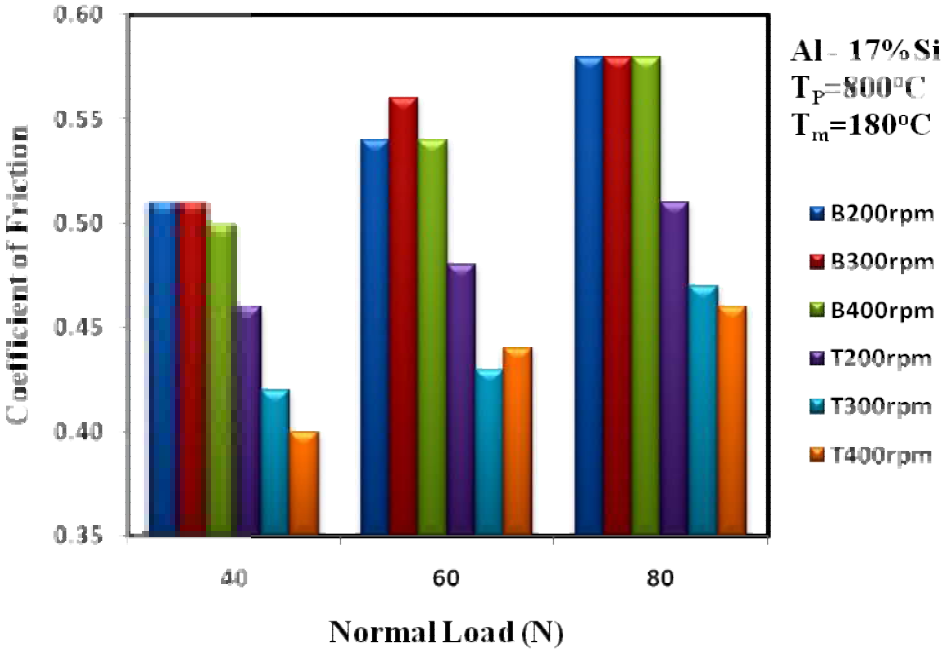

Fig. 4.62 COF of Al-17wt%Si FGM vs Normal load of the casting for 800°C melt temperature with preheating the mold.

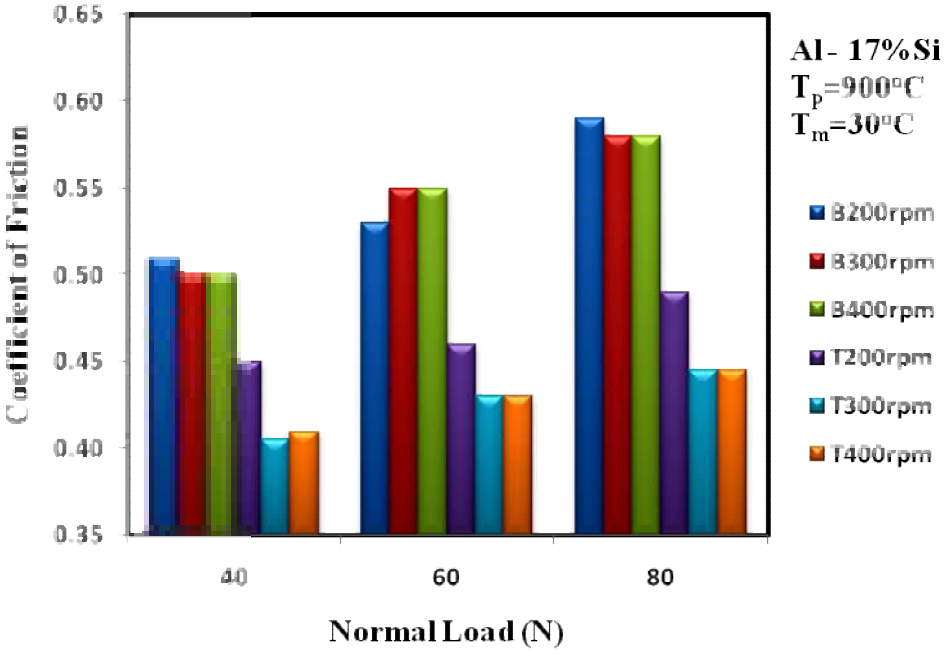

Fig. 4.63 COF of Al-17wt%Si FGM vs Normal load of the casting for 900°C melt temperature without preheating the mold.

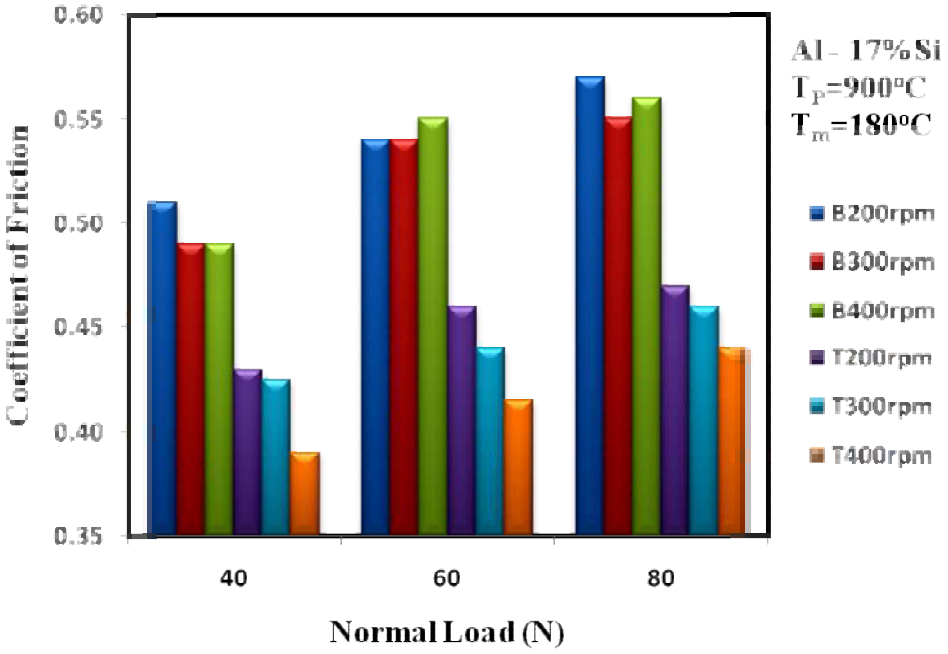

Fig. 4.64 COF of Al-17wt%Si FGM vs Normal load of the casting for 900°C melt temperature with preheating the mold.

4.3.4 Wear Analysis of the Al-Si FG Alloy

The effect of centrifuge process and processing parameters, presented earlier provide sufficient evidence that the process is suitable for producing Functionally Graded Material and further by properly controlling the process parameters such as rpm, mold temperature and teeming temperature it is seen that the percentage of the hard phase and its distribution along the length of the specimen can be controlled. For both the Al-Si alloys discussed earlier, the values of percentage of primary Si at the top end, its extension up to a certain distance from the top end known as rim thickness and constituents at the bottom of the specimen were different under different processing parameters. This was evident from the microstructural and hardness studies. It is thus expected that the two ends of the specimen of the FGMs would show different wear characteristics and it was confirmed by the results of wear test. The FG alloy specimens showed different wear rates for sample taken from the extreme ends of the specimen. The wear mechanisms generally observed could be (i) abrasive wear, (ii) delamination wear and (iii) adhesive wear. It was found that, for the Al-Si FG alloys

tested at the primary Si rich top end and hypoeutectic bottom end, combination of the above-mentioned mechanisms and a different wear mechanism or same was operative. SEM examination of the worn surfaces of the specimens taken from the extreme ends showed that the bottom end was dominated by abrasive and delamination wear, while the top end was dominated by delamination wear. The SEM photographs and EDS spectrum of the worn surface and the wear debris for the bottom region of the specimen are shown in Fig. 4.65. EDS on all the worn samples were carried out on an area using a 20kV electron beam. This gives the average composition on that surface.

At low magnification, the worn surface of the specimen from the bottom end was characterized by long ploughing lines that run parallel to the direction of sliding, as shown in Fig. 4.65(c). Such features suggest abrasive wear during sliding against the steel counter face. The scouring seen in the micrographs may be due to abrasion by tapped debris or due to work hardened deposits on the counter face or by hard asperities on the hardened steel counter face. Furthermore, upon closer examination, shallow craters and holes of varying sizes, as well as cracks perpendicular to the sliding direction were commonly observed and also extensive plastic flow and cracking was observed. These are the two likely modes of crack initiation and propagation.

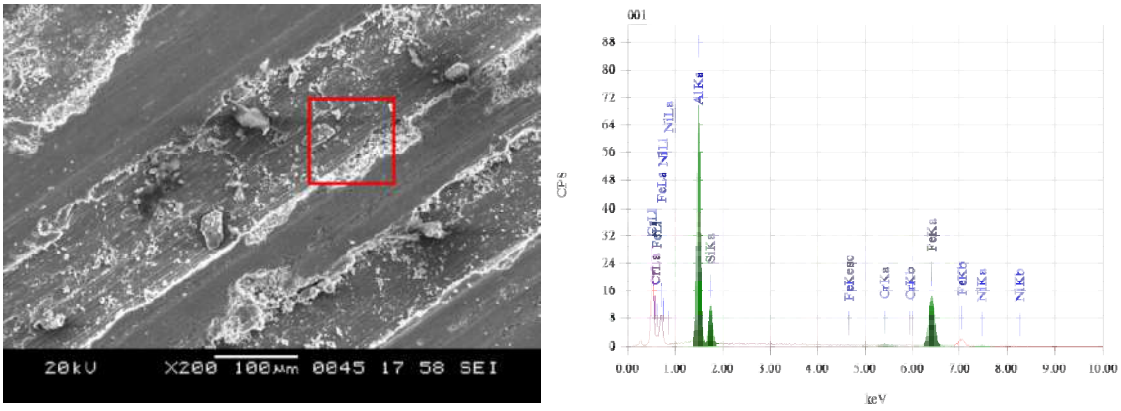

Fig. 4.65 a) Long, shallow craters of varying sizes caused by delamination on the bottom surface b) EDS spectrum showing the adhesion of Fe

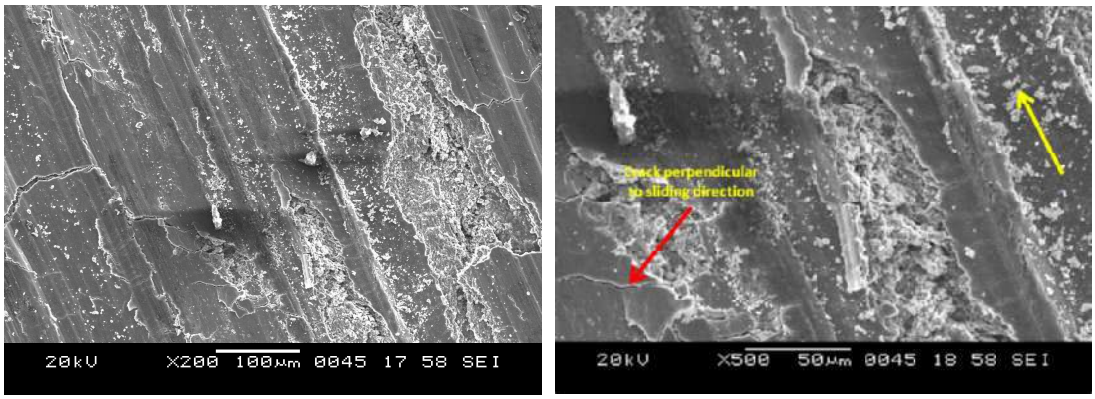

Fig. 4.65 c) Cracks and holes caused due to delamination on the surface at lower and higher magnification

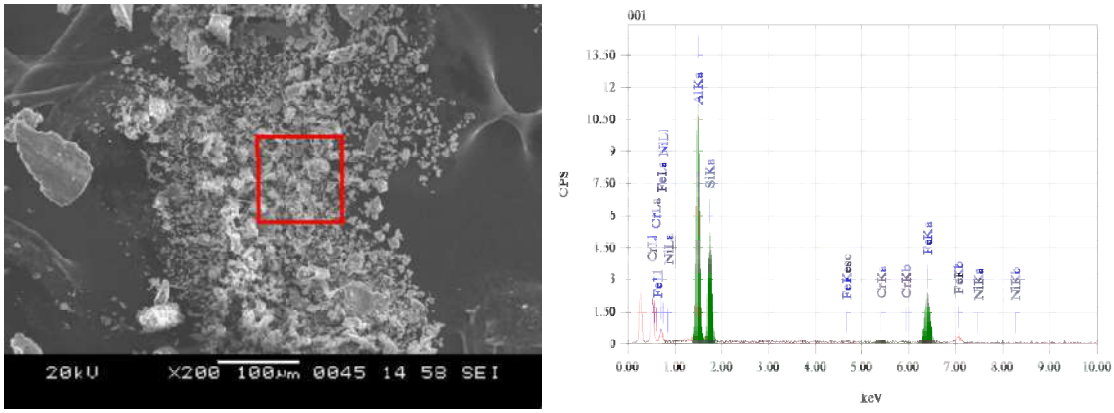

Fig. 4.65 d) SEM of Wear debris e) EDS spectrum of the wear debris

Fig. 4.65 SEM photographs and EDS spectrum of the bottom part of the casting.

Cracks may initiate in the highly work hardened layer, particularly in the sub surfaces region. When cracks grow and get interconnected, a layer of metal is removed. This is delamination of wear. The presence of these cracks and formation of such holes and craters during sliding of the specimens has been associated with the process of delamination on several occasions by other researchers (Nai et al 2003), (Dwivedi 2009), (Reddy et al 2009).

In case of the top end of the specimen the microstructure reveals that the delamination mechanism is more predominant. The SEM photographs and EDS spectrum of the worn surface and the wear debris for the top region of the specimen are shown in Fig. 4.66.

Delamination is the propagation of cracks preferentially along the sliding direction, which gives rise to the detachment of wear debris in the form of sheets. In case of the specimen from the top end of Al-Si FGM, delamination wear was confirmed by the presence of abundant flake-like wear debris collected from the wear of top end as shown in Fig. 4.66 (d). It is also seen in the photographs that long and continuous grooves appear at lower loads, but these grooves get wider and fine cracks start to appear as the load is increased. At the same time the top end has a tendency to flake. The EDS spectrum of these wear specimen shows the presence of iron, indicating that the material transfer from wear disc surface occurred across the interface during the wear tests. At high loads high interface temperature may increase the back transfer of Fe, which may diffuse into the near sliding surface and change the composition.

EDAX analysis of wear debris (Fig. 4.66e) clearly shows the presence of Fe, Al, and Si. The diffusion of Fe into the alloy may cause precipitation/dispersion hardening by reacting with different alloying elements. Opportunities to form such hard intermetallic compound will be less in the bottom of the casting because of smaller counter face wear. Hardening in the presence of alloying element may be a possible reason for higher seizure resistance of top surface compared to the bottom surface.

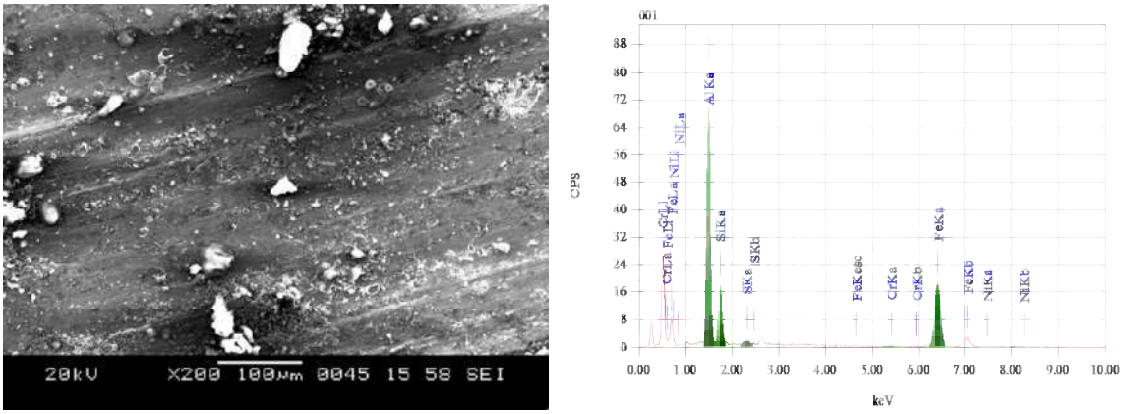

Fig. 4.66 a) Long, shallow craters of varying sizes caused by delamination on the surface of the top end b) EDS spectrum showing the adhesion of Fe on the top end of the specimen

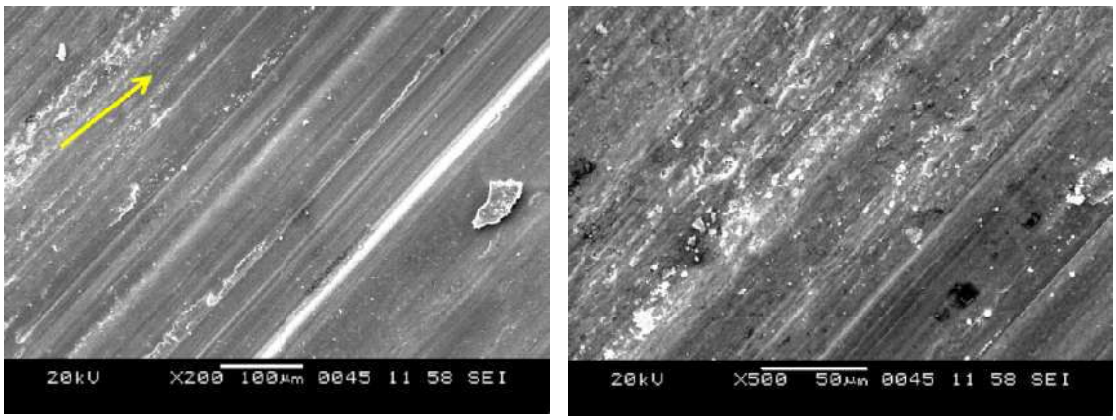

Fig. 4.66 c) Cracks and holes caused by delamination on the surface of top end at 2 magnifications.

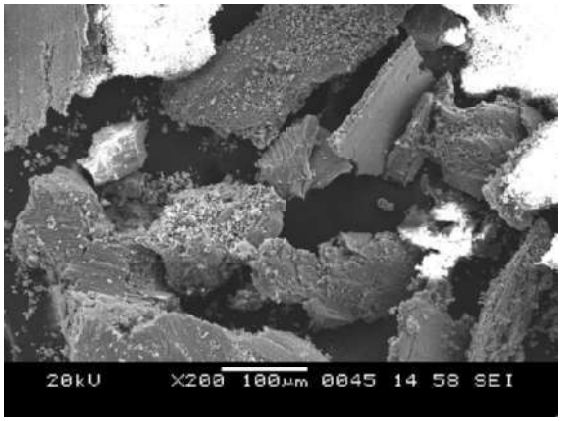

Fig. 4.66 d) Flake Wear debris from the top end

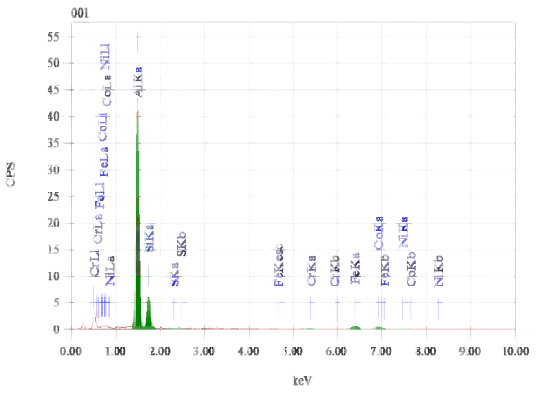

Fig. 4.66 e) EDS spectrum of the debris collected from the top end

Fig. 4.66 SEM photographs and EDS spectrum of the top of the Al-Si FGM specimen subjected to wear.

It has been reported that friction also depends on material properties such as hardness, strain, density, shear strength, modulus of elasticity and ultimate strength (Sarkar et al 1975). High hardness of the top surface compared to the bottom surface may explain the reduced incidence of fracture and deformation of surface asperities with its small contact area. This also explains low COF in sliding for the top surface than that of the bottom surface under similar conditions. Friction force arises from two main reasons: (a) force required to shear minute welds formed at contact points between two rubbing surfaces and (b) force required to blow the hard asperities over a soft surface. At high loads, the formation and large growth of junction asperity in

contact regions, increases the force required to shear off the junction to maintain the relative motion. This explains the higher COF at higher normal loads.

4.4 Al-Si- SiC_P Composite system

High strength, thermal stability, and wear resistance of Aluminum based Metal Matrix Composites (MMCs) in general and particle reinforced composites in particular are used extensively in the automotive industry. It is also established that increasing the volume fraction of the reinforcement increases the performance of the MMCs. These composites however do not show improved performance for load bearing applications. Functionally Graded MMCs (FGMMCs) are new class materials intended to eliminate the drawback of the MMCs in which the surface of one side provides higher hardness but the interior region will have higher resistance towards the crack growth. On account of low dissipation of energy due to the high segregation of SiC_P at the boundary, the fracture toughness is low for small crack lengths in case of Al-Si- SiC_P composite system (Castro et al 2002).

The Al-Si- SiC_P FGMMCs show a gradual change in the volume fraction of the SiC particle along the length of the casting. The gradient in the SiC particles is seen because of the application of the G force on the particle during casting. The moving direction of the particle under the centrifugal force is determined by the relative magnitudes of densities. The densities of SiC_P and molten Al-Si matrix are 3150 kg/m^3 and 2400 kg/m^3 respectively. Hence, SiC particles move towards the bottom of the casting under the action of a centrifugal force. Since the melting point of SiC_P is higher than the processing temperature, these particles remain as solid phases in a liquid matrix during the application of the centrifugal force.

In this study SiC particle reinforced Al-Si alloy based FGMMCs have been produced by centrifuge casting process. The castings were produced at 200, 300 and 400rpm of the mold. The two alloys studied earlier namely Al-17wt%Si and Al-12wt%Si were used as matrix material with 2, 4 and 6 weight % of SiC_P added as reinforcement to the matrix. The samples were cast at 900^{o}C teeming temperature and

mold temperature of 180°C. The graded composites were tested for volume fraction of SiC particles and hardness along the length of the sample. The wear tests were conducted on the top and bottom surfaces of the casting.

4.4.1 Microstructure

4.4.1.1 Al-17wt%Si-SiC

The microstructure of the FGMMC with 2% SiC_P cast at 200, 300 and 400rpm is shown in Fig. 4.67.

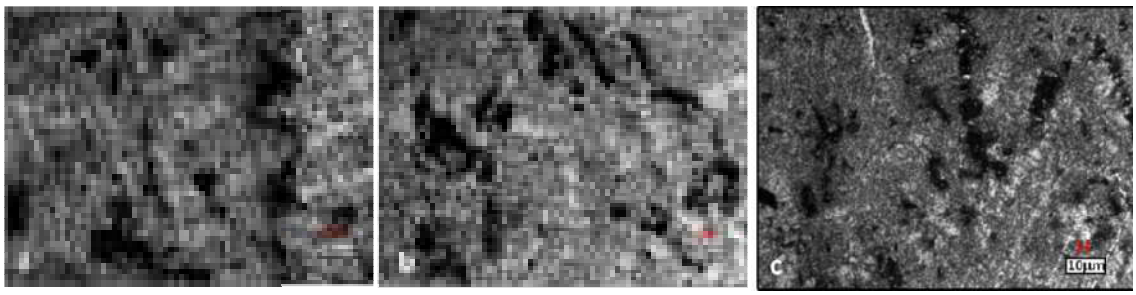

Fig. 4.67 Microstructure of Al-17wt%Si-2% SiC_P system at 200, 300 and 400rpm

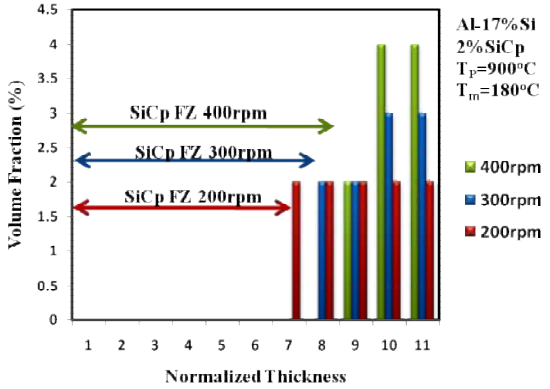

Fig. 4.68 Distribution of SiC_P along the length of the sample for 2wt% reinforcement.

The segregation of SiC_P is more at 400rpm when compared to the other two rpm's. For 2% SiC_P reinforcement the amounts of enrichment at the lower surface of casting are 2%, 3% and 4% respectively at 200, 300 and 400rpm. The rim thicknesses of the SiC_P rich zone from the bottom of the casting are 16mm, 12mm and 8mm

respectively. The volume fraction of SiC_P and SiC_P free zone with respect to the bottom end are shown in Fig. 4.68.

With increase in volume fraction of SiC_P from 2% to 4% the segregation of SiC_P at the bottom end of the casting increased to 5, 7 and 8% at 200, 300 and 400rpm respectively, while the rim thickness remained same as in the case of 2% and further similar trend was observed at 6% SiC_P with the amount of segregation increasing to 6%, 8% and 10% as shown in Fig. 4.69.

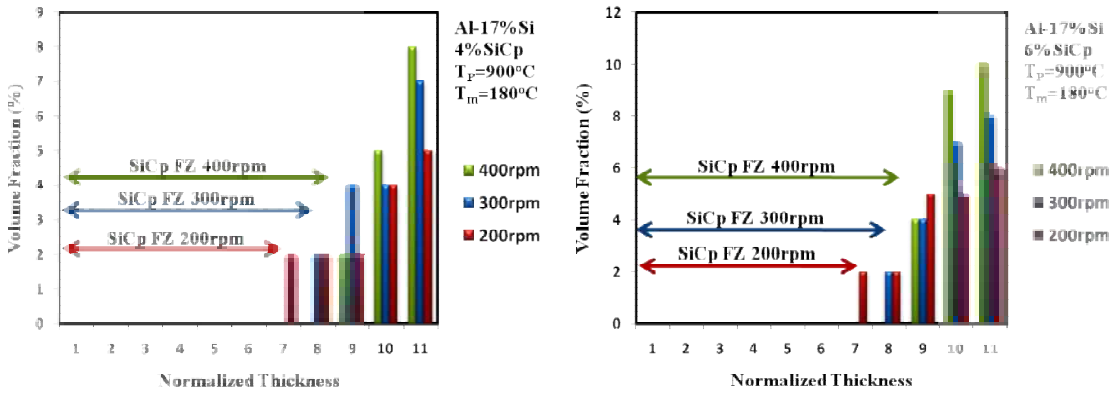

Fig. 4.69 Distribution of SiC_P along the length of the sample for 4wt% and 6wt% reinforcement.

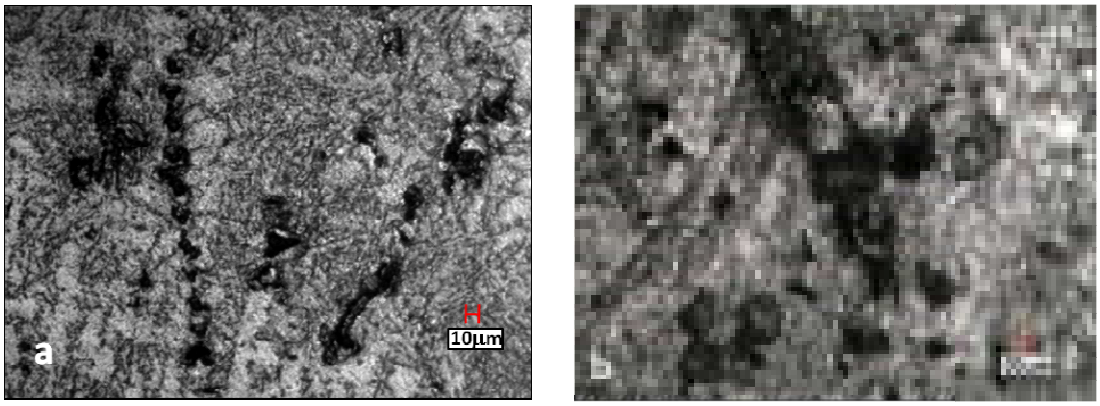

Fig. 4.70 Microstructure of FGMMC by a) Conventional stir casting technique, b) Centrifuge technique

The distribution of SiC particles in the Al- 17% Si castings is better when it is cast centrifugally than by the conventional stir casting method (Fig. 4.70). This is due to the fact that alloy solidification takes place in a very restricted zone at the interfaces between particles; the quick transport process of particles in liquid aluminum alloy promotes the homogeneous nucleation of matrix alloy during solidification. The fine equiaxed primary α-Al can be achieved in this zone, and the solidification front of primary α-Al pulls SiC particles to the interface between thin primary α-Al phases. The larger the number of primary α-Al grains, the more uniform is the distribution of SiC particles. In the free particle zone, the centrifugal agitation prevents the growth of eutectic silicon and dendritic primary α-Al, and low under cooling leads to a coarse primary α-Al. Therefore, thin granular eutectic Si phase and coarse non-dendritic or dendritic primary α-Al are observed in this zone.

4.4.1.2 Al-12wt%Si-SiC

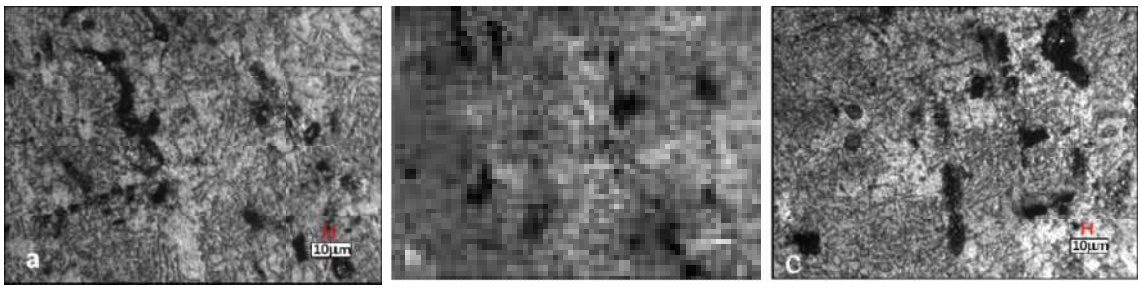

Fig. 4.71 Microstructure of Al-12wt%Si-2% SiC_P system at 200, 300 and 400rpm

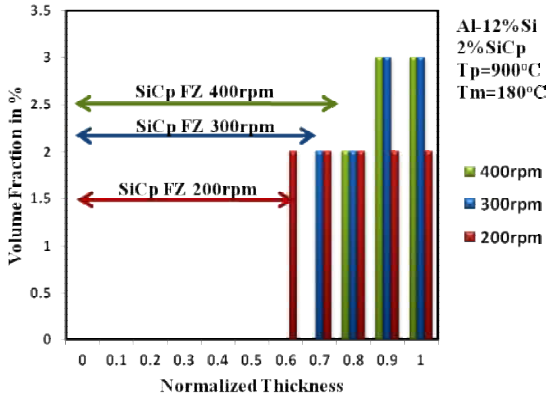

Fig. 4.72 Distribution of SiC_P along the length of the sample for 2wt% reinforcement.

FGMMCs cast using 12wt%Si with different wt % of SiC particulates has shown an increased volume fraction of SiC_P at the bottom of the casting. At 2% reinforcement the segregation is found to be 3%, 3% and 2% for 400, 300, 200rpm with rim thickness of 16mm, 12mm and 8mm respectively. The melting points of SiC particles are higher than processing temperatures and these particles remain as solid phases in the liquid matrix during application of the centrifugal force. The distribution conditions of SiC particles in a viscous liquid influence the microstructural characteristics in centrifugal casting of composites. The morphology of primary α-Al in turn affects the distribution of SiC particles. At the bottom of the casting as it is having primary α-Al dendrites particle entrapment and engulfment are expected during solidification giving rise to the uniform distribution of SiC particles. Fig. 4.71 also clearly indicates good interface bonding between SiC particle and the metallic matrix. The volume fractions of SiC_P and SiC_P free zone with respect to the bottom end are shown in Fig. 4.72.

With increase in volume fraction of SiC_P to 4%, the segregation of SiC_P at the bottom of the casting FGMMC measured was 7%, 7% and 5%, for 400, 300, 200rpm and the rim thickness changed to 8mm, 12mm and 16mm respectively. Similarly at 6% SiC_P the corresponding values were 8%, 7% and 6% and 8mm, 12mm and 20mm respectively as shown in Fig. 4.73.

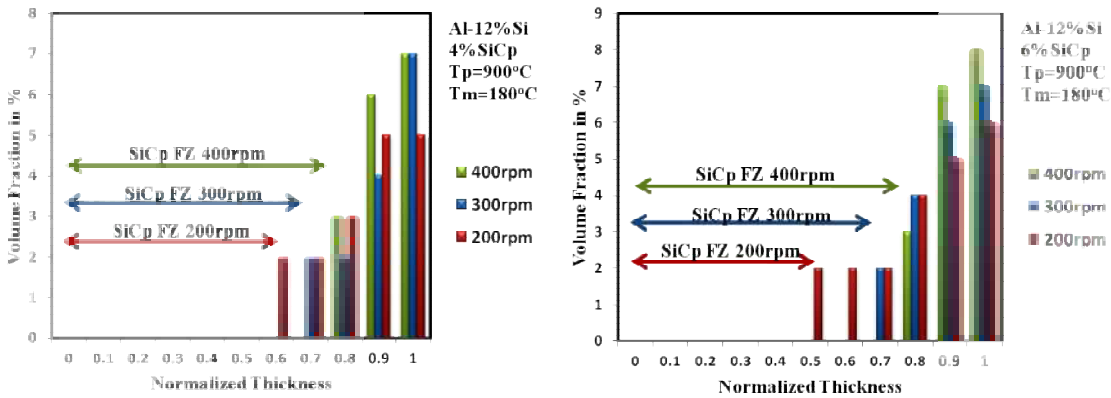

Fig. 4.73 Distribution of SiC_P along the length of the sample for 4wt% and 6wt% reinforcement.

4.4.1.3 Effect of rotational speed

During the centrifuge casting, segregation of particles takes place in the melt due to the movement of particles resulting from the difference in densities of the particles and the melt, and also due to the centrifugal acceleration. The solid particles are subjected to radial buoyancy (F_c) and radial moving velocity (V_c) as given by equations 4.1 and 4.2.

$$F_c = \frac{\pi d^3 (\rho_p - \rho_l) \omega^2 r}{6} \quad 4.1$$

$$V_c = \frac{d^2 (\rho_p - \rho_l) \omega^2 r}{18 \eta_c} \quad 4.2$$

where d is the diameter of the reinforced particle (m), ρ_p and ρ_l are the densities of the particle and the liquid (kg/m^3), ω is the angular velocity of the mold (rad/s), r is the distance of the particles from the axis of rotation (m), and η_c is the viscosity of the liquid with solid particles (Pa.s). If $\rho_p < \rho_l$, then $V_c<0$, the particles move toward the top part of the casting, whereas if $\rho_p > \rho_l$, then $V_c>0$, the particles move away from the axis of rotation (bottom of the casting). In this Al-Si- SiC_P system, the density of the SiC particles is higher than that of the liquid metal, and hence, the particles are pushed toward the bottom surface of the casting.

From the Figs. 4.72 and 4.73 it can be observed that the thickness of the particle segregated region decreases with the increase in rotational speed of the mold. It is also noted that at relatively lower rotational speeds, there is a section near the bottom of the casting in which the final volume fraction of the particulates is equal to that of the initial volume fraction in the melt. This signifies that the melt in contact with the mold solidifies so rapidly that no particulate is able to migrate into or out of this melt. Beyond this small section, the volume fraction of the solid particulates increases rapidly, reaching the maximum in the segregation pattern. The thickness of

this section decreases with the increase in the rotational speed of the mold (Fig. 4.74) and the density difference between the particle and the melt.

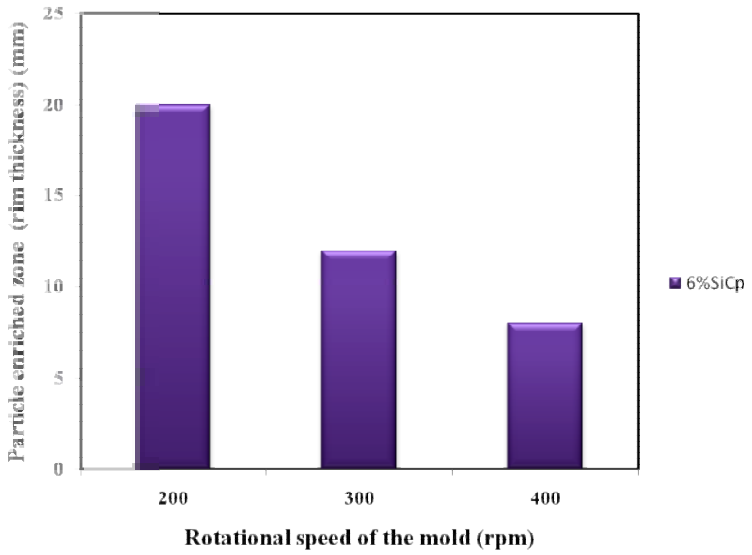

Fig. 4.74 Effect of speed on rim thickness

This can be further explained as the effect of chilling. At lower rotational speeds, the velocity of the solidification front at the mold is greater than the particle velocity. As a result, particles originally present in the region are trapped and no new particles are able to reach this region before melt solidified. Gradually, as the solidification front moves to the interior of the casting, the time required to solidify a volume segment having the same dimensions increases, giving the particles more time to move toward the bottom part of the casting, which subsequently leads to a segregated region next to the section. As the centrifugal force on the particles increases with increasing rotational speed of the mold, the velocity of the particles soon exceeds the velocity of the solidification front, leading to a shortened section. It has been established that for aluminum, the heat transfer coefficient at the metal/mold interface increases with an increase in the rotational speed and at a higher rotational speed, liquid metal exerts a larger pressure on the solidified layer, which, in turn, results in a better physical contact between the solidified layer and the mold wall, improving the heat transfer coefficient at this interface (Shamsi et al 1993).

4.4.1.4 Effect of Temperature

The previous discussion on Al-Si FG alloy shows that, with an increase in initial pouring temperature, the thickness of the particle-rich region shrinks. The higher initial pouring temperature essentially means that the larger amount of heat has to be removed from the melt before solidification begins. Hence, the metal matrix composite takes longer time to solidify, and during this extra time, the reinforcement particles are able to segregate more, forming a denser segregation pattern. With higher initial mold temperature, the rate of heat withdrawal from the melt to the mold is reduced because of the reduced thermal gradient. As a result, the solidification time is increased, allowing extra time for solid particulates to segregate and pack into thinner regions.

4.4.1.5 Effect of Matrix and Reinforcement

At 2% and 4% reinforcement the segregation of the SiC particles towards the bottom is almost increased by 100% whereas for 6% reinforcement it is 66% in Al-17wt%Si. This may be attributed to the fact that the increase in % of the SiC has decreased the fluidity of the system which in turn decreased segregation. In centrifuge casting process, where high centrifugal forces are involved, the particles are restricted to move in the direction of the centrifugal force with increasing radial speeds at increasing angular velocities. The solidification front, on the other hand, moves in the opposite direction with a variable speed toward the axis of rotation. Moreover, it has been observed and reported (Castro et al 2002) that cooling rate is enhanced with increasing mold rotation speed because of better heat transfer, i.e high centrifugal forces produce a tight contact between the mold wall and the melt and also due to the presence of thermally insulating SiC particles, higher SiC particulate contents reduce the amount of heat to be removed and this causes an increase in the solidification rate. The high cooling rate gives rise to a much finer cast microstructure.

From the microstructure of Al-12wt% Si matrix reinforced with different wt % of SiC particles, it can be noted that the amount of SiC particles segregated at the

bottom of the casting in Al-12wt% Si is less compared to the segregation of the SiC particles in Al-17wt%Si. This is due to the fact that the increase in Si increases the fluidity and castability (Apelian, 2009), (Campbell et al 2003). So the decrease in Si content has decreased the fluidity and increased the solidification rate. Eutectic alloy freezing range is much less compared to a hypo or hyper alloy. This will drastically reduce the segregation time for the SiC particle. The movement of the SiC particle is now totally affected due to the fluidity and solidification rate. This has resulted in a reduced concentration of SiC particles towards the bottom end of the cast specimen.

The comparison of distribution pattern of centrifuge cast silicon carbide particles reinforced Al-17wt%Si and Al-12wt% Si alloys show that there is a more SiC enriched zone in Al-17wt%Si compared to Al-12wt%Si. This is obviously due to solidification range being larger in 17% alloy. The difference in freezing range (longer freezing range of Al-12wt%Si) and viscosity of the alloy (Rajan et al 2009).

The SiC particle distribution graphs show that the gradient of SiC is more steep in case of Al-17wt%Si compared to Al-12wt%Si. For Al-12wt%Si at 200rpm the SiC particles are spread for 20mm from the bottom whereas for Al-17wt%Si they are spread for 16mm only.

It has been noted that the segregation for SiC particles towards the bottom end of the casting depends not only on the speed of rotation of the mold but also on the matrix. The 'G' factor forces the SiC particle towards the bottom end along its direction due to the density difference between the melt and the SiC particle. The content of the Si in the matrix affects the fluidity which reduces the temperature range solidification which in turn increases the rate of phase transformation allowing very less time for particle movement.

4.4.2 Hardness

As evident from the Figures 4.75 to 4.80 in case of FGMMCs there is a substantial increase of hardness at the bottom of the casting. Further the hardness yielded best results at 6% SiC_p reinforcement for both the matrix materials. At the top region, leading to segregation of Si, hardness similar to alloy FGM was obtained. Thus a middle region of comparatively lower hardness is sandwiched between harder top and bottom.

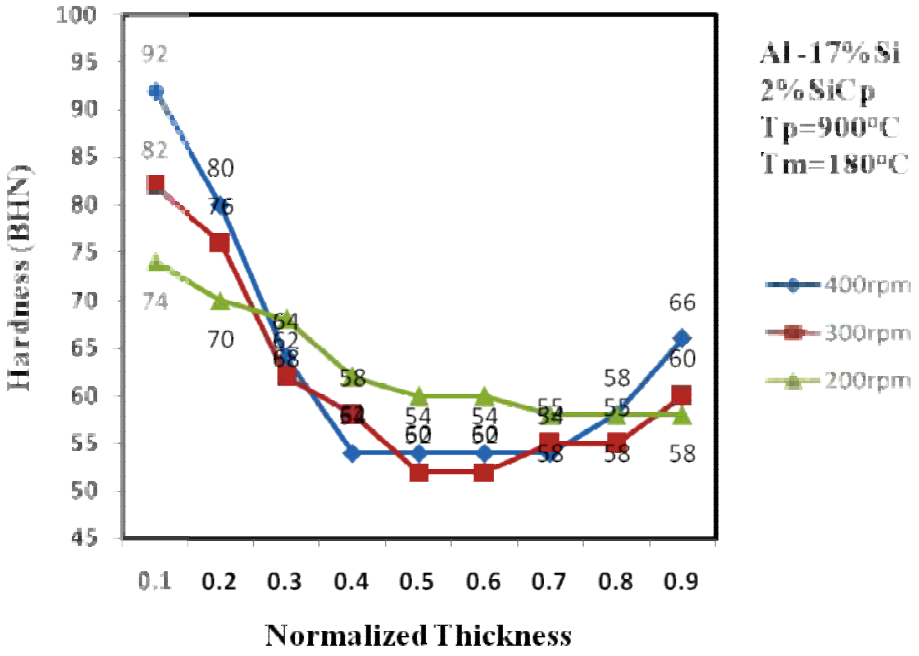

Fig. 4.75 Hardness values along the length of the casting for Al-17wt%Si-2wt% SiC_P FGMMC.

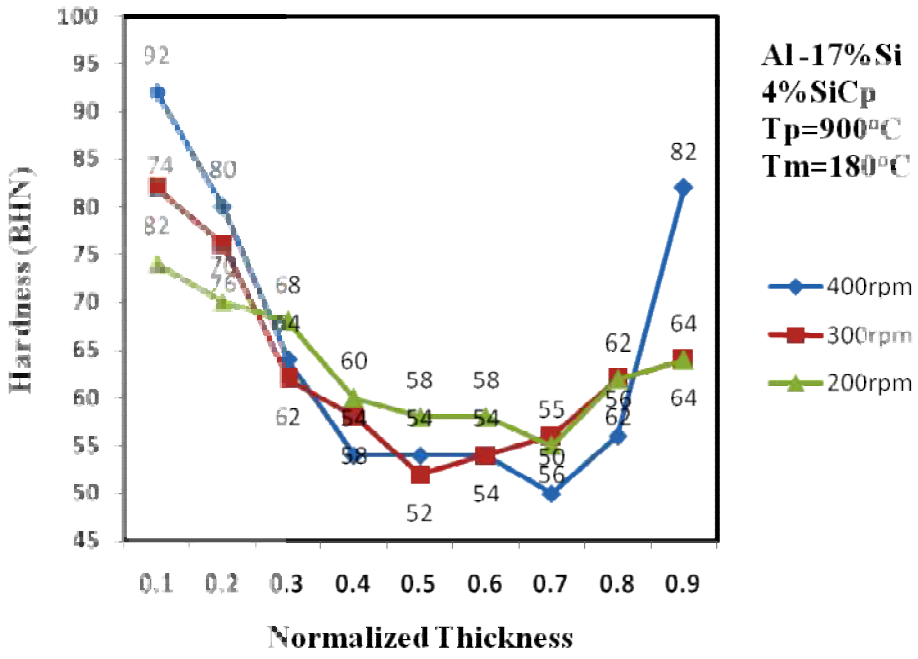

Fig. 4.76 Hardness values along the length of the casting for Al-17wt%Si-4% SiC_P FGMMC.

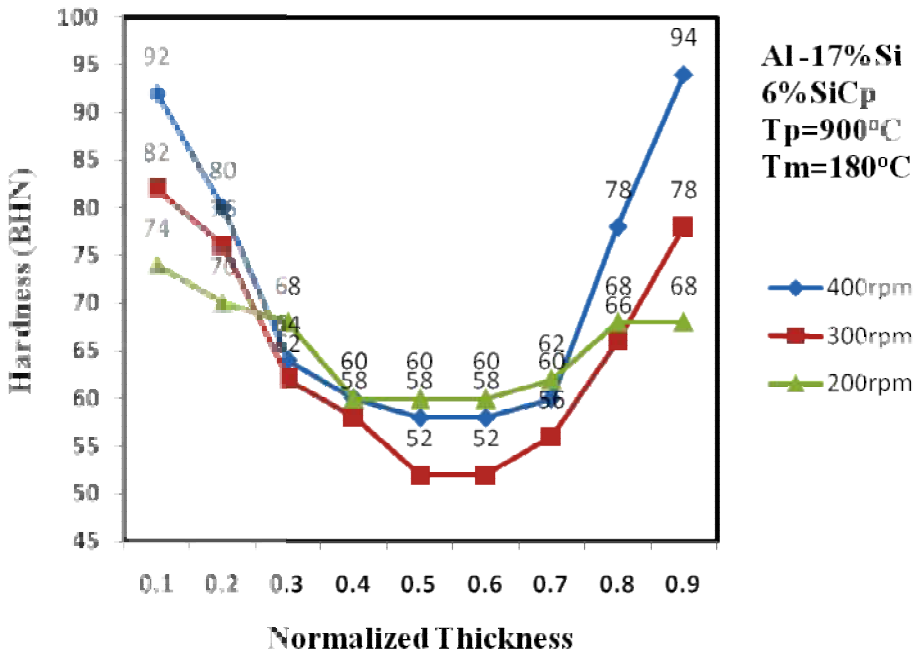

Fig. 4.77 Hardness values along the length of the casting for Al-17wt%Si-6% SiC_P FGMMC.

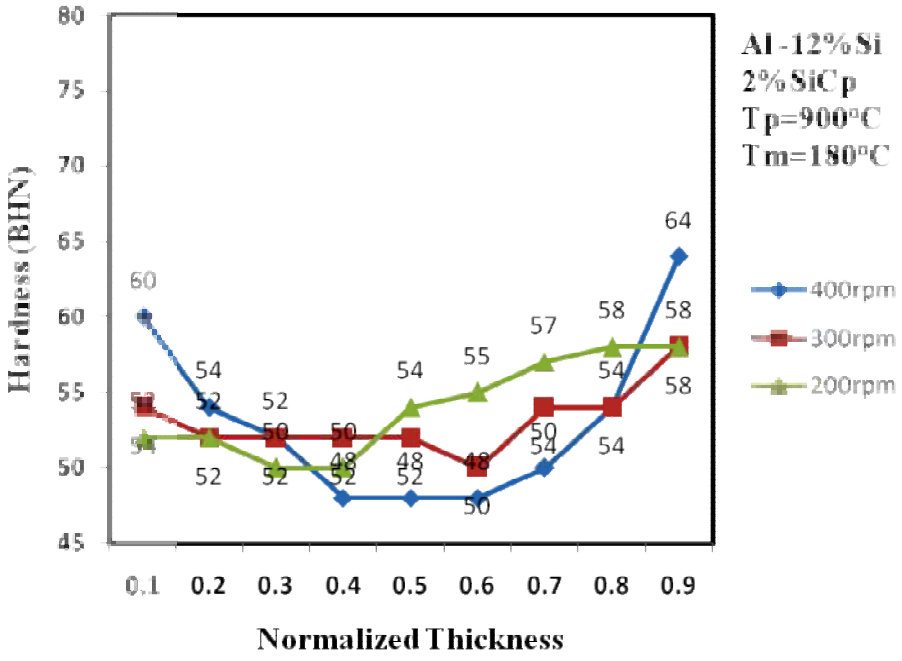

Fig. 4.78 Hardness values along the length of the casting for Al-12wt%Si-2% SiC_P FGMMC.

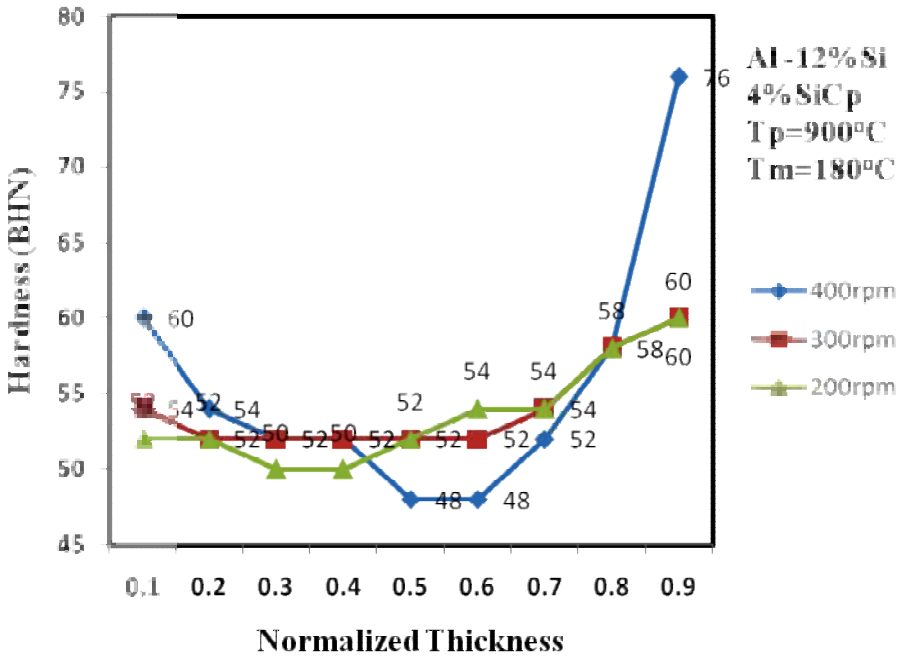

Fig. 4.79 Hardness values along the length of the casting for Al-12wt%Si-4% SiC_P FGMMC.

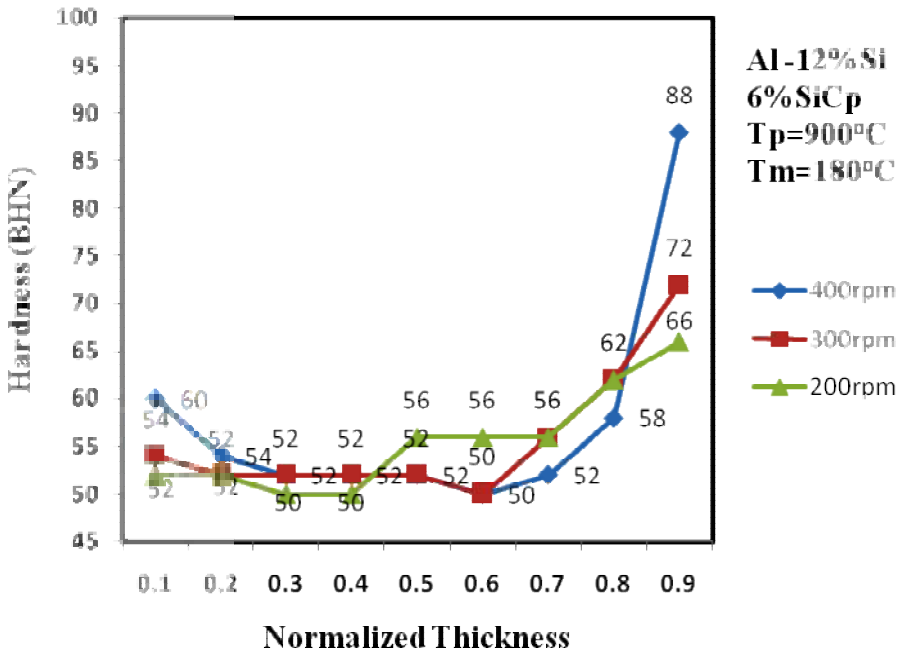

Fig. 4.80 Hardness values along the length of the casting for Al-12wt%Si-4% SiC_P FGMMC.

For Al-17wt% Si matrix alloy a reinforcement of 2% SiC_P yielded a maximum hardness of about 66BHN at 400rpm while for 4% and 6% the hardness was found to be 82 and 94BHN. Similarly for Al-12wt% matrix hardness of 64, 76 and 88BHN is achieved at the bottom of the casting for 2%, 4% and 6% reinforcement respectively.

In centrifugal castings solidification progresses radially inwards from the outside surface. This is due to the fact that the outside and bottom surfaces are in contact with the mold surface and the top surface is free. The liquid also undergoes certain amount of shear and mixing possibly preventing the formation of a crust on the top surface. High pressures developed due to the centrifugal force, in addition, delay the air gap formation, and make the air gap smaller. This enhances the heat transfer rate at the outer surface. High rates of heat transfer, and therefore solidification, leads to refined structure. We can see that by reducing the heat transfer rate the solidification rate of the casting can be reduced. This reduced solidification rate gives more time for the SiC particles to segregate towards the bottom of the casting. The segregation can be enhanced by increasing the pouring temperature and

mold temperature. In the following explanation the heat transfer between the liquid metal and the mold is enumerated with the aid of Fig. 4.81.

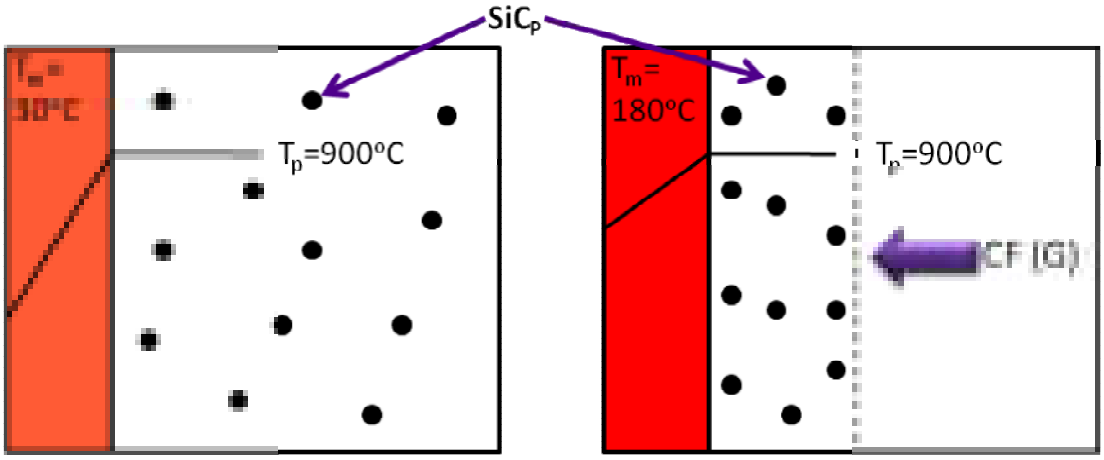

Fig. 4.81 Mold temperature gradient and centrifugal force

When the mold temperature is low (room temperature) and the liquid temperature is 900^{o}C, a steep temperature gradient at the mold is expected. The higher difference in temperature causes faster heat transfer at the mold-liquid interface. This results in higher solidification rate. As the mold temperature is increased, the temperature gradient gets reduced. This results in a decrease of the heat transfer coefficient at the casting mold interface, leading to a slower solidification rate. At a slower solidification rate, more time is available for SiC particles to segregate better under G forces and this results in higher hardness compared to that at higher solidification rate.

4.4.3 Wear

The top and bottom regions of the specimens were subjected to wear test at ambient temperature under dry sliding condition. The aim of this study is to find the volume loss, coefficient of friction variation under different loads. The wear mechanism causing the loss of the material during the friction and wear for the FGMMCs castings with 2, 4 and 6% SiC_P reinforcement in Al-17%Si and Al-12%Si alloy are the key points of this study.

4.4.3.1 Al-17wt%Si-SiC

The dry sliding behavior of the Al-Si/ SiC_P FGM under different loads of 40, 60 and 80N at 1.446 m/s sliding speed is evaluated. The wear mechanism causing the loss of the material during the friction and wear is investigated.

Volume loss of Al-17wt%Si-SiC_P FGM composite at both top end and bottom end of the casting is determined as a function of the applied load at sliding speed of 1.466 m/s. The weight loss of both the ends having SiC_P and Si respectively increases with the increase of the applied load. It may be noted that in the composite specimens the bottom end (having segregated SiC_P) exhibited significantly lower volume loss than the corresponding Functionally Graded Al-Si alloy. In case of FGMMC, the top end of the casting has segregated Si and thus shows lower volume loss compared to the middle region which has neither the SiC_P nor the primary Si segregation. It is also evident from the graph that there exists a certain applied load, i.e. a transition phenomena at which there is a sudden increase in the wear loss, in the matrix alloy, while there is no evidence of transition load in the composite tested at that test load.

As the volume percent of reinforcement influences the wear rate in a composite material, it is of interest to know the percentage variation in the wear rate for every increment of the reinforcement volume percent at a particular test load. However, in order to know whether this variation depends on the magnitude of the test load as well, the specific wear rate of the various composites tested have been calculated for three test loads.

From Figs. 4.82 to 4.84 at different test loads, for 2 volume percent of SiC_P reinforcement in Al-17%Si alloy/MMC, SWR decreased by about 11.3%, 8% and 10.34% at 40, 60 and 80N respectively at sliding speeds of 1.446m/s for castings produced at 400 rpm compared to 200rpm. For 4% of SiC_P reinforcement produced at 400rpm it has been noted that the SWR decreased by 15.8, 14.46 and 13.8% for 40, 60 and 80N test loads in comparison with 2% of SiC_P reinforcement FGMMC. But there is a significant improvement in case of 6% SiC_P reinforcement wherein the

SWR decreased by 36.9%, 30.8% and 23.2% for 40, 60 and 80N test loads in comparison with 4% of SiC_P reinforcement FGMMC. This clearly shows that the additions of SiC_P to Al-Si alloys enhance the strength of matrix, reducing contact area at any given load leading to reduction in SWR. From these results, it is clear that the effect of increase of test load in improving the wear resistance is higher in MMCs with harder reinforcement particles embedded in softer matrix and vice versa. The decrease of SWR with increase in test load can be attributed to higher strain hardening of matrix.

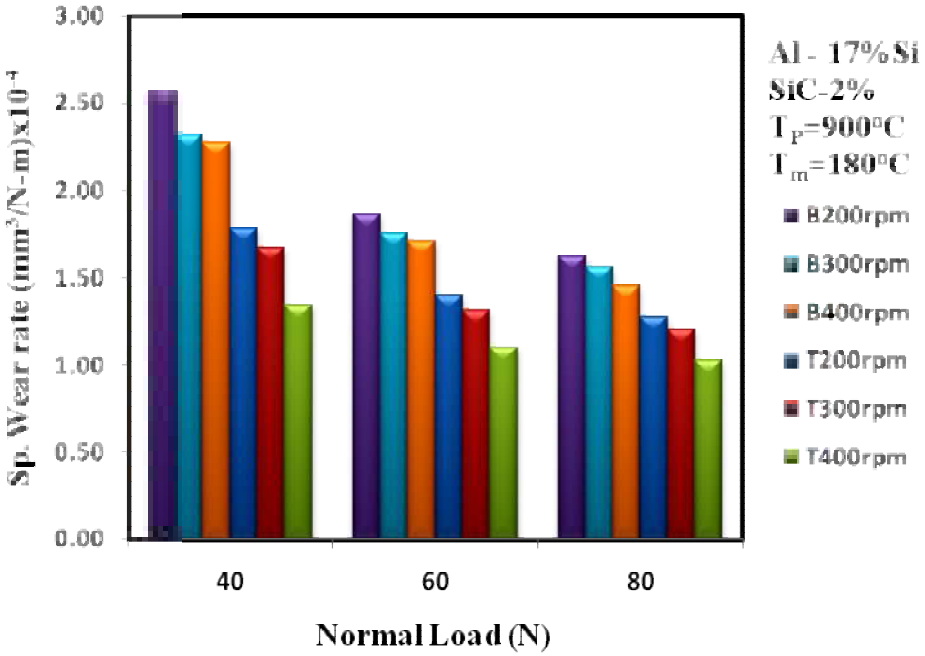

Fig. 4.82 Specific Wear rate of Al-17wt%Si-2% SiC_P FGMMC.

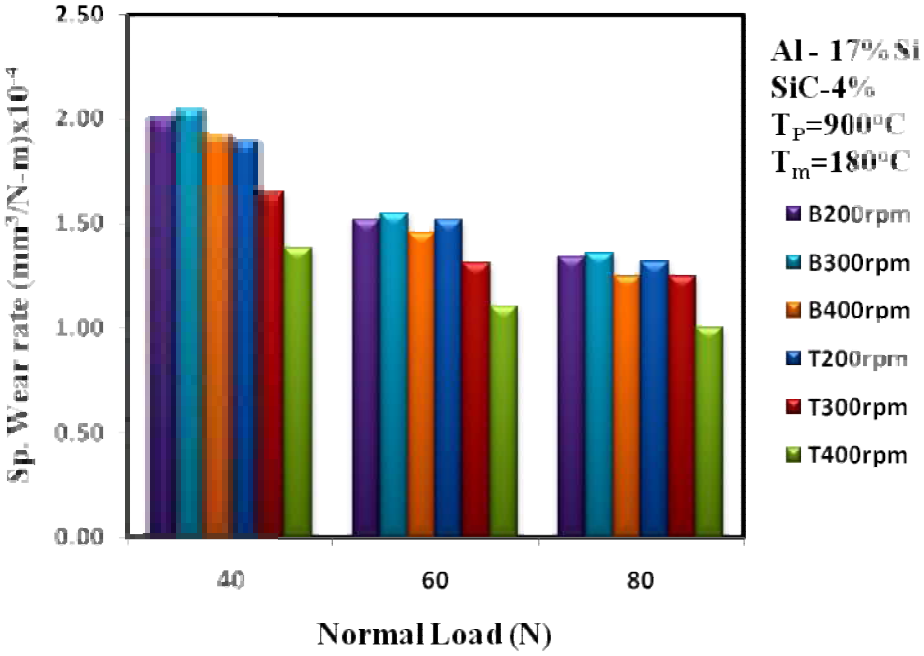

Fig. 4.83 Specific Wear rate of Al-17wt%Si-4% SiC_P FGMMC.

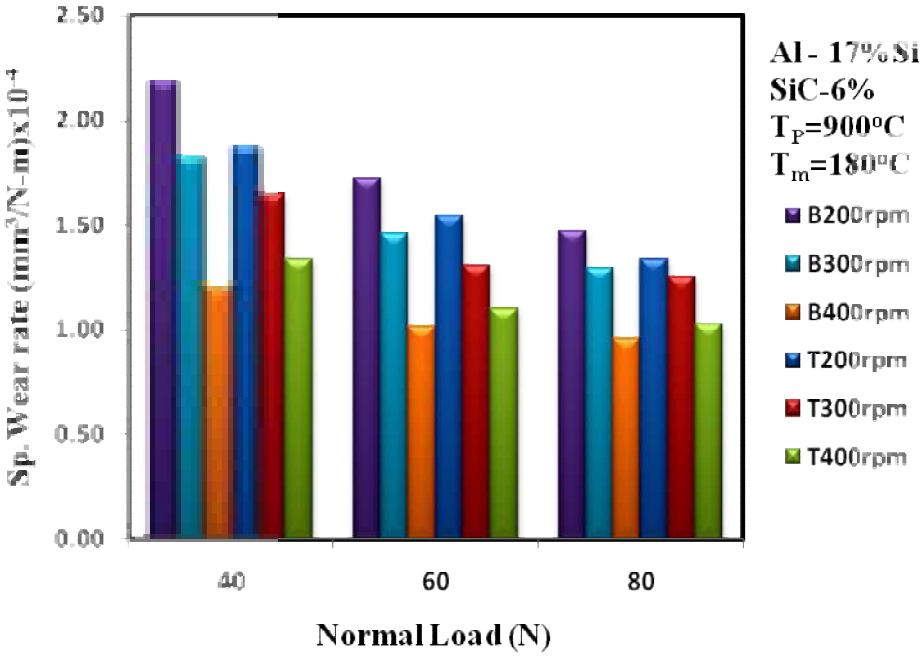

Fig. 4.84 Specific Wear rate of Al-17wt%Si-6% SiC_P FGMMC.

Figs. 4.85 to 4.87 shows the variation of Coefficient of Friction (COF) during wear test. The COF increased to a maximum as the rotating disc, of pin on disc wear testing machine, reached its set speed on starting and then smoothly decreased to a constant value. At the start of the test, due to changes in pin and disc surfaces, the COF rises with time in the beginning and remains constant. The Al-Si eutectic with 23% free Si at the top end apparently shows lower COF. Whereas the lower end shows higher COF. The reinforcement of the 2% SiC_P led to no significant improvement in terms of wear and its properties. Comparison of COF at the bottom end of both FG alloy and SiC_P 2% reinforced FGMMC has shown a very little difference at all test loads.

With further increase in volume percent of SiC_P the coefficient of friction was found to decrease at the bottom end for different normal loads. On an average at different loads and at 1.446m/s, for an increment of 2 volume percent of SiC_P reinforcement, the coefficient of friction decreased by about 4% and for a increment of 4% COF decreased by 7%.

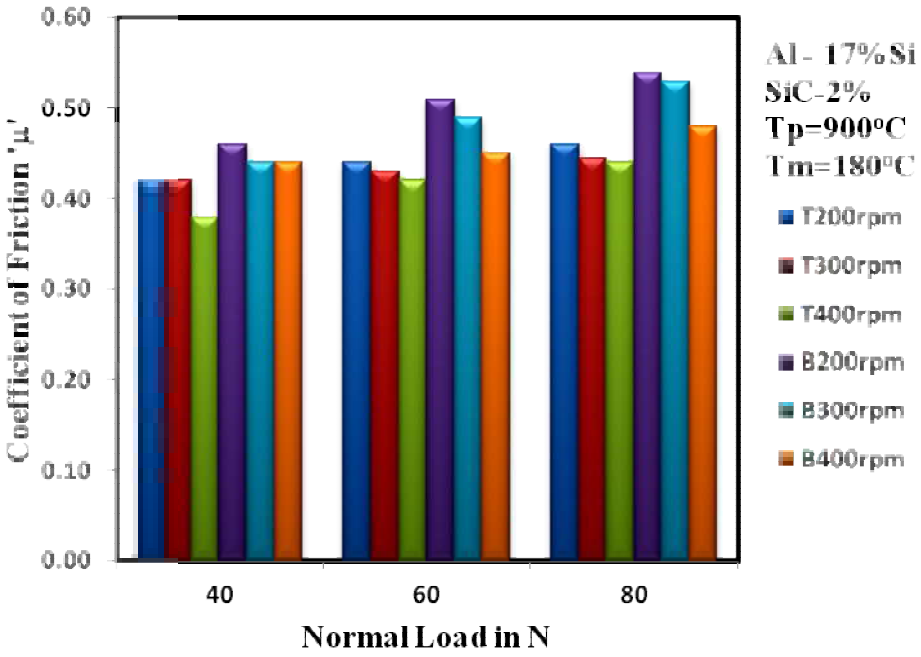

Fig. 4.85 COF of Al-17wt%Si-2% SiC_P FGMMC.

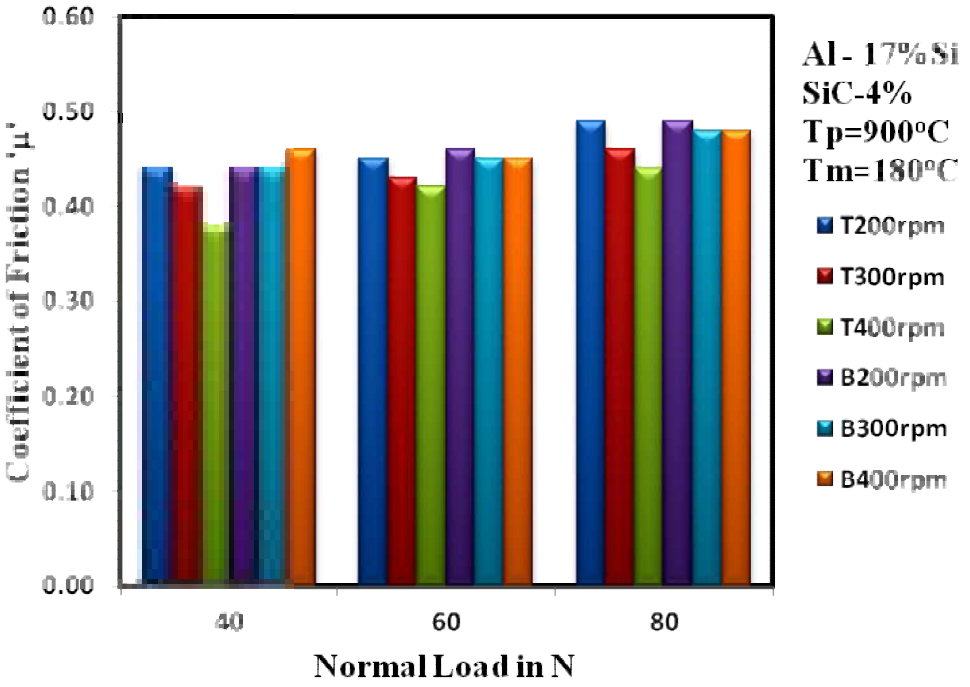

Fig. 4.86 COF of Al-17wt%Si-4% SiC_P FGMMC.

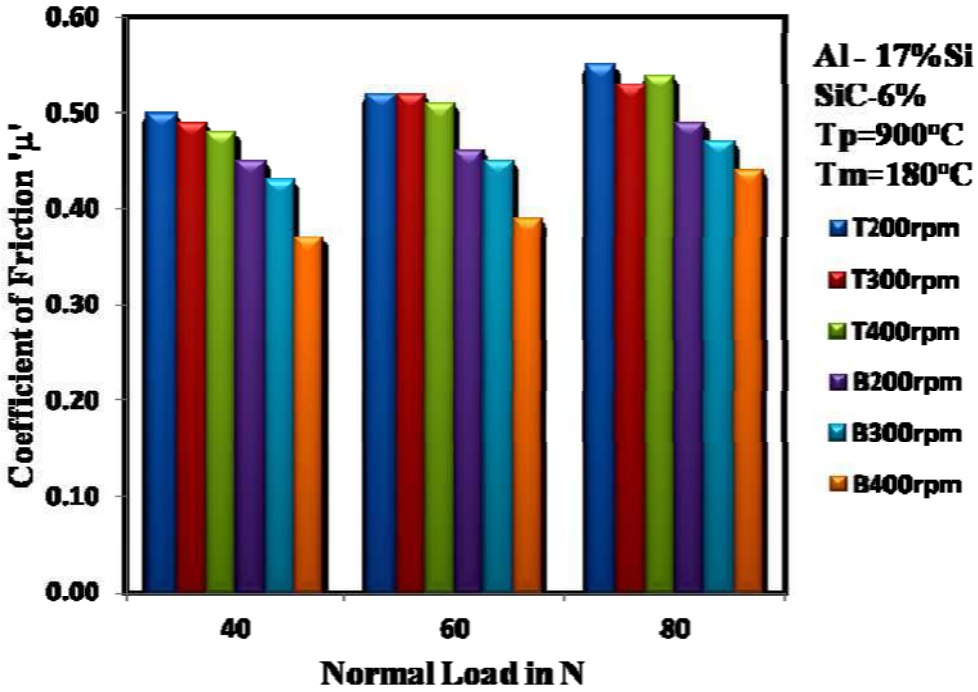

Fig. 4.87 COF of Al-17wt%Si-6% SiC_P FGMMC.

From the above test results, it is evident that aluminum-Silicon alloy matrix composites reinforced by SiC particles possess very good wear resistance, much better than that of the matrix alloy. This is in line with the theory which proposes that the material for anti-friction bearing alloy should be soft matrix scattered with hard particles, which can support the load, while the soft matrix can secure the hard particles and transport the load from matrix to hard particles. In the SiC particle reinforced aluminum matrix composite, the SiC particles support the load, so as to lessen the contact area between composite and counter disc surface and decrease the friction coefficient, and can also prevent the scratch and cut from the hard little asperities of counter face and improve the wear resistance of the composite largely. But under very high-applied load, the SiC particles will not be effective due to reasons explained as follows: Under high loads, the protective action of the reinforcing particles can no longer remain stable under the ploughing and micro-cut action, and the abrasion grooves formed are very distinct in worn surfaces. The material loss during the process is in the form of small pieces resulting in the formation of flake type and stringer type debris. The shear strains induced in the process are transmitted to the matrix alloy and the wear mechanism proceeds by subsurface crack propagation leading to the delaminating wear. This is shown and explained in micrographs later (Fig. 4.95). Das et al. suggested that in delaminating wear, the subsurface cracks, which may either exist or get nucleated due to the stresses, propagate during the course of test. When such subsurface cracks join the wear surface, delamination is the dominant wear mechanism (Das 2004,). Suh et al have described the delaminating wear of metal/material and state that the large plastic strain in the deformed layers gives rise to void nucleation and subsurface crack initiation and propagation (Suh 1980). The surfaces of materials are removed and the cracks get nearer to the surface and the shear strain is increased, thus causing the removal of the surface layers by delaminating. It follows from the above observations that the main wear mechanism at high loads is delaminating wear causing excessive fracture of the reinforcement and the matrix, resulting in deterioration of the wear resistance of the composite.

4.4.3.2 Al-12wt%Si-SiC

In case of Al-12%Si alloy, at normal test load of 40N and for an average increment of 2 % in SiC_P reinforcement, SWR decreased by 11.73% at 400rpm compared to casting produced at 200rpm as seen in Fig. 4.88.

As shown in Figs. 4.89 and 4.90 casting produced with 4% SiC_P has yielded better results with decreased volume loss at higher G (89.42). The SWR for this is found to decrease by 8.9% compared to casting produced at 22.3G. For 6% SiC_P at 400rpm (89.42G) SWR decreased by 37.36% and 31.67% compared to casting produced at 22.3G and 50.3G.

Table 4.5 SWR for Al-12%Si- SiC_P FGMMC at 400rpm

		SWR (mm^3/N-m)x10^{-4}		
	$SiC_P \rightarrow$	2%	4%	6%
Load (N)	40	2.01	1.83	1.25
	60	1.53	1.43	1.01
	80	1.34	1.29	1.00

Referring to Table 4.5 for a given rpm, the SWR for FGMMC with a given % of SiC_P decreased as the load is increased from 40N to 80N. From the table it can be deduced that compared to 40N at 80N load the SWR decreased by 33.3%, 29.5%, 20% for 2, 4, 6% reinforcement respectively. For the same mold rotational speed increasing the SiC_P has shown a decrease in SWR for all the test loads. At 40N load the SWR decreases by 37.8% for 6% reinforcement compared with 2%. For 60, 80N the SWR decreases by 33.9% and, 25.37% respectively. Thus increase in load at lower % of SiC_P helps in reducing SWR significantly whereas at higher given % of SiC_P the reduction is marginal.

The castings produced at higher G in combination with higher volume percent of reinforcement provided better results compared to other cases.

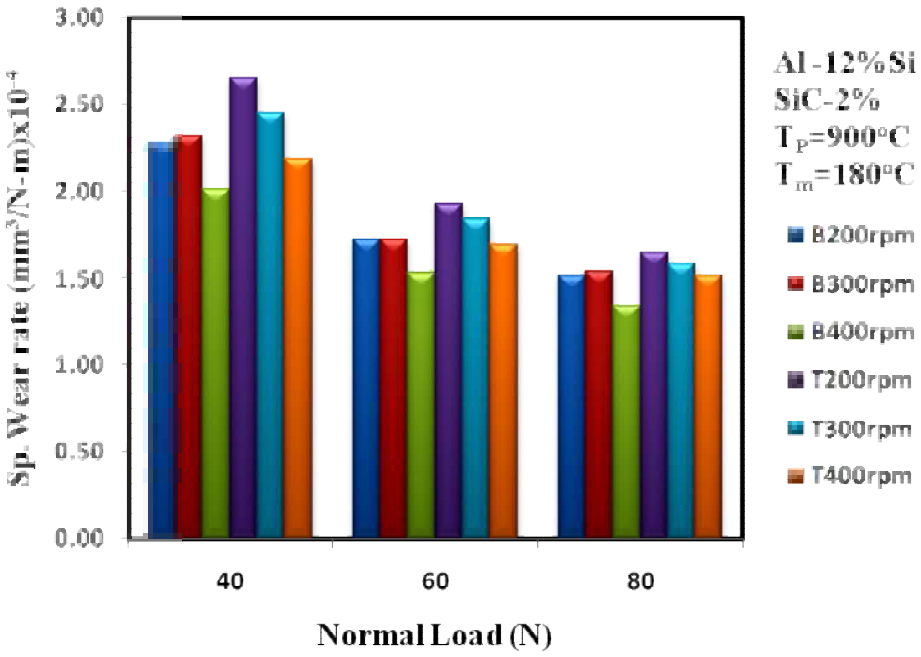

Fig. 4.88 Specific Wear rate of Al-12wt%Si-2% SiC_P FGMMC.

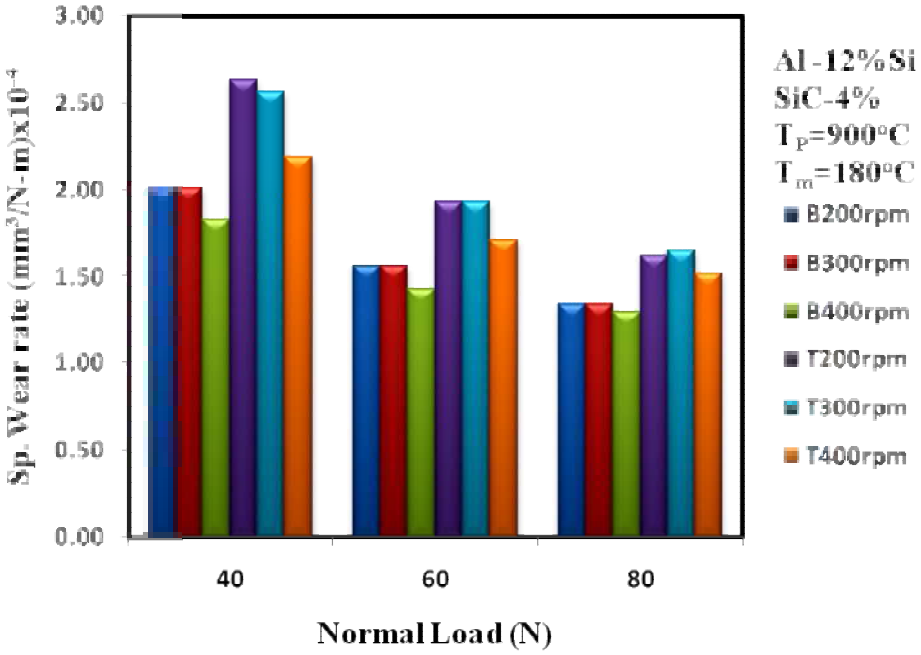

Fig. 4.89 Specific Wear rate of Al-12wt%Si-4% SiC_P FGMMC.

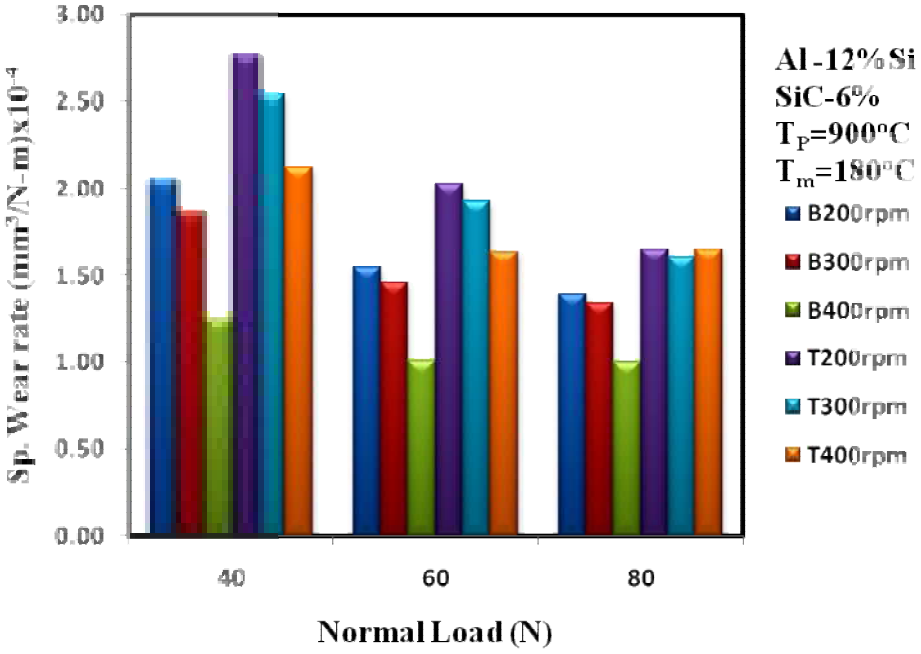

Fig. 4.90 Specific Wear rate of Al-12wt%Si-6% SiC_P FGMMC.

The variation of COF with load is shown in Figs. 4.91 to 4.93. At 40N test load, COF decreased by 2.17% for 2% SiC_P reinforcement at higher 400rpm i.e. 89.42G, compared to casting produced at 200rpm i.e 22.3G. Similarly casting produced with 4% SiC_P has yielded better results by decreasing the COF at higher G (89.42) by 4.4%. Results obtained from these figures clearly show that the COF of the casting produced using 6% SiC_P at 89.42G decreased by17.7% compared to casting produced at 22.3G. Similar trend was observed at 60N and 80N for 4% and 6% SiC_P reinforcement.

Table 4.6 COF for Al-12%Si- SiC_P FGMMC at 400rpm

		COF		
	$SiC_P \rightarrow$	2%	4%	6%
Load (N)	40	0.45	0.43	0.37
	60	0.46	0.45	0.39
	80	0.49	0.47	0.44

As the SiC_P is increased the COF decreased at all loads. It is evident in Table 4.6 that COF decreased by 17.7% for the 6% SiC_P compared to 2% reinforcement tested at 40N. Similarly COF decreased by 15.2% and 10.2% for the castings produced at 60N and 80N. It is also seen that the COF is higher for larger test load. The results in Table 4.6 reveal that with increase in load from 40N to 80N the COF increased by 8.88%, 9.3%, 15.1% for 2%, 4%, 6% reinforcement respectively. This increase in COF can be attributed to the increase in load and the relation between the applied load and COF i.e, $F=\mu R_N$, where F= Normal applied load, R_N=Reaction, μ=COF. From the results we can conclude that the increase in SiC_P has resulted in decreased values of COF for a particular load. Similarly increasing the speed also resulted in decrease in COF for all the percentages of SiC_P reinforcement.

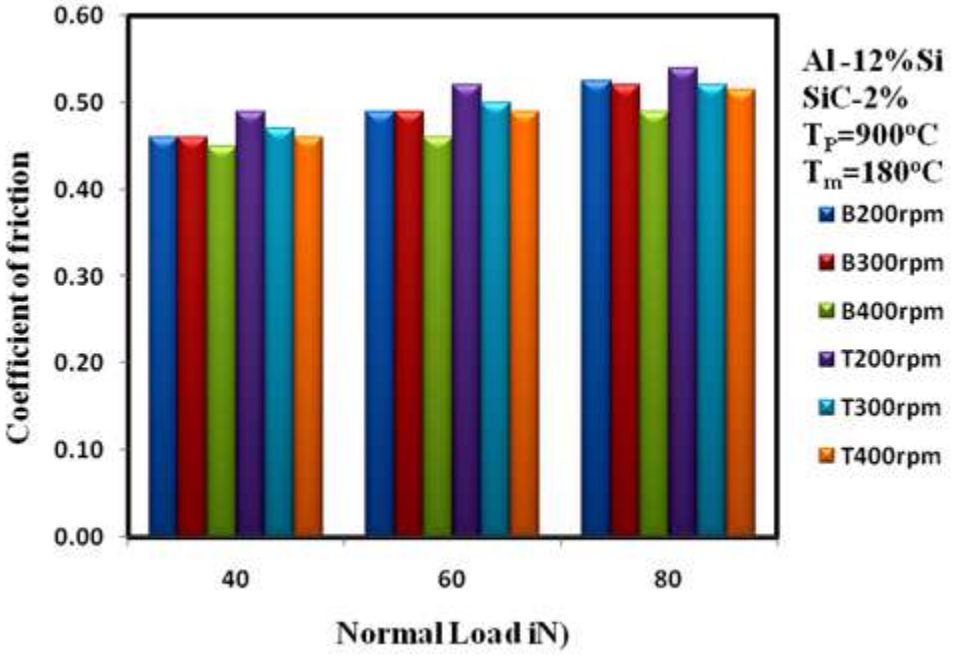

Fig. 4.91 COF of Al-12wt%Si-2% SiC_P FGMMC.

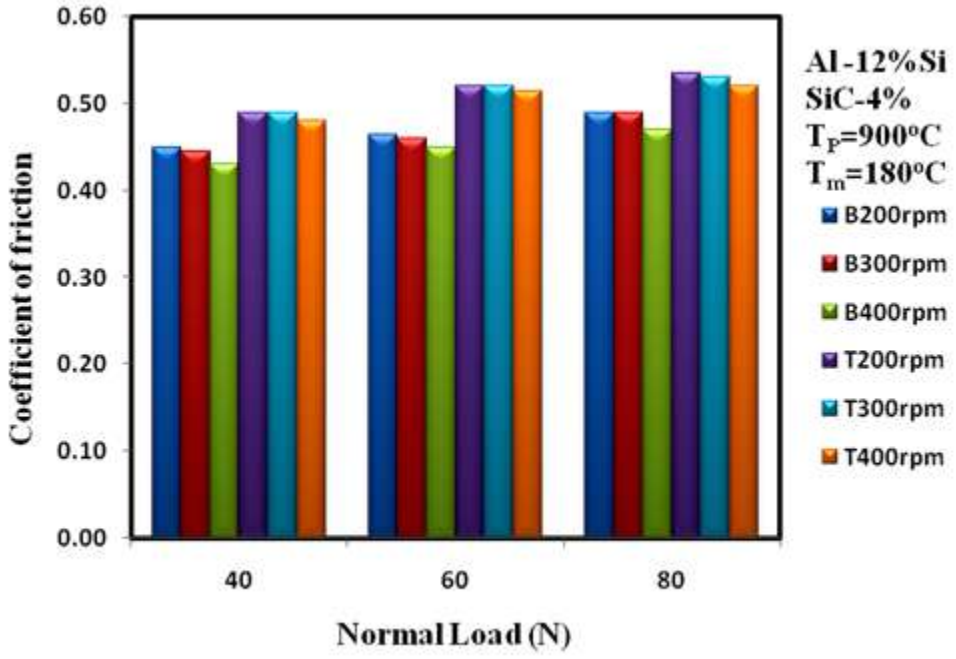

Fig. 4.92 COF of Al-12wt%Si-4% SiC_P FGMMC.

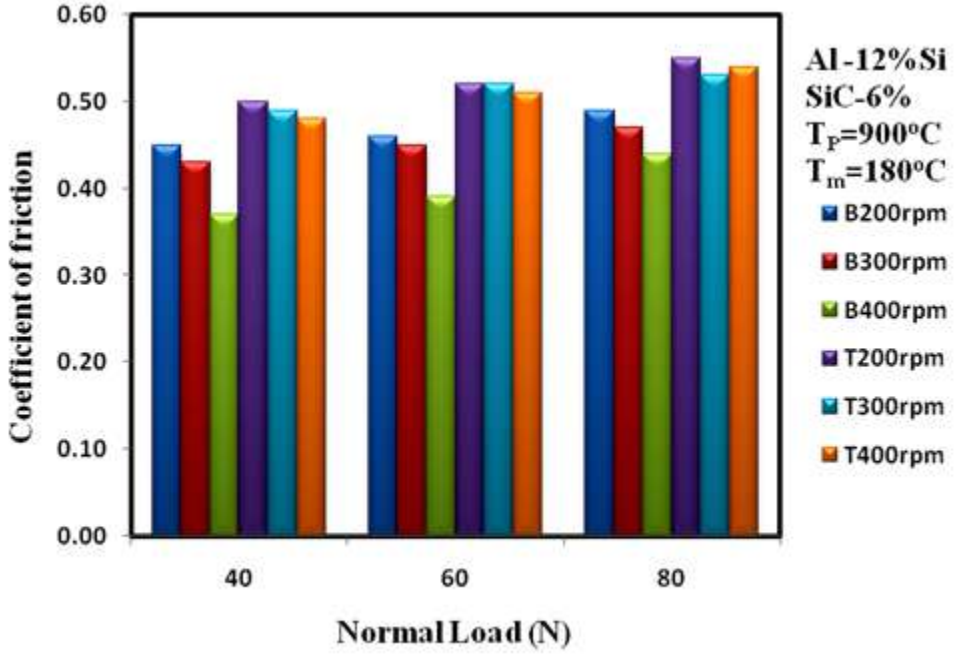

Fig. 4.93 COF of Al-12wt%Si-6% SiC_P FGMMC.

The results of sliding wear tests against steel counter face show the effect of applied load on the wear rate. Reinforcing with the SiC particulates enhanced the sliding wear resistance of the bottom end of the cast FGMMC. The SiC_P reinforced FGMMC showed better wear resistance than the FGM without particulate reinforcement. Furthermore, it should be noted here that the wear volume increased while the SWR decreased as the applied load increased. However, since by definition the wear rate is the volume loss per unit normal force per unit sliding distance and the wear volume is the total volume loss, this opposite tendency between the wear volume and the wear rate is not surprising.

SiC particles act as load-bearing elements during wear at low loads. Thus, in the FGMM composites, the SiC particles help to carry a greater portion of the applied load, thereby reducing the load on the base metal. In addition, the SiC particles in the FGMM composites could help to shield the matrix from the gouging action of the abrasive, thus helping the FGMMC to continue performing their wear resisting function longer than Al based FGM alloy. Moreover, it has been reported that the critical load required to cause fracture of SiC particles increases with increasing the number of particles. Thus, in the composite containing a proportion of particles, the critical load for particle fracture would be higher than that in the FG alloy, which contains only Si. Thus, the inclusion of SiC particles in the composite clearly helps in improving the wear resistance of the bottom end of the cast specimen compared to the top surface.

4.4.3.3 SEM Analysis of FGMMCs

SEM examinations of the worn pin surfaces and debris collected after the wear test under dry sliding wear conditions have shown different wear mechanisms like abrasion, delamination, adhesion and thermal softening and melting operating either individually or in combination. Slightly different wear mechanisms are noted for samples with different percentages of reinforcement tested at different loading conditions.

At lower loads the pin surface is having numerous grooves and scratch marks parallel to the sliding direction. Grooving and scratching appear more severe at the lower loads. Such features are characteristics of abrasion, in which hard asperities on the steel counter face or hard particles in between the contacting surfaces, plough or cut into the pin, causing wear by the removal of small fragments or ribbon like strips or small flakes of the material (Fig.4.94). This occurrence suggests that abrasion takes place primarily via ploughing, in which the material is displaced on either side of the abrasion groove without being removed or through wedge forming, where tiny wedge shaped fragments are torn only during the initial contact with an abrasive particle (Zhang et al 1995). Examination of the wear debris reveals the presence of steel, which indicates abrasion of the steel which is the counter surface. This can be attributed to the fact that reinforced hard SiC particles would have led to the cutting of the counter face. In addition, fractured SiC particles trapped between the sliding surfaces would also cause abrasion of the steel disc, as would work hardened fragments of matrix alloy and steel.

Visual inspection reveals that the surfaces of the pins tested under the lower load appear dark (4.103) while those at the higher load retain their metallic luster. The debris collected by this are fine powders. These characteristics are indicative of oxidative wear, in which frictional heating during sliding causes oxidation of the surface, with wear occurring through the removal of oxide fragments. Over repeated sliding, oxide wear debris fills out the valleys on the pin surface, and becomes compacted into a protective layer, thus metallic contact is prevented and wear rates drop accordingly (Wilson et al 1997). The SiC particle reinforcement facilitates the compaction of the oxide film in between the particles. Fragments of fractured SiC particles might also be mixed with the oxide layer, enhancing the hardness and wear resistance of the film. Finally, the higher hardness of the composites would provide better support for the oxide film, thus improving its stability and load bearing capacity. The benefits of SiC particle reinforcement are evident in the generally lower wear rates of the composites when oxidative wear predominates.

Pins made of material with low reinforcement percentage tested at higher load have exhibited series of short cracks roughly perpendicular to the sliding direction. The intersection of these cracks result in the detachment of sheet like wear particles, causing shallow craters. This is a fatigue wear mechanism in which repeated sliding induces subsurface cracks that gradually grow and eventually shear to the surface, forming wear sheets (Fig. 4.95). This is known as delamination wear. This is observed to be more extensive under the higher load. Since the delamination involves subsurface deformation, crack nucleation and crack propagation, an increase in load will hasten these processes and produce greater wear (Fig. 4.96). Delamination caused by the excessive fracture of reinforcements the SiC_P and the matrix would badly affect the wear resistance due to the additional void nucleation sites, as well as preferential crack propagation paths. For the low reinforcement (2%) a large shear strain is induced in the subsurface during the wear. The magnitude of this strain depends on the load and sliding speed. This tends to induce the dislocations. Then the subsurface region is fragmented and redistributed near the surface region. This leads to a hardened layer. Referring to Fig. 4.97, this layer contains some iron and fragmented phase (hypo eutectic). This iron originated from the steel disc and is caused by metal transfer across. Repeated sliding between the pin and the disc results in the formation of cracks and subsequent delamination (Fig. 4.98) of the hardened layer from the pin (Tjong et al 1997).

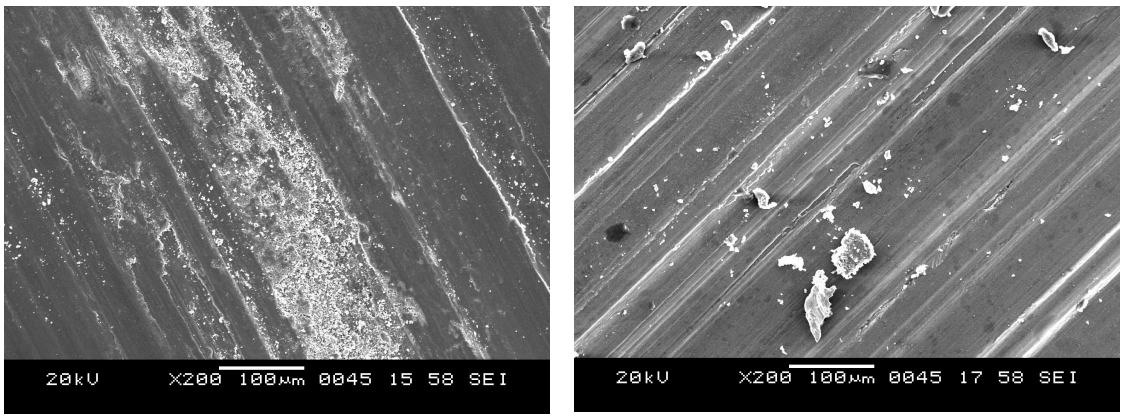

Fig. 4.94 Grooves and scratch marks on the pin surface indicating abrasion

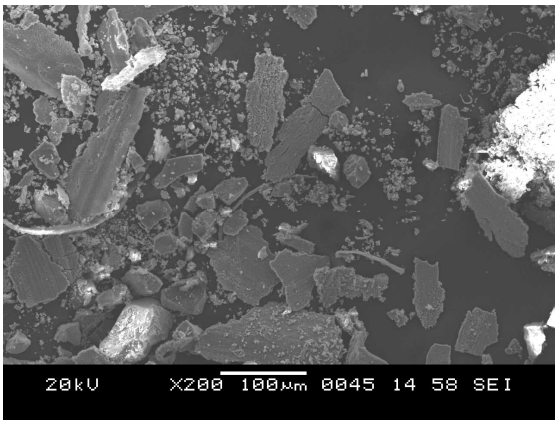

Fig. 4.95 Flake or sheet like wear debris of delamination

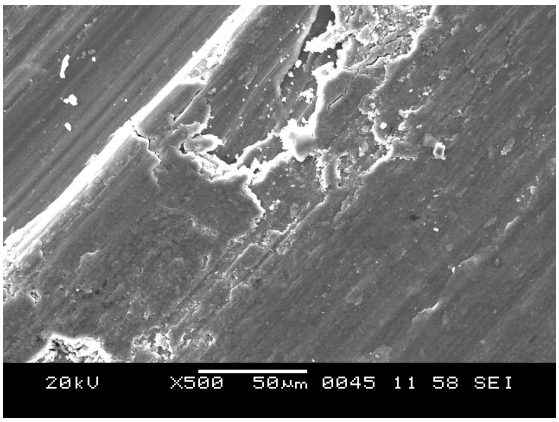

Fig. 4.96 Fine cracks associated with delamination

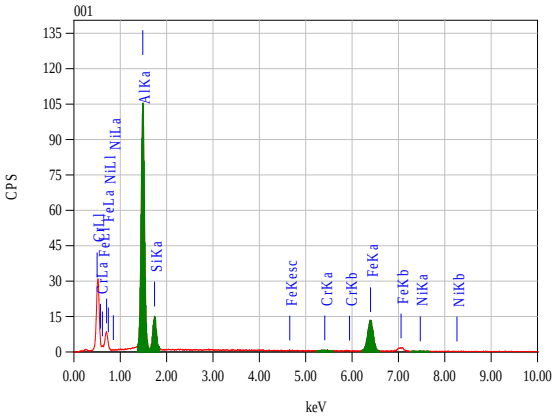

Fig. 4.97 EDAX showing material transfer of Fe on to Pin surface

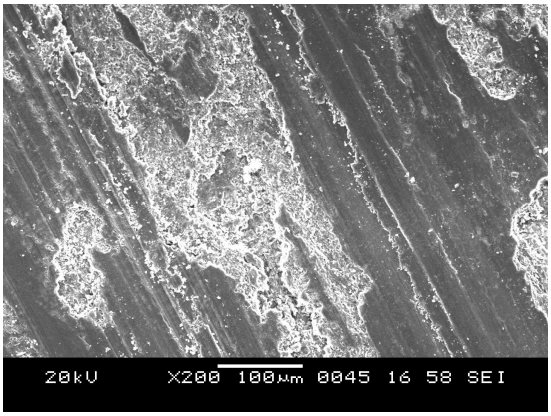

Fig. 4.98 Shallow crater showing material worn by delamination

At higher loads (80N) delamination wear is gradually replaced by rows of furrows. Material transfer is evident from the pin surfaces and there are also signs of smearing and plastic deformation. Under higher loads, the wear track on the disc is covered with a discernible layer of transferred material. The extensive transfer of material suggests that wear is of adhesive type (Fig. 4.99). The pins of the FGMMC specimens containing more SiC show lesser evidence of adhesion. This is in accordance with Archard's (Archard, 1953) law that the wear rate of a material is inversely proportional to its hardness. It can be seen from the wear surface, that grooves formed have progressed and increased the wear. The grooves are formed at the locally fractured area of reinforcements and the matrix. Although less friction forces are active on the wear surface, localized fracture has taken place by high

localized friction forces which come from the non-uniform nature of the counter material surface and defective areas of the wear surface. The groove growth is advanced by the fracture of the wear (Lee et al 1992).

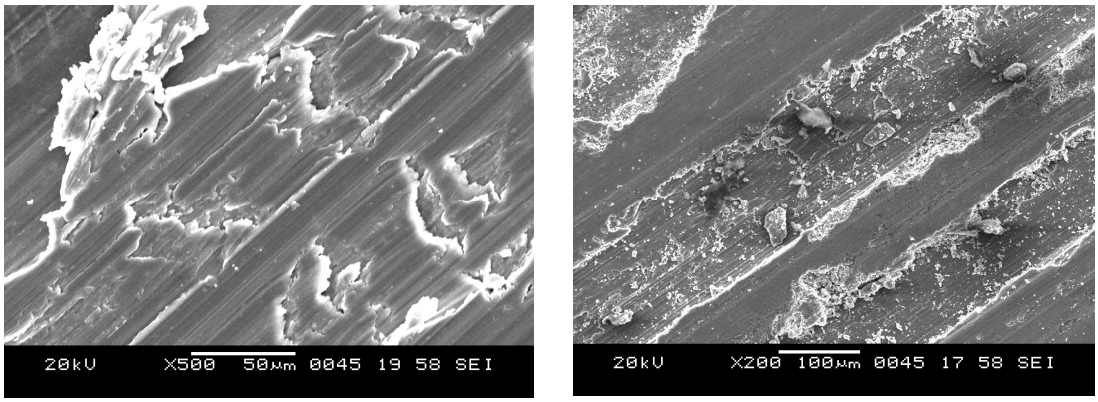

Fig. 4.99 Furrows due to adhesion on the Pin surface

At higher loads, layers of material are seen protruding slightly at the trailing edge. Large irregular lumps, quite distinct from the debris collected are found. It is also observed that a gross plastic deformation of the pin surface occurs and the material is extruded from the interface before welding around the periphery of the pin (Fig. 4.102). Extensive material transfer is found with large sheets of wear debris (Figs. 4.100 and 4.101). These observations are associated with the softening and melting of the matrix material caused by frictional heating at the sliding interface. When the sliding speed and applied load reach certain critical value, flash temperature at contacting asperities could exceed the melting point of the matrix alloy, thus increasing bulk temperature and causing gradual softening of the matrix (Straffelini et al 2004). Continued sliding would raise the temperature further, leading to melting. The presence of SiC_P reinforcements lowers wear rate and delays the onset of these thermally activated deformation processes to higher loads (Bai et al 1992). This has been linked to the higher thermal stability of the composites, which allows them to retain their strengths at higher temperature.

The various wear mechanisms and their regions of dominance show that transitions of wear from one group of mechanism to another are found to be dependent on reinforcement and load. Under lower load, the effects of these are

mitigated by the presence of Al_2O_3 oxide film which forms a stable protective layer. Under the higher loads the rate of removal of the oxide film exceeds that of its formation and a transition from oxidation to delamination and abrasion occurs. This increases the wear rate with the particulate-matrix interface initiating crack nucleation and growth. At higher loads a gradual transition occurs from delamination to adhesion. The higher hardness because of increased addition of reinforcement SiC_P improves the load bearing capacity and imparts better resistance to adhesive wear. Further softening and melting gives rise to gross plastic deformation of the pin surface, which marks the useful limit of the FGMMCs.

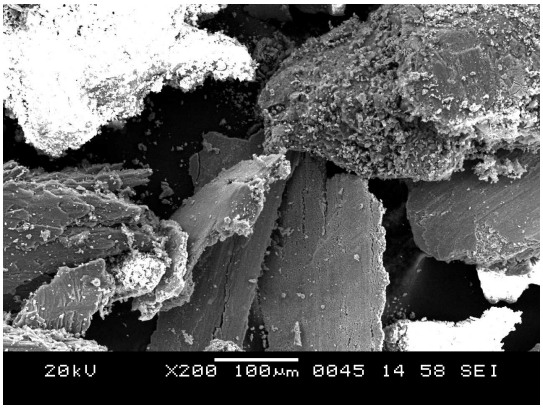

Fig. 4.100 Large sheets in the wear debris from the spalling of transferred pin material on the wear track

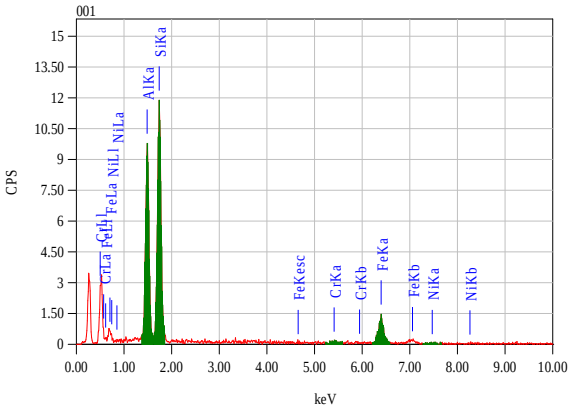

Fig. 4.101 EDAX showing material transfer

Fig. 4.102 Optical micrograph showing extruded layer of the pin surface

Fig. 4.103 Pin surface with oxide film

4.5 L/D Ratio

The microstructure and distribution of primary Si particles in a casting depend on several parameters (Halvaee et al 2001). These parameters include the size, centrifugal force and cooling rate controlled by mold temperature, pouring temperature and heat transfer between the mold and melt.

In order to access the size effect, experiments are conducted keeping influential parameters viz. pouring temperature, centrifugal force, and mold temp fixed except the length to diameter (L/D) ratio of the casting. The material used is Al-17%Si alloy. The experimental parameter details are given in Table 4.7

Table 4.7 L/D experimental parameters

Constant	Length (L)mm	Diameter (D) mm	L/D
Casting Diameter	20	40	0.5
	40	40	1.0
	60	40	1.5
Casting Length	40	20	2.0
	40	40	1.0
	40	60	0.67

Table 4.8 Primary Si and hardness values for different L/D ratios

Constant (C)	**L**	**D**	**L/D**	**V**	**A**	**V/A**	**Pri Si (%)**	**H**
D=C	20	40	0.50	25172	5034.4	5.00	8	63
	40	40	1.00	50344	7551.6	6.67	22	73
	60	40	1.50	75516	10068.8	7.50	26	89
L=C	40	20	2.00	12586	3146.5	4.00	6	60
	40	40	1.00	50344	7551.6	6.67	22	73
	40	60	0.67	113274	13215.3	8.57	32	102
L: length of the Casting mm, D: Diameter of the casting mm, V: Volume of the Casting mm^3, A: Cooling Surface Area mm^2, H: Hardness at top end of the casting BHN.								

The results of the experiments are given in Table 4.8. When 'L' is held constant, the maximum hardness and primary Si is obtained for the case of lowest L/D ratio of 0.67. With ' D ' held constant at lowest L/D ratio of 0.50, the hardness and primary Si is obtained are lowest. This can be explained better by the equation 4.3.

$$t_f = \frac{\rho_f H}{h(T_m - T_0)} \times \frac{V}{A} \qquad 4.3$$

where t_f is the solidification time, h is the heat transfer coefficient, H is the latent heat of solidification, ($T_m - T_0$) is the temperature difference across the interface, A is the cooling surface area and V is the volume of the casting. As the L/D ratio is increased the volume of the casting is increased. This, in turn, increases the solidification time (Campbell et al 2003). It has been well established that the interaction between solidification fronts and particles as well as size of the continents of the matrix structure are responsible for the final distribution of the particles in the casting. In centrifugal casting where high centrifugal forces are involved, the particles are restricted to move in the direction of the centrifugal force at increasing angular velocities. The solidification front on the other hand moves in the opposite direction with a variable speed towards the inner circumference of the casting. It is well established that cooling rate is decreased by increasing the volume / thermal mass of the casting. From the data obtained we can clearly conclude that the L/D ratio does not have any effect on the mechanical and tribological properties of the casting. It is purely dependent of the ratio V/A of the casting.

4.6 Diametral Compression Test

In FGMs the properties vary from one end of the specimen to the other end. Therefore it becomes very difficult to establish the mechanical properties such as tensile and compressive strength of the specimen by conventional method. This section gives an insight into the diametral compression test conducted on the sample from bottom and top of the casting for both Al-Si FG alloy and Al-Si-SiC_P FGMMC.

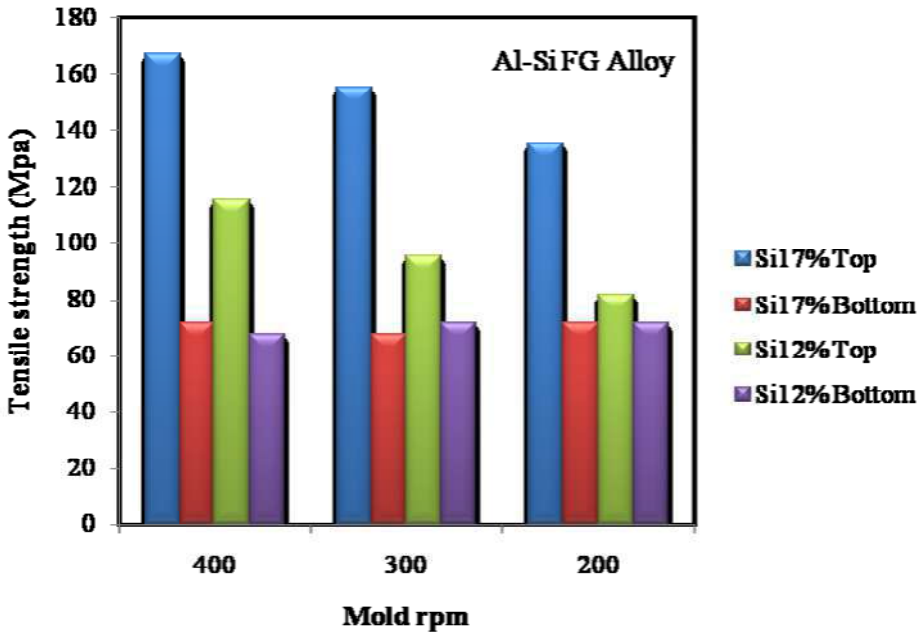

Fig. 4.104 Tensile strength of the Al-Si FG alloy for different mold rotational speeds

The tensile strength of the sample from the bottom of the Al-Si FG alloy castings is shown in Fig. 4.104. The tensile strength of the castings remained almost same while the tensile strength of the FG alloy at the top of the casting increased as the mold speed is increased for both 12 and 17% Si alloy system. For Al-12%Si alloy the tensile strength of the casting at the top is 68MPa at 200 rpm. 20.8% increase in tensile strength is obtained for casting produced with 300rpm. Similarly an increase of 41.4% is observed for 400rpm compared to 200rpm. Comparing the top and bottom of the casting, the top region of the casting shows more strength. For casting produced under 200rpm mold rotation the tensile strength for top region is 13.9% greater than

that for the bottom. Similarly increases of 33.3 and 70.5% occurred for castings produced at 300rpm and 400rpm respectively.

For Al-17%Si FG alloy the tensile strength drastically increased at the top region compared to Al-12%Si FG alloy. The top region of the castings produced at 200rpm mold speed had a tensile strength of 135MPa, whereas the castings produced at 300rpm and 400 rpm showed improvements of 18.8% and 23% respectively.

The results obtained confirm the previous findings in terms of primary Si and hardness. The enhancement of the tensile strength at the top regions compared to the bottom regions clearly signifies the gradation in properties from top to bottom of the FG alloy and confirms the other properties reported. It also confirms the effect of mold rotational speed (G factor) on the gradation and enhanced properties at the top region.

The stress state inducing the failure of composites during diametral compression is determined. The extraction of the tensile strength of the material, requires an effective tensile stress state inside the specimens. The predictions of the theory of elasticity, i.e. a tensile state in the x-direction along the diameter, are helpful in this matter. The introduction of SiC_P into the Al-Si matrix to form FGMMC has improved the performance of the casting at the bottom region of the casting as compared to the Al-Si FGM. The effect of volume percent of reinforcements on percentage increase in tensile strength was found almost similar for both the matrix materials considered and the same is depicted in the form of bar chart in Figs. 4.105 and Fig.4.106. A 135% improvement of tensile strength is noticed in case of the bottom region of the Al-12%Si with a reinforcement of 6% SiC_P at 400rpm. This is the highest change among all the combinations. From the previous findings it is observed that an increase in mold rotational speed (G factor) has increased the primary SiC_P percentage. Further tensile strength from the diametral compression test has also confirmed similar variations.

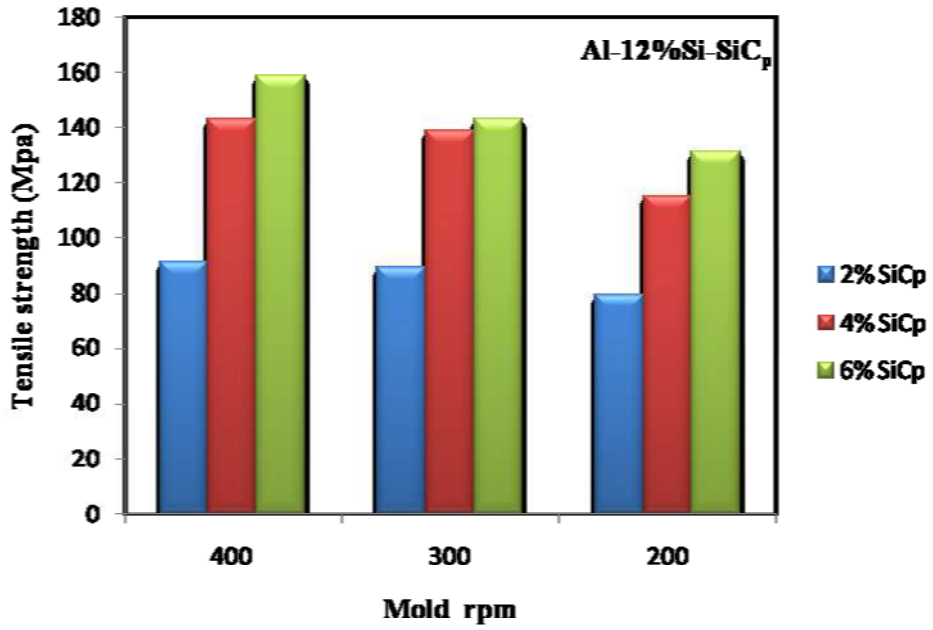

Fig. 4.105 Tensile strength of the bottom region of the Al-12% Si- SiC_P FGMMC casting

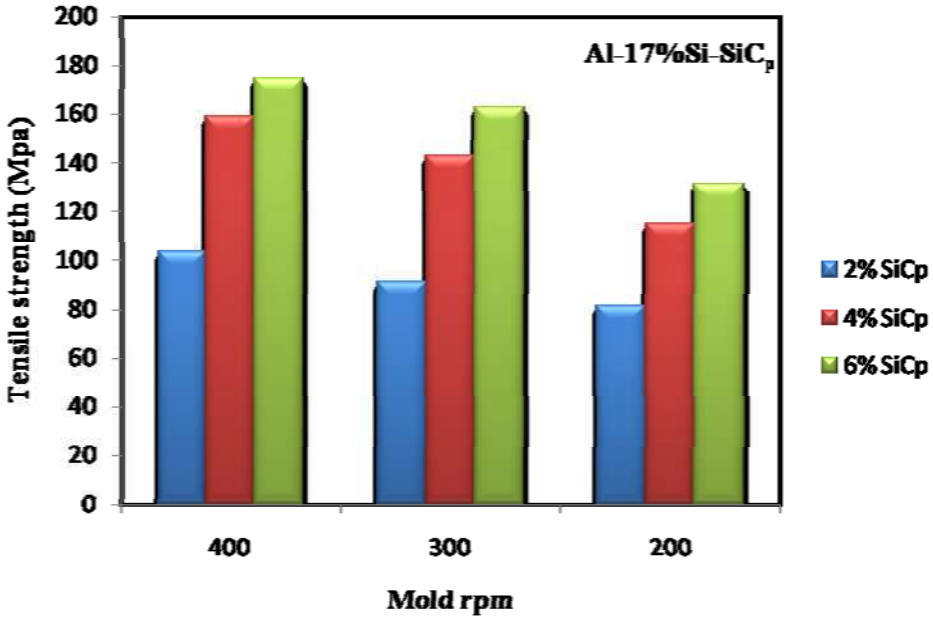

Fig. 4.106 Tensile strength of the bottom region of the Al-17% Si- SiC_P FGMMC casting

Compared to the tensile strength of the bottom region of the FGMMC (Table 4.9), FG alloy shows a linear increase with the mold rotational speed. At lower reinforcements the material behaved in a ductile manner whereas for higher reinforcement and at higher mold rotational speed the bottom region of the casting was similar to a brittle material which can be attributed to the more segregation of reinforcement particles which renders the bottom region to be brittle.

Table 4.9 Tensile strength at bottom region of FGMMCs

		RPM	**SiC_P**		
			2%	**4%**	**6%**
MATRIX	**Al-12%Si**	400	35	112	135
		300	25	94	100
		200	11	61	83
	Al-17%Si	400	44	122	144
		300	35	112	141
		200	14	61	83

The photographs of the test specimens subjected to diametral compression test are shown in Fig. 4.107. In general, the application of compressive load on the disc along the diametral plane induces tensile stresses normal to the diametral plane causing the failure of the material along the diametral plane. Macroscopic examination of the specimens tested indicated an approximately diametral crack on each surface of the disc. In most cases, the test disc was not fully cracked at the end of the test. From subsequent observations it is noticed that the fracture resulted throughout the disc via bending and mechanical means. For large number of the discs, fracture was observed in the central part. This tends to indicate that, for all the materials investigated, the crack begins in the central section of each disc, which is the most severely stressed, subsequently growing and propagating in two opposite directions towards the periphery.

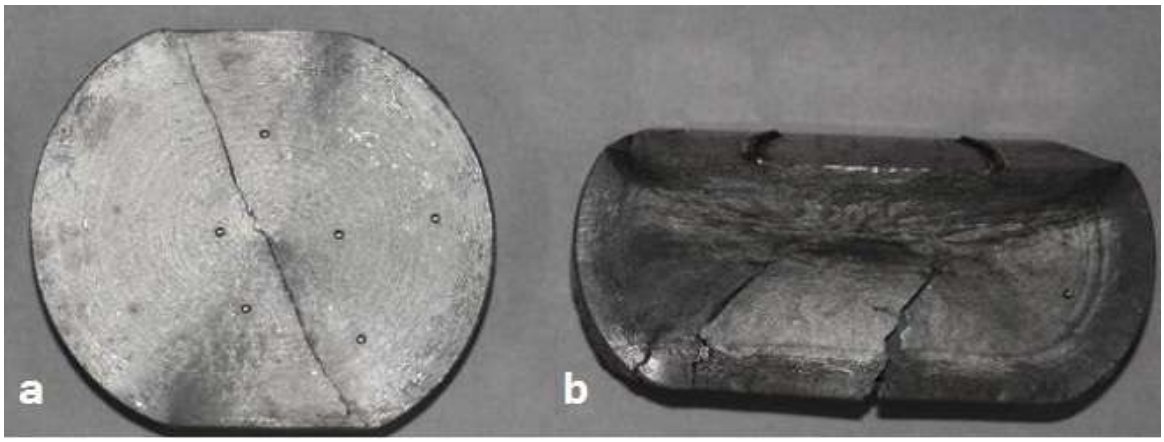

Fig. 4.107 Mode of failure under the diametral test for Al-Si FG alloy a) Top region, b)Bottom region

In case of Al-Si FG alloy the fracture along the diametral plane was not formed at bottom part of the casting due to its ductile nature and the material was compressed as shown in Fig.107(b). In top region which is hypereutectic in nature, the fracture was observed from the centre of disc approximately at an angle of 45^{o} to the diametral plane as shown in Fig.107(a). The crack formation shows to an extent brittle tendency of the material and the crack at an angle to diametral plane is indicative of failure on the shear plane.

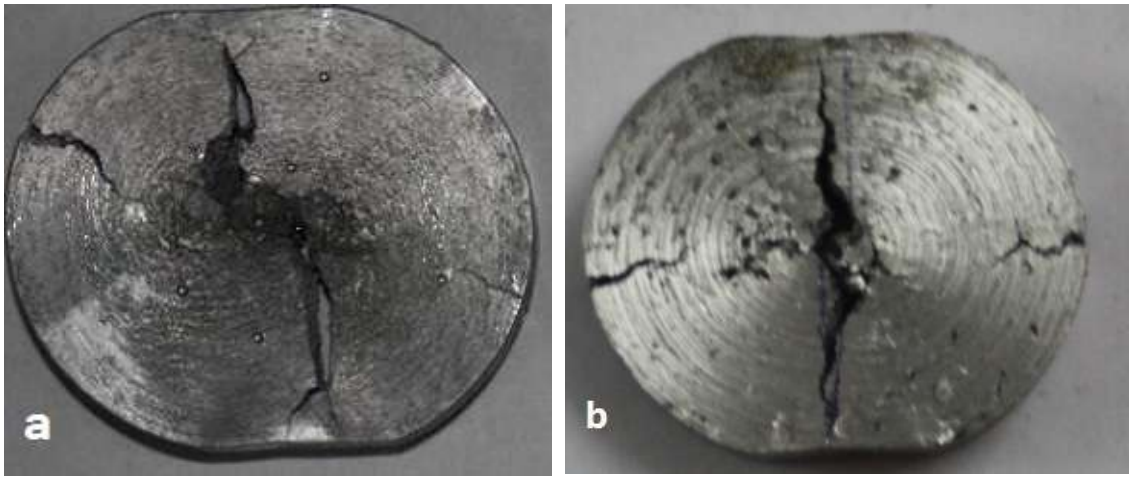

Fig. 4.108 Fracture for the bottom region of the FGMMC. a) Al-12%Si- SiC_P, b) Al-17%Si- SiC_P

The crack formation for the bottom region of the SiC_P reinforced Al-Si alloys is shown in Fig. 4.108 and it is found to be severe and exact along the diametral plane. This confirms that due to diametral compressive load, in high hardness and relatively more brittle materials, the stress causing the failure is tensile. In all FGMMCs considered, the failure of the material was found to be along the vertical diameter which is due to the tensile stress induced in a direction perpendicular to the load direction. The crack formation along the diametral plane was found to be continuous and clear.

5. CONCLUSIONS

In the present investigation centrifuge casting technique is utilized for producing functionally graded material in the form of solid cylindrical shape. The centrifuge casting technique is exploited basically on the grounds that it also allows the molten metal to be poured into the mold when it is stationary. The effect of mold rotational speed (G factor), pouring temperature and mold temperature are investigated. Two Al based FGMs were developed one using Al-Si alloy and another Al-Si alloy composite reinforced with SiC particles. The castings have been characterized with respect to their microstructure, hardness, wear properties and diametral compression strength properties. The major observations and the conclusions drawn are as follows:

1. Under the action of centrifugal force during the centrifuge casting, both the Al-Si alloys (Al-12wt%Si and Al-17wt%Si) showed gradation in the distribution of Si phase from the top of the casting to the bottom of the casting. The gradation is characterized using percentage of primary Si segregation and the rim thickness. Three different rpms (400, 300 and 200) were used and observing the values for percentage of primary Si segregation and the rim thickness, it is concluded that the mold rpm has a significant effect on gradation and higher the mold rpm better is the gradation.

2. At each rpm of the mold the effect of pouring temperature and mold temperature was studied. From the results the conclusion drawn is that, higher pouring temperature and higher mold temperature provide better gradation at each rpm. The main reason for this is attributed to the temperature difference resulting in solidification which allow time for primary Si to grow from the melt. Further higher teeming temperature helps in retaining the melt for a long time in the two phase region above the eutectic temperature. The primary silicon gets more time to float to the top, the time the liquid spends in the mold under the centrifugal force is

increased and as a result the particles are pushed towards the top and segregate.

3. For both the alloys the gradation characteristics were better at higher values of rpm, melt temperature and mold temperature.

4. The gradation is characterized by percentage of volume fraction of primary Si and the rim thickness at the top end of the casting. In case of both the alloys the percentage of volume fraction of primary Si is higher at the top end of the casting compared to the bottom end. Further under favorable conditions of rpm, teeming temperature and mold temperature this volume fraction improved and also produced better (lower) rim thickness values. The results of hardness and wear studies further substantiated the above observations i.e., the microstructural and experimental studies through hardness and wear tests were in good agreement with each other. This conclusion is based on the fact that the Si being a harder phase, the region where it is segregated is expected to show higher hardness and lower specific wear rate.

5. By properly controlling the centrifuge casting parameters viz., the rpm, teeming and mold temperature it should be possible to produce FG Al-Si alloys containing the majority of primary Si segregated at the top end of the casting while the bottom end having Al- dendrites with no free Si.

6. In the Al-Si / SiC_P MMC system the gradation occurred in terms of the reinforcement as well as the alloying element. The cast specimen showed the segregation of SiC_P at the bottom while Si at the top. The segregation and movement of SiC_P to the bottom and Si to the top is influenced by the mold rpm. Higher the rpm better the gradation at the both the ends of the casting. Further the pattern in gradation remained same for all percentages of SiC_P and only the percentage segregation increased with increase in weight percentage of SiC_P.

7. The experiments on hardness and wear corroborated the microstructural studies and as expected higher hardness lower specific wear rates were observed at the bottom of the casting compared to top end of the casting. The SEM studies of the worn pin surface further substantiated the presence of harder and heavier SiC_P phase at the bottom of the casting while the less harder and lighter Si phase at the top.

8. From the experiments conducted on castings produced with different L/D ratio, it is concluded that L/D ratio does not have any effect on the mechanical and tribological properties of the FG casting and only the V/A ratio of the casting has an effect on gradation and hence on the mechanical and tribological properties.

9. The diametral compression test can successfully utilized to validate the gradation in the cast FG alloy. In the present investigation it is confirmed that due to the gradient distribution of Si in the FG casting, the DC test showed higher strength at the top region than the middle and bottom region of the casting.

6. BIBILIOGRAPHY

Alam, R I Marshall and S Sasaki (1996). Metallurgical and tribological investigations of aluminum bronze bushes made by a novel centrifugal casting technique. *Tribology International*, 29, No 6, 487-492.

Amoros J.L., V. Cantavella, J.C. Jarque, C. Fel, (2008). Green strength testing of pressed compacts: An analysis of the different methods. *Journal of the European Ceramic Society* , 28(4), 701-710.

Apelian, (2009). *Aluminum cast alloys:Enabling tools for improved performance.* NADCA.

Archard, (1953). Contact and rubbing of flat surfaces. *Journal of applied Physics*, Vol 24, pp 981-988.

ASM, (1992). Casting. In P.-á.-M. S. Alain Royer and Stella Vasseur, *ASM Hand Book Vol15, Casting* (p. Vol15). ASM International.

ASTM-3-95E, (1995). Standard practice for preparationof Metallographicspecimens. *ASTM* .

ASTM-E1245, (1995). Standard practice for determining the inclusion or second-phase constituent content of metals by automatic image analysis. *ASTM* .

ASTM-E562, (1995). Standard test method for determiningvolume fractionby systematic manual point count. *ASTM* .

ASTMG40, (n.d.). Corrosion Standards and wear standards. *ASTM G40* .

ASTMG-99, (1995). standard test method for wear testingwith a pin-on-disk apparatus. *ASTM standards* .

Bai Pramila, Biswas S K, (1987). Charecterization of dry sliding wear of al-Si alloys. *wear* , Vol 120, 61-74.

Bai Pramila, Rameash B S, M K Surappa, (1992). Dry sliding wear of A356-Al-SiCp composites. *Wear* , vol 157, pp 295-304.

Blau, (1981). Interpretation of the friction and wear break-in behavior of metals in sliding contact. *Wear* , 71 (1), 29.

Basavakumar, Madhusudan charaborty, Mukunda, (2006). Effect of grain refinement and modification on microstructure and impact properties of Al-12Si and Al-12Si-3Cu cast alloys. *Trans. Indian Inst. Met* , V59, 399-406.

Basavakumar, Madhusudan charaborty, Mukunda, (2008). Influence of grain refinement and modification on microstructure and mechanical properties of Al-7Si and Al-7Si-2.5Cu cast alloys. *Materials Charecterization* , 59, 3, 283-289.

Basavakumar, Madhusudan charaborty, Mukunda, (2007). Influence of grain refinement and modification on dry sliding wear behaviour of Al-7Si and Al-7Si-2.5Cu cast alloys. *Journal of Materials processing technology* , Vol 186, 236-245.

Beal, Erasenthiran, Hopkinson, Dickens, Ahrens, (2006). The effect of scanning strategy on laser fusion of functionally graded H13/Cu materials. *International Journal for Advance Manufacturing* , 30, 844-852.

Bever, Duwez, (1972). 'Gradients in Composite Materials', Materials Sc. Engg. 10, 1972, 1-8. *Materials Sc. Engg*,

Bialo D, Zhou J, Duszczk J, (2000). The tribological characteristic of the Al-20Si-3Cu-1Mg alloy reinforced with Al_2O_3 particles in relation to the hardness of a mating steel. *Journal of Materials Science* , 35, 5497-550.

Birman victor, Larry W Byrd, (2007). Modeling and Analysis of Functionally Graded Materials and Structures. *Transactions of the ASME* , 60, 195-215.

Bollono F, Moret A, Gallo S, Mus C, (2004). Cylinder liners in aluminum matrix composite by centrifugal casting. *La metallurgia italiana* , 6, 49-55.

Bonollo F, Molinas, Tangerini I, and Zambon A. (1994). Diametral compression testing of metal matrix composites. *Material Science and Technology* , 10(6), 558-564.

BSSA, (2012). *Factors affecting wear and galling*. Retrieved from www.bssa.org.uk.

Campbell, (2003). *Castings.* Burlington M A: Butterworth Heinemann.

Carneiro F, Barcellos A, (1953). Concrete tensile strength. *Union of testing and research laboratories for Materials and structures* , 13.

Castro Rodri´guez, Kelestemur, (2002). Microstructure and Mechanical behavior of functionally graded Al A359/SiCp composite. *Materials Science and Engineering A* , 323, 445-456.

CastroRodri´guez, Kelestemur, (2002). Processing and microstructural characterization of functionally gradient Al A359/SiCp composite. Journal of materials Science , 37, 1813-1821.

Cetinel, Uyulgan B, Tekmen C, Ozdemir I, Celik E. (2003). Wear properties of functionally gradient layers on stainless steel substrates for high temperature applications. *Surface and Coatings Technology* , Vol 174-175, 1089-1094.

Chen Chao-Shi, Pan Ernian, Amadei bernard (1998). Determination of deformability and tensile strength of anisotropic rock using Brazilian tests. *International Journal of Rock Mechanics and Mining Sciences* , 35 (1), 43-61.

Chen G, Tong M, Zhu Z, (1999). Study on the macrosegregation of aluminium in centrifugal-cast ZA27 alloy. *Material Science and Engineering A* , 265, 306-309.

Chirita G, Soares D, Silva F S, (2008). Advantages of the centrifugal casting technique for the production of structural components with Al-Si alloys. *Materials & design* , 29, 20-27.

Chirita G, Stefanescu I, Soares D, Silva F S, (2007). Mechanical resistance as a function of local properties. *International Conference on diagnosis and prediction in mechanical engineering systems* (pp. 45-49.). Galati, Romania: The Annals of university.

Chirita G, Stefanescu I, Barbosa J, Puga H, Soares D, Silva F S, (2009). On assessment of processing variables in vertical centrifugal casting technique. *International journal of cast metal research* , 22, No. 5, 382-389.

Chirita G, Stefanescu I, Cruz D, Soares D, Silva F S, (2010). Sensitivity of different Al-Si alloys to centrifugal casting effect. *Materials & design* , 31, 2867-2877.

Clarke J, Sarkar A D, (1979). Wear characteristics of as-cast binary aluminium-silicon alloys. *Wear* , 54, 7-16.

Darvell B W, (1990). Uniaxial compression tests and the validity of indirect tensile strength. *Journal of Material Science* , 25, 757-780.

Das S, (2004,). Development of Aluminum alloy composites for engineering applications. *Trans. Indian Inst. Met.* , Vol.57, No. 4, pp. 325-334.

Deuis R L, Subramanian C, Yellup Deius J M, (1996). Abrasive wear of aluminum composites-a review. *Wear* , 201, 132-144.

Duque N B, Melgarejo Z H, Suárez O M, (2005). Functionally graded aluminum matrix composites produced by centrifugal casting. *Materials Charecterization* , 55, 167-171.

Dwivedi D K. (2009). Adhesive wear behaviour of cast aluminium–silicon alloys: Overview. *Materials and Design* , 31 (5), 2517-2531.

Dwivedi D K, Sharma Ashok, Rajan T V, (2001). Friction and wear behaviour of cast Al-Si base alloys. *Indian foundry Journal* , Vol 47, 18-22.

Dwivedi D K, Arjun T S, Thakur P, Vaidya H, Singh, (2004). Sliding wear and friction behaviourof Al–18%Si–0.5%Mg alloy. *Journal of Material Processing Technology* , Vol152, 323-328.

Fahad M K, (1996). Stresses and failure in the diametral compression test. *Journal of Material Science* , 31, 3723-3729.

Fairhurst, (1964). On the validityof the brazialian test for brittle materials. *International journal of rock mechanics mining scienec* , 1, 534-546.

Fell J T, Newton J M, (1970). Determination of tablet strength by the diametral-compression test. *Journal of Pharmaceutical Sciences* , 59(5), 688-691.

Fukui Y, Yamanaka N, Enokida Y, (1997). Bending strength Al-Al_3Ni functionally graded material. *Composites Part B* , 28B, 37-43.

Fukui Y, (1991). Fundamental Investigation of Functionally Gradient Material Manufacturing System using Centrifugal Force. *JSME International Journal, Series III* , 34(1), 144-148.

Fukui Y, Okada H, Kumazawa H, Watanabe Y, (2001). Near-Net-Shape forming of Al-Al3Ni functionally graded material over eutectic melting temperature. *Metallurgical and Materials Transaction A* , 31A, 2627-2636.

Gao J W, Wang C Y, (2000). Modeling the solidification of functionally graded materials by centrifugal casting. *Material Science. Engineering A* , A292, 207-215.

Gomes J R, Robeiro A R, Vieira A C, Miranda A S, Rocha L A, (2005). Wear mechanisms in Functionally Graded Aluminum Matrix Composites: effect of the Lubrication by an Aqueous Solution. *Materials science and engineering* , 492-493,33-38.

Gupta M, Lai M O, Srivatsan T S, (2002). Synthesis and Characterization of a free standing, one dimensional, Al-Cu/SiC based functionally gradient material. *Journal of material Synthesis and Processing* , 10, 2, 75-81.

Gupta M , Nai S M L, Lim C Y H, (2003). Synthesis and wear characterization of Al based, free standing functionally gradient materials: effects of different matrix compositions. *Composites Science and technology* , 63, 1895-1909.

Gupta M, Loke C Y, (2000). Synthesis for free standing, one dimensional, Al/SiC based functionally gradient materials using gradient slurry disintegration and deposition. *Material Science Engineering A, ,* 276, 210-217.

Gupta M, S M L Nai, (2002). Synthesis of Al/SiC based functionally gradient materials using the technique of gradient slurry disintegration and deposition: effect of stirring speed. *Material Science Engineering A* , 18, 633-641.

Gruzleski J E, Closset B M, (1990). The treatment of liquid Aluminum-silicon alloys. *AFS* , 127-143.

Halvaee A, Talebi A, (2001). Effect of process variables on microstructure and segregation in centrifugal casting of C92200 alloy. *Journal of Materials Processing Technology* , 118, PP 123–127.

Hertz. (1895). Gesammelte Werke. *Aufbua* , 1, 155.

Hinoki T, Lara-Curzio E, Snead L L, (2008). Evaluation of Transthickness Tensile strength of SiC/SiC composites. *27th Annual Cocoa Beach Conference on Advanced Ceramics and Composites: B: Ceramic Engineering and Science Proceedings*, (pp. vol 2, issue 4.401-406).

Holling G E, Lee M, (1996). Tensile strength measurement using a diametral compression test on a small disc with central hole. *Key Engineering Materials* , 118-119, 279-286.

Hondros et al, (1959). The evaluation of Poisson's ratio and the modulus of materials of a low tensile resistance by the Brazilian (indirect tensile) test with particular reference to concrete. *Australian Journal of Applied Science* , 10, 243-267.

Hooper J A, (1971). The failure of glass cylinders in diametral compression. *Journal of the Mechanics and Physics of solids* , 19(4), 179-188.

Huisman W, Graule T, Gauckler L J, (1995). Alumina of High Reliability by centrifugal casting. *Journal of the European ceramic Society* , 15, 811-821.

Hwu B K, Lin S J, and Jahn M T, (1996). The interfacial compounds and SEM fractography of squeeze casting SiCp/6061 Al composites. *Material science Enggineering* , A206, 110-119.

Ibrahim A, Mohamed F A, Lavernia E J, (1991). Particulate reinforced metal matrix composites-a review. *Journal of Material Science*, 26, 1137-1156.

Jahanmir, Suh N P, (1977). Mechanics of subsurface void nucleation in delamination wear. *Wear* , 44(1), pp17-38.

Janco, N. (1998). *Centrifugal casting.* American Foundry Society.

Jasim K M, Dwarakadas E S, (1987). Wear in Al–Si alloys under dry sliding conditions. *Wear* , Vol119, 119–30.

Kaczmar J W, Pietrzak K, Wlosinski W, (2000). The production and application of metal matrix composite materials. *Journal of Material Processing Technology* , 106, 58-67.

Kai Wang, Xue Han-song, Zou Mao-hua, Liu Chang-ming, (2009). Microstructural characteristics and properties in centrifugal casting of SiCp/Zl104 composite. *Transactions of Non ferrous Metals Society of China* , 19, 1410-1415.

Kang C C, Rohatgi P K, (1996). Transient Thermal Analysis of solidification in a centrifugal casting for composite materials containing particle segregation. *Journal of metallurgical and materials transaction B* , 27B, 1025-1029.

Kato K, Kurimoto M, Shumiya H, Adachi H, Sakuma S, Okubo H, (2006). Application of Functionally Graded Material for Solid insulator in Gaseous Insulation System. *IEEE Transactions on Dielectrics and Electrical insulation* , 13, Feb, 362-372.

Kawasaki A, Watanabe R, (1997). Concept and P/M Fabrication of Functionally Graded Materials. *Ceramics International* , 23, 73-83.

Kawasaki A, Watanabe R, (1990). Microstructural Designing and Fabrication of Disk Shaped Functionally Gradient Material by Powder Metallurgy. *Journal of the Japan Society of Powder and Powder Metallurgy* , vol. 37, 253-258.

Kiebact B, Neubrand A, Riedel H, (2003). Processing Techniques for Functionally Graded Materials. *Materials Science and Engineering A* , 362, 81- 05.

Kim K H, Cho S , Yoon K J, Kim D J, Ha J, Chun D, (2002). Centrifugal casting of alumina tube for membrane application. *Journal of Membrane Science* , 199, 69-74.

Kim K H, Cho S J, Kim D J, Yoon K J, (2000). Centrifugal casting of large alumina tube with low rpm. *American Ceramic Society Bulletin* , 77, 95-98.

Koizumi, (1997). FGM activities in Japan. *Composites Part B* , 28B,1-4.

Kok M, (2006). Abrasive wear of Al_2O_3 partocle reinforced 2024 aluminum alloy composites fabricated by vortex method. *Composites part A: Applied Science and Manufacturig* , 37(3), 457-464.

Korachkin D, Gethin D T, Lewis R W, Tweed J H, Guyoncourt D M M, (2008). Measurment of Young's modulus and tensile failure properties of green powder compacts. *Powder Metallurgy* , 51(2), 150-158.

Kumar S, Subramaniya Sarma V, and Murty B S, (2010). Functionally Graded Al Alloy matrix in-situ composites. *Metallurgical and materials transactions A* , 41A, 242-254.

Lee C S, Kim Y H, Han K S, Lim T, (1992). Wear behaviour of aluminum matrix composite materials. *Journal of Material science* , vol 27, pp 793-800.

Lin C Y, Bathias C, McShane H B, Rawlings R D, (1999). Production of silicon carbide Al 2124 alloy functionally graded materials by mechanical powder metallurgy technique. *Powder Metallurgy* , 42, No 1, 29-33.

Liu B B, Xie J X, Hui Qu X, (2008). Fabrication of W-Cu functionally graded materials with high density by particle size adjustment and solid state hot press. *Composites science and technology* , 6, 68, 1539-1547.

Ludema K. C. (2000). Sliding and Adhesive wear. ASTM, *Friction, Lubrication and Wear technology, Vol18.* ASTM International.

Marion, Robert H. Johnstone, Keith J. (1977). A parametric study of the diametral compression test for ceramics. *American Ceramic Society Bulletin* , 56 (11), 998-1002.

Matsuura K, Ohmi T, Kudoh M, Takahashi H, Kinoshita H, Suzuki K, (2004). Dispersion Strengthening in a Hypereutectic Al-Si Alloy Prepared by Extrusion of Rapidly Solidified Powder. Metallurgical and Materials Transcations A , V35, 333-339.

Melgarejo, Duque N B, Sua rez O M, (2005). Functionally graded aluminum matrix composites produced by centrifugal casting. *Materials Characterization* , 55, 167-171.

Melgarejo K, Marcelo S, Sridharan K, (2008). Microstructure and properties of functionally graded Al-Mg-B composites fabricated by centrifugal casting. *Composites: Part A* , 39, 1150-1158.

Melgarejo K, Marcelo S, Sridharan K, (2006). Wear resistance of a Functionally graded aluminum matrix composites. *Scripta materialia* , 55, 95-98.

Mishina H, Inumaru Y, Kaitoku K, (2008). Fabrication of ZrO_2/AlSi316L functionally graded materials for joint prostheses. *Materials Science and EngineeringA.* , 475, 1-2.

Mondal D P, Das S, Rao R N, Singh M, (2005). Effect of SiC addition and running-in-wear on the sliding wear behaviour of Al–Zn–Mg aluminium alloy. *Materials Science and Engineering A* , Vol 402, 307–319.

Mondolfo (1976). *Al alloys: Structure and properties.* London, Boston: Butterworths.

Muller, Drasar, Schilz, Kaysser, (2003). Functionally Graded Materials for Sensor and Energy applications. *Materials Science and Engineering A.* , 362,17-39.

Murray J, (1992). Alloy Phase Diagrams. ASM, *ASM Hand Book.* ASM International.

Nai, Gupta, Lim, (2003). Synthesis and wear characterization of Al based, free standing functionally graded materials: effects of different matrix compositions. *Composites Science and Technology* , Vol63, 1895-1909.

Nath D, Rohatgi P K, (1981). Segregation of mica particles in centrifugal and static castings of aluminium/mica composites. *Composites* , Apr, 124-128.

Ogawa T, Watanabe Y, Sato H, Kim L S, Fukui Y, (2006). Theoretical study on fabrication of functionally graded materials with density gradient by a centrifugal solid-particle method. *Composites, Part- A: Applied science and Manufacturing* , 37, 2194-2200.

Ovri, Davies, (1987). Diametral compression of silicon nitride. *Mater. Sci. Eng.* , 96,109-116.

Pace, (2011). *Metallographic hand book.* Tucson, Arizona: Pace Technologies.

Panda E and Mazumdar D, Mehrotra S P, (2006). Mathematical Modeling of particle segregation during centrifugal casting of metal matrix composites. *Metallurgical and materials transactions A* , 37A, 1675-1687.

Peng X, Yan M, Shi W, (2007). A new approach for the preparation of functionally graded materials via slip casting in a gradient magnetic field. *Scripta Materialia,* , 56,907-909.

Pintsuk, Smid, Döring, Hohenauer, Linke, (2007). Fabrication and characterization of vacuum plasma sprayed W/Cu-composites for extreme thermal conditions. *Journal of Material Science* , 42, 30-39.

Pompe, Worch, Epple, Friess, Gelinsky, Greil, Hempel, Scharnweber, Schulte, (2003). Functionally Graded Materials for Biomedical applications. *Materials Science and Engineering A.*, 362, 40-60.

Potekhin, Il'yushin, Khristolyubov, (2009). Effect of casting methods on the structure and properties of Tin Babbit. *Metal Science and Heat Treatment* , Vol 51, 7-8, pp378-382.

Prasad, Venkateswarlu, Modi, Jha, Das, Dasgupta, Yegneswaran, (1998). The effects of primary silicon particles on the sliding wear behavior of aluminum-silicon alloys. *J Mat Sc.* , 17, 1381-3.

Procopio, Zavaliangos, Cunningham, (2003). Analysis of the diametral compression test and the applicability to plastically deforming materials. *Journal of Materials Science* , 38, 3629-3639.

Proveti J R C, Michot G, (2006). The brazilian test: a tool for measuring the toughness of a material and its brittle to ductile transition. *Internation Journal Fracture* , 139, 455-460.

Qudong W, Yongjun C, Wenzhou C, Yinhong W, Chunquan W, Wenjiang D, (2005). Centrifugally cast Zn-27Al-xMg-ySi alloys and their in situ (Mg2Si+Si)/ZA27 composites. *Materials science & engineering A* , Vol304, pp425-434.

Rajan T P D, Pai B C, (2009). Formation of solidification microstructures in centrifugal cast functionally graded aluminum composites. *Transactions of the Indian Institute of Metals* , 62, Issues4-5, 383-389.

Rajan T P D, Pillai R M, Pai B C, (2008). Functionally graded Al-Al3Ni in situ intermetallic composites: Fabrication and microstructual characterization. *Journal of Alloys and Compounds* , 453,1-2.

Rajan T P D, Pillai R M, Pai B C, (2006). Functionally graded Al-Al_3Ni on situ intermetallic composites: fabrication and microstructural characterization. *Journal of alloys and Compounds* , 453, L4-7.

Raju, Mehrotra, (2000). Mathematical modeling of centrifugal casting of Metal matrix composites. *Materials Transactions, JIM* , 41, No. 12, 1626-1635.

Rao P, Iwasa M, Tanaka T, Kondoh I, (2003). Centrifugal casting of Al2O3-15wt%ZrO_2 ceramic composites. *Ceramics International* , 29, 209-212.

Reddy T V S, Dwivedi D K, Jain N K, (2009). Adhesive wear of stir cast hypereutectic Al–Si–Mg alloy under reciprocating sliding conditions. *Wear* , 266, 1–5.

Reddy S A, Bai P, Murthy B S S, Biswas S K, (1995). Mechanism of seizure of aluminium silicon alloys dry sliding against steel. *Wear* , 181-183,658-667.

Reddy S A, Bai P, Murthy B S S, Biswas S K, (1994). Wear and seizure of binary Al-Si alloys. *Wear* , 171, 115-127.

Revankar , (2000). Mechaniacl testing and evaluation. In A. International, *ASM hand book.* ASM International.

Rohatgi, (1991). Cast aluminum-matrix composites for automotive applications. *JOM*, 43, 10-15.

Royer A, (1988). Horizontal centrifugation: A technique of foundry well adapted to the processing of high reliability pieces. *Journal of material shaping technology* , Vol.5, No.3, pp 197-209.

Sarkar A D, Clarke C J, (1980). Friction and wear of alumimun-silicon alloys. *Wear*, vol 61, 157-67.

Sarkar A D, (1975). Wear of aluminium-silicon alloys. *Wear* , 31,331-343.

Schulza U, Petersa M, Bachb W, Tegederc G, (2003). Graded coatings for thermal, wear and corrosion barriers. *Materials Science & Engineering A* , 362, 61-80.

Shamsi, Mehrotra, (1993). A two-dimensional heat and fluid-flow model of single-roll continuous-sheet casting process. *Metallurgical And Materials Transactions B* , Volume 24, Number 3, 521-535,.

Shaw, Braiden, Desalvo, (1975). The disk test for brittle materials. *Journal of Engineering for Industry, Transactions of the ASME* , 77-87.

Shivnath, PK Sen Gupta, TS Eyre,, (1977). Wear of aluminium-silicon alloys. *Br. Foundryman* , 70, 349-356.71.

Silaeva I, Prusakov B A, Éskin G I, (2000). Effect of microalloying on the structure and properties of alloys in the Al-Si-Cu system. *Metal Science and Heat treatment* , Vol 42, 241-245.

Song C J, Xu Z M, , Li J G, (2007). Fabrication of in-situ Al/Mg_2Si functionally graded materials by electromagnetic separation method. *Composites Part A:Applied science and manufacturing* , 38, 427-433.

Song C J, Xu Z M, , Li J G, (2007). In situ Al/Al_3Ni functionally graded materials by electromagnetic separation method. *Materials Science & Engineering A* , 445-446, 148-54.

Song C J, Xu Z M, , Li J G, (2005). In situ multi-layer functionally graded materials by Electromagnetic Separation method. *Materials Science & Engineering A* , 393, 164-169.

Song C J, Xu Z M, , Li J G, (2007). Structure of in situ Al/Si functionally graded materials by electromagnetic separation method. *Materials & Design* , 28, 1012-1015.

Song C J, Xu Z M, , Li J G, (2006). Study of in-situ Al/Mg_2Si functionally graded materials by electromagnetic separation method. *Materials Science & Engineering A* , 424, 6-16.

Srivatsan T S, Ibrahim I A, Mohamed F A, Lavernia E J, (1991). Processing techniques for particulate-reinforced metal matrix Aluminum matrix composites. *Journal of Material Science* , 26, 5965-5978.

Straffelini G, Pellizzari M, Molinari A, (2004). Influence of load and temperature on the dry sliding behaviuor of Al-based metal-matrix-composites against friction material. *Wear* , vol 256, pp754-763.

Subramanium, (1991). Effects of sliding speed on the unlubricated wear behavior od Al-12.3wt%Si alloy. *Wear* , Vol 151, 97-110.

Suh, (1980). Fundamentals of Friction and Wear of Materials. *ASM* , pp43-72.

Surappa, (2003). Aluminium matrix composites: Challenges and opportunities. *Sadhana* , Vol. 28, Parts 1 & 2, pp. 319–334.

Takagi, Shaw, (1981). Evaluation of fracture strength of brittle tools. *CIRP* , Vol1,53-57.

Thimoshenko, (1982). *Theory of elasticity.* Newyork: McGraw-Hill.

Tjong, Wu S Q, Liao H C, (1997). Wear behaviour of an Al-12%Si alloy reinforced with a low volume fraction of SiC particles. *Composites Sciece and Technology* , vol 57, pp 1551-1558.

Torabian H, Pathak JP, Tiwari SN, (1994). Wear characteristicsof Al-Si alloys. *Wear* , 172, 49-58.

Vassiliou, Pantelis,Vosniakos, (2008). Investigation of centrifugal casting Conditions. *Proceedings of the 3rd International Conference on Manufacturing Engineering* (pp. 347-356). Chalkidiki, Greece: ΕΕΔΜ and PCCM.

Velhinho, Botas, Ariza, Gomes, Rocha, (2004), Tribocorrosion Studies in Centrifugally Cast Al-Matrix SiCp - reinforced Functionally Graded Composites. *Material Science Forum* , Vol 455-456, 871-875.

Wilson, Alpas, (1997). Wear mechanism maps for metal matrix composites. *Wear* , vol 212, pp 41-49.

Wright, (1955). Comments on an indirect tensile test on concrete cylinders. *Magazine of Concrete Research* , 7(20), 87–95.

Wright, (1955). Comments on an indirect tensile test on concrete cylinders. *Magazine of concrete research* , 87.

Xiandong S, Chengping L, Zhuoxuan L, Liuzhang O (1997). The fabrication and properties of particle reinforced cast metal matrix composites. *Journal of Materials Processing Technology* , 63, 426-431.

Xie J X, Liu BB, QuXH, (2005). Design of component and structure for W/Cu heat sink Gradient materials. *Chinese journal of Rare metals* , 29(5), 757-761.

Xuhong H A O, Changming LIU, Dengliang PAN, (2011). Microstructure and Mechanical Behavior of in Situ Primary Si/Mg_2Si Locally Reinforced Aluminum Matrix Composites Piston by Centrifugal Casting. *Chinese Journal of Mechanical Engineering* , 22, No. 5, 1-5.

Watanabe Y, Kurahashi M, Kim I S, Miyazaki S, Kumai S, Sato A, Tanaka S, (2006). Fabrication of fibre-reinforced functionally graded materials by a centrifugal in situ method from Al-Cu-Fe ternary alloy. *Composites part A* , 37, 2186-2193.

Wayne S F, Baldoni J G, Buljan S T, (1990). Abrasion and erosion of WC-Co with controlled microstructures. *Tribology Transactions* , 33, 4, 611-617.

Watanabe Y, Yamanaka N, Fukui Y, (1998). Control of composition gradient in a metal-ceramic functionally graded material manufactured by the centrifugal method. *Composites part A* , 29A, 595-560.

Watanabe Y, Sato H, FukuI Y, (2007). Effects of Platelet size and mean volume fraction on platelet orientation and volume fraction distributions in functionally graded material fabricated by centrifugal solid-particle method. *Journal of engineering material and Technology, ASME* , 129, 2, 304-312.

Watanabe Y, Eryu H, Matsuura K, (2001). Evaluation of three-dimensional orientation of Al_3Ti platelet in Al-based functionally graded materials fabricated by a centrifugal casting technique. *Acta Materialia* , 49, 775-783.

Watanabe Y, Oike S, (2005a). Formation mechanism of graded composition in Al-Al_2Cu functionally graded materials fabricated by a centrifugal in situ method. *Acta Materialia* , Vol: 53 (6),1631-1641.

Watanabe Y, Nakamura T, (2001). Microstructures and wear resistances of hybrid Al-(Al_3Ti+Al_3Ni) FGMs fabricated by a centrifugal method. *Intermetallics* , 9, 33-43.

Watanabe Y, Oike S, (2005b). Microstructures of functionally graded materials fabricated by centrifugal solid-particle and in-situ methods. *Metals and Materials International* , Vol11, 5, 391-399.

Watanabe Y, Fukui Y, Okada H, Kumazawa N, (2001). Near-Net-Shape forming of Al-Al_3Ni functionally graded material over eutectic melting temperature. *Metallurgical and Materials Transaction A* , 31A, 2627-2636.

Watanabe Y, Kawamoto A, Matsuda K, (2002). Particle size distributions in functionally graded materials fabricated by the centrifugal solid-particle method. *Composites science and Technology* , 62, 881-888.

Ogawaa T, Watanabea Y, Satob H, Kima I S, Fukui Y, (2006). Theoretical study on fabrication of functionally graded material with density gradient by a centrifugal solid-particle method. *Composites part A* , 37, 2194-2200.

Watanabe Y, Yamanaka N, Fukui Y, (1999). Wear behavior of Al-Al_3Ti composite manufactured by a Centrifugal method. *Metallurgical and Materials Transaction A* , 30A, 3253-3261.

Watanabe Y, Sato R, Kim IS, Miura S, Miura H, (2005c). Functionally Graded Material Fabricated by a Centrifugal Method from ZK60A Magnesium Alloy. *Materials Transactions* , Vol. 46, No. 5, pp. 944 to 949.

Yan-bo Z, Chang-ming L, WANG Kai, Mao-hua Z, Yong X, (2010). Characteristics of two Al based functionally gradient composites reinforced by primary Si particles and Si/in situ Mg_2Si particles in centrifugal casting. *Transactions of Non ferrous Metals Society of China* , 20, 361-370.

Yanwei Sui, Bangsheng Li, Aihui Liu, Jingjie Guo, Hengzhi Fu, (2010). Evolution of microstructure in centrifugal cast Al-Cu alloy. *China Foundry* , 7, No. 1, 43-46.

Zhou B L, (1999). Functionally graded Al/Mg_2Si in situ composites prepared by centrifugal casting. *Journal of material science letters* , 17, 1677-1679.

Zhanga J, Fana Z, Wangb Y, Zhoub B, (2000). Hypereutectic aluminum alloy tubes with graded distribution of Mg_2Si particles prepared by centrifugal casting. *Materials and Design* , 21, 149-153.

Zhang W Q, Yang Y S, Liu Q M, Zhu Y F, Hu Z Q, (1998). Structural transition and macrosegregation of Al-Cu Eutectic alloy solidified in the electromagnetic centrifugal casting process. *Metallurgical and materials transactions A* , 29A, 404-408.

Zhang Z F, Zhang L C, Mai Y W, (1995). Wear of ceramic particle reinforced metal matrix composites, Part I, Wear mechanisms. *Journal of Material Science* , Vol 30, pp 1961-1966,.

Zhang, Zhongtao, Li, Tingju, Yue, Honyun, Jian, Li, Jie, (2009). Study on the preparation Al/Si functionally graded materials using power ultrasonic field. *Materials and design* , 30, 851-856.

Zhiqiang S, Di Z, Guobin L, (2005). Evaluation of dry sliding wear behavior of silicon particles reinforced aluminum matrix composites. *Materials and Design* , Vol26, 454–458.

Zhou Z J, Yum YJ, G CC, (2010). The recent progress of FGM on Nuclear materials-Design and fabrication of W/Cu Functionally Material High Heat Flux Components for Fusion reactor. *Material Science Forum* , 631-632, 353-358.

Zhu J, Lai Z, Yin Z, Jeon J, Lee S, (2001). Fabrication of ZrO2-NiCr functionally graded material by powder metallurgy. *Materials Chemistry and Physics* , 68,130-135.

Technical research papers published based on this thesis

Category Details

1.Journal paper, full paper reviewed 2.Journal paper, abstract reviewed 3.Conference/Symposium paper, full paper reviewed

4.Conference/Symposium paper, abstract reviewed 5.Others (in Workshops, NITK Research Bulletins, Short notes etc.)

Sl. No.	Title of the Paper	Authors	Name of the journal/ Conference/Symposium Vol., No., Pages	Month & Year of publication	Category
1.	Characterization of Al-Si Functionally Graded material using Centrifuge Casting Method	Kiran Aithal Vijay Desai Narendranath S P G Mukunda	International review of Mechanical Engg. Vol.3, N.5	Sep. 2009	1
2.	Effect of L/D ratio on Al-Si Functionally Graded Material cast through Centrifuge Technique	Kiran Aithal Vijay Desai Narendranath S P G Mukunda	Advanced Materials Research Journal *Vol. 213 pp 281-285*,	Oct. 2011	1
3.	Evolution of Microstructure and Hardness of Al-Si Functionally Graded Material Cast through centrifuge Technique using Hypereutectic and Eutectic Al-Si	Kiran Aithal Vijay Desai Narendranath S P G Mukunda	International Journal of Mechanical and Materials Engineering Vol 6, No2, pp 275-279	Jan. 2011	1
4.	Microstructure, Hardness and Wear characterization of Al-Si FGMs	Kiran Aithal Vijay Desai Narendranath S P G Mukunda	Indian Foundry Journal, Vol58, No.5, pp39-48	May 2012	1
5.	Fabrication and Characterization of AL/17%Si Functionally Graded Composite Material using Centrifuge casting method	Kiran Aithal Vijay Desai Narendranath S P G Mukunda	National conference of ETME-09, Oxford College, Bangalore	Mar. 2009	3

6	Wear Characterization of Al/17wt% Si Functionally Graded Material	Kiran Aithal Vijay Desai Narendranath S P G Mukunda	Tribo-India Conference. **IIT Delhi**	Dec. 2009	3
7	Microstructure and Wear Characterization of Hypereutectic Al-Si FGM	Kiran Aithal Vijay Desai Narendranath S P G Mukunda	**TMS2010,** 139th Annual Meeting and Exhibition, 2010, **USA**	Feb. 2010	3
8.	Characterization of Al-Si Functionally Graded Material Cast through centrifuge technique	Kiran Aithal Vijay Desai Narendranath S P G Mukunda	ICFIME- May 2010, **NITK Surathkal**, India	May 2010	3
9	Evaluation of Microstructure and Hardness of Al-17wt%Si-7wt%SiC Functionally Graded Composite	Kiran Aithal Vijay Desai Narendranath S P G Mukunda	AMMMT 2010, SIT Tumkur.	Nov. 2010	3
10	Microstructure, Hardness characterization of Al-Si FG alloy and Al-Si- SiC_P FGMMC	Kiran Aithal Vijay Desai Narendranath S P G Mukunda	3rd Asian Conference on Mechanics of Functional Materials and Structures, **IIT Delhi**	Dec 2012	3
11	Effect of process parameters on centrifugally cast Al-Si FGM	Kiran Aithal Vijay Desai Narendranath S P G Mukunda	**TMS2013,** 142nd Annual Meeting and Exhibition, 2013, **USA (Accepted)**	Mar, 2013	3